Integrated trailing edge flap track mechanism for commercial aircraft

Integrated Trailing Edge Flap Track Mechanism for Commercial Aircraft

by

Sven P. Schoensleben

Master Thesis

Winter Term 2005/06
at the Center of Structure Technologies
Prof. Dr. Paolo Ermanni

Reference Number: IMES-ST-05-198

Advisor: Christof Ledermann

Eidgenössische Technische Hochschule Zürich
Swiss Federal Institute of Technology Zurich

Abstract

Flap track fairings are familiar features of every modern commercial aircraft. In recent developments much has been done to decrease fairing drag with sophisticated aerodynamic design. But a significant parasite drag always remains which is particularly substantial at high airspeed during cruise, a flight phase not requiring any flap track actuation, the fairings thus being responsible for part of the parasite drag and unnecessary fuel consumption. Avoidance of this fairing drag could therefore lead to an improvement in the aircraft's operating costs as well as a payload increase due to less fuel consumption.

Since in the retracted state flap loads are minimal when compared to a final approach configuration where stiff, strong and thus voluminous flap supports are needed, a 'weaker' and smaller mechanism and flap support system would suffice during cruise.

This thesis presents how a basic concept for an integrated flap track mechanism could be designed, fitted into the wing strake in the flaps up position, while aerodynamic flap setting requirements are satisfied. Various realistic constraints are taken into account.

Rather than pure theoretical reasoning a pragmatic hands-on approach was chosen for this project. The results are obtained by mostly intuitive and experimental construction work, while always accounting for requirements resulting from the professional background and application of the project.

The first three chapters represent a semester thesis by the same author. The introducing chapter gives a rough estimation of the economic benefit for a typical airliner when integrated flap tracks are used. Second, a comprehensive look into current systems is presented. The third chapter shows all necessary components with detailed descriptions and finally the full mechanism in conceptual form.

The actual master thesis begins with chapter 4, at first outlining various constraints and considerations for the detailed design process which is explained extensively in chapter 5 based on a fully working demonstrator model of the mechanism. Further structural details are outlined in chapter 6 together with a CAD model, which is the basis for a set of movies and some selected FEM analyses in chapter 7. Finally, a conclusion in chapter 8 gives a brief summarization of pros and cons as well as an outlook.

Acknowledgements

This report presents the results of a semester and master thesis carried out at the Center of Structure Technologies of the Swiss Federal Institute of Technology ETH Zurich.

I would like to thank my advisor Mr. Christof Ledermann and Prof. Dr. Paolo Ermanni, who allowed me to do this equally challenging and exciting project, the basic idea of which came to my mind on one of my many flights.

My thanks also go to Mr. Fritz Zaugg and Mr. Robert Krueger of SR Technics, Zurich Airport, Switzerland, as well as Mr. Daniel W. Knecht of the Swiss Aircraft Accident Investigation Bureau. I would like to thank as well Mr. Ben Holert from the Aircraft Systems Engineering Department of the Technical University of Hamburg-Harburg, Germany, for his valued expert tips.

Disclaimer & Conditions

Any information or opinions presented in this report are entirely the author's and do not necessarily comply with those of either ETH Zurich, any company mentioned, or any other party involved. Any liability in connection with this report and its pertaining project will be declined.

The new technical principles presented in this report must be used, under any circumstances, for peaceful purposes only. Usage in aircraft and other devices intended for and/or involved in any armed forces operation is strictly prohibited. This prohibition includes application on military derivatives of commercial aircraft.

The invention as presented in this report is subject of a patent application filed with the United States Patents and Trademark Office on June 2, 2005. Licensing requests are welcome and may be addressed to:

Technology Transfer
Swiss Federal Institute of Technology Zurich
ETH Transfer
Raemistrasse 101
CH-8092 Zurich
Switzerland

Table of Contents

Nomenclature

Latin Symbols, Abbreviations

a	Sonic speed	[m/s]
AOA	Angle of attack	
C_D	Drag coefficient	[-]
C_{D0}	Drag coefficient at $\alpha = 0°$	[-]
C_L	Lift coefficient	[-]
c_{TJET}	Specific fuel consumption for turbojet aircraft	[1/h]
D	Drag	[N]
DOC	Direct operating costs	
e	Oswald factor	[-]
G	Weight	[N]
m	Mass	[kg]
S	Surface area	[m^2]
STOL	Short takeoff & landing	
T/O	Takeoff	
v	Speed	[m/s]

Greek Symbols

α	Angle of attack	[°]
α_{max}	Stalling angle of attack	[°]
Λ	Wing aspect ratio	[-]
ρ	Density	[kg/m^3]

Chapter 1

Introduction

1.1 Motivation

Flap track fairings are familiar features of every modern commercial aircraft. While the size of flap track mechanisms in proportion to aircraft tended to increase in recent developments much has been done to decrease fairing drag with sophisticated aerodynamic design.

However, a significant drag always remains, and it goes exponentially with airspeed. Thus there is a particularly substantial parasite drag at high airspeed during cruise, a flight phase not requiring any flap track actuation. It is a legitimate question why this approach must be kept in future.

One reason is that significant loads act on a flap system including its fairings, and that these loads should be distributed to rather big parts and areas to avoid exceeding of material limits. Such big parts cannot be reasonably built into the main wing structure as fuel and other systems leave only very little space for any other mechanism.

On the other hand, since in the retracted state flap loads are minimal when compared to a final approach configuration, a ‘weaker’ (so smaller) mechanism and flap support system would suffice during cruise. It could be devised in a way that it builds up to a stronger system when flaps are extended. It is the main aim of this study to investigate whether this is at all possible.

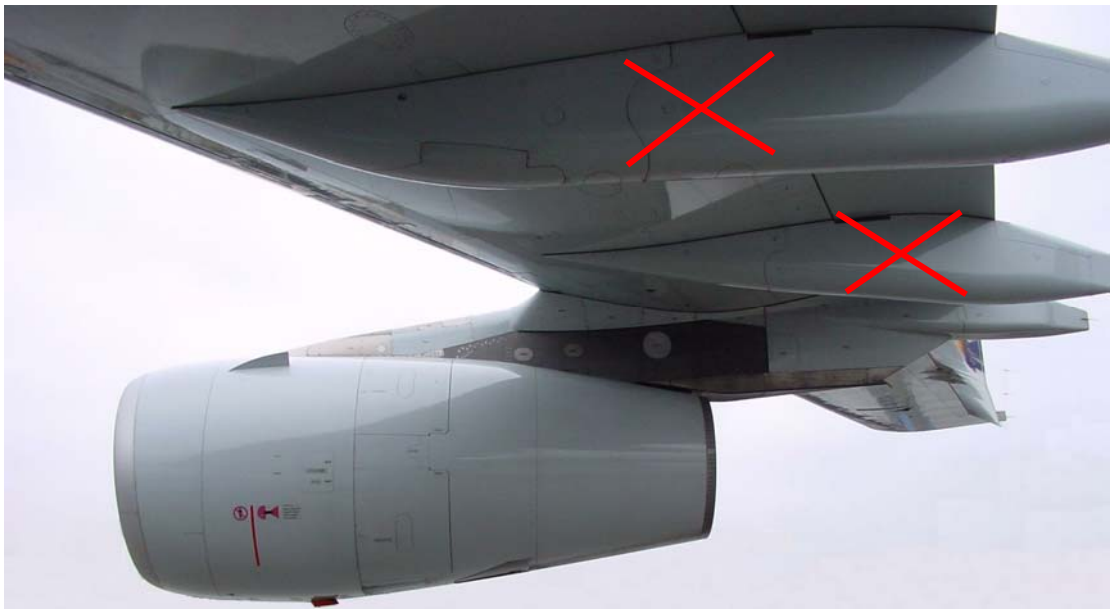

Photo © Max Koerte

Figure 1.1 The goal of this project — in short

1.2 Economic Advantage Estimate

As with any technical innovation the question of the economic benefit is a valid one. This subchapter is intended to give a rough estimate in terms of fuel savings or range improvement.

The following investigation is done on the basis of the A340-300. However, it is not in any way intended to be exact, but rather to give an order of magnitude, which is also valid for other aircraft of the same class. Thus some rough assumptions are made and explained at the appropriate locations.

First a drag coefficient must be specified for a typical fairing. As can be seen in figures 1.1 and 1.3 they do not all have exactly the same shape but are rather designed to minimize drag at their specific location on the wing. Note that in figure 1.3 the outermost fairing is from the outer engine pylon; the three flap track fairings of the outer flap are shown. The fourth flap track fairing for the inner flap can be seen in figure 1.4.

For the purpose of this rough estimate they will all be dealt with as the same, disregarding their aerodynamic differences. Exact drag data is not freely available, but literature suggests that $c_{D,Fairing} = 0.05$ is a reasonable assumption for such kinds of roughly spindle-shaped bodies, with the maximum cross section perpendicular to the airflow as the reference area S [3]. As shown in figure 1.2 below this area is about $S = 0.6m \times 0.5m = 0.3m^2$.

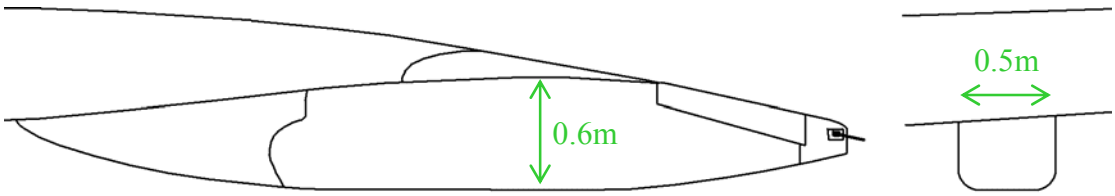

Figure 1.2 Side and front view with approximate dimensions

The following A340-300 data is taken from [2], [3] and [5].

Reference Wing Area	363.10 m^2
Economic Cruise	M = 0.84 @ Flight Level 390 = 11890m
Service Ceiling	Flight Level 410
Range	6750NM = 12500km
MTOW	257000kg, whereof 113000kg fuel
Drag Polar	$c_D = 0.0165+0.0435*c_L^2$
Aspect Ratio & Oswald Factor	$\Lambda = 9.5$, e = 0.77

Figure 1.3 A340-300 wing view — 'clean' cruise configuration

Figure 1.4 A340-300 final approach — landing configuration
(at Juliana International Airport, St. Maarten, D.W.I.)

ICAO Standard Atmosphere (from [2]):

Altitude	0m	11890m
Barometric Pressure p	1013.25hPa	196.172 hPa
Density ρ	1.225 kg/m^3	0.324 kg/m^3
Temperature T	288.15K = 15°C	210.93K = -62°C
Mach Speed a	340.9m/s = 662.65kts	291.66m/s = 567kts

Now the actual calculations are carried out:

***Step 1:* Speed**

$$M = 0.84, a = 291.66 m/s \Rightarrow v = M \cdot a = 245 m/s = 476 kts = 882 km/h$$

***Step 2:* $C_{L,max\ range}$, $C_{D,max\ range}$**

Drag polar (symmetric polar assumed): $C_D = C_{D0} + k \cdot C_L^2 = 0.0165 + 0.0435 \cdot C_L^2$
Follows with formula from [2] for maximum range of jet aircraft:

$$C_{L,max\ range} = \sqrt{\frac{C_{D0}}{3 \cdot k}} = \sqrt{\frac{0.0165}{3 \cdot 0.0435}} = 0.356$$

which, inserted in the drag polar, yields

$$C_{D,max\ range} = C_{D0} + k \cdot C_{L,max\ range}^2 = 0.0165 + 0.0435 \cdot 0.356^2 = 0.022$$

***Step 3:* Drags**

To avoid any coefficient and reference area mismatch all drags are first expressed in actual forces rather than directly evaluating a 'weighted' overall C_D.

Overall drag @ cruise:

$$D_{ovrl@cruise} = C_{D,max\ range} \cdot S_{wing,ref} \cdot \frac{\rho}{2} \cdot v_{cruise}^2 = 0.022 \cdot 363.1 \cdot \frac{0.324}{2} \cdot 245^2 = 77677 N$$

Fairing drag @ cruise:

$$D_{fairing@cruise} / fairing = C_{D,fairing} \cdot S_{fairing,ref} \cdot \frac{\rho}{2} \cdot v_{cruise}^2 = 0.05 \cdot 0.3 \cdot \frac{0.324}{2} \cdot 245^2 = 145.86 N$$

Follows with a total of 8 flap track fairings: $D_{fairing@cruise} = 1167N$

(Assumptions: additional economization of interference drag by removing the fairings and thus additional edges is not considered here; therefore this approach is conservative. Further $C_{L,max\ range}$ is assumed to be constant.)

Overall drag @ cruise with 'integrated' flap tracks, i.e. no fairings:

$$D_{ovrl@cruise,new} = D_{ovrl@cruise} - D_{fairing@cruise} = 77677N - 1167N = 76510N$$

***Step 4:* New C_D & lift/drag ratio**

Inverting the steps above yields the new overall drag coefficient:

$$C_{D,max\ range,new} = \frac{D_{ovrl@cruise,new}}{S_{wing,ref} \cdot \frac{\rho}{2} \cdot v_{cruise}^2} = \frac{76510}{363.1 \cdot \frac{0.324}{2} \cdot 245^2} = 0.02167$$

Old lift/drag ratio: $\left(\frac{C_L}{C_D}\right)_{old} = \frac{0.356}{0.022} = 16.1818$

New lift/drag ratio: $\left(\frac{C_L}{C_D}\right)_{new} = \frac{0.356}{0.02167} = 16.4282$

Ratio of both values: $\frac{16.4282}{16.1818} = 1.0152$

Aerodynamic efficiency thus increases by about **1.5%**.

Step 5: **New range or fuel consumption**

The range is calculated by means of the following formula (for turbojet aircraft) taken from [2]:

$$\text{Range} = \frac{1}{c_{TJet}} \cdot \sqrt{\frac{2}{\rho} \frac{G}{S_{wing,ref}}} \cdot \frac{C_L^{1/2}}{C_D} \cdot \ln\left(\frac{m_{T/O}}{m_{T/O} - m_{Fuel,Used}}\right)$$

With only C_D changing the following ratio comes up (same as for lift/drag ratio):

$$\frac{\text{Range}_{new}}{\text{Range}_{old}} = \frac{C_{D,old}}{C_{D,new}} = \frac{0.022}{0.02167} = 1.0152$$

Thus the range increases by about **1.5%** or about 200km on a 12500km flight if the same amount of fuel is consumed. This is enough to reach an alternate airport in many cases.

If the range is the same and fuel savings are of interest the following equation needs to be solved (with $C_L = 0.356$, $m_{T/O} = 257000$kg, $m_{Fuel,Used,old} = 113000$kg):

$$\text{Range}_{new} = \text{Range}_{old} \Rightarrow \frac{C_L^{1/2}}{C_{D new}} \cdot \ln\left(\frac{m_{T/O}}{m_{T/O} - m_{Fuel,Used,new}}\right) = \frac{C_L^{1/2}}{C_{D old}} \cdot \ln\left(\frac{m_{T/O}}{m_{T/O} - m_{Fuel,Used,old}}\right)$$

Solving yields $m_{Fuel,Used,new} = 111743$kg,
i.e. a saving of $m_{Fuel,Used,old} - m_{Fuel,Used,new} = 1257$kg
or about $m_{Fuel,Used,saved}/m_{Fuel,Used,old} =$ **1.1%**

Literature suggests that about 30% of a long-haul aircraft's DOC are due to fuel costs. 1.1% of these 30% would therefore reduce the DOC by 0.3% [2].

This may seem only very small savings and not worth considering. However, today's aviation is a field of extreme economic competition, with low airfares leaving the financial excess revenue (i.e. gain not only paying for the flight's operation costs) per seat and flight for an airline only at sometimes very few dollars.

If, for example, DOC for a specific long-haul flight may be US$ 50k, the avoidance of fairings could generate an excess revenue per flight of 0.3% of US$50k, i.e. US$150. This is indeed very low, but as explained may be still of importance for low-cost carriers. It must be noted, however, that these figures are extremely dependent on general fuel cost, which tend to increase.

These considerations did not account for any additional maintenance costs which are likely to increase with complexity of the system. Thus an integrated flap track should not be so complex and costly in maintenance as to outweigh any savings achieved. But, according to maintenance engineers, the handling of flap track fairings on current aircraft is extremely tedious and costly, with the consequence that they are not removed for track inspection unless absolutely necessary. Eliminating of these fairings could therefore reduce costs from this point of view and may also allow for easier inspection. Overall maintenance costs may thus remain the same even with more complex flap tracks.

For an airline, more important than range increase or fuel savings is the higher payload capacity. In this context the anticipated payload increase of 1257kg for a given range due to fuel savings becomes very attractive. This could mean an additional loading of ten paying passengers including their luggage (tickets of which may generate an additional combined revenue of US$5000 and up) or the equivalent in cargo, where over one metric ton generates already a relevant revenue also for non-low-cost carriers. But again the flap track's weight increase due to complexity should not outweigh these savings, although a somewhat heavier system might not be avoided.

Thus the most important — while trivial — insight gained from this chapter for the project at hand is as follows: integrated flap track mechanisms should not be of a complexity which increases overall maintenance costs and weight so much that any additional payload revenue either becomes unattractive or at all impossible.

If this can be avoided, usage of integrated flap track mechanisms could lead to a significant economic benefit for an airline, even though reducing the aircraft's DOC only marginally.

Chapter 2

State of the Art

2.1 Technical and Legal Aspects

Flaps are extremely loaded parts, and so are the flap tracks made up of their structural parts and actuators; besides, in every flap track unit each part must be allowed to fail without the whole assembly getting unstable. Thus the different load cases are more varying than in most other parts of an aircraft. This leads to generally very robust and rather heavy parts. A number of airworthiness directives related to various failures in flap track systems of different aircraft types clearly show that these issues are not to be underestimated.

Still, all of these mechanisms are to consume the least space possible, particularly those parts which need a fairing outside the actual wing structure. Within the wing space is usually very limited since the torque box should be as large as possible to fulfill its purpose and accommodate the most fuel, leaving little space for other systems. The latter are often stored behind the rear spar of the torque box, the space which would also be needed by an integrated flap track. It is part of this project to investigate if this clash of interests can be solved.

The deployment of trailing edge flaps always entails a considerable decrease of α_{max}, i.e. the angle of attack at which the wing airflow would stall. Thus before any flaps are moved the leading edge slats are deployed and a slot opens there through which an airflow can pass and regenerate the upside wing boundary layer. This increases α_{max}, compensating for the impact of the flaps. If the slats are inoperative for any reason the use of flaps is prohibited.

Again for boundary layer regeneration reasons one ore more slots are opened at the flaps when they are deployed. Highly efficient but complicated systems may have up to three slots opened in their fully extended (flaps down) position.

Federal and Joint Airworthiness Regulation FAR/JAR 25.701(a) require the synchronization of flap surfaces on both sides and suggest a mechanical link between them or another safe and reliable method (see appendix). Modern high-lift systems in transport aircraft usually have a mechanical shaft transmission system and a central power drive unit synchronizing the flap panels. Should the flap system fail to extend or retract on one side of the aircraft a torque limiter automatically shuts down and freezes flap movement to avoid a highly asymmetric lift distribution, a dangerous condition which cannot be trimmed out on most commercial aircraft.

2.2 Current Technologies

2.2.1 Integrated Flap Tracks Already Developed

It is noteworthy that in earlier years of aviation integrated flap tracks were more common than nowadays. This is partly because of then less 'packed' wings; since they were mainly empty, relatively big mechanisms could be stored inside the wing. Two similar patents filed 1945 and 1950, respectively, show such flap tracks.

These two patents show an efficient combination of translating tracks and programming elements, a similar system used today for (always integrated!) leading edge slat devices. It is currently not used in this way for trailing edge flaps, however.

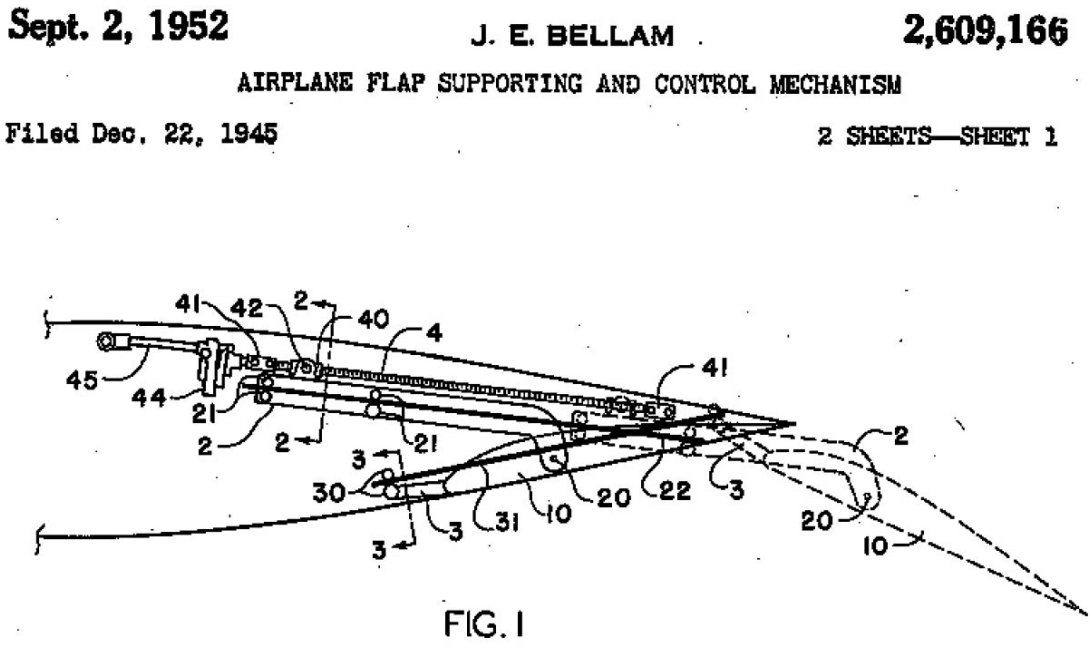

Figure 2.1 Extract from a patent document [10] filed 1945

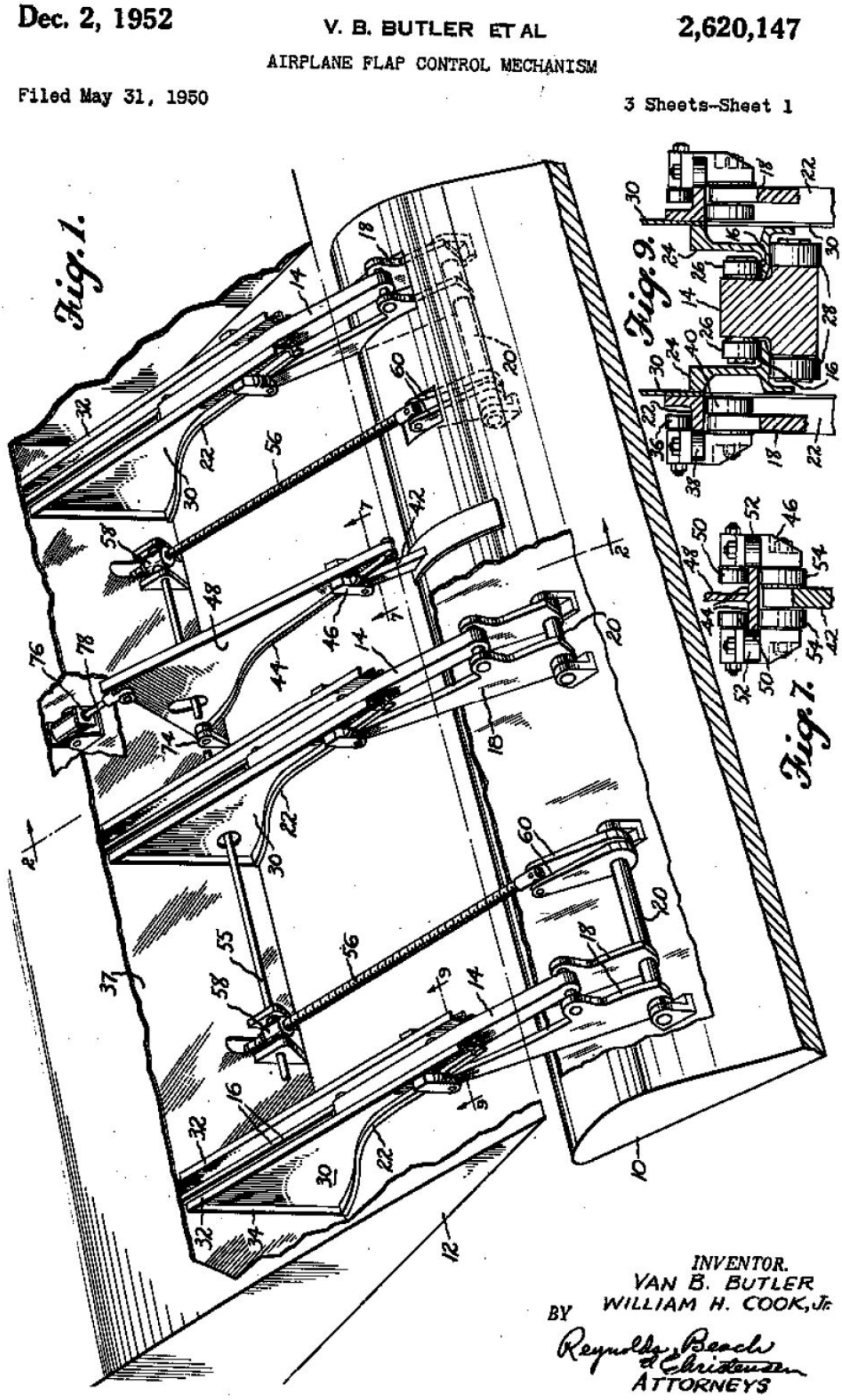

Figure 2.2 Extract from a patent document [11] filed 1950

2.2.2 Flap Systems for Small Transport Aircraft

Although not the main topic of this project, studying flap tracks of smaller aircraft gives a broader view on the field.

Figure 2.3 Cessna Grand Caravan (at St. Barts, F.W.I.)

The Cessna Grand Caravan is a rugged aircraft used on difficult airfields (including STOL). Therefore it needs fowler flaps the small guide tracks of which can be seen in figure 2.4 below, but since it is not a top-notch aircraft anyway from the aerodynamic point of view there are no fairings on the rear tracks.

Figure 2.4 Cessna Grand Caravan flap tracks (at Philipsburg, St. Maarten, D.W.I.)

Figure 2.5 De Havilland Canada DHC6-300 Twin Otter

Originally designed for the rough arctic of northern Canada the very robust De Havilland Canada DHC6 Twin Otter became a widely used and extremely reliable aircraft flying different types of missions all over the world. It may operate from bumpy STOL airfields (with approach angles up to 30°) but also from huge international airports, which calls for a wide range of approach and departure speeds. This is accomplished by a sophisticated and very efficient flaperon high-lift system: the double-slotted flaps extend over the whole wingspan up to the wing tips. The flap supports and tracks have a pivot point at their lowest point; since the ailerons are part of the flap systems they must be controlled via the tracks. The aileron (here flaperon) control rod can be seen in figure 2.6 below.

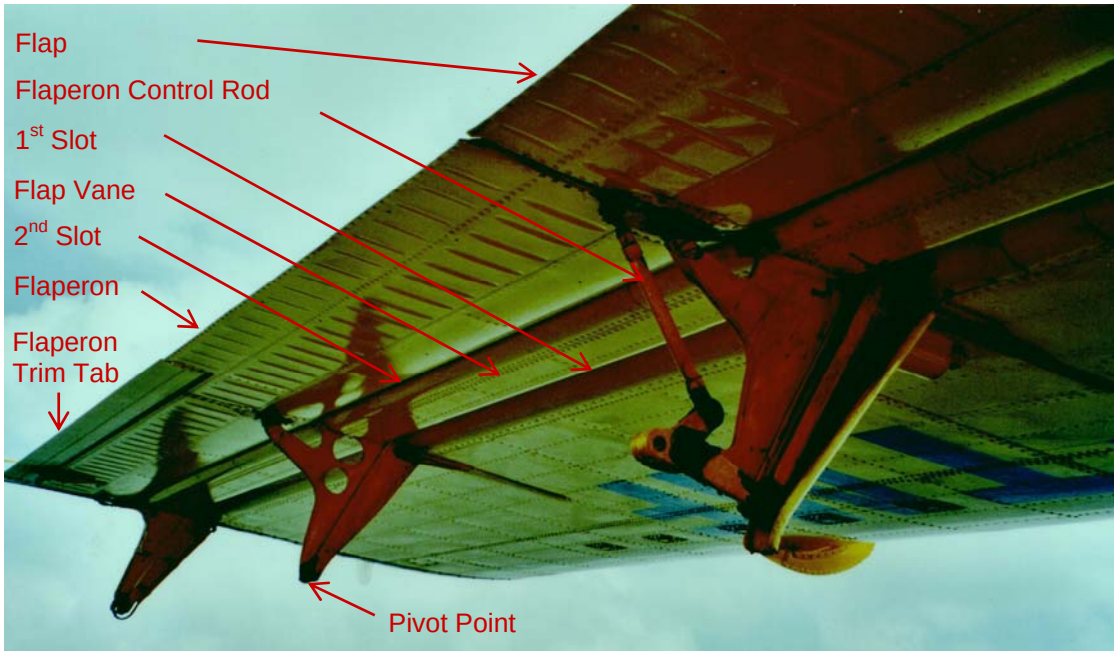

Figure 2.6 Twin Otter flaperon tracks in flaps up position

The outer parts of the tab are used as ailerons (thus called flaperons), while the inner parts are the actual flaps and are tilted a bit further when compared to the flaperons; the flaps down position can be seen in figures 2.7 and 2.8 below.

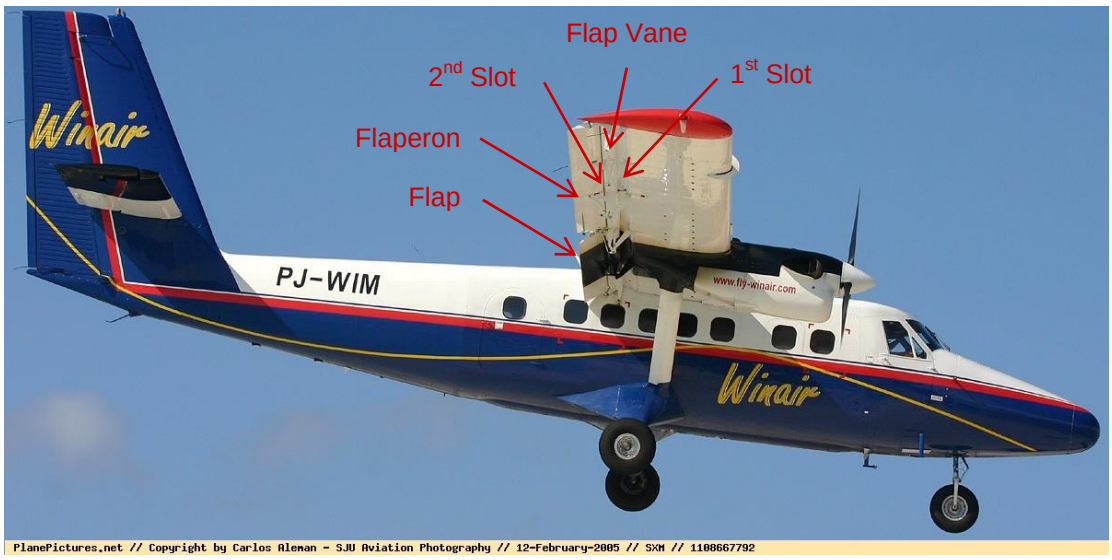

Figure 2.7 Twin Otter landing configuration (final approach, St. Maarten, D.W.I.)

Figure 2.8 Twin Otter landing configuration
(steep angle approach into St. Barts, F.W.I., real!)

Although dating back from the sixties this flaperon system might prove to be path breaking for future developments, where such systems extending over the whole wingspan will probably play a major role.

ATR aircraft have a similar but simpler system where the whole flap pivots around a specified line under the wing; the fairings thus seem to ‘spread’. This system was also successfully applied on large aircraft by McDonnell Douglas.

Figure 2.9 ATR42 landing configuration

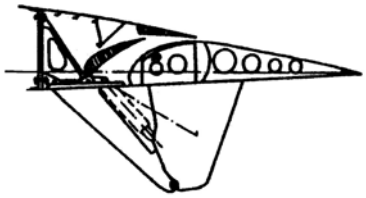

Figure 2.10 Flap track with fixed pivot point, from [4]

2.2.3 The Boeing Approach

Boeing is known to screw highly complex flap track mechanisms onto their aircraft. They are admirable engineering work and very compact especially in the flaps up position, keeping ‘useless drag’ at a minimum. High maintenance expenditure due to many joints and parts are some disadvantages, however. Most Boeing aircraft have double slotted flaps, at least for the inner flaps. The basic principle is a slotted fowler flap (i.e. first increasing wing surface, then tilting the flap), with the second slot opening in landing configuration by moving the tab. The flaps are moved by a rotary actuator which transmits a yaw motion from a central command unit. This actuator extends almost throughout the wing span and needs to withstand all wing movements including oscillations due to turbulence, besides a relatively high bias torque.

Figure 2.11 Boeing 767-300 taking off (at Amsterdam-Schipol, Netherlands)

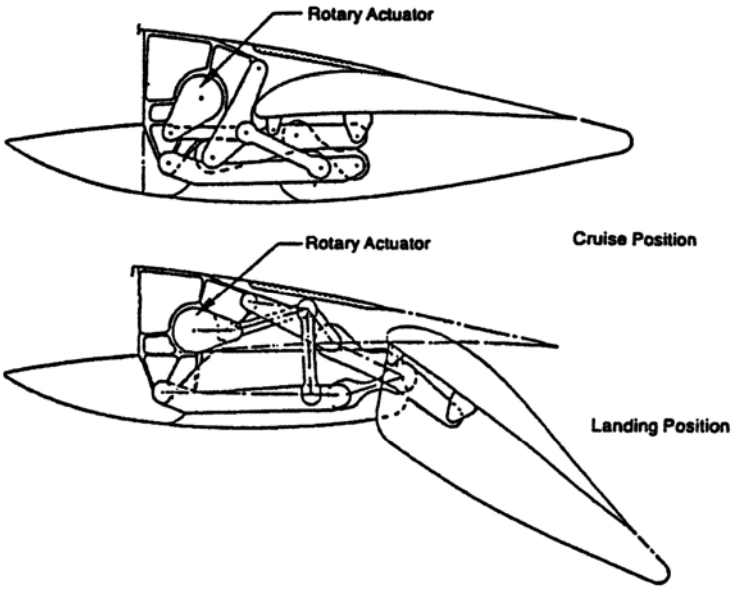

Figure 2.12 B767 outer flaps (single-slotted), from [4]

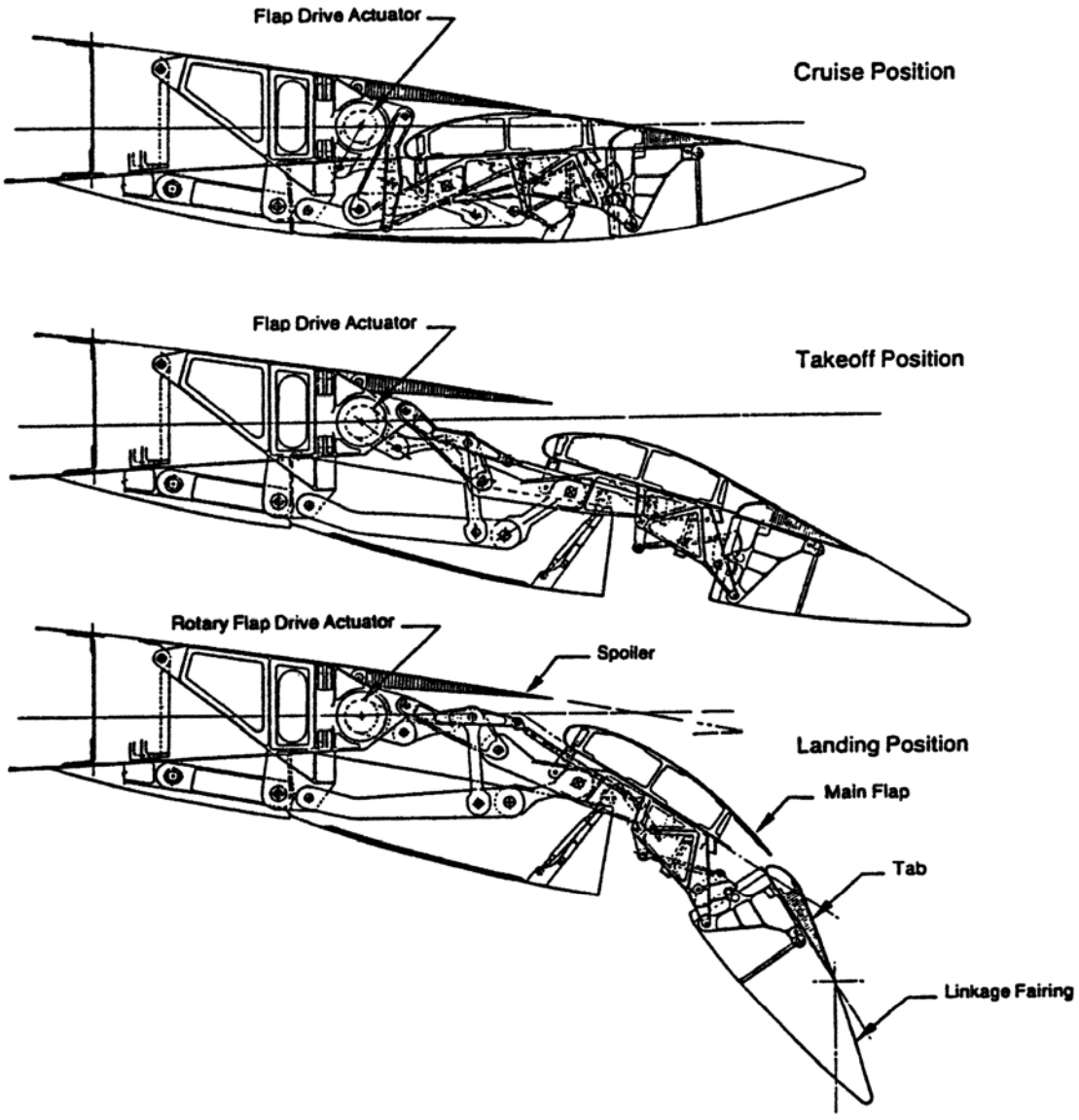

Figure 2.13 B767 inner flaps (double-slotted for landing), from [4]

2.2.4 What Airbus Did

Unlike Boeing, Airbus used robust and rather big guide tracks in their early models. They work well, but their fairings are more voluminous than those of Boeing, since there is no ‘folding and stowing’ of the mechanism.

The flaps were mainly double-slotted and moved by a system of rotating shafts and translating ball screw link actuators. They allow accurate positioning, are relatively light and very efficient, but due to high rotation rates of the parts there is a need for high quality bearings as well as intensive lubrication.

Figure 2.14 Airbus A300 (at Male, Maldives)

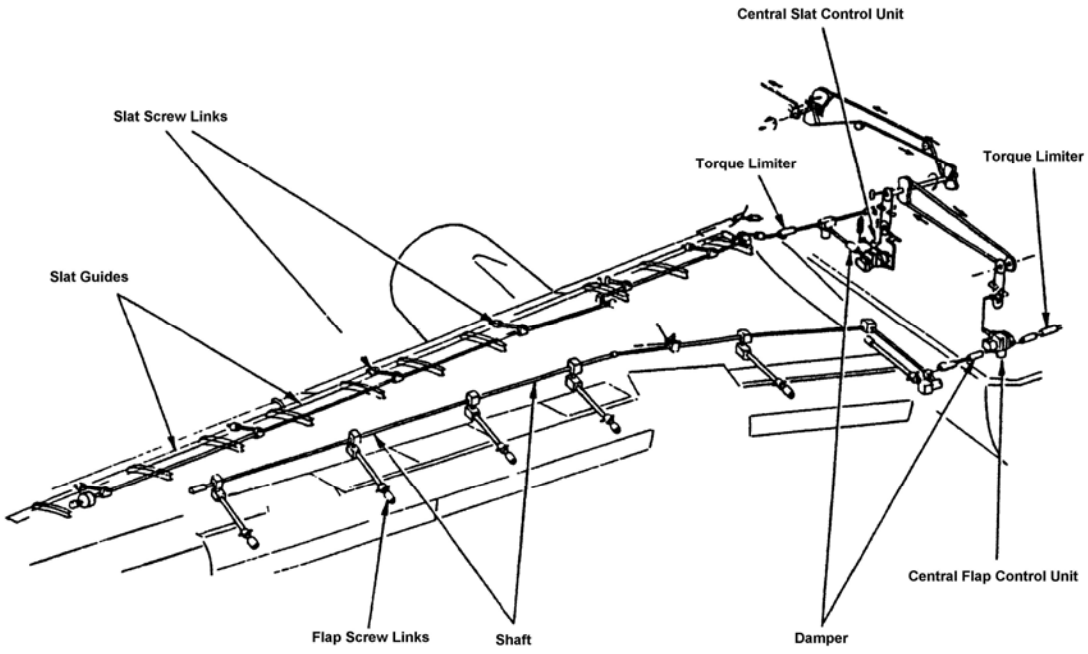

Figure 2.15 A300 flap/slat control through shafts, from [4]

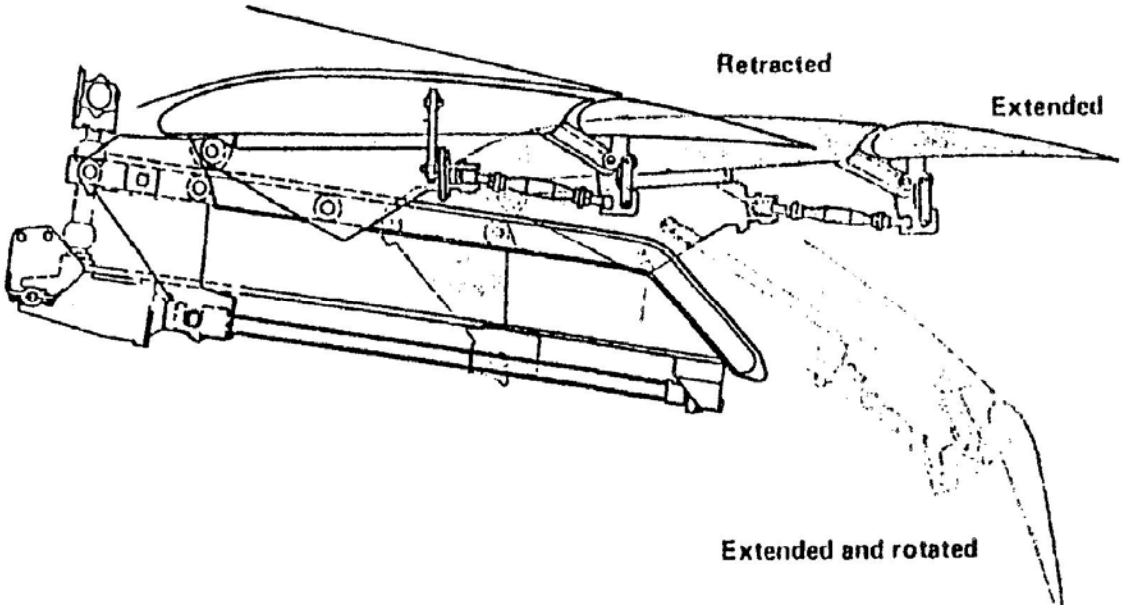

Figure 2.16 A300 flap track and operation, from [4]

Figure 2.17 A300 flap track structural part (made from one raw material block)

Figure 2.18 A300 flap track assembly

More recent Airbus aircraft feature a slightly different flap track system. Having a single-slotted system, the A340 features a track/carriage system with a rear link; the whole is no longer operated by a translating ball screw link but by a hinged type actuator which makes a yaw motion of about 120°. The A330 flap tracks are identical to those of the A340, and the A320 family uses the same concept too.

Figure 2.19 A340-300 (at Zurich, Switzerland)

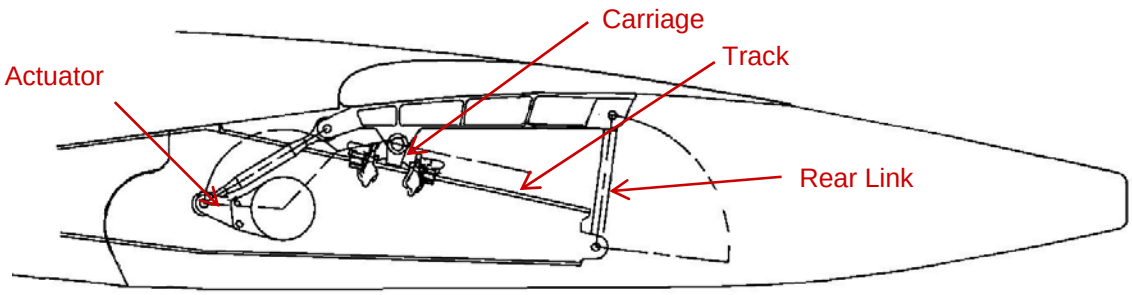

Figure 2.20 A340 flap track, according to [13]

The newest product of Airbus, the A380, goes without any carriage but uses a pure linkage system which keeps maintenance at a minimum. Unlike the A340, the outermost fairing (i.e. the pylon fairing) is a flap track fairing at the same time (see figure 2.23). This efficient combination is not new, as will be shown in the next chapter.

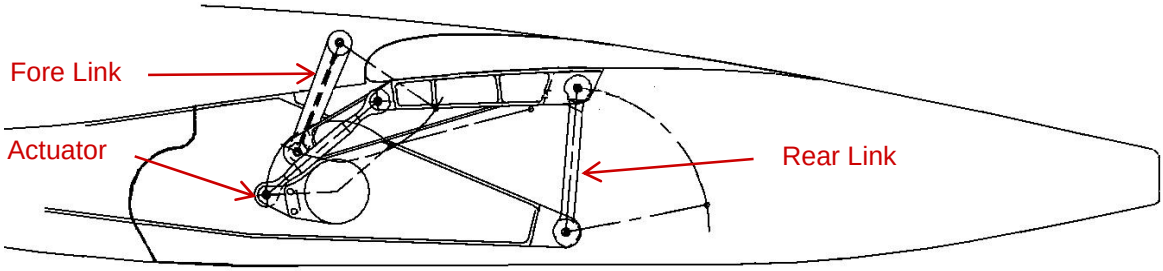

Figure 2.21 A380 flap track (not drawn to scale with Figure 2.20!), according to [13]

Figure 2.22 A380-800 roll-out

Figure 2.23 A380-800 wing view

2.2.5 The British Aerospace Brainstorm

British Aerospace use an innovative flap track fairing approach on their BAE146/AVRO series originate back from the 1970s. Two of three main fairings are integrated in the (inevitable) engine pylon, as shown in figures 2.25 and 2.26, thus avoiding additional drag. The flap tracks themselves are carriage type.

Figure 2.24 BAE146-200 (at Salines Intl Airport, Grenada, W.I.)

However, as seen in figure 2.25, the 'useless drag' problem remains for the third flap track fairing as well as the fairings of small tab controls (which open a second slot in landing position).

This flap-pylon double fairing works well with this specific high-wing aircraft configuration. It allows plenty of engine nacelle ground clearance even though these are mounted quite low with respect to the wing, keeping the flap and particularly the fairing off the hot exhaust blast also in landing configuration. With other standard low-wing configurations this double fairing is usually not feasible because of exhaust blast interference. Exceptions are aircraft with very high engine bypass ratio, i.e. a small hot blast (see A380). With conventional aircraft an inner aileron could be placed there instead of a flap; small tab parts kept off the blast have also been investigated (see chapter 2.3.3).

Figure 2.25 BAE146 flap track fairings

Figure 2.26 BAE146 flaps — up/takeoff/landing configurations

2.3 Future Trends

2.3.1 As Simple as Possible

As seen with the evolvement of Airbus flap tracks simple systems are used nowadays. Single-slotted systems prevail, and their disadvantages (when compared to more complicated systems) are compensated for by the simpleness and maintenance savings.

This is done even though this entails rather big flap tracks, leaving most of the voluminous fairing 'empty' and drag-producing.

In [1], P. K. Rudolph writes: 'In the field of high-lift systems, Airbus has done extremely well and has four airplane models flying with single-slotted flaps that provide adequate maximum lift, airplane attitude and very good takeoff L/D. Many experts in the field believe that Airbus has actually overtaken Boeing in several airplane technologies, especially in high lift.'

However, given actual and future concerns on fuel efficiency and environmental friendliness as well as the fact that current airplane concepts are thought to be exhausted, any improvement possible should be thoroughly investigated. The question whether integrated flap tracks are feasible is therefore a useful one, even though such a system will most probably come up more complex.

2.3.2 Non-mechanical Flap Synchronization

As outlined in chapter 2.1, FAR/JAR 25.701(a) require the synchronization of flap surfaces on both sides. While a mechanical link is suggested other possibilities to ensure symmetric flap deployment are currently investigated, since the regulation makes provision for 'approved equivalent means.' With the background of future 'all-electric planes,' electronic control is a useful approach. However, as with any critical system in the aircraft, failure probability must be demonstrated to be 10^{-9}.

2.3.3 Adaptive Wing Approach, Multifunctional Wing

As mentioned in chapter 2.2.2 efficient flaperon systems are expected to play a major role in the future. Among other reasons a high lift/drag ratio with high drag enables an aircraft to descend steeper than the present 3° on final approach which is very desirable from a noise point of view.

On current aircraft the lift distribution is usually far from the most drag-efficient ideal one. This is partly due to the engine pylons: since there are often no flaps and/or slats at these locations no additional lift is produced there when flaps are extended (see figure 2.27). Further, there is no additional lift at the ailerons, although they are sometimes used as flaperons.

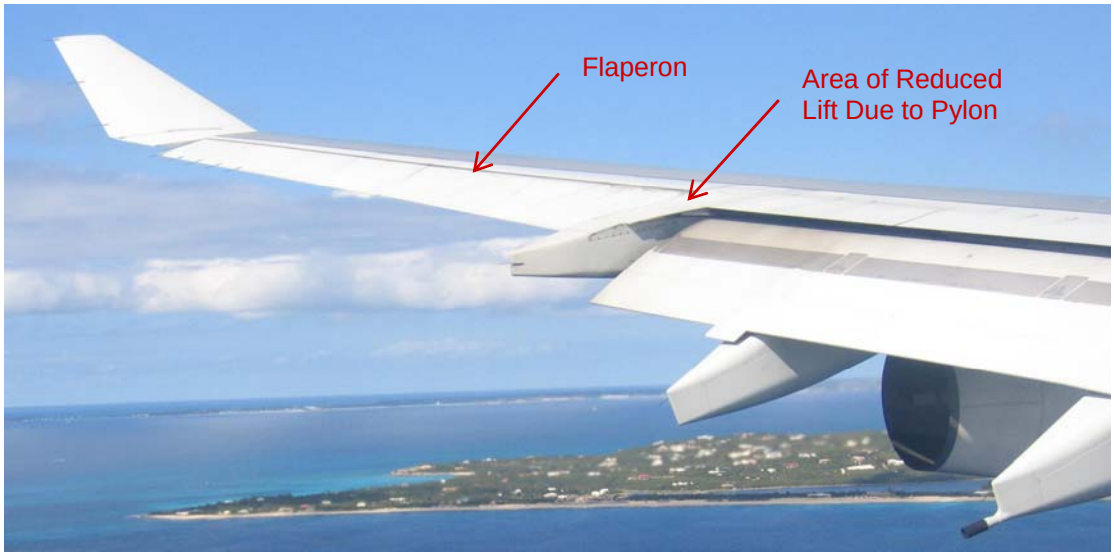

Figure 2.27 A340-300 outer wing in landing configuration
(on final approach to RWY09, St. Maarten, D.W.I.)

For these reasons current research looks into the possibility of extending the spoiler and flap system up to the wingtip, combined with a differentially controllable tab system at full span of the trailing edge. This would allow to generate an almost ideal lift distribution, high drag where needed (i.e. for a steep final approach), while avoidance of engine blast is possible by appropriate tab control at these locations. Besides, it allows very efficient gust load and roll control. Despite of more complexity its high flexibility also makes it an interesting candidate for aircraft families.

This kind of first-generation adaptive wing with its multifunctional flap system was introduced in a similar way with the Twin Otter in the sixties and seems to be successfully on line for larger aircraft.

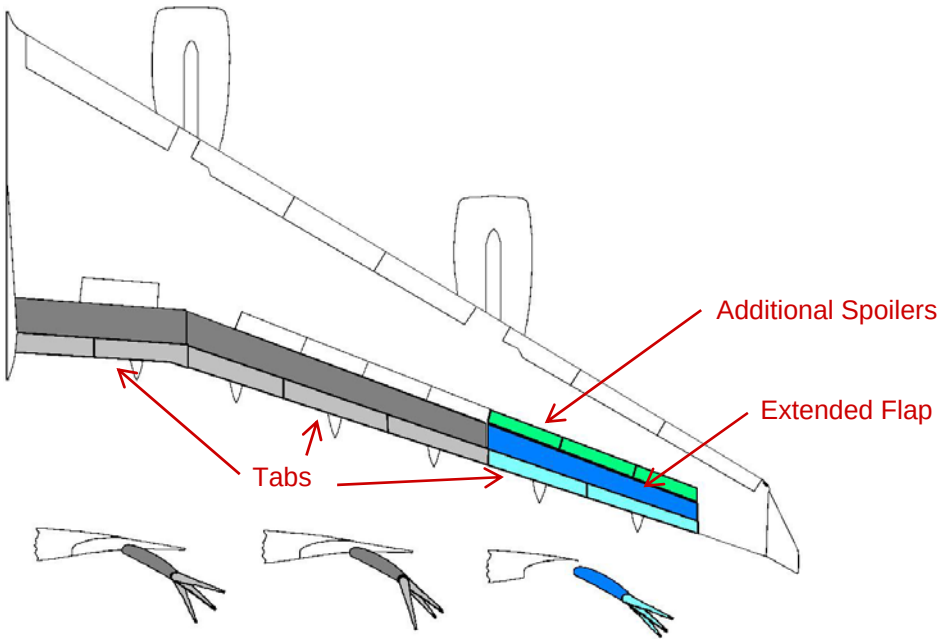

Figure 2.28 Future multifunctional flap system, according to [12]

Chapter 3

Design Approaches for Integrated Flap Tracks

3.1 Design Premises

3.1.1 The Standard Package

There are three basic design concepts which prevail in aerospace design:

- **Safe-life:**
  part/system is designed such that no catastrophic failure can occur during the full service life (i.e. flight hours or cycles). Example: nose gear

- **Fail-safe:**
  redundant load paths exist, of which each is able to bear the full load should one path break down completely. Example: at least two main wing spars where one can bear the full load

- **Damage-tolerant:**
  damages such as cracks may be tolerated to a certain length and are not relevant to flight safety, but it must be insured they do not grow to a hazardous extent and are detected at the latest at the next routine inspection. Example: various parts with notches due to rivets

It is apparent that the safe-life method leads to rather heavy parts since they must withstand particularly dynamic loads. Further, expensive high-strength materials would be used for such components, partly again for weight reasons.

Fail-safe layout, on the other hand, comes up with lighter single structures. However, since there are at least two load paths, the weight advantage is somewhat relativized. But these at least two structures can be arranged in such a way that a new function can be achieved (such as both spars used as the bordering elements of the main wing integral tank, or a symmetric load distribution). For these reasons fail-safe design is mainly applied in this project, but only where it is reasonable from a technical point of view.

3.1.2 Other Premises for this Project

As explained in chapter 2.3 adaptive multifunctional wings will probably become more important in the future, therefore the integration of the pertaining mechanisms will be of interest. Single-slotted flap systems prevail now and are mainly considered in this project, but the integration of at least one additional slot will be investigated since the tab acts again as a camber flap on the flap body itself which may cause

stalling if there is no boundary layer regeneration. Further, mechanical flap panel synchronization is not of primary concern since efforts are undertaken to achieve this by other means.

All of this likely entails a more complicated system than current developments, but given the benefits as anticipated in chapter 1.2 this might still be worth a try.

3.2 Component Concepts

In the following figures the arrows have the following meaning:

→ indicates a motion

→ pointer for explanations

3.2.1 Guides

As seen in chapter 2 the actual flap motion and force transmission may be accomplished by guides or by linkages. Again, a closer look back gives a hint on how integrated flap tracks could be built. Slat tracks have always been integrated, and as can be seen in figure 3.1 below this is accomplished using a combination of translating track supports, fixed programming cams and actuators (rotary actuator in this case).

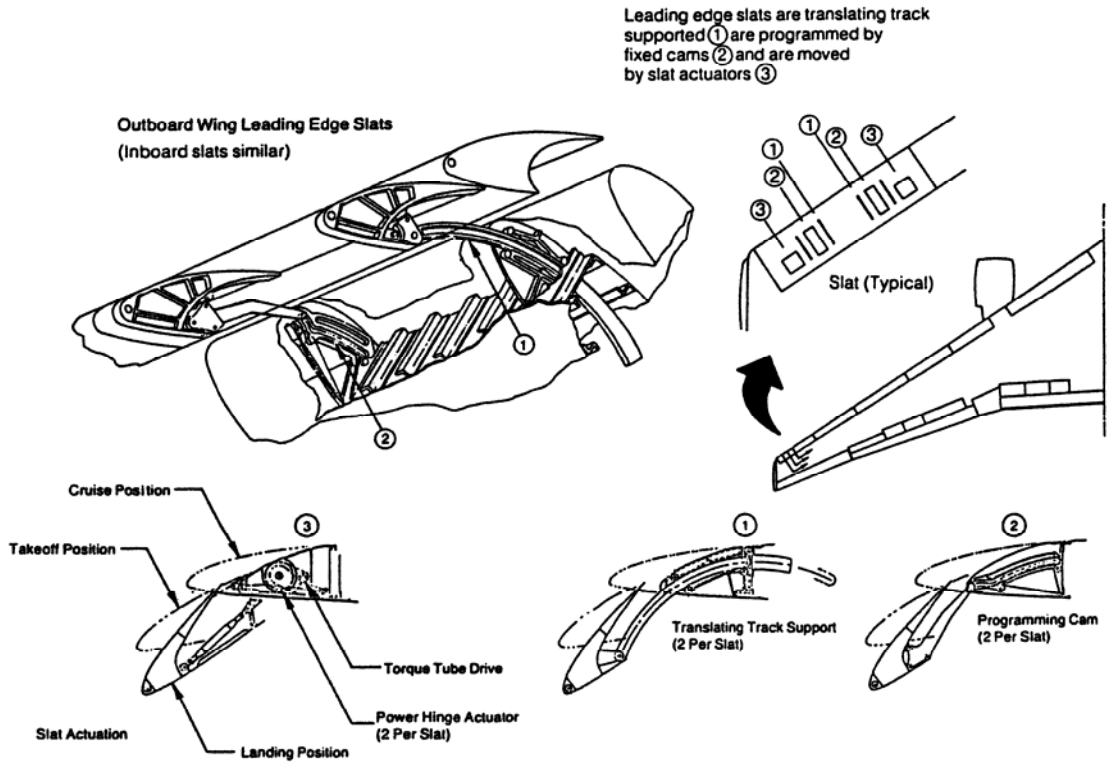

Figure 3.1 B767 wing leading edge slats, from [4]

These components are usable for trailing edge devices too. However, the translating track should not intrude the spars if possible due to structure and integral tank sealing problems.

There are several kinds of translating tracks already developed; most of them have in common that they use open profiles only. While this is not ideal from a structural design point of view one needs to bear in mind that all parts in an aircraft must be visitable by eye and (semi-)optical tools, and should not trap any moisture because of corrosion problems. This point, however, might become less important through the use of composite materials.

The detailed design of guides and bearings is done later in a detailed construction. But, as a possibility, if a standard I-type beam is used as a translating track (slider) then guides/supports with rolls could look as follows:

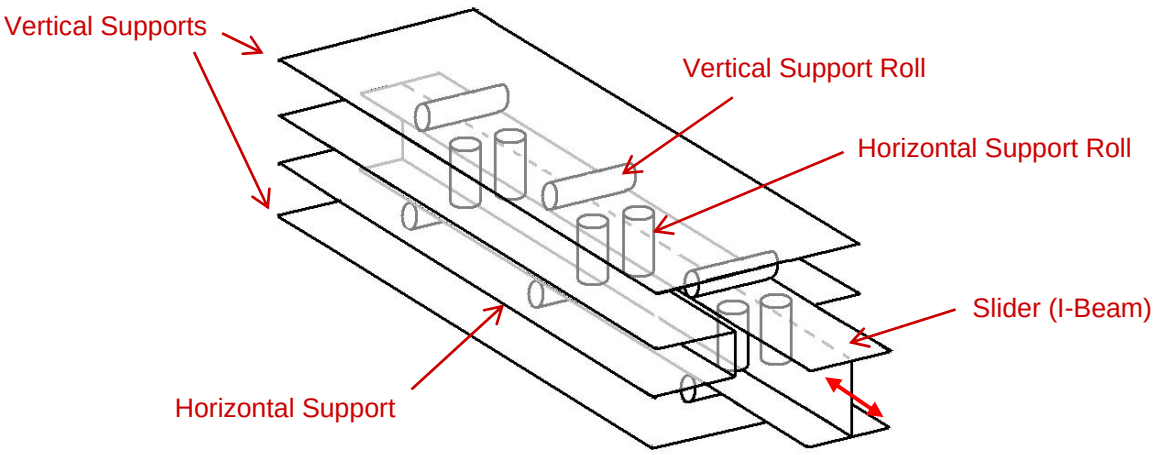

Figure 3.2 I-beam translating track supported by rolls

Of course the rolls should not ‘float’ freely. They could either be fixed to the slider, which would be a useful method for the horizontal support rolls, or they could be placed in cavities in the supports as shown below.

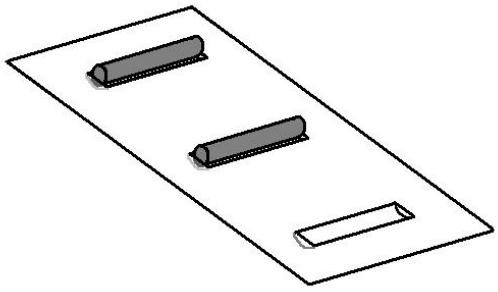

Figure 3.3 Simple roll bearings

It is desired that there be only one actuator on each flap track, with any necessary differential translating track movements directly linked to it. Besides simplification this would ensure exactly the same expected movement at each flap deployment, which may not be absolutely guaranteed with actuators on each translating track.

This can be achieved by the use of programming cams, as shown in figure 3.4 below. At least two slider links are needed, with a bolt at their connection sliding along the cam and thus lengthening or shortening the distance between the two slider parts (d, blue in the figure) as required. This distance depends on the programming cam shape, which must be a specific mathematical curve chosen appropriately in order to generate a desired overall slider motion as shown in the plot on the right side of figure 3.4.

For stability reasons (too high forces acting on link/cam etc) the angles in the linkage should be kept small, not much more than shown in the figure. Therefore, with only two links the spectrum of distance shortening/lengthening is rather limited. It could be increased by using more than two links folding up in a zigzag scheme, but this could again lead to some stability problems and complexity.

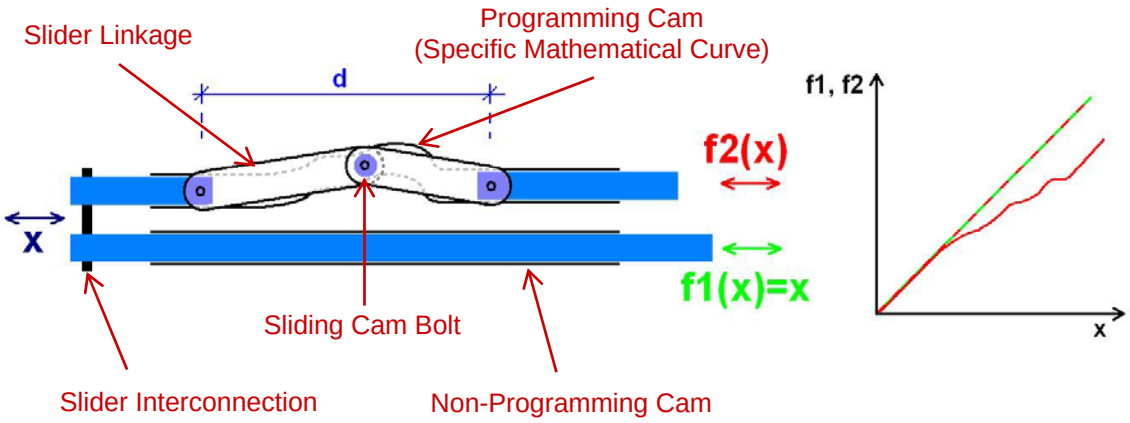

Figure 3.4 Effect of programming cam

3.2.2 Actuation

There are many system components (going to the outer wing) located right behind the rear spar, so there is very limited space to pack any additional mechanisms into it. Rotary actuators economize space as seen with the B767 (see figures 2.12 and 2.13), but as described they may have a weight problem due to high loads. Similar considerations apply to hinged type actuators as used in Airbus aircraft.

Screws with jacks are more lightweight actuators, with a very high power to weight ratio. This would make them attractive for lightweight structures and systems. However, as seen in the A300 example, they need relatively much longitudinal space, which is very limited and precious for an integrated flap track mechanism. Therefore, the following arrangement has been conceived for this project.

Since there is usually enough space in the lateral direction of a wing for parts like a thin rotary actuator or a screw, such a screw could be mounted laterally behind the rear spar. By means of an appropriate linkage system effective slider control is achieved while keeping longitudinal space consumption at a minimum.

Figure 3.5 below shows the complete fail-safe design of the actuation system. Since the two main sliders are directly interconnected mechanically (not only in the attached flap), this symmetric approach minimizes slider bending and lateral loads on the main guide track. However, for fail-safe design reasons each side must be able to bear the full load in the event of any failure, including lateral loads not encountered in normal operation (for example due to the failure of one main link, which leaves a lateral force on the guide tracks). The two auxiliary sliders may also be connected mechanically, at least in the flap body itself. With this design it is ensured that any part can break without the whole system failing or even loosening of the flap assembly.

In the actual construction attention needs to be paid to extra loads on the screw due to wing bending and possibilities to avoid bending of the screw. The screw itself comes in two physically separate parts (one for each side), but both being interconnected in the drive unit. Flap loads in longitudinal direction would still have a significant impact on the screw by inducing a bending loading case. A detailed construction would need to minimize this screw bending by absorbing longitudinal flap loads for example in a separate screw jack guide, leaving only the actual screw moving load in its longitudinal direction.

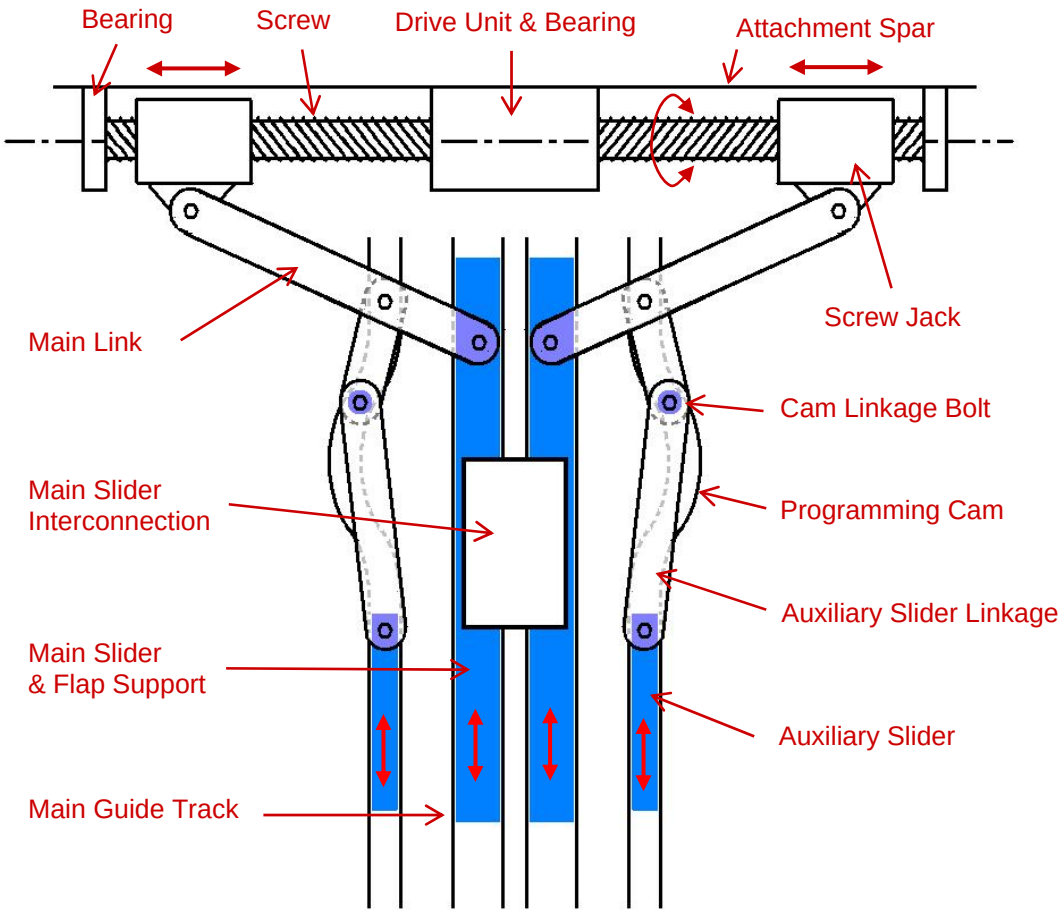

Figure 3.5 Fail-safe symmetric ball screw actuation concept

As mechanical flap panel synchronization is no longer an absolute must, an electric motor could be considered at each flap track drive unit; the screw or any connected driving parts do not need to extend over the whole wingspan, which allows them to have just the length needed to fulfill the purpose of moving the jack.

Still, there are significant problems with this symmetric fail-safe approach. Some of them are due to relatively high forces occurring on the main links and screws near the flaps up position. To reduce these forces the angle between the screw's axis and the main sliders should be as wide as possible, but this entails a rather long system (measured in the plane's longitudinal direction). The space needed may not be available especially with highly packed integrated flap tracks.

Another problem arises because the attachment spar (in most cases this would be the rear spar of the wing's torque box) must be perpendicular to the slider actuation direction. On most commercial aircraft this is only the case for the inner flaps, where a secondary spar behind the main gear well (see figure 3.6) is indeed almost perpendicular.

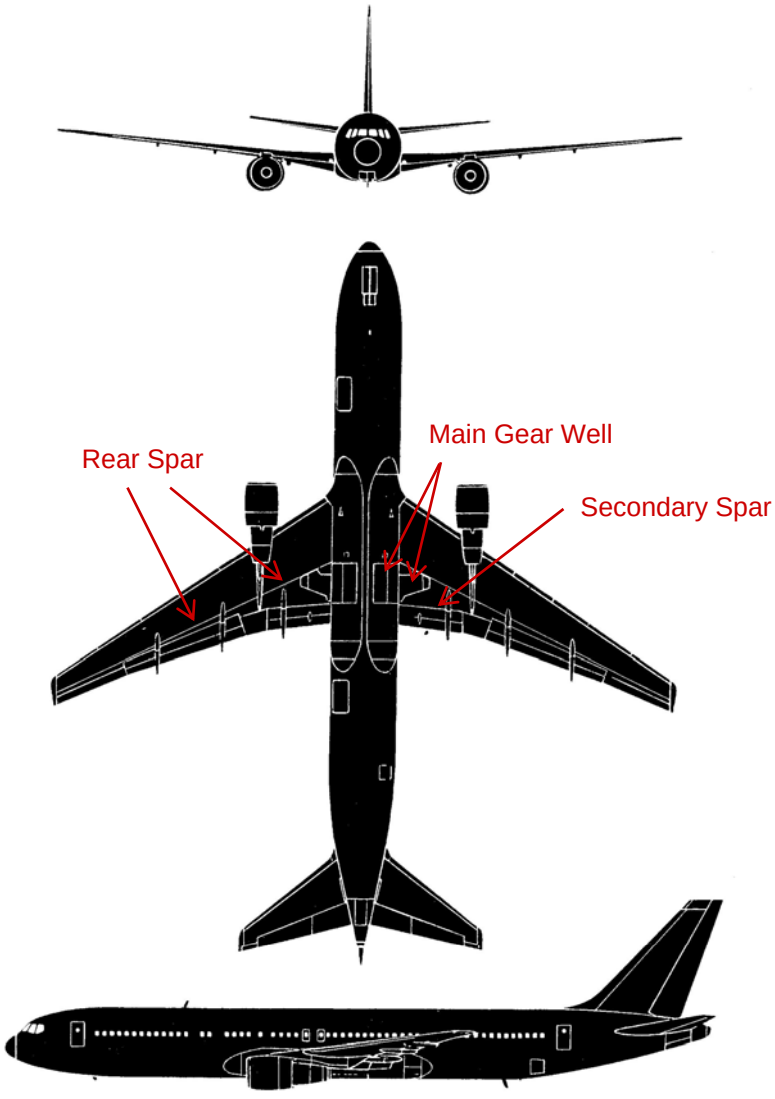

Figure 3.6 B767 views, from [5]

For the outer flaps the above symmetric concept would not work since the rear spar to which the whole system needs to be attached to is not perpendicular, and the flaps must be deployed parallel to the flight direction. The following mechanism may be useful in this case.

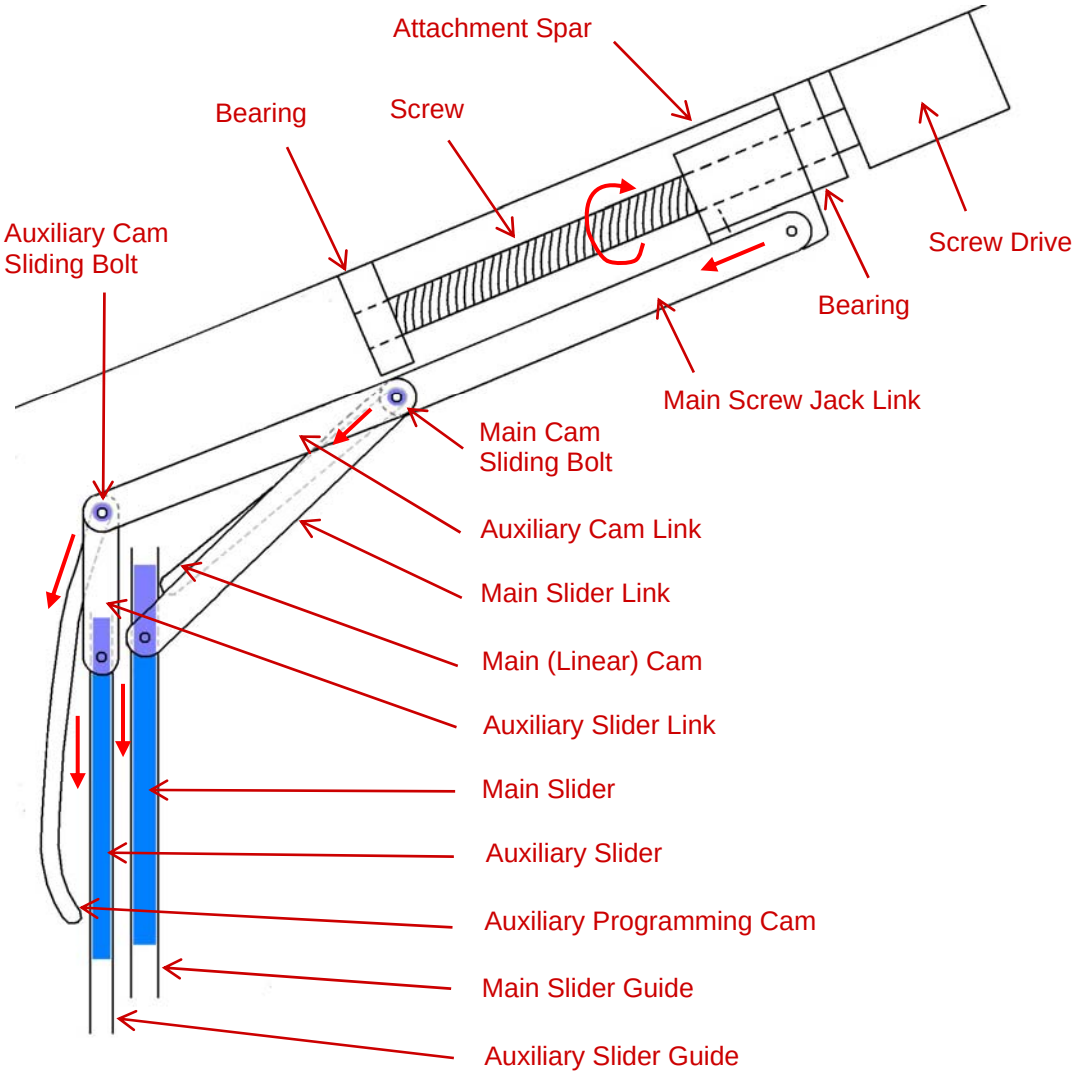

Figure 3.7 Non-perpendicular spar ball screw actuation concept

With the dimensions shown it is ensured that no sliding bolt goes into a locking position (i.e. pushing 90° to a cam border etc), and lateral force on the screw is kept small: most of the force in the slider's moving direction is absorbed in the main cam. The main cam is shown linear in the figure above, but could also be shaped to meet specific requirements.

As opposed to a system with perpendicular spar, this system comes up with another problem: As shown below the screw rotary axis and the slider hinge line are no longer parallel. Therefore the main link attachment plane on the screw jack needs to tilt via another joint to become parallel to the slider plane.

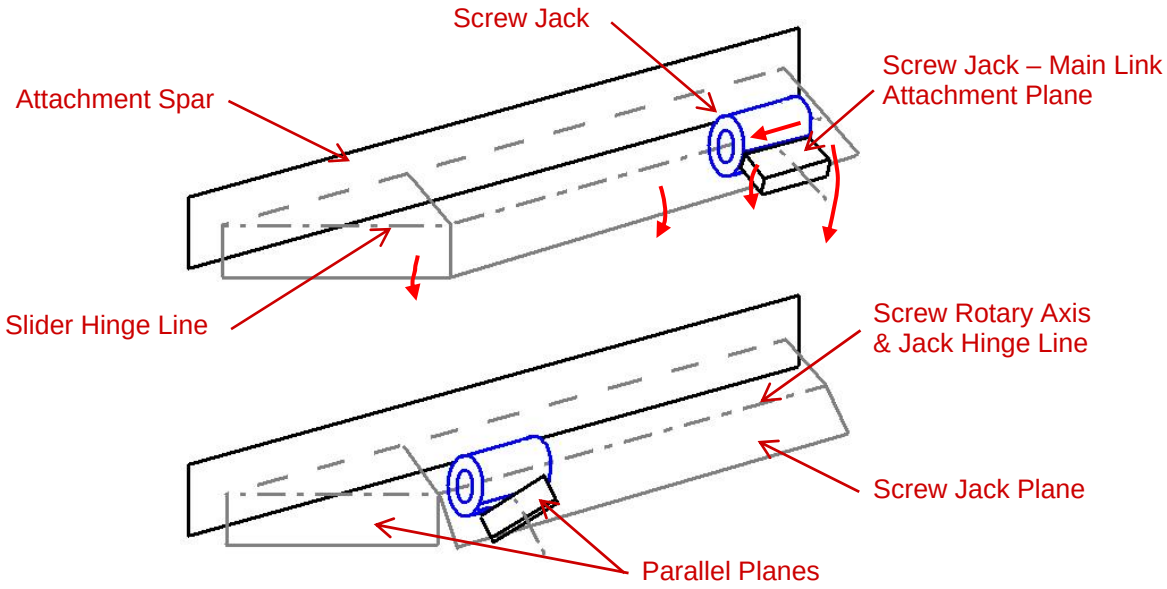

Figure 3.8 Hinged screw jack main link attachment

A symmetric fail-safe approach as shown in figure 3.5 is not possible here; simply putting another screw on the other side would not work since acute angles would occur between the links, which would entail high forces if not making a smooth sliding bolt motion impossible. Therefore a fail-safe design is achieved by simply doubling the elements and glueing them, with each part of these doubled elements being able to bear the full load. As the only part the screw needs to be designed safe-life.

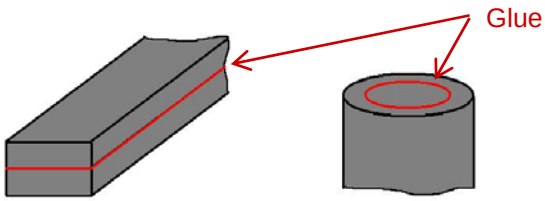

Figure 3.9 Fail-safe link/slider and bolt

3.2.3 Flap Angle Control

Besides just moving the flap back- and downwards its angle must be appropriately set at each position. Therefore the following simple control method is found to be suitable.

At every wing profile there is a center of pressure (similar to aerodynamic center), a specific point at which the resultant aerodynamic force acts. This point is located between about 25% and 35% of the chord line, dependent on the incidence angle of the airflow. Since there is no moment about this point it is advisable to attach the main flap support at this location in order to minimize loads on other supports.

These other supports control the angle of the flap by means of a linkage as shown in figure 3.10 below. The attachment/pivot point at the flap must be located a bit up such that the linkage never attains an angle of 180°, since this could block the mechanism. The precise motion of this auxiliary flap control and linkage can be achieved by programming cams as described in chapter 3.2.1. Note that only a rather small relative motion is needed between auxiliary and main slider (as indicated by the arrow on the slider in the figure below) to achieve a considerable flap angle.

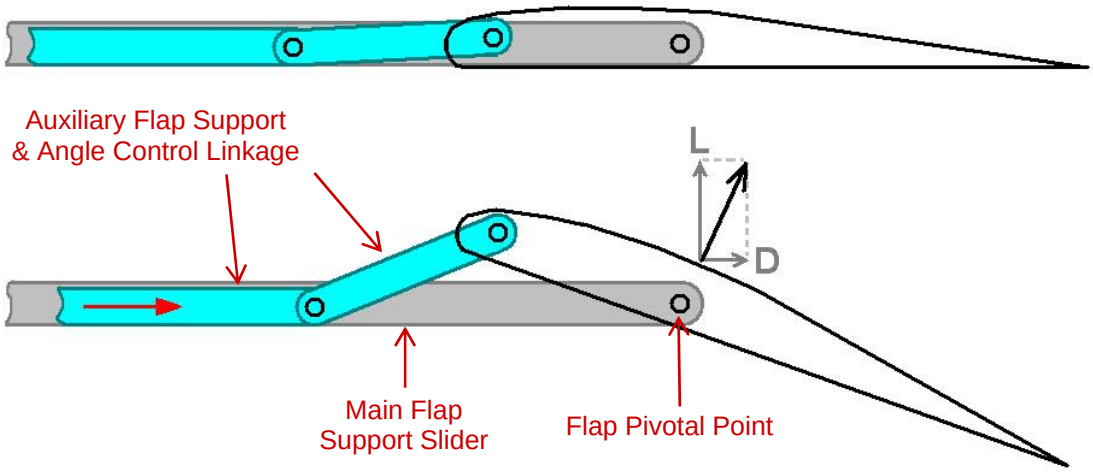

Figure 3.10 Flap angle control concept

This approach means that standard lightweight structure design with shells and stringers cannot be applied throughout the span of the flap body, since other than with conventional approaches this integrated track automatically entails a cut in a standard lightweight structure, at least where the supports are located. This will be an issue to be addressed in the detailed construction.

3.2.4 Main Flap Support Angle Control

The flap including its supports also needs to move downwards. There are some force transmission issues too: as shown in figure 2.12 (B767 outer flaps) these loads are absorbed in a main suspension element (containing a bearing for the rotary actuator) attached to the rear spar. The loads from the flaps pass into both the top and bottom of this element, which allows transmission of the moment (due to flap load) while the forces at the spar remain as small as possible with the dimensions at hand.

This basically two-point bearing force absorption approach is also necessary for an integrated flap track to keep bearing loads small. This can be accomplished together with a support angle control mechanism as shown on the next page. With this linkage design the linkage slider load decreases with flap extension, even though the actual flap loads increase considerably: the main force flow passes through the two back links of the angle control linkage (i.e. suspension link and main slider angle link) and goes directly into the main suspension, with the linkage slider and the angle control link only having a supporting function.

Again to avoid blockage of the mechanism no angle should ever attain 180°. The angles as shown below allow an appropriate linkage positioning. Note: due to flap weight the support would move automatically downwards even if some links attain 180°. However, this is true for ground operation only. In flight conditions are conceivable where aerodynamic forces exactly balance the flap's weight, thus the 'bended links' approach is still necessary here.

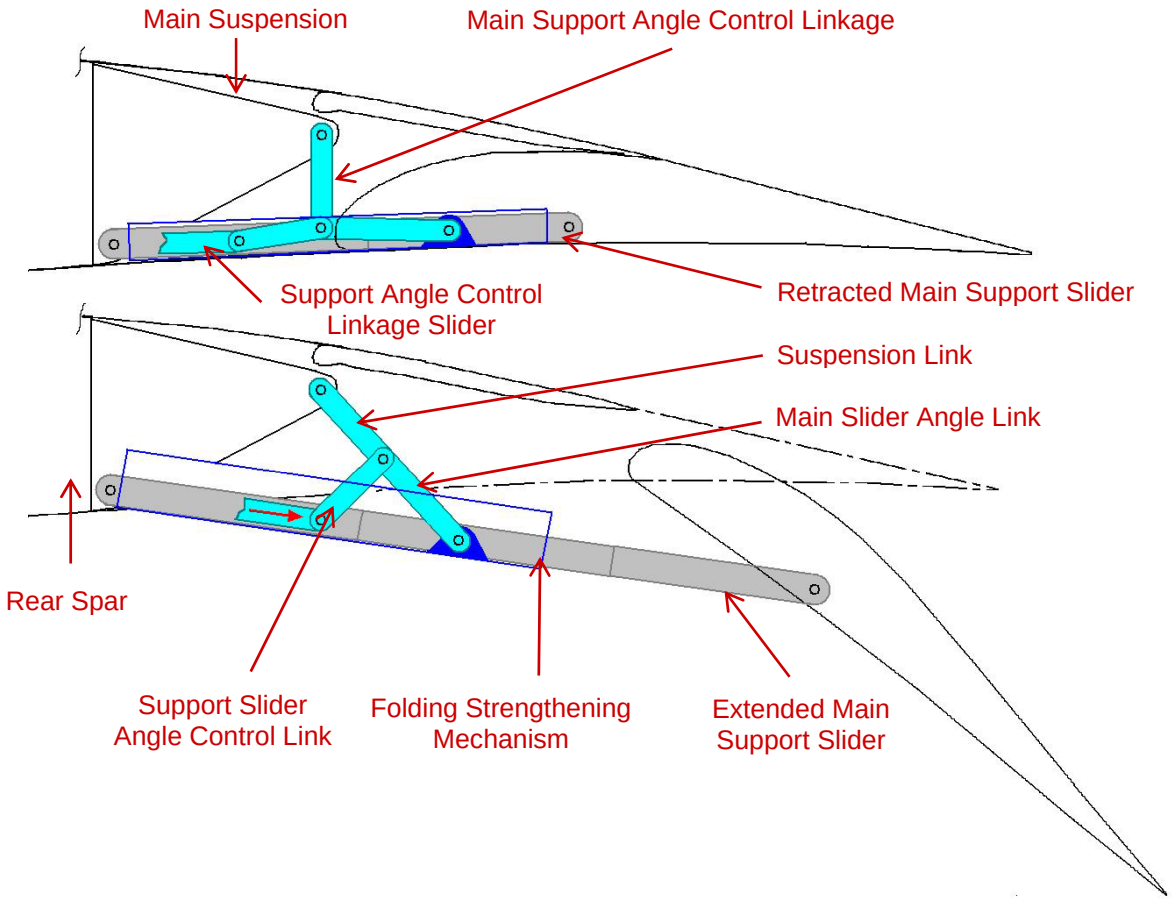

Figure 3.11 Flap downward motion control concept

With the geometric dimensions shown in figure 3.11 above, already a very small angle control linkage slider actuation in the flaps up position would lead to a significant downward motion of to main support slider. While this may be desired for some aerodynamics premises it automatically entails a rather high force on the linkage slider near the flaps up position. In the actual construction this must be accounted for; a method of applying a 'locking device' attached to the main slider will be considered.

In the following figures of this subchapter (all top views) different flap settings are labeled accordingly for easier reference (seven settings for these examples, '0' corresponds to flaps fully retracted). The exact dimensions would need to be deduced from the aerodynamic requirements and the general mechanism proportions, which is to be done accurately in a detailed construction. Filled arrows indicate the respective flap extension motions.

The mechanism shown in figure 3.12 below both reduces loads on an actuator and allows accurate control of the support angle control linkage slider even when it moves only very little near the flaps up position. Magenta on the right side are support angle control linkage slider positions; on the bottom in red a perpendicular and basically linear ‘transformation and locking cam’ is shown. Green is a link A (in different positions) with one end attached to the slider and the other, sliding along the cam, is attached to an actuator (other link, leverage etc) basically pushing the link horizontally. As can be seen with the label positions this mechanism transforms the highly nonlinear motion of the slider into a more steady cam motion. This ‘linearization’ also applies to the forces encountered.

In the ‘0’ position this green link firmly locks the slider, since the link’s cam-sliding end pushes 90° towards the cam (which then absorbs the full load on the slider) and thus theoretically no horizontal actuator force is required; the actuator would have a supportive function. In the ‘6’ position the whole mechanism could not be moved back if the cam were fully linear (90°-pushing problem again, but now undesired). Therefore the cam is bent between position ‘5’ and ‘6’; i.e. the 90° angle is reduced to about 80°, which is enough since the actual forces on the slider between ‘5’ and ‘6’ are small, as the slider and its attached link only have a supporting function there; see also figure 3.11.

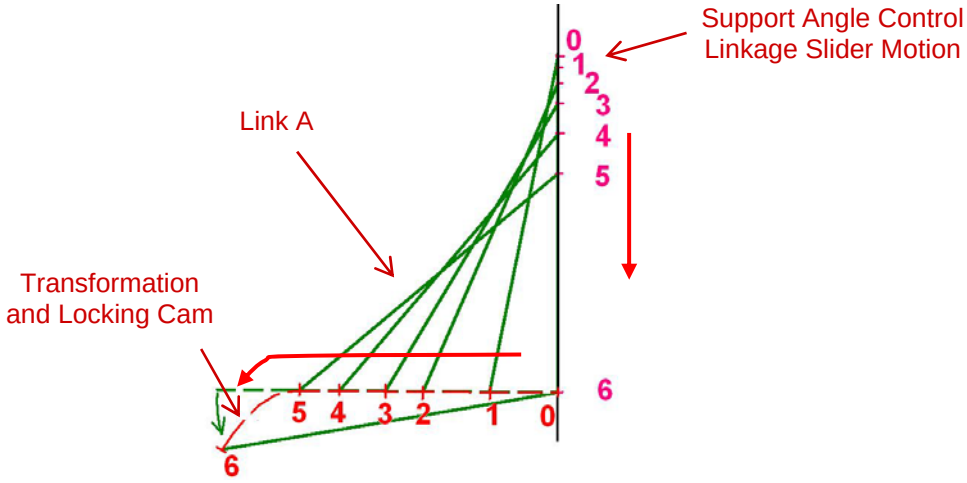

Figure 3.12 Transformation and locking cam

The guides for the sliders should all be mounted onto a single plate the bottom of which is identical to the aerodynamic wing strake in the flaps up position; this approach comes up with the least joints. All cams and the fixed pivot points shown in subsequent figures would also need to be attached to this mounting plate in order to avoid additional joints.

Basically the main slider motion must be converted to a desired support angle control linkage slider, as shown in figure 3.13 on the next page. The main slider motion is introduced to this mechanism by a fixed appendage which moves exactly in parallel to the main slider (see also figure 3.25 on page 43).

As displayed in figure 3.13 the main slider moves only little between ‘5’ and ‘6’ when compared to the other positions. This is due to aerodynamic requirements: in the last stage of flap deployment, the flap does basically not move backwards but more downwards (therefore the support angle control linkage slider moves a long way between ‘5’ and ‘6’) while increasing its angle of attack considerably at the same time.

Again to ‘linearize’ the main slider motion a link C is attached to both the main slider appendage and the (only rotating) lever B. This is achieved successfully, as can be seen in with the different label positions.

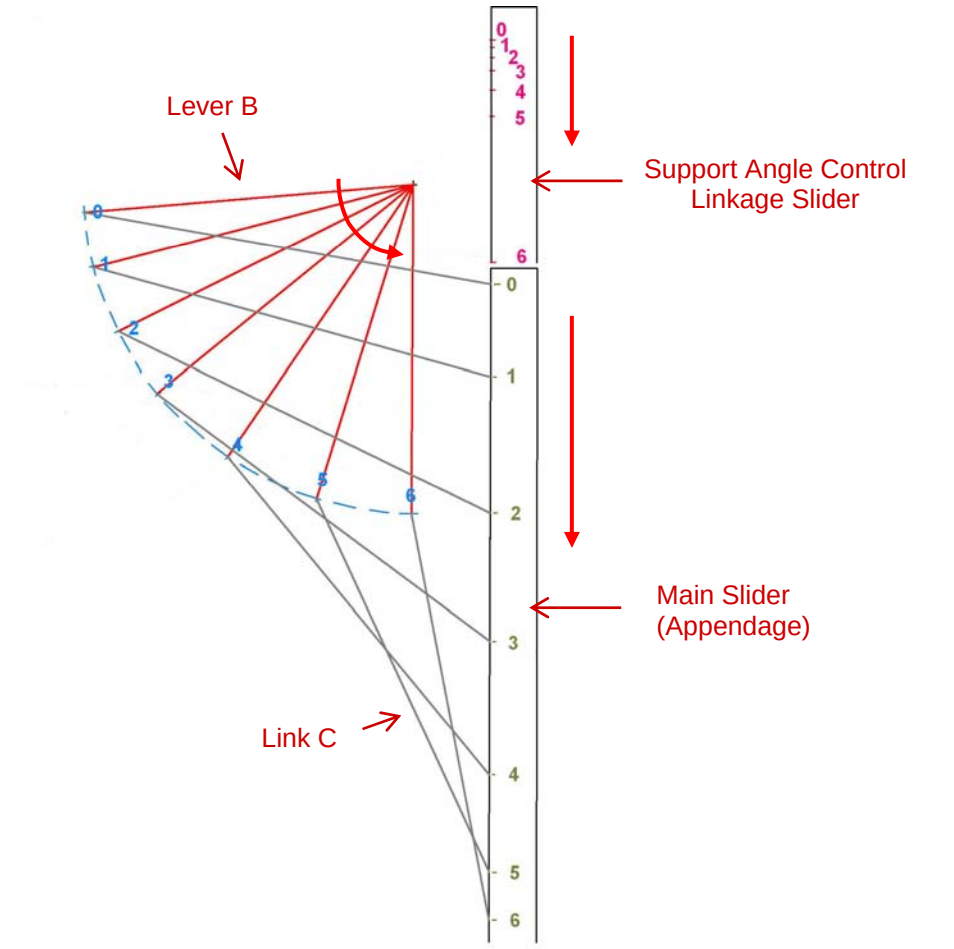

Figure 3.13 Main slider motion transformation mechanism

Now this rotation of lever B needs to be transformed into a more linear motion of link A. This cannot be done by a single link as the motions are basically opposite to each other, and neither do they have exactly the same subdivision proportions for the different settings. Therefore introducing another programming cam is appropriate here and is done using the following mechanism.

Link D is attached at about the middle of Lever B, and also fixed to a triangle-shaped lever E. Lever E, which basically inverts the motion of lever B, is attached to link A via the links F and G, with the bolt connecting F and G sliding along a programming cam. The bolt connecting G and A slides along the transformation and locking cam.

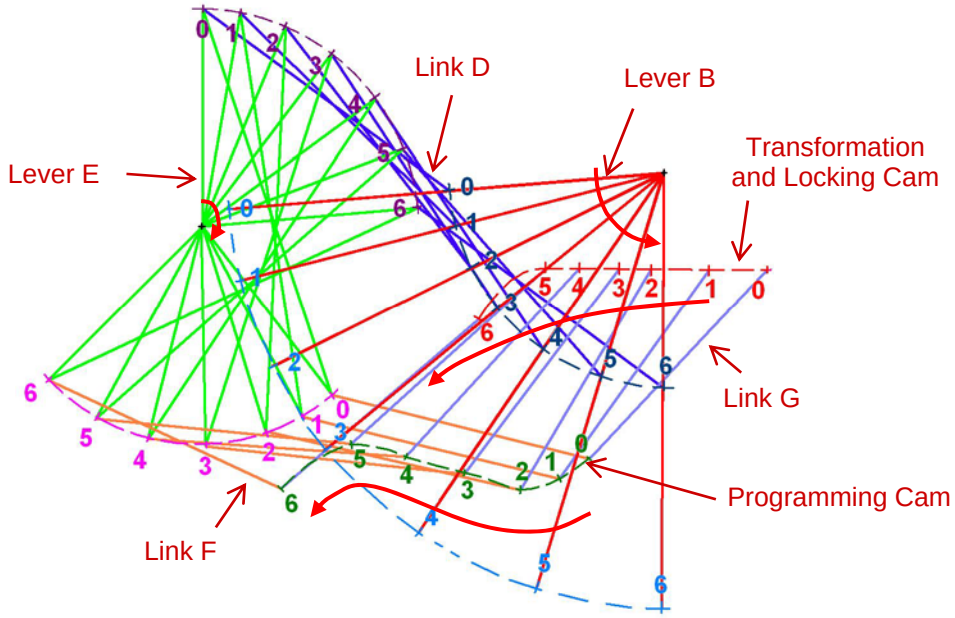

Figure 3.14 Motion inversion and programming cam

Although this mechanism is rather complicated no other means was found to fulfill requirements of exact slider control, small element loads, no blockage (90°/180° situations), plus fitting into the very limited space available in the retracted position.

The following figures show the mechanism with drawn elements in retracted and extended position (cams are still displayed schematically).

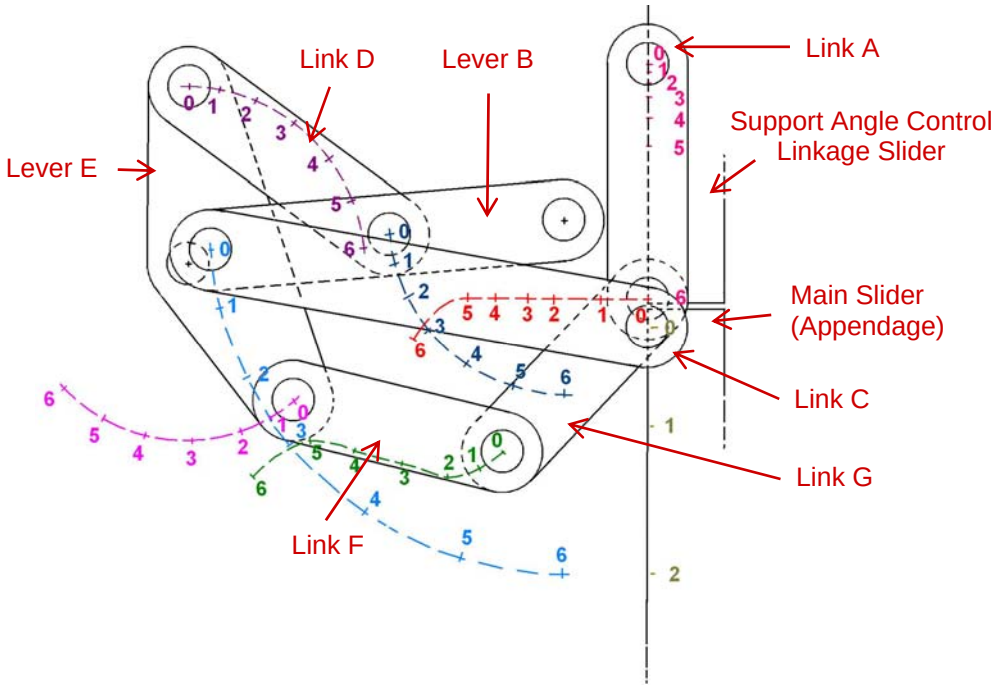

Figure 3.15 Transformation and locking mechanism — retracted position

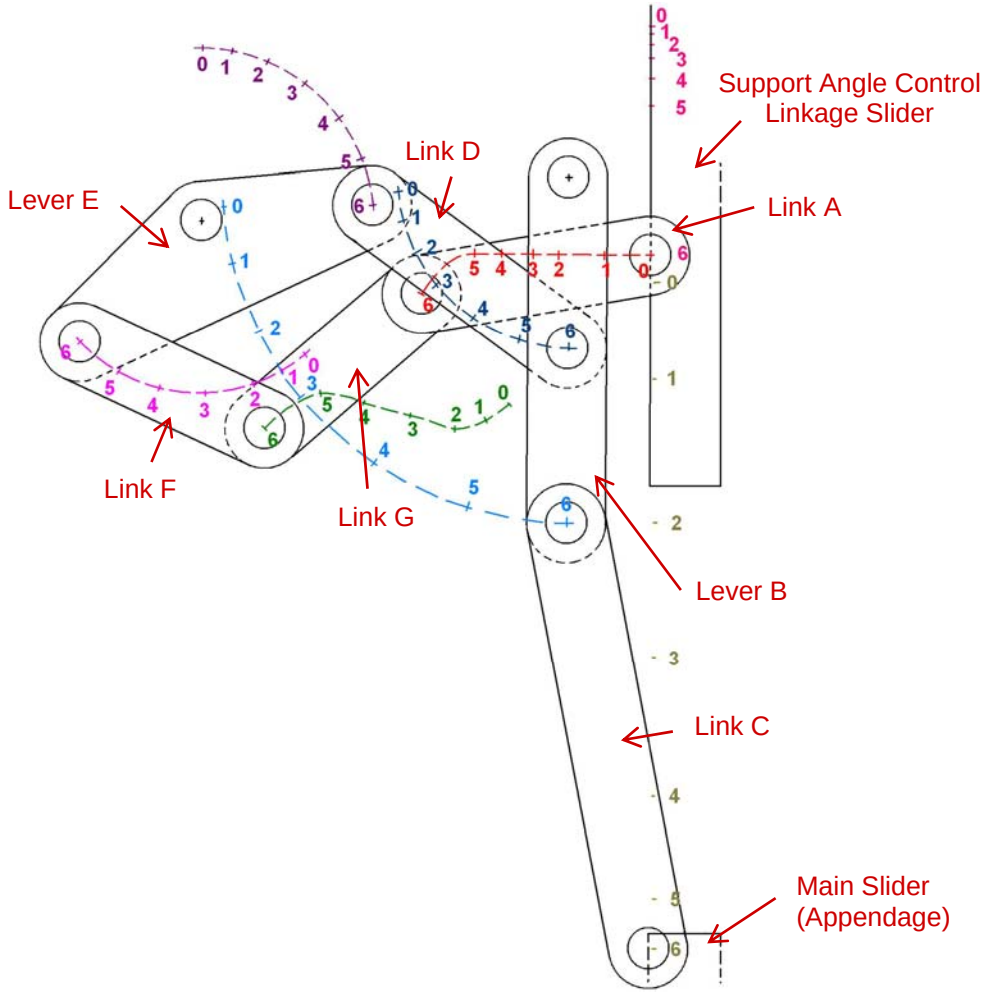

Figure 3.16 Transformation and locking mechanism — extended position

3.2.5 Folding Strengthening Mechanism

If needed there is also a folding strengthening mechanism which contains the main support slider guides and absorbs most of the bending moment on the sliders produced by the flap load. These loads are minimal in the retracted position, but rather high when flaps are extended. This means strong and big guides etc are needed with flaps extended, but smaller and less strong components are sufficient when flaps are retracted.

As mentioned in the preceding chapter, the guides for the sliders are all fixed to a single mounting plate. While this plate is probably stiff enough to withstand any moments encountered with flaps up this may no longer be the case with fully extended flaps where a high bending moment acts on the guides and the rather (last but not least for weight reasons) thin mounting plate. If this should be the case, to stiffen this plate when needed a strengthening mechanism could be attached to the plate via hinges, which basically folds up another plate on each side and thus increases the mechanism's overall moment of inertia (i.e. increases its flexural strength).

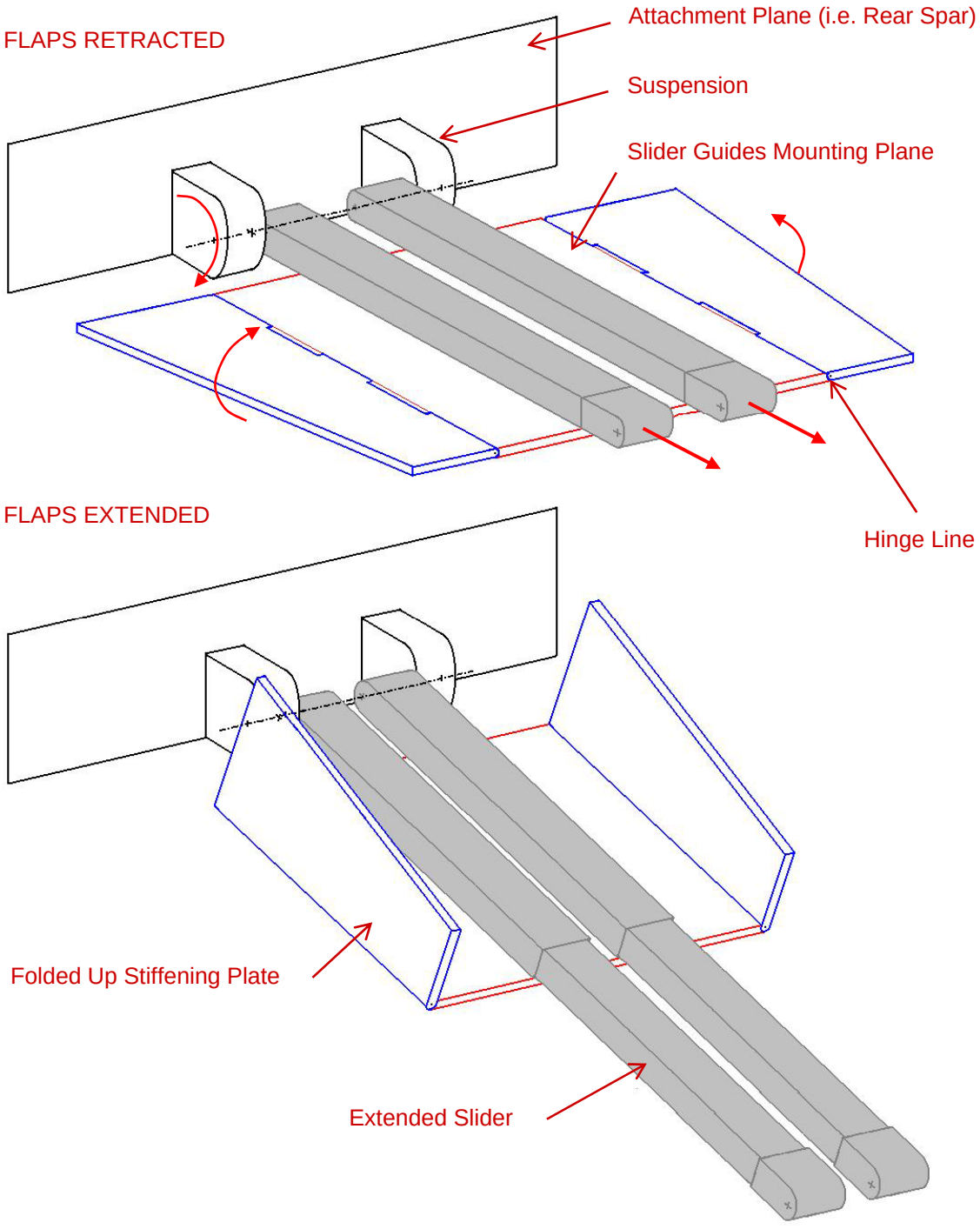

Figure 3.17 Folding strengthening mechanism

3.2.6 Tab Actuation

Since in a multifunctional wing the tab is part of the flap body, as opposed to a flaperon directly attached to the wing's main structure, its actuator must be located either within the flap body or this task needs to be accomplished from outside and via leverages or other means. There is probably not enough space left within the flap body due to the integrated track and support which take much volume; there are concerns of power transmission, too. If hydraulically actuated the respective pipes and hoses need to move a rather long way which makes them vulnerable for fatigue, stone hits if hanging exposed, or even corrosion.

To be effective an aileron or a camber flap should not be deflected by more than 30° to each side. But this is already quite much from an actuation point of view: in current aileron systems, actuated by cylinders and leverages, there are often bulges in the wing strake (at least at the bottom surface) to accommodate for the levers in fully deflected aileron position. As long as pure lever systems are used this cannot be avoided unless very high forces are encountered on short levers.

These problems may be avoided with the following approach as shown in figure 3.18 on the next page. Besides support ribs the tab contains at least one actuation rib which features some kind of spike. This spike is designed such that it fits exactly into the flap body (i.e. its strake) when the tab is fully deflected to either side. There is a facet on its tip which is needed to allow for a smooth slide in the actual actuator: the laterally moving tab angle control slider features a cam which the spike is forced to follow and thus a rotation is induced in the tab. This slider cam can be linear (in the back view) or may be shaped as a specific programming cam, but in the latter case the actuation rib spike facet needs to be rounded.

The slider is actuated via a shaft as shown in figure 3.18. This is basically an extendable spline shaft, attached to the main slider and designed to follow both the main support slider's extension and downward motion. It also needs to allow for the flap angle adjustment motion as described in chapter 3.2.3 above, and this is accomplished using a cardan joint with its kinematic center located exactly on the main support slider's hinge line.

Note that usually there is a taper angle other than zero at least on outer flaps. This means that the flap's leading and trailing edge are not parallel, and this angle too can be accounted for using that same cardan joint.

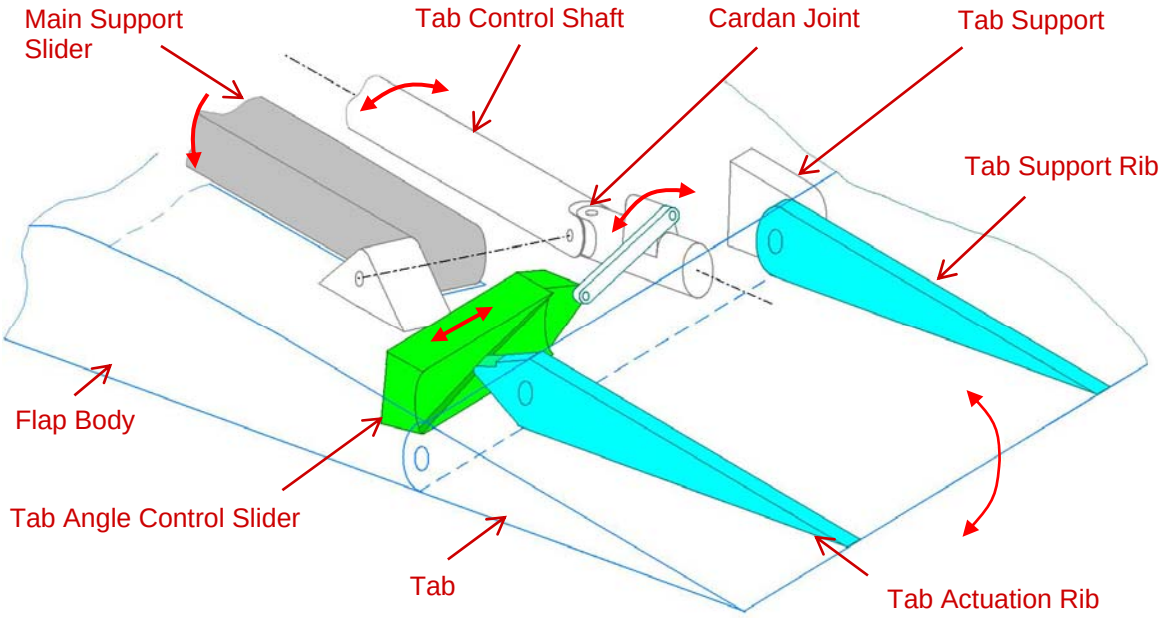

Figure 3.18 Tab actuation mechanism

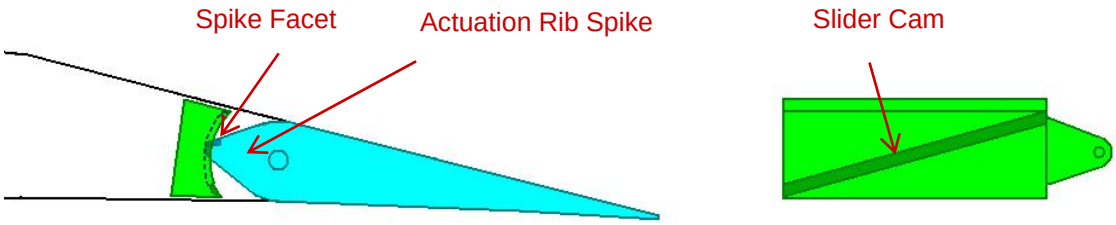

Figure 3.19 Tab angle control slider — side and back view

3.2.7 Flap Vane Actuation

With the introduction of a tab as explained in the last subchapter, the flap body becomes basically like a conventional wing. The tab acts as a simple camber flap on the actual flap body, with all its problems including reduction of α_{max} as explained in chapter 2.1. Therefore it is advisable to include a flap vane in the system which opens up an additional slot on flap deployment, thus acting like a slat for the flap body. Such a vane becomes effective only at rather high back- and downward position of the flap; the pertaining mechanism should thus open the slot only at and after this point. Besides, aerodynamics require specific overlaps and gaps (as shown in figure 3.20) for each flap position which need to be accounted for.

Basically the same actuation/programming system as for the B767 slats (see figure 3.1) can be applied for the most accurate positioning of the flap vane. A simplified system is shown in figure 3.21: it is assumed that the vane moves on a circular track with specific radius.

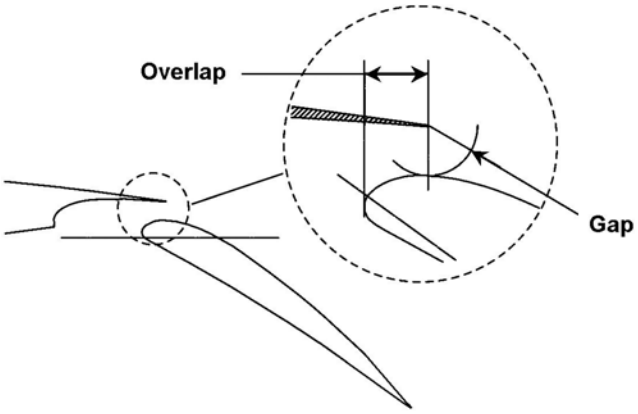

Figure 3.20 Overlap and gap specifications, according to [13]

The support slider (which is firmly fixed to the vane) thus has a circular shape with this radius, moving on support rolls. It is attached to the main support slider via the cam link and the main slider link; they are joint in a bolt which is forced to follow a programming cam.

As explained above the vane should be actuated only after a significant backward and tilting motion of the flap body has taken place. The main slider would move during any position change of the flap; therefore the programming cam features two parts. The first is circular with its center at the joint location of the retracted slider and radius equal to the cam link's length, i.e. this part of the cam is non-actuating as the cam link follows a circle around its joint with the flap vane slider. Thus the latter encounters no moving force for this cam part. The second part of the cam is now designed such that the vane follows the desired path.

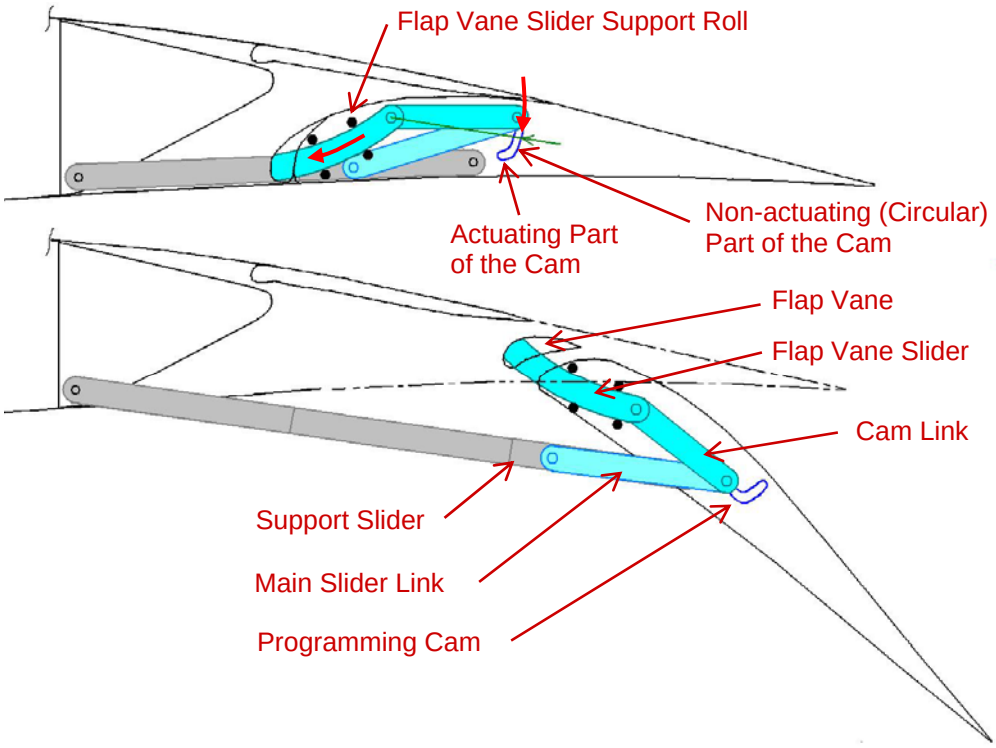

Figure 3.21 Flap vane actuation

3.3 Assembled Mechanism

Now the component concepts as outlined above are combined to one single flap actuation mechanism. In order not to overload the figures below, they do not show the flap vane and tab actuation mechanisms, neither are spoilers and their support ribs displayed.

The flap track/support should allow the following motions (color groups for the individual motions will be kept for this chapter):

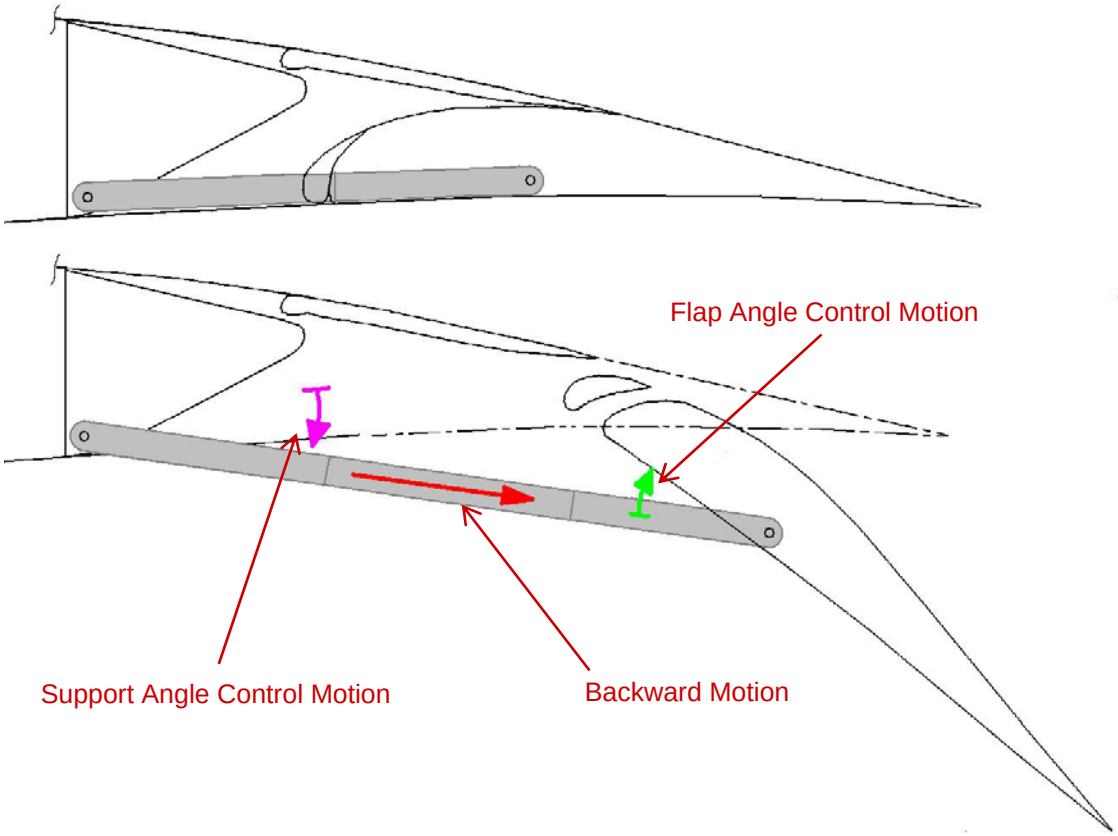

Figure 3.22 Flap track mechanism — main motions

The figures on the following two pages show the assembled mechanism in both the flaps up and flaps down position. All labeling is consistent with chapter 3.2; for easier identification programming cams are always drawn grey, even where they are actually masked by other elements (but there the borders are shown in dashed lines). The legend may be useful for reference.

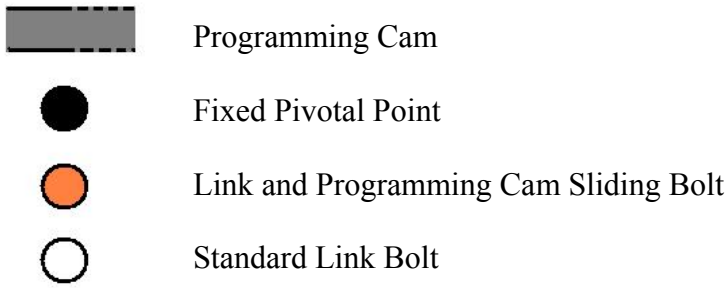

Figure 3.23 Elements legend

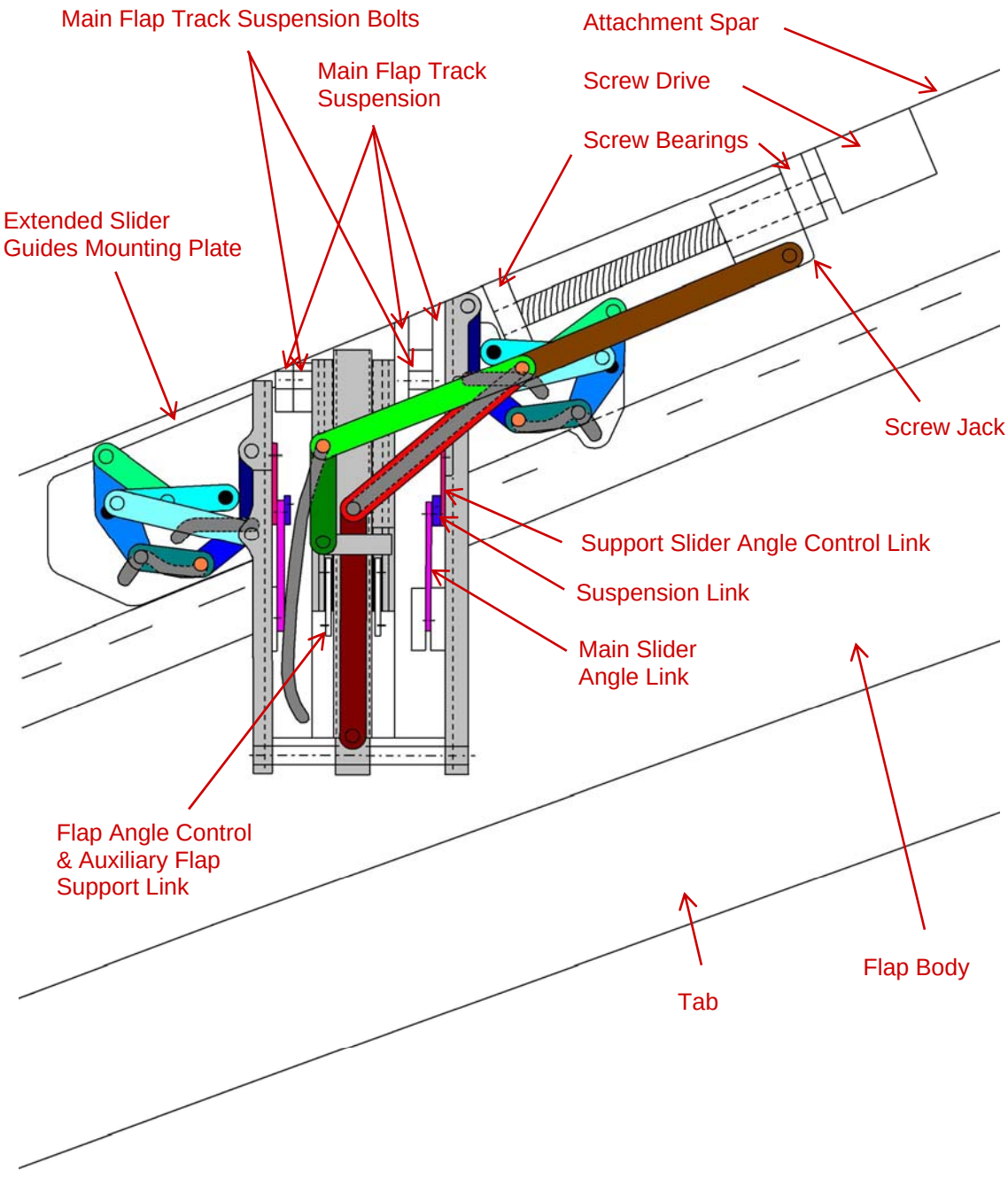

Figure 3.24 Flap track mechanism — flaps fully retracted

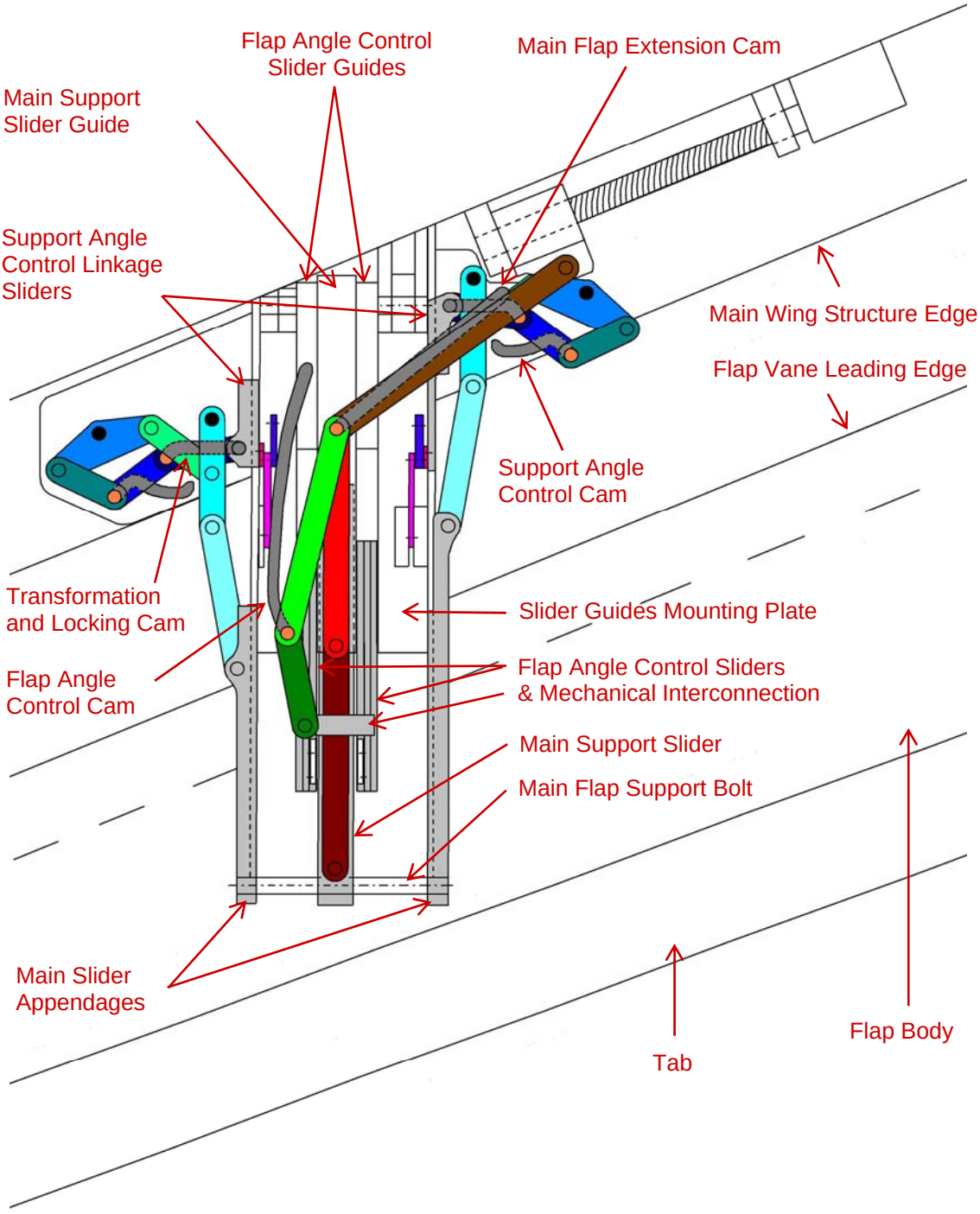

Figure 3.25 Flap track mechanism — flaps fully extended

Although mainly a task to be done in the detailed construction, the slider profiles are suggested as shown in figure 3.26 below. Fail-safe design can be achieved by glueing (red lines) two parts.

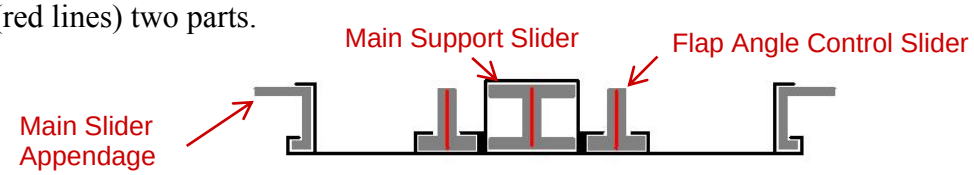

Figure 3.26 Recommended slider profiles

An inverted T-beam profile was chosen for the flap angle control sliders as with this profile both a firm guiding as well as accommodation of the flap angle control and auxiliary support link are possible.

For the main slider actuation, note that there is an additional link (dark red) when compared to figure 3.7 on page 29. This is necessary because the main support slider guide, having to bear a very high load especially in extended position, is a closed profile and should not be slotted. This additional link slides on top of this guide and is connected to the main slider only after the guide's end.

This mechanism concept basically proves to fit within the wing strake in the flaps up position. Note that the support angle control linkage including its sliders needs to be slightly different for each side: while the transformation and locking mechanism itself is perfectly symmetric, the support angle control mechanism and its sliders are somewhat distorted to fit into the very limited space available in the retracted state. A small cam part is still interfering with the flap's leading edge in the retracted position (see figure 3.24).

Solving these and other problems as well as the exact vertical 'layering' of all leverages etc remains to be done in a detailed construction, but does not affect the basic working principles. This mechanism takes all requirements (as outlined in chapter 3.1) into consideration.

Chapter 4

Preliminary Considerations For Detailed Design

4.1 Nomenclature

‘airfoil’ (US) or ‘aerofoil’ (UK): another expression for an aerodynamic wing profile

‘inboard:’ refers to parts, assemblies etc closer to the fuselage/center of an aircraft

‘outboard:’ refers to parts, assemblies etc farther from the fuselage/center of an aircraft

‘flap track station:’ refers to a full flap track assembly at a specific location on the wing including all supports, guides and actuators; there are at least two such stations per flap. Usually they are numbered as ‘Station 1’, ‘Station 2’ etc, the lowest number being allocated to the station closest to the center of an aircraft. For a given set of stations to which a flap is attached one station is the ‘master station’ while the others are the ‘slave stations’.

‘chord line:’ roughly refers to the line from a airfoil’s leading edge to its trailing edge. Its length is usually referred to as ‘chord’.

‘sweep:’ refers to the angle between fuselage (longitudinal) and mean wing spar direction, normally represented by the 0.25 chord line of the wing or less often also the leading edge. Many smaller aircraft with this angle being perpendicular (normal direction) have unswept wings, while most current large airliners feature backswept wings. The difference between actual mean wing spar angle and normal direction is referred to as ‘sweepback angle,’ or, in some less common designs where the wing is inclined in forward direction, as ‘sweepforward angle’.

‘taper:’ basically, a wing (or flap, aileron, rudder etc) with parallel leading and trailing edge is untapered (a so-called trapezoidal wing with parallel leading and trailing edge) and otherwise is tapered, regardless of its sweep angle. A tapered wing has therefore different chords at the wing tip and root; ‘taper ratio’ (tip chord divided by root chord, or sometimes also by equivalent centerline chord) is used to describe this wing characteristic. Untapered wings have a taper ratio of 1.

4.2 Design Environment

4.2.1 Coordinate Systems

A standard aircraft-fixed coordinate system is commonly used in aerospace technology, with the x-axis pointing forward along the aircraft's longitudinal axis, the z-axis pointing earthward and the y-axis chosen according to the right-hand rule. The coordinate system's origin is often chosen at the center of gravity or nearby, but sometimes also more forward, especially if further lengthened versions of the aircraft are planned. The origin is placed on the plane of symmetry if the plane is symmetric, which is almost always the case.

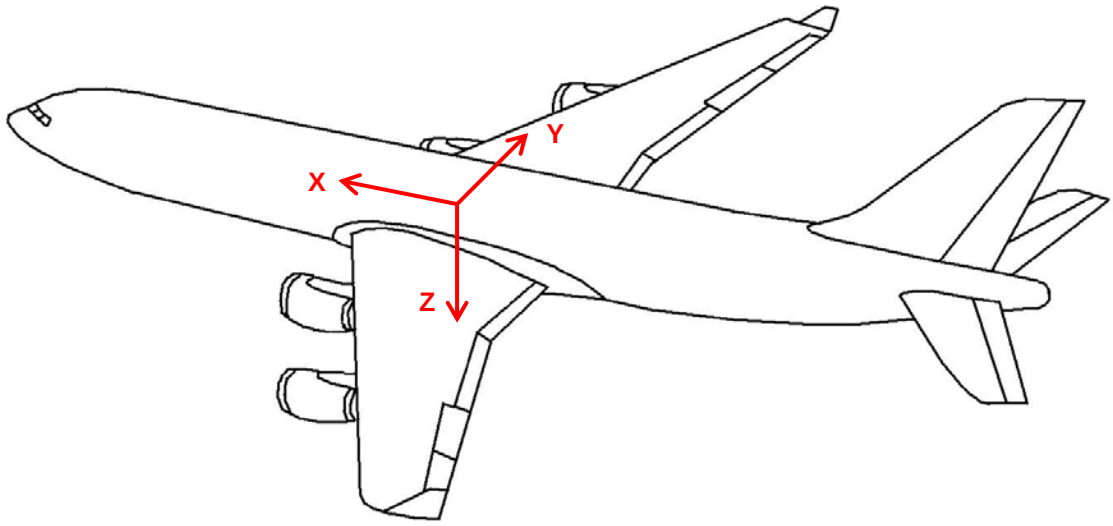

Figure 4.1 Coordinate system normally used

For this project another approach is applied: since the rear spar makes a good reference and most dimensions of interest are located behind it and all detailed construction in this project will be done on the left wing (arbitrary but not uncommon), the coordinate system being used is chosen in such a way that the least possible negative values appear. The origin is located at the outer skin of the wing's bottom shell and on the back plane of the rear spar. The y-axis points toward the trailing edge with the z-axis pointing upwards, and the x-axis pointing from inboard to outboard on a left wing situation.

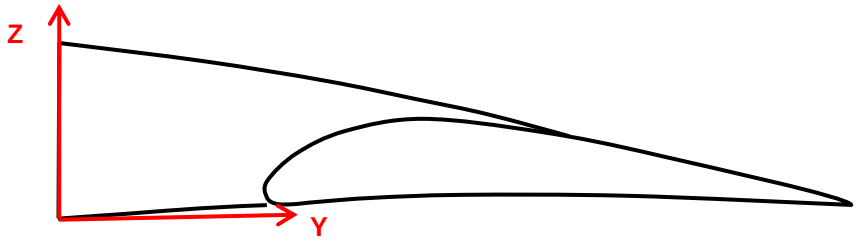

Figure 4.2 Coordinate system used in this project

4.2.2 Dimensions

For the purpose of this thesis the B767 outboard flap's dimensions are being used approximately, and the inner station thereof. This approach is mainly chosen to get realistic results, and because with this station the flap suspensions are attached exclusively to the main wing rear spar (see fig. 4.5) rather than several attachment points on the wing's lower side (compare approach of Airbus).

As this project is mainly about developing an integrated flap track mechanism it is beyond its scope to demonstrate structural stability of the main wing with this flap track attachment method, but since it apparently works in a widely used aircraft there is good reason to apply it in the following design work without further specific investigation.

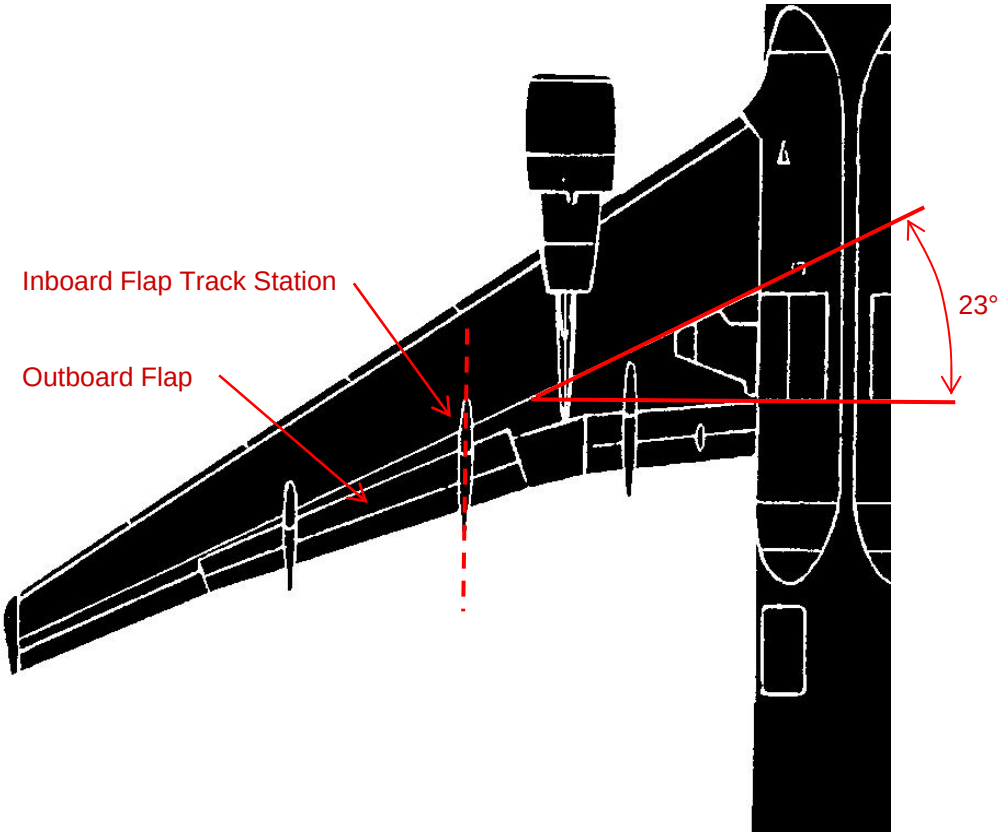

Figure 4.3 B767 wing lower side: flap track station used

A rear spar sweepback angle of 23° is chosen from fig. 4.3 above as a realistic reference for this project. For the purpose of flap load calculations the following approximate flap dimensions are used (similar to a B767 outboard flap):

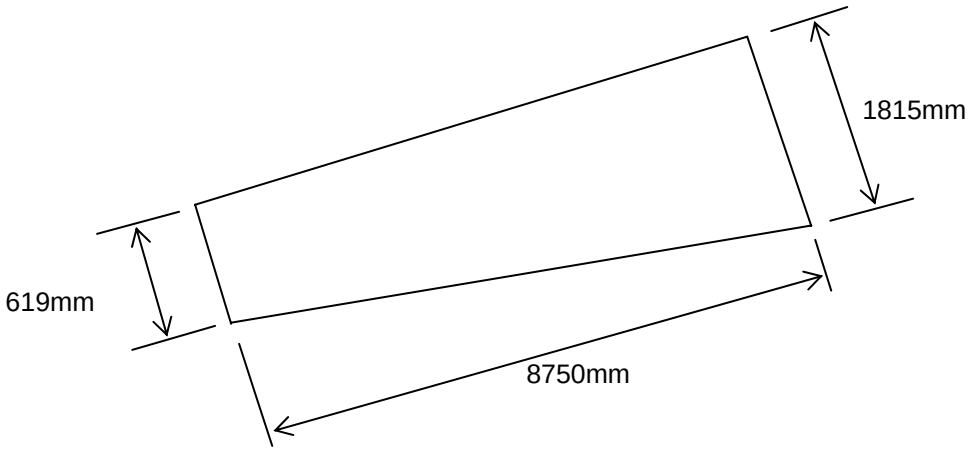

Figure 4.4 Flap dimensions

The basic section shapes and dimensions are shown in fig. 4.5 below. They are derived from the B767 outboard flap track mechanism, see also fig. 2.12 on page 14.

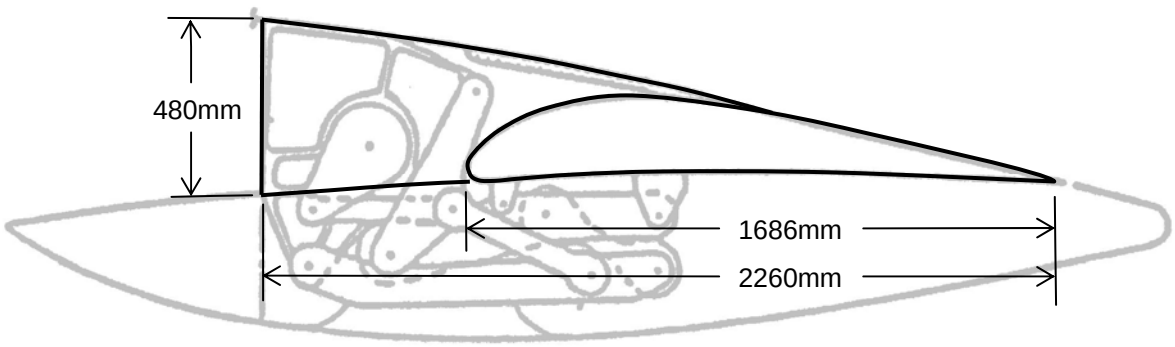

Figure 4.5 Basic section shapes and dimensions

To be efficient the tab needs to have sufficient chord; it also acts as a standard camber flap or aileron for the flap body which then becomes similar to a wing itself. Literature suggests [2,3] that such a camber flap/aileron chord should be around 25% to 33% of the wing chord, and maximum deflection should be 30° up or down. In this case attention must be paid to avoidance of collision with the spoiler, but with the dimensions shown in figure 4.5 above this is not a problem.

For these reasons the length from the tab pivot/attachment point to its trailing edge is set to 560mm, which is about 33% of the flap's chord 1686mm, and the maximum deflection is 30°.

4.2.3 Flap Extension Characteristics

The exact backward/downward positions and corresponding angles of the flap are defined by the aerodynamic requirements. For this project no such data is available, but the different positions as shown in fig. 4.6 below are a realistic reference and will be used this way.

Colors go from green to red for the different flap extension states. The flap vane is deployed only in the last three states, where they are also shown in figure 4.6 below. The tab is shown only with the fully extended flap position. The different flap chord angles are labeled appropriately.

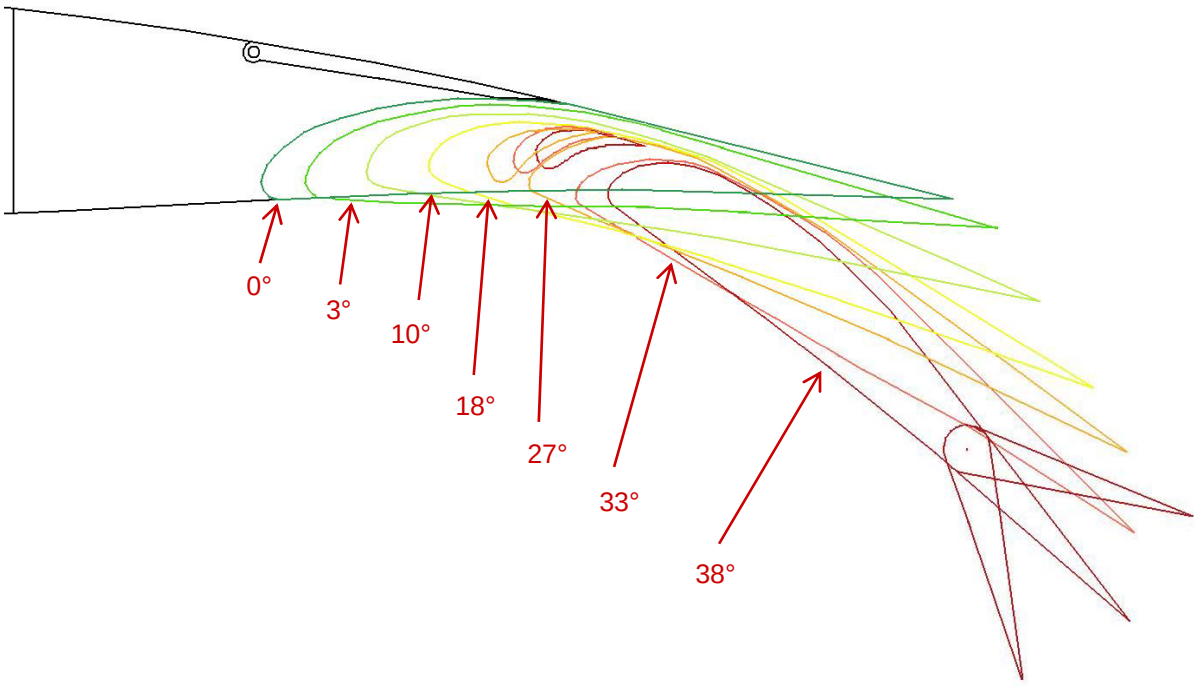

Figure 4.6 Flap extension characteristics

4.2.4 Three-Dimensional Flap Deployment With Swept Wings

As opposed to unswept wings with untapered flaps perpendicular to the flight path, fowlering with swept wings is more complicated. The flap body no longer moves solely on a cylindrical surface, but performs a complex three-dimensional motion. This usually entails ball joint suspensions. For swept wings there are two basic flap extension principles as shown on the following two pages.

Trapezoidal Fowlering:

Where a flap is untapered but swept it usually moves on a cylindrical surface as shown in fig. 4.7. The flap suspension motions form a trapezoidal shape as shown in blue. Note that this surface is not necessarily circular but defined by aerodynamic requirements, and that since the flap is swept this cylinder is oblique, i.e. its axis is not perpendicular to the sections.

Trapezoidal fowlering is often used in inboard flaps which are untapered on most common airliners (see also B767 in fig. 4.3 above). An advantage of this principle is that theoretically exactly identical flap track stations could be used for such flaps, although this is rather uncommon. Besides, an untapered flap with identical sections throughout its span may be built with only one rib shape.

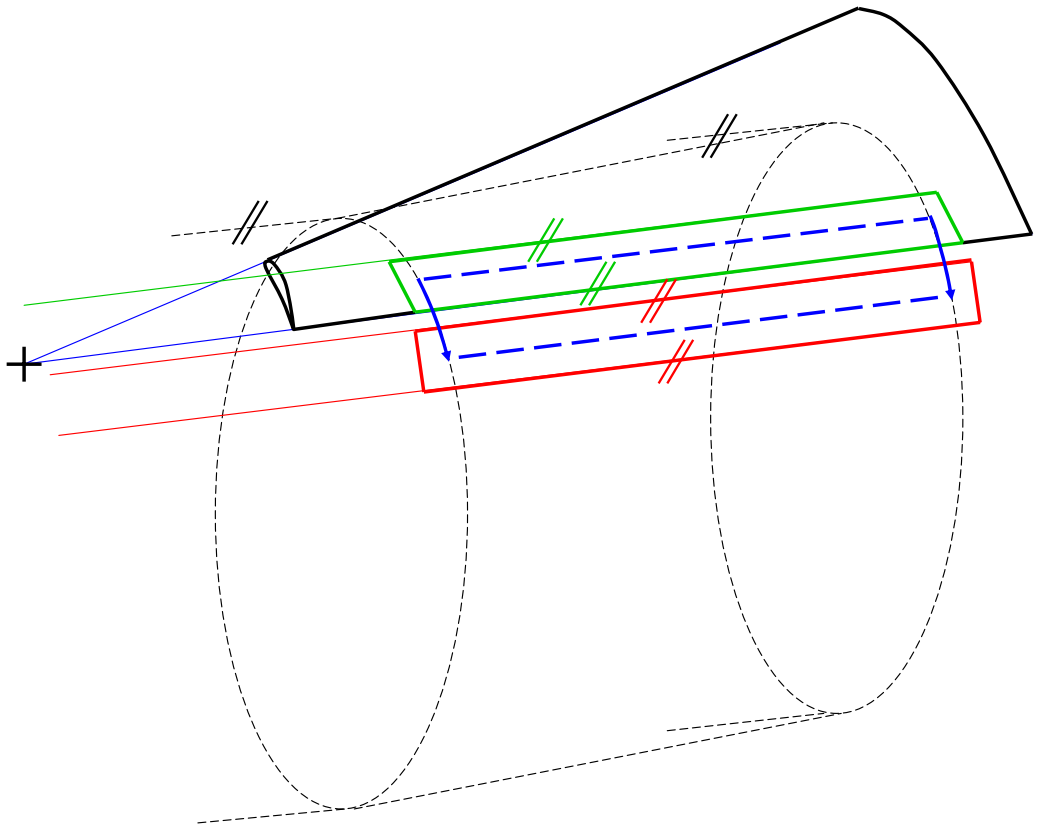

Figure 4.7 Trapezoidal fowlering principle

Conical Fowlering:

When a flap is tapered and swept the intersection point if its trailing an leading edge is often identical to that of the wing's leading and trailing edge. The flap usually moves on a conical surface as shown in fig. 4.8. The flap suspension motions form a conical surface shown in blue, as opposed to the trapezoidal shape depicted on the preceding page. Note that this cone surface is again not necessarily circular and its axis is not perpendicular to the sections.

Conical fowlering is almost always used in outboard flaps, which are mostly tapered to a certain degree. The taper ratio with reference to the span is often identical or close to that of the wing as this allows to place the rear spar as far backward as possible. With this principle no two flap track stations are exactly identical. Further, depending on the exact aerodynamic requirements, some of these tracks need to be installed somewhat offset of the aircraft's longitudinal axis. With conventional systems this entails a wider fairing and thus more parasite drag (Airbus A380 is a good example). With integrated flap tracks this disadvantage can be fully eliminated.

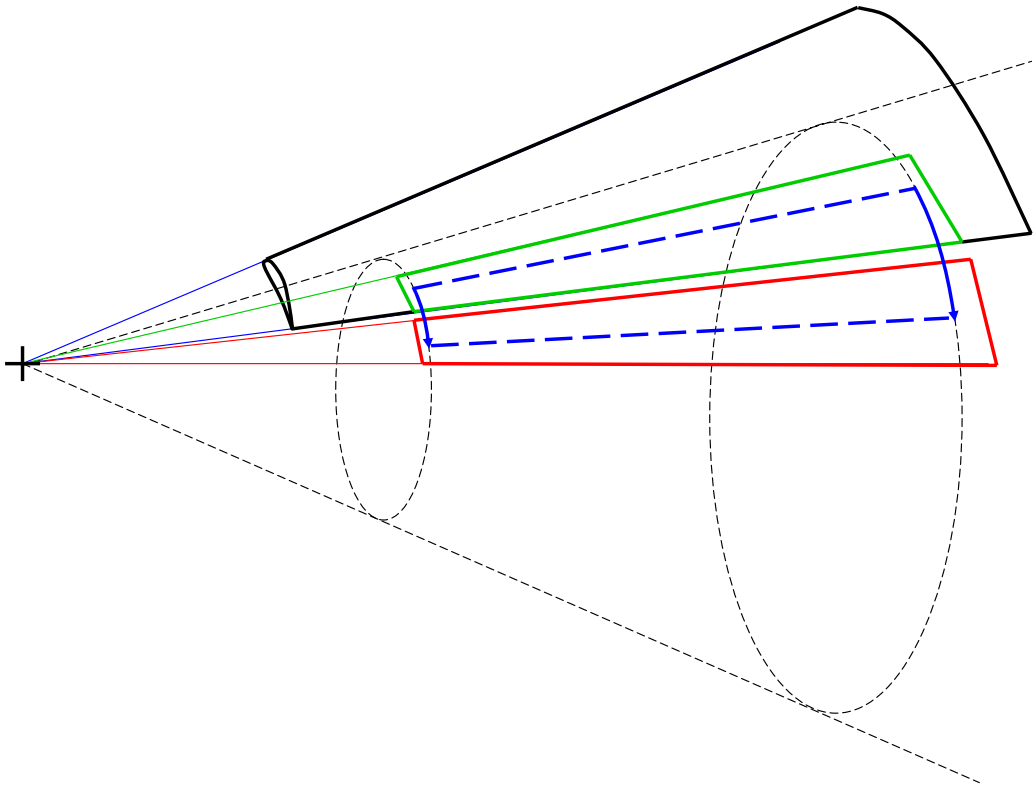

Figure 4.8 Conical fowlering principle

In this project only trapezoidal fowlering will be considered, as this allows a much simpler production process of the demonstrator model and besides, two identical flap track stations can be used in the CAD model. This approach has no negative impact on the aim of the thesis which is to demonstrate that the mechanism as depicted in chapter 3 basically works.
The flap's 3D rotation around its main suspension point can be split into three separate rotation angles, each of which is relevant for the suspension ball joint design. Therefore these three angles need to be derived approximately already at this stage. In the following three figures these rotations are shown; green is the flap plane before and red after rotation, respectively. The angles are α, β and γ, but in this subchapter they have no reference to other variables such as the angle of attack, for example.

First, besides a backward translation typical for fowlering, the flap is rotated about a parallel to the aircraft's Y-axis (see fig. 4.1 above), i.e. the direction perpendicular to fuselage and flight path. This is approximately the main flap angle and is indicated as α in figure 4.9 on the next page. The blue line represents the projection of the 'raw' wing plane onto the deployed flap in the following three figures, and the dash-dot lines are the respective rotation axes. In the α rotation it is identical with the blue projection line.

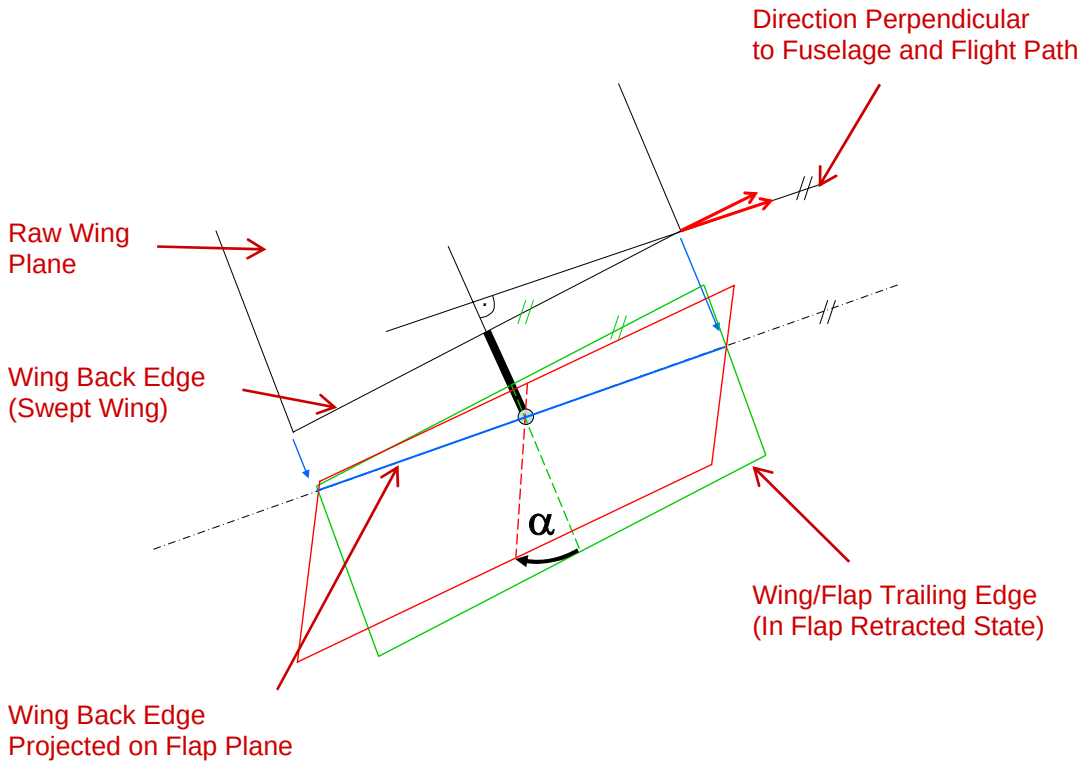

Figure 4.9 α flap plane rotation

Since the flap plane must be parallel to the wing's back edge (in untapered flaps, otherwise same central point), it needs to be rotated such that this blue projection line comes up parallel to the wing's back edge. This rotation angle will be called β and is shown in figure 4.10 below.

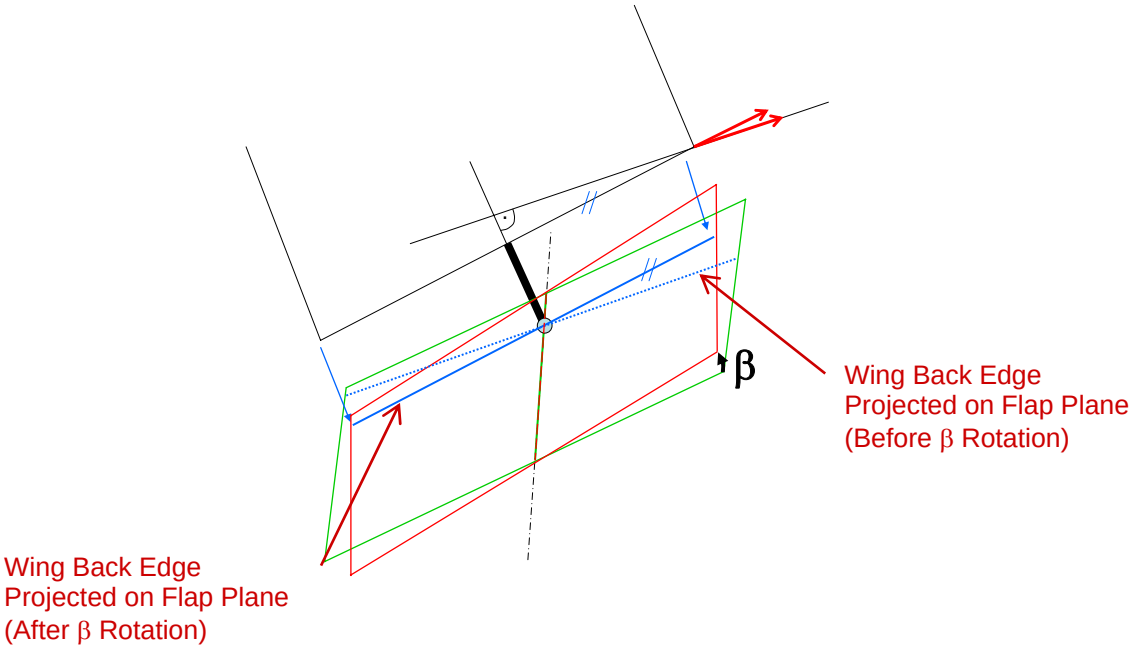

Figure 4.10 β flap plane rotation

Finally, the flap's leading edge must be made parallel to the wing's back edge. This is the intention of the γ rotation as shown in figure 4.11 below. The axis is perpendicular to the flap plane, so the blue projection line will of course remain the same.

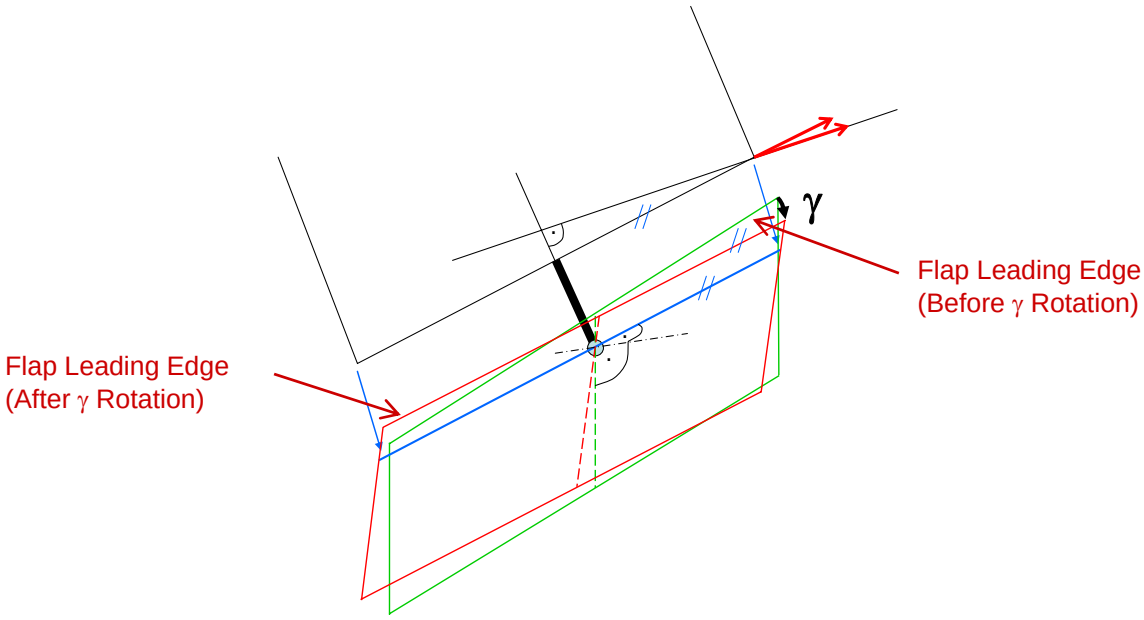

Figure 4.11 γ flap plane rotation

These three angles are calculated using a Mathematica Notebook 'FlapRotation.nb' (see Appendix B), using vectors and appropriate rotation matrices. For a sweep angle of 23° and a maximum flap angle of 38° approximately the following angles are obtained: **α = 38°, β = 15°, γ = 5°**

Note that this calculation does not take into account the main suspension angular motion; the corresponding angular value would need to be subtracted from the α value above, and it depends on the actual main suspension layout and dimensions. Therefore, if a standard ball joint is used it must allow for a rotation of less than 38° around its main axis and about 15° in the lateral direction.

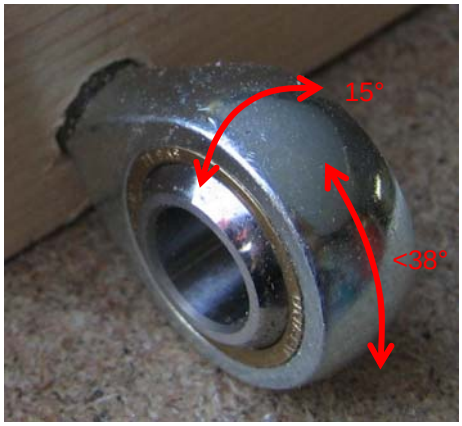

Figure 4.12 Ball joint rotation angles

4.2.5 Flap Loads

The actual loads on a flap and its tracks depend on many different parameters. Even though nominal aerodynamic loads are already significant, the various failure loading cases have even more impact and are often dimensioning. There are actually several hundreds up to thousands of such failure cases which need to be considered in an actual aircraft certification process. Some of them involve jamming of sliding ball joints, a failure case also appearing in technically immaculate aircraft: it is not very uncommon that a mechanic puts his screw-wrench into such a joint box and soon forgets he has done so. Although there are torque limiters on flap track actuators the loads resulting from jamming may exceed aerodynamic loads by 20% up to 70%. Nominal flap loads include forced flap deformation (bending and torsion) and loads due to wing bending. The maximal aerodynamic load is often encountered in a 'return-to-land' situation, i.e. when an aircraft still gets airborne after a technical failure, dumps fuel and immediately lands again with its maximum allowable landing weight.

Wing and resulting flap bending also entail a lateral motion of the flap body. To avoid high lateral loads on flap tracks there is one master station which absorbs all lateral loads; all other slave stations allow the flap body to move freely in the lateral direction.

Within the scope of this thesis only very basic loading cases are considered, since the main intention is to develop a working mechanism. According to the FARs/JARs the operating range for a commercial airliner is -1.0g to +2.5g. The maximum nominal aerodynamic loads are attained with fully deployed flaps on final approach.

Therefore, the following loading cases will be considered in this thesis, all of them for a flap angle of 38° and a speed of 140 knots (with ICAO Standard Atmosphere conditions at sea level):

+2.5g and tab up 30°

+2.5g and tab down 30°

-1.0g and tab up 30°

-1.0g and tab down 30°

Besides a basic safety factor of 1.1, to account for jamming loads another safety factor of 1.7 is applied. Rather small basic safety factors are used in aerospace engineering since on one hand the operational range includes unusually high loads, and on the other hand failure characteristics of the various materials are mostly well known.

As realistic flap load data is difficult to obtain freely, and varies widely depending on the aircraft itself with its design, loading and flight configuration, a rough calculation based on theoretical premises is carried out in this project. This gives a rough idea of the actual flap loads, although far from being exact. Appendix C shows the various formulas and steps needed to get these loads, which are finally computed using the Mathematica Notebook FlapLoad.nb (see Appendix D).

4.3 Flap Structure

4.3.1 State of the Art

Basically, a flap body is simply a wing also from a structural point of view. The standard lightweight thin-walled design approaches are as well applied, with shells, spars and stringers. Trade-off studies are done to attain the most favorable results as to the number of spars and stringers to be used; it is not uncommon that three or more spars are built into a flap body. The trailing edge part is often made up of a covered honeycomb structure.

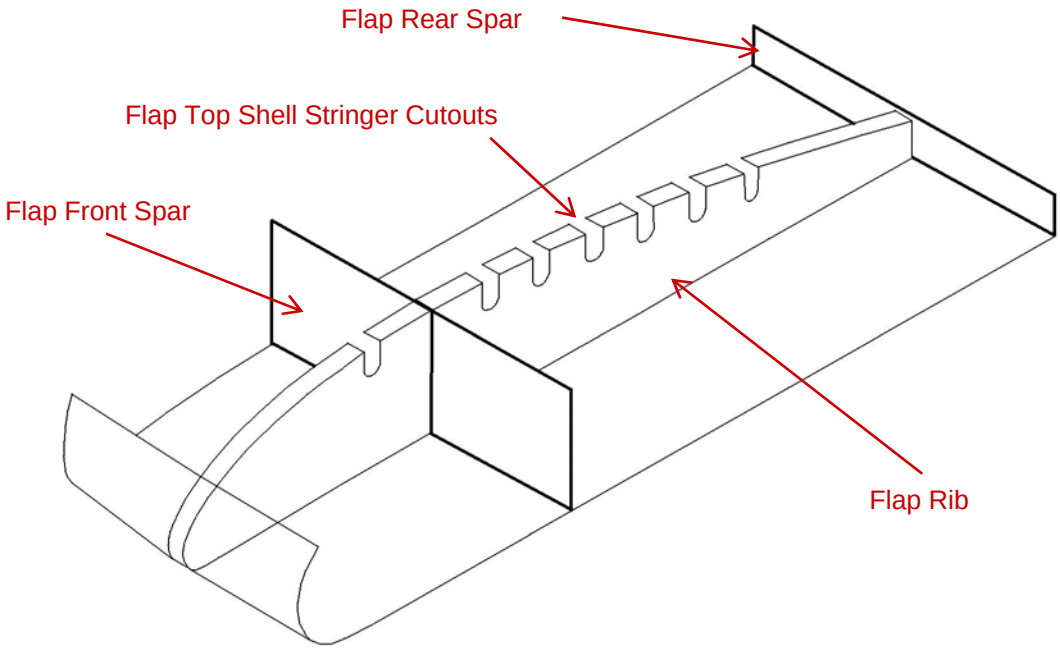

Figure 4.13 A330/340 standard flap body structure

Figure 4.14 A330/340 standard flap track

Fig. 4.13 above shows a common structure which is applied on the A330/340 aircraft families. A front and a rear spar are connected by ribs; only the top shell is stiffened by stringers. This forms a torque box with the flap nose not being a relevant part of it.

Figure 4.14 shows the flap track mechanism as used on the A330/340 aircraft. Since the element connecting the flap to the carriage is mounted fully on its outside, the flap's lightweight structure shell is not impaired, apart from some rivet and screw holes.

With the application of an integrated flap track as depicted in chapter 3 it is not possible to keep this design approach fully. At least one side of the shell needs to be cut in order to accommodate the main slider and pertaining guides in the flaps retracted position. Any deviation from membrane loads through cutouts and similar leads to a heavier system than what could be achieved ideally; therefore such disruptions must be kept at an absolute minimum.

4.3.2 The B747SP Approach

Coming up with an aircraft for very specific applications, Boeing also introduced a new kind of flap track mechanism with the B747SP ('Special Performance'). This aircraft was designed for ultra long haul trips and can be recognized by its very short fuselage. The flap track mechanisms are integrated to a high degree, but there are still small flap track fairings as shown in fig. 4.15 below.

Figure 4.15 B747SP with partially integrated flap tracks

The fact that this flap track mechanism has so far only been used on this (old) aircraft shows that there are some serious issues to be considered which are also relevant for this project.

The mechanism itself is fairly simple, as fig. 4.16 below shows. A two-link approach produces satisfactory flap extension characteristics, although they are only an approximation to the ideal, which may be a disadvantage from an efficiency point of view. However, the simplicity of the system is a huge advantage for maintenance.

Figure 4.16 B747SP partially integrated flap track system

As explained in the preceding subchapter the main problem with this and any 'integrated' flap track approach is the disruption of a standard thin-walled lightweight flap body structure common to all other standard flap suspension methods. With the B747SP this is particularly evident as can be seen in figures 4.17 and 4.18 on the following page where large cutouts on the flap body top sides are visible. This design entails a rather heavy system, particularly since the top side of the lightweight structure is disrupted. Still, the cutouts are needed since the rear link connects flap and suspensions about in the middle of the flap.

Figure 4.17 B747SP flap structure cutouts

Figure 4.18 B747SP fully extended flaps

As depicted in fig. 4.18 above the flap suspensions act like ‘thorns’ disturbing the airflow in the flaps extended position. As particularly the top part of the airflow around an airfoil is very susceptible to disturbances, discontinuities on the top side lead to considerable efficiency losses due to boundary layer separation. With this approach, however, there are flap body cutouts anyway at these locations which would not act as an efficient airfoil.

If the top side of the wing and flap combination could be kept clear of any disruption this would likely lead to an increase in efficiency compared to the B747SP approach.

4.3.3 Approach for This Project

The state-of-the-art approach as explained in chapter 4.3.1 should be kept wherever possible. A two-spar structure will be applied with at least one spar kept continuous; it is obvious that this is possible with the rear spar only and thus there is not much sense in introducing more than one additional spar. The tab should be attached right at the back of this rear spar and the main flap support right in front of it.

Thus only the front spar needs to be cut and only in its lower part, the size of the cutout depending on the dimensions of the main slider and pertaining guides. The latter also affect the size and placement of the stringers; therefore their vertical dimensions should be as small as possible to keep weight increases at a minimum. On the other hand the main slider’s vertical size should be as large as possible to provide for a high geometrical moment of inertia and a favorable weight-to-strength ratio. These conflicting requirements need to be addressed also from a main support bearing point of view: as explained in the preceding chapters the main suspension attachment point needs to be a ball joint/bearing, and such ball joints need to have a specific minimal size for given materials and load. This bearing must also be able to follow rotating motions as explained in chapter 4.2.4.

To avoid some of the problems with the B747SP approach, again ‘Don’t touch the top side of the flap body’ wherever possible is therefore the way to go in this project.

Intentionally left blank

Chapter 5

Detailed Mechanism Design and Demonstrator Model

5.1 Overview

The demonstrator model is built in scale 1:4. Apart from the calculation in chapter 5.2.3 all dimensions are shown in demonstrator size, i.e. four times smaller than what they would be on a real airplane like the B767. To keep a better overview these dimensions are depicted only for some elements explained at the beginning of this chapter; this allows the reader to get an impression of the actual proportions. The main intention of this chapter, however, is to give an insight into the full design process and caveats which would be encountered when applying this concept to a real airliner.

Figure 5.1 below shows the finished demonstrator model; the span of the wing section used is about 1m. As can be seen on the bottom right picture, it is indeed possible to leave the flap's top structure intact and to ensure a smooth airflow on the top side.

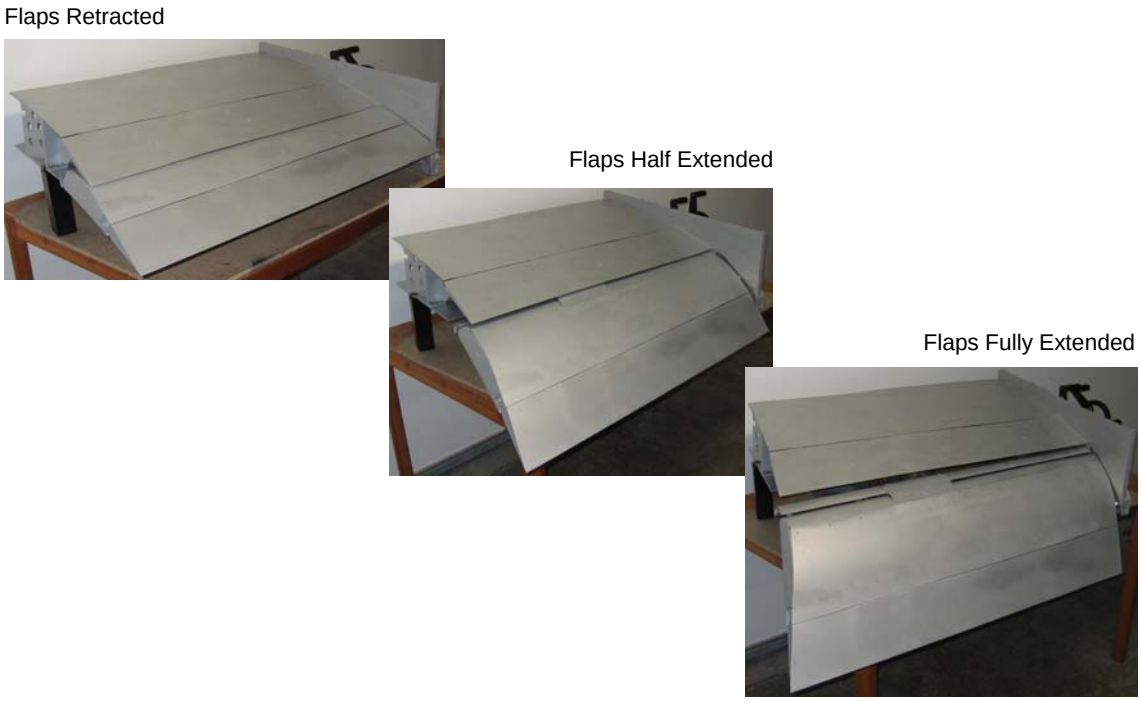

Figure 5.1 Assembled demonstrator model

As explained in chapter 4.1, the flap needs to be suspended on at least two stations. Since building two identical integrated flap track mechanisms would be too time-consuming and not of any additional benefit for this project, only one such mechanism is built and the other is a simulated station 1 flap track, i.e. built into the fuselage structure and thus of a much simpler nature (it shall be explained in chapter 5.13). A section of the fuselage is included in the demonstrator as can be seen in fig. 5.1 above.

The next figure shows that the task of integrating the flap track into the wing strake and thus eliminating a fairing can indeed be accomplished using the concept presented in chapter 3.

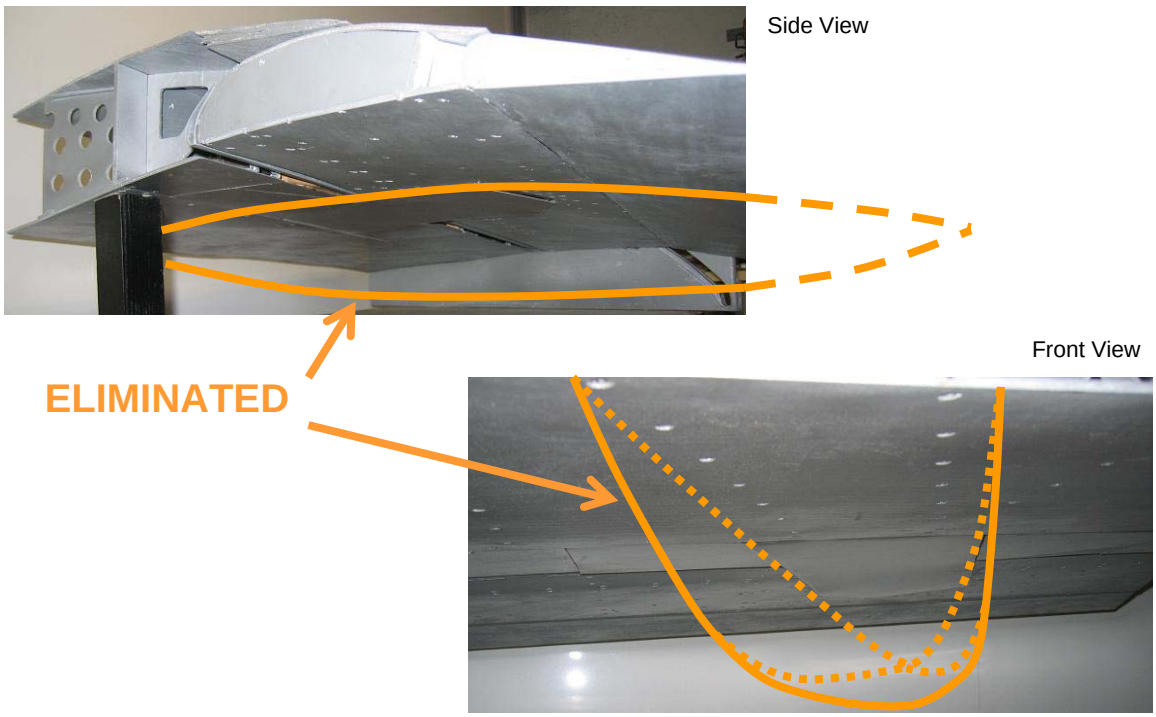

Figure 5.2 Task accomplished!

Chapter 5 shows the necessary design steps in a straightforward way wherever possible. However, choosing the appropriate dimensions and design is, as often in engineering, a highly iterative process; therefore references to later subchapters cannot be avoided at each point. The results as presented herein show a feasible approach, although far from being optimized in every detail.

The materials used for the demonstrator model are mainly plywood and aluminum; for some parts stainless steel, brass and copper are used as well. Lubrication is provided by a low viscosity lube oil for metal-to-metal sliding surfaces; for all other sliding contact surfaces (metal-to-wood and wood-to-wood) a special lubricant Waxilite® has been used which is a substance based on paraffin and specially designed for such purposes.

As an overview, figure 5.3 shows the finished main mechanism assembly.

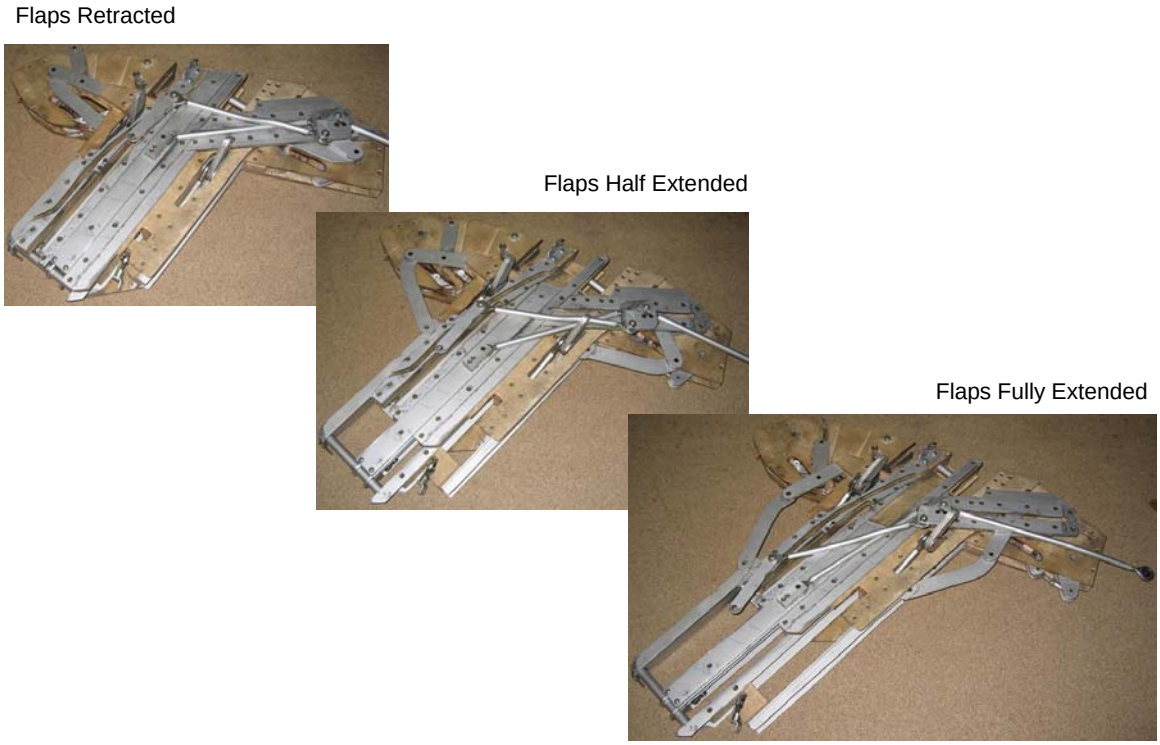

Figure 5.3 Main mechanism assembly

Figure 5.4 below shows its nomenclature, consistent with chapter 3 wherever possible.

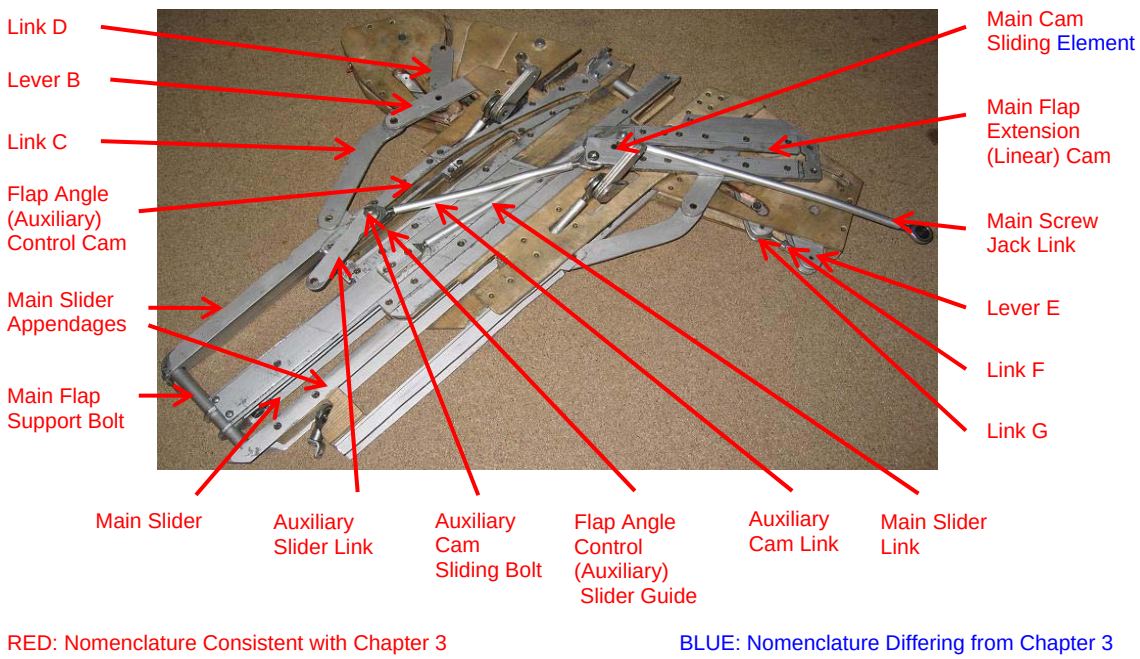

Figure 5.4 Main mechanism assembly nomenclature

5.2 Main Slider and Support Fitting

5.2.1 Main Suspension Flap Attachment Location

As a first design constraint the main flap attachment point should be close to the flap's aerodynamic pressure point, so at about 25%-30% of the flap chord. This minimizes the load on the secondary suspensions due to flap moment; however, there will be a considerable moment when the tab is deflected.

On the other hand, the attachment point should be located as far to the back as possible to allow for a maximum overlap of the main slider and its guide in the flaps fully extended position (see fig 5.5 below); if it is too small then the main slider bearings in the guide and the main slider itself might get overstressed. An overlap of about half of the main slider's length should be sufficient.

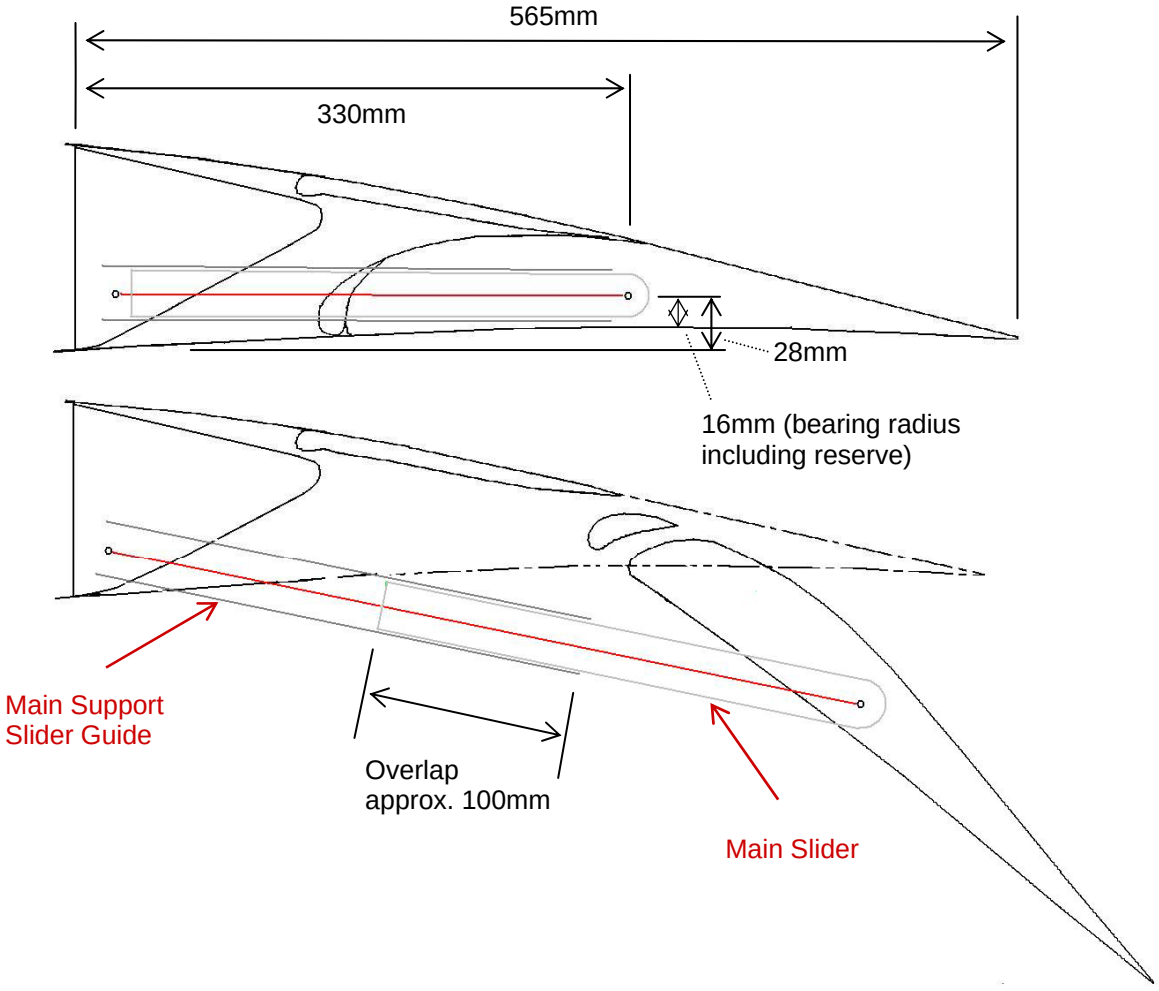

Figure 5.5 Flap suspension and main slider overlap

An attachment point too far to the back is not useful either since this entails a large cut in the lightweight structure. To keep most of the standard flap structure shown in fig. 4.13 on page 55 the rear spar should not be cut in any way, and the tab with its bearings and actuators should be accommodated right behind the rear spar.

As explained in chapter 4.3.3 the flap's top structure should not be touched either for the same reasons. When setting the vertical flap attachment position attention must be paid to allowing enough room for the stringers (also considering the flap's 3D motions, see also figure 5.69). Therefore it should be located as close as possible to the bottom surface of the flap, while just letting enough room for the flap main bearing and the main slider guide bearings. The slider guide structure height will therefore come up at about the flap main bearing diameter, but not much more. The main bearing diameter needs to be calculated roughly already at this stage, and for the given loads about 60mm result (see Appendix E), or 15mm in demonstrator scale. 30mm will be used as a reference for the structure's height, leaving about 20mm for the main slider's height.

Taking all these constraints into consideration the main suspension flap attachment location has been set as shown above in fig. 5.5. Thus only the nose section of the flap top part needs to be cut (besides the flap vane), and given that this section is not normally designed as a part of the load path this does not have a significant impact on the stiffness of the flap top structure.

5.2.2 Main Suspension Wing Attachment Location

Again for the purpose of maximizing slider overlap, the corresponding main suspension attachment point at the wing structure should be located as close as possible to the main wing rear spar. On the other hand there must be sufficient room for the attachment bolt, also taking into consideration this bolt's dimensions in the x direction.

Affecting the vertical attachment location, another constraint is the concave shape of the flap bottom surface: the main support slider guide must not collide with it. As described on page 31 the main suspension element it is attached to needs to transfer the moment produced by the flap load into the rear spar. In order to minimize the pertaining loads the main suspension wing attachment point should be located as close as possible to the bottom surface. A tangential configuration (including allowance for bearings etc) is therefore the best trade-off. The following figure 5.6 shows the selected dimensions.

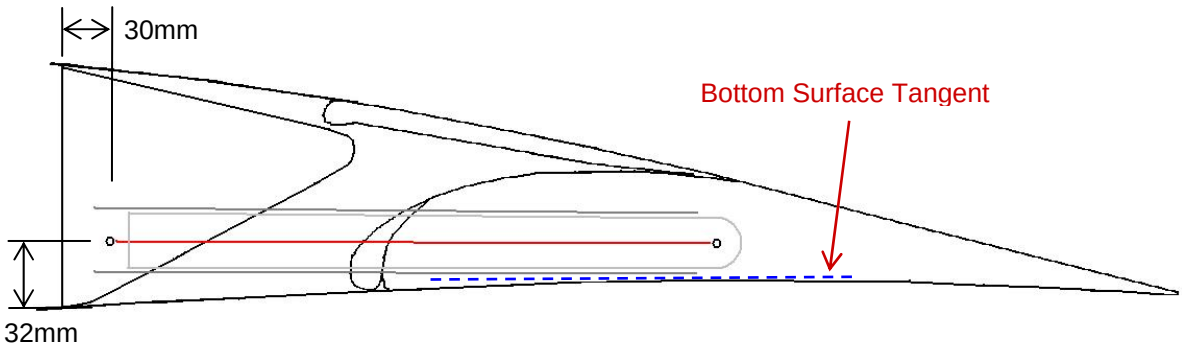

Figure 5.6 Main flap suspension wing attachment location

5.2.3 Main Slider Dimensions

It is only now that an actual very rough dimensioning of the main slider can be done. As explained in chapter above, it must not be higher than 20mm. Therefore its width and thicknesses must be chosen accordingly. Figure 5.7 below shows the front part of the slider, which is designed fail-safe by gluing together two standard profiles (see also figure 3.26 on page 43). These combined profiles make up the main slider width which is 30mm, a dimension obtained through various iterations and taking into account many different constraints.

Figure 5.7 Main slider (raw)

A bolt attachment element is added to the main slider. The main flap support bolt is inserted there and finally the main flap support ball joint.

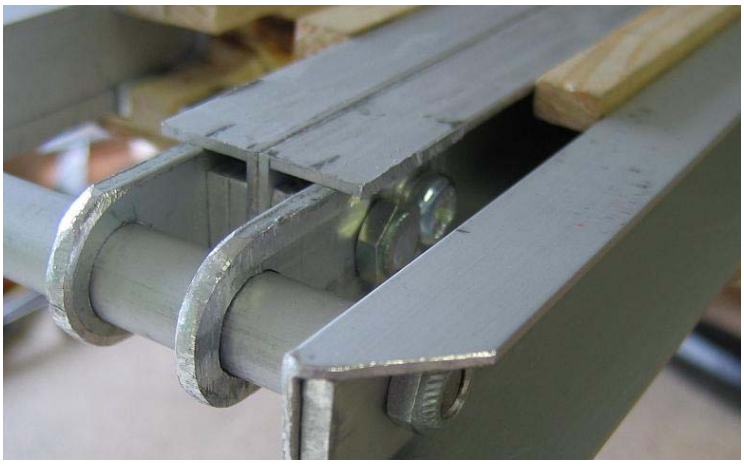

Figure 5.8 Main slider with bolt attachment element

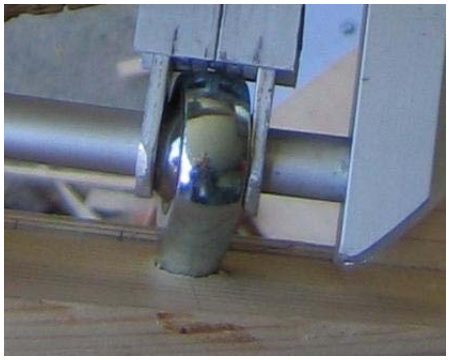

Figure 5.9 Flap main support ball joint attached to main slider

With the dimensions shown in figures 5.5 and 5.6 above, an approximately 300mm long main slider results, with a minimum guide overlap of 100mm. Therefore, in the flaps fully extended position the main slider lever arm is about 200mm long. For stress calculations real dimensions must be used, i.e. in the following calculation the arm length is 800mm and the maximum slider height 80mm, the width being 120mm.

The loading case +2.5g / tab 30° down with flaps extended yields the highest bending stress on the main slider since this is the point where the highest loads occur (see graph in appendix D). Half of the respective lift value of L = 81kN will be used in the calculation since two flap track stations bear the flap load (main support angle will be neglected). Two factors of 2.5 (operation range +2.5g) and 1.1 (standard safety factor) are applied. As the design is such that jamming of ball joints etc anywhere in the mechanism does not influence the main slider directly, a jamming safety factor of 1.7 is not applied here. However, fatigue is an issue which must be accounted for, so as a first measure a safety factor of 2 is appropriate, and it is introduced as a multiplication of the load rather than a reduction of the material constant since the latter is not yet known.

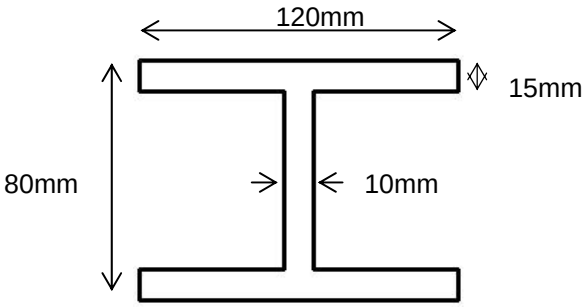

Figure 5.10 Main slider dimensions

$$M = 200mm \cdot \left(\frac{81kN}{2} \cdot 2.5 \right) = 20250kNmm$$

$$I = \frac{120 \cdot 80^3}{12} - \frac{(120-10) \cdot (80-2 \cdot 15)^3}{12} = 3.97 \cdot 10^6 mm^4$$

with $z_{max} = 80mm/2 = 40mm$

$$\sigma = \frac{M}{I} \cdot z_{max} = 204 N/mm^2$$

Therefore, with a standard safety factor of 1.1 and another one of 2 for fatigue show that the main slider material should have an elastic limit of at least 450N/mm^2, a value attainable with many steel and titanium alloys. Due to fatigue issues aluminum is not recommended for the main slider, even though the necessary strength may be attained.

This calculation proves the selected dimensions to be appropriate as a first design, though not optimized. So in demonstrator scale the dimensions of the main slider are a height of 20mm and a width of 30mm.

5.2.4 Guide Structure Assembly

So far dimensions have only been set for the y and z directions, respectively. Figure 3.24 on page 42 already showed some basic proportions, and is displayed again below in fig. 5.11. A mounting plate has been suggested in chapter 3; the red lines roughly outline this plate. Note that with this mounting plate layout the actuation screw needs to be placed somewhat further away than shown below.

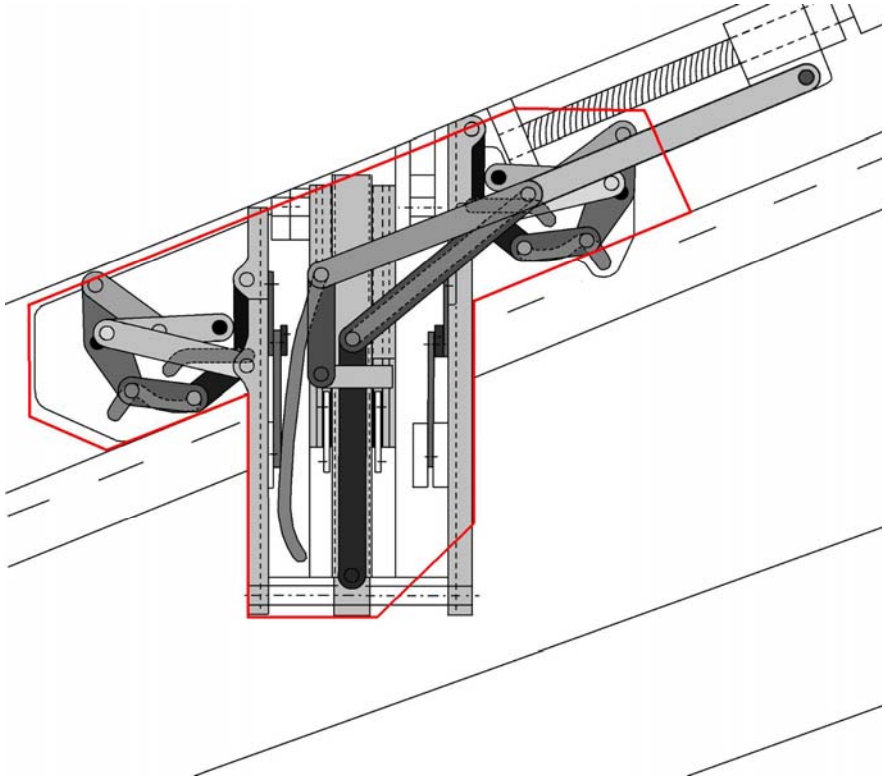

Figure 5.11 Mounting plate environment

In the following figure the dimensions used in the demonstrator model are shown. The blue dash-dot line is equal to the main flap suspension wing attachment location as explained in chapter 5.2.2 above and is therefore one of the main flap hinge lines. The red dashed line is the reference line for the figures above which show the configuration in y-z direction.

The width is chosen to be 170mm, which is basically the result of an iterative process (as well as the other dimensions shown). It should not be much wider than current flap track fairings so as not to impair flap efficiency too much in comparison to current flap track systems. Figure 1.2 on page 2 shows the approximate width for an A340 fairing to be about 0.5m, or 125mm in demonstrator scale. The chosen width is therefore about a third larger than this reference.

The reason for chamfering the bottom right corner will be explained later in chapter 5.7.2; it is done to avoid collision with the flap's top structure due to the β flap rotation angle as well as structural problems.

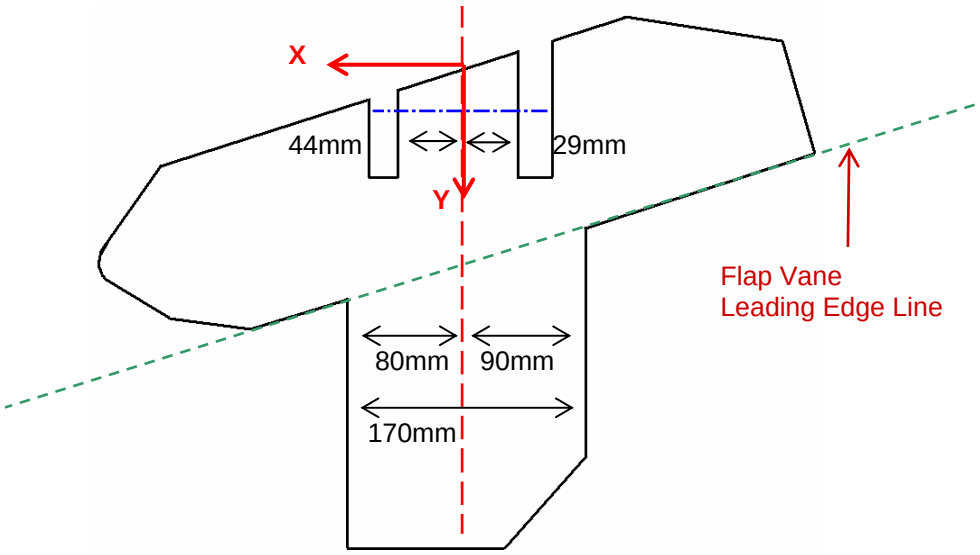

Figure 5.12 Mounting plate basic dimensions

There are two main suspension elements which on one hand allow a fail-safe design and on the other hand permit lengthening the main slider if the main suspension bolt is doubled rather than a single bolt. Another advantage of two suspensions is that lateral forces can better be absorbed. The distance between them should therefore be as large as possible, but it is limited by various constraints which will be discussed later. The dimensions shown in fig. 5.12 above are found to be practical. Dimensions not shown are either given by the design environment (such as the flap vane's leading edge line) or will be introduced in the appropriate chapter.

The raw mounting plate of the demonstrator looks as follows (with some guide elements already mounted).

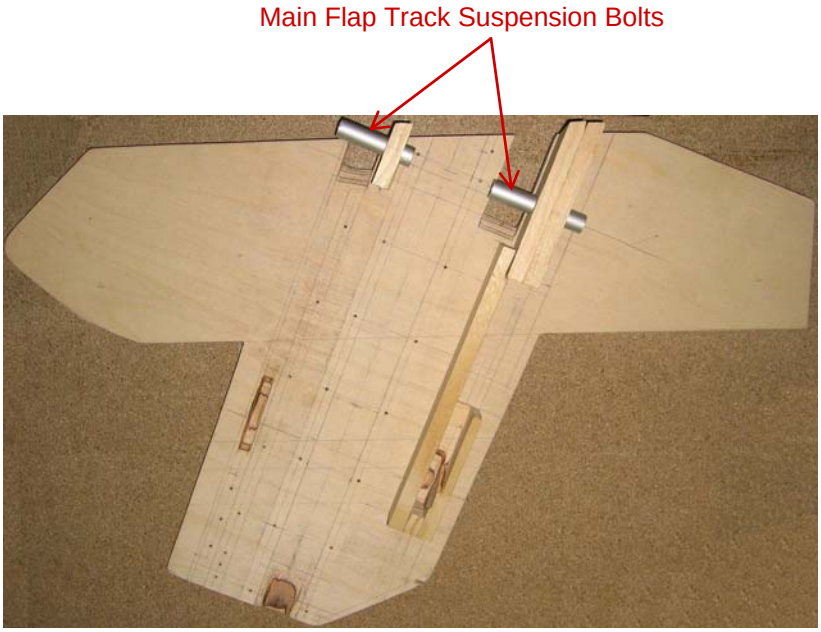

Figure 5.13 Mounting plate with main suspension bolts

Fig. 5.14 below shows the main slider in flaps retracted state, embedded between its guides which are fixed to the mounting plate.

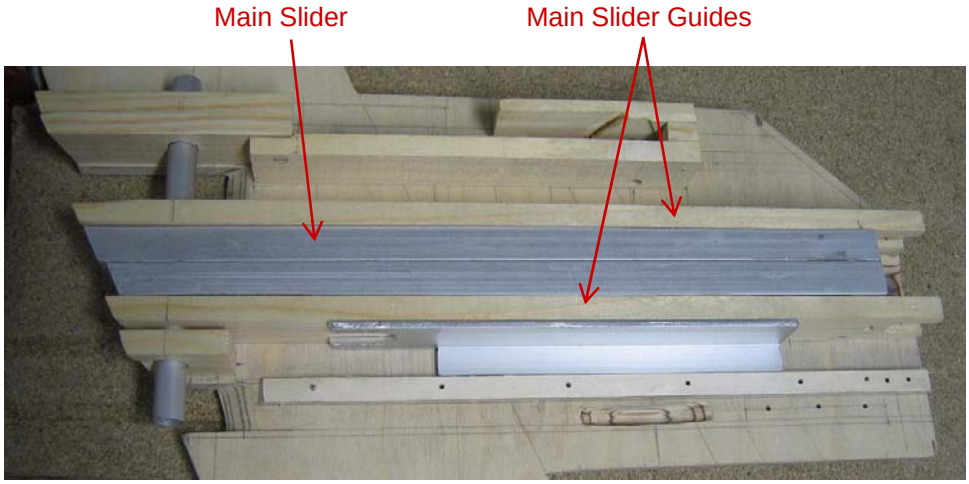

Figure 5.14 Embedded and retracted main slider with guides

Since the guides are fixed on the mounting plate they can as well act as distance pieces, or as a web rib if embedded in a lightweight construction: a cover plate, basically the same part as the mounting plate is attached at the top of the guides. This cover then acts as a flange, greatly increasing the bending stiffness of the assembly. As the main slider dimensions are already chosen such that it is able to bear real flap loads, there is good reason for assuming that the guide structure assembly will do so as well. A folding strengthening mechanism as described in chapter 3.2.5 will therefore not be included in the demonstrator.

The cover acts, at the same time, as a base for both the auxiliary cam and the main slider control link/cam. Fig. 5.15 below shows the mounted cover with some cam elements attached (it equally shows the transformation locking mechanism which will be explained in chapter 5.4). Figure 5.16 shows a side view of the built-in full guide structure assembly with the relevant features visible.

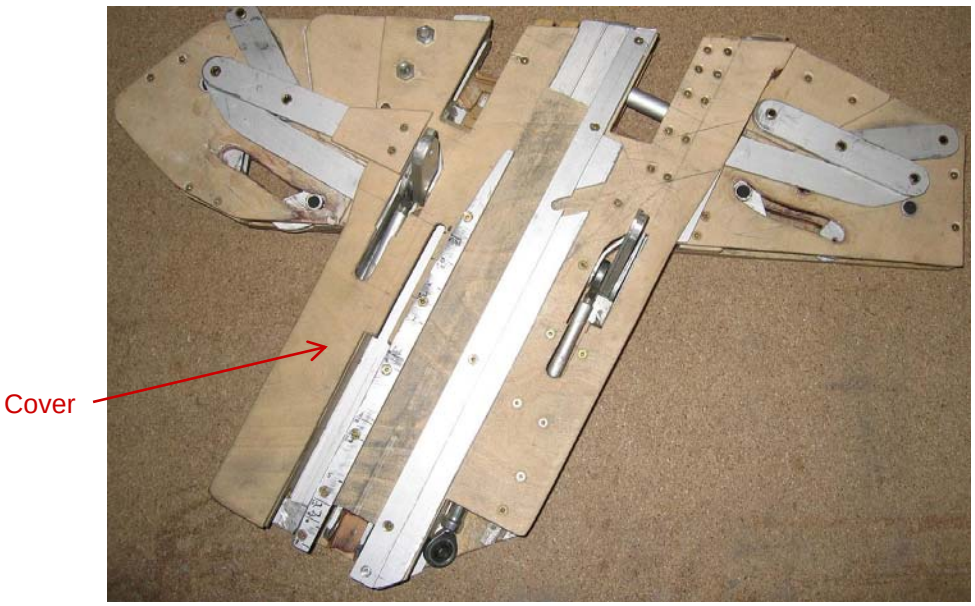

Figure 5.15 Guide structure assembly with cover attached

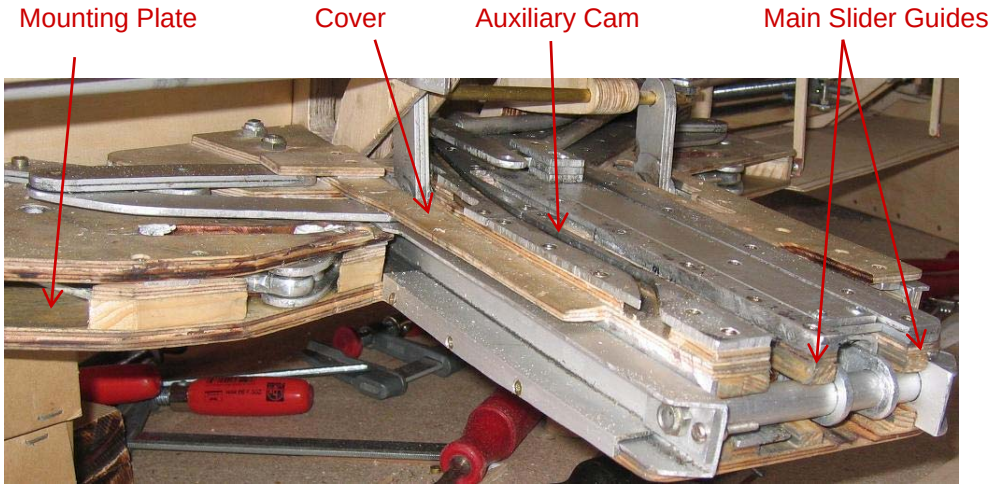

Figure 5.16 A first functional check of the guide structure assembly

It does make sense to attempt to design this guide structure assembly in way that it can be easily detached as a whole, both from the flap and the main wing structure, while moving parts like sliders and levers remain in this assembly. This allows better and less costly maintenance (better access if detached) and replacement, if needed; i.e. such a unit could be replaced quickly as a whole without the aircraft being grounded for a long time.

5.3 Support Angle Control Linkage

5.3.1 Vertical Section Dimensions

As with the main slider positioning there are again several contradicting requirements with the support angle control linkage.

First, the secondary suspension point must be specified. It should be as much up as possible (flap moment) and be at a backward position where it does not interfere with spoiler attachments and actuators. Here the approach of using two main suspension elements in conjunction with a swept wing may create problems since the inboard element would protrude into the spoiler (see also figure 5.17 on the next page), which must be kept at a minimum. It is also intended to attach the spoiler directly to these main suspension elements to save the weight of other extra spoiler suspensions.

Another constraint is the suspension link's angular position in the flaps retracted position. An approximately vertical position as shown in fig. 5.17 is considered optimal to direct the load flow in a way that the support slider angle control link is not overly stressed. In order to keep the suspension link from penetrating the flap's top structure, the backward position as shown in figure 5.17 is deemed best with all constraints taken into account. Note that due to the main wing sweep angle the problem is more prominent with the inboard support angle linkage; but the dimensions as shown in fig. 5.17 are chosen such that the inboard suspension link only collides with the nose section of the flap's top structure ─ a part which is not considered relevant for the flap top stiffness and removed anyway for the guide structure assembly.

The position and angle of the suspension link having been set, this leaves only small margins for its length. On one hand it must not penetrate the wing surface bottom, and preferably it should neither do so with the mounting plate if possible. On the other hand, in order to avoid blocking as explained on page 32 in chapter 3.2.4, no angle may attain 180° or 90° in the flaps retracted position.

Finally, the main slider angle link must be specified. Again, the blocking avoidance approach applies, which entails that this link must be tilted downwards as much as possible. On the other hand, since the load flow produced by the flap moment must be as straight as possible, this link should be attached as far on the back as possible of the guide structure assembly, a requirement conflicting to the one just explained above. Furthermore, too long links are more likely to bend under compression load (which is the primary loading case due to aerodynamic lift of the flap). Therefore, the main slider angle link length is chosen such that it meets an additional requirement: to relieve the support slider angle control link as much as possible in the flaps extended position, both the suspension link and the main slider angle link should be parallel, i.e. the load flows directly through these two elements and into the main suspension element. With an attachment point on the guide structure assembly as close as possible to the bottom surface the length of the main slider angle link can be derived.

The setting as shown in fig. 5.17 on the next page shows a feasible approach which meets all of the above requirements as far as possible.

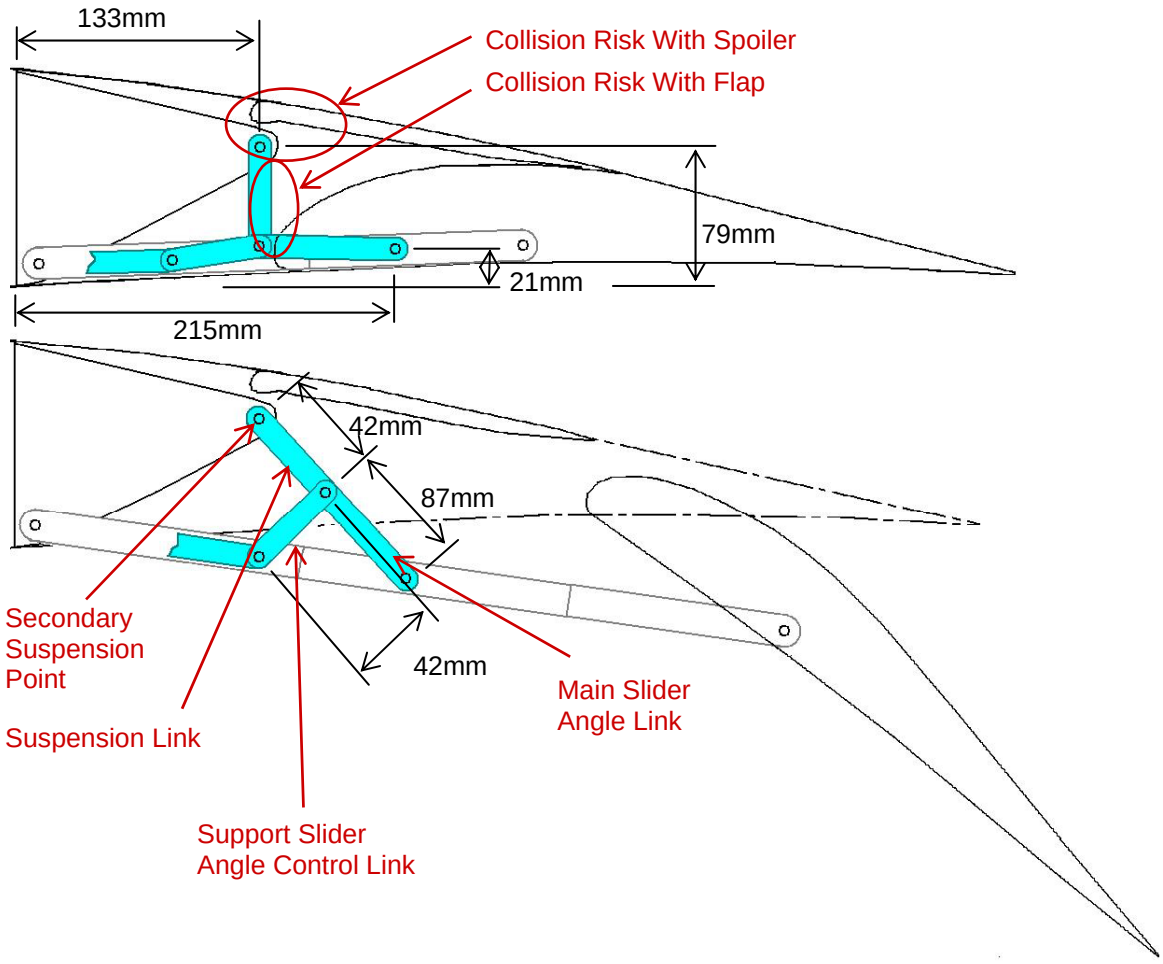

Figure 5.17 Support angle control linkage y and z dimensions

5.3.2 Lateral Configuration and Dimensions

Fig. 5.18 on the following page shows the actual layout of the support angle control linkage. In order to avoid tensions, joints are, wherever possible, designed as ball joints in aerospace engineering. For the linkage at hand this design is only applied for the main slider angle link. If the suspension link were equipped as well with ball joints the whole linkage would likely collapse under compression loads due to flap lift. Therefore, in order to prevent bending of the linkage, the suspension link is designed with axial bearings rather than ball joints.

Figure 5.18 Support angle control linkage (outboard)

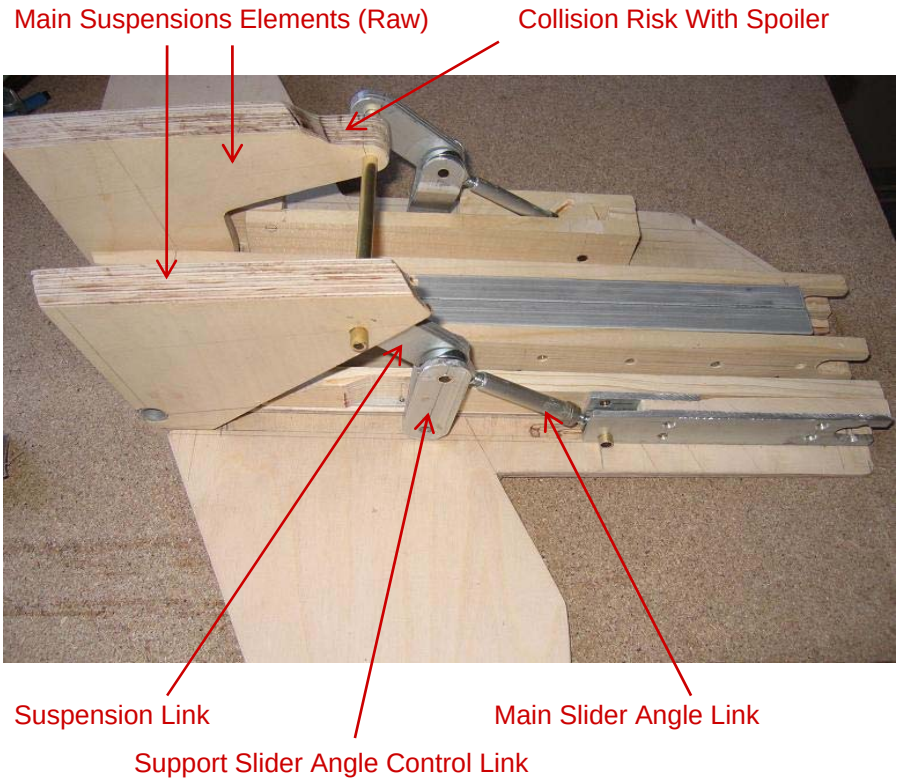

Figure 5.19 Support angle control linkage functional check

The inboard and outboard linkage assemblies are not exactly symmetric, as can be seen in figures 5.19 and 5.21. The reason is shown in fig. 5.20 on the next page: at the outboard linkage there is a collision risk between the main slider angle link and the auxiliary cam, therefore this link must be placed as far to the outboard side as possible. For the inboard linkage the collision risk arises between the main slider linkage and the suspension link, which entails that the suspension link must be placed as far to the inboard as possible.

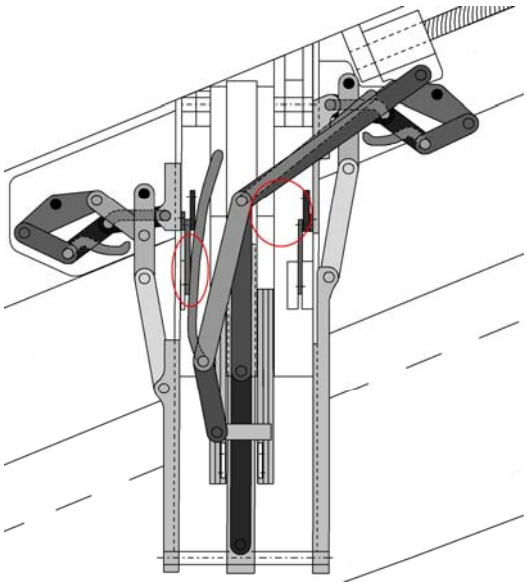

Figure 5.20 Support angle control linkages collision risk

Again, the exact positions of the individual links are the result of an iterative process which takes the auxiliary and main slider control linkage into consideration. The following figure shows the dimensions as they were determined accounting for all requirements.

Figure 5.21 Support angle control linkages x dimensions

5.3.3 Support Angle Control Linkage Sliders and Main Slider Appendages

As mentioned in chapter 3, the support angle control linkage sliders and main slider appendages are different on each side. The outboard slider looks as follows:

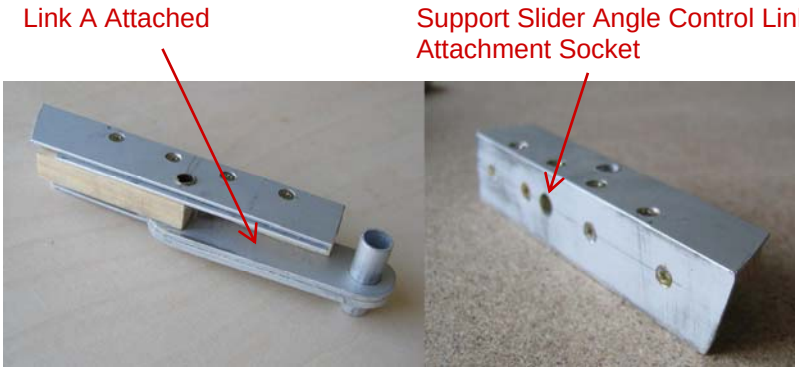

Figure 5.22 Outboard support angle control linkage slider (outboard/inboard view)

The slider has two guide elements on the inboard and outboard side. Note that the outboard guide needs to be designed in a way that it allows free motion of link A, while still providing satisfactory guidance to the slider when it is at a far aft position, i.e. the flaps extended position (see fig. 5.2.1 on the preceding page). In the model this is accomplished by a cut in the guide element as shown in fig. 5.23 below.

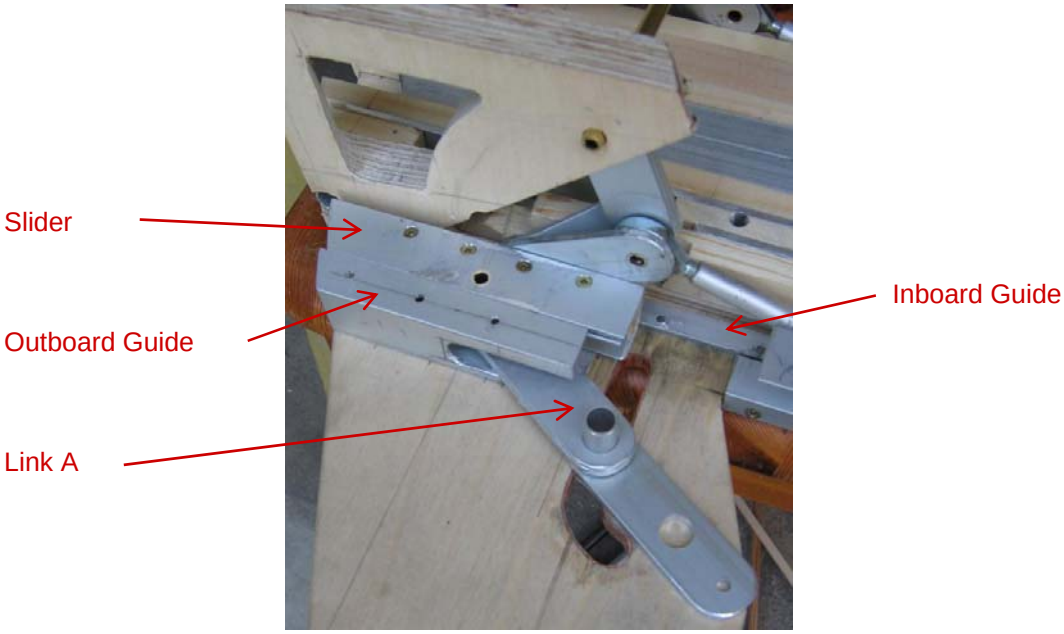

Figure 5.23 Installed outboard support angle control linkage slider

The outboard main slider appendage has essentially the same profile. On one hand, this avoids collision problems with guides of the support angle control linkage slider. On the other hand, this allows for an improved additional locking possibility if the appendage is designed such that it just meets with support angle control linkage slider in the flaps up position. The appendage is guided by a simple L-profile attached to the guide structure assembly.

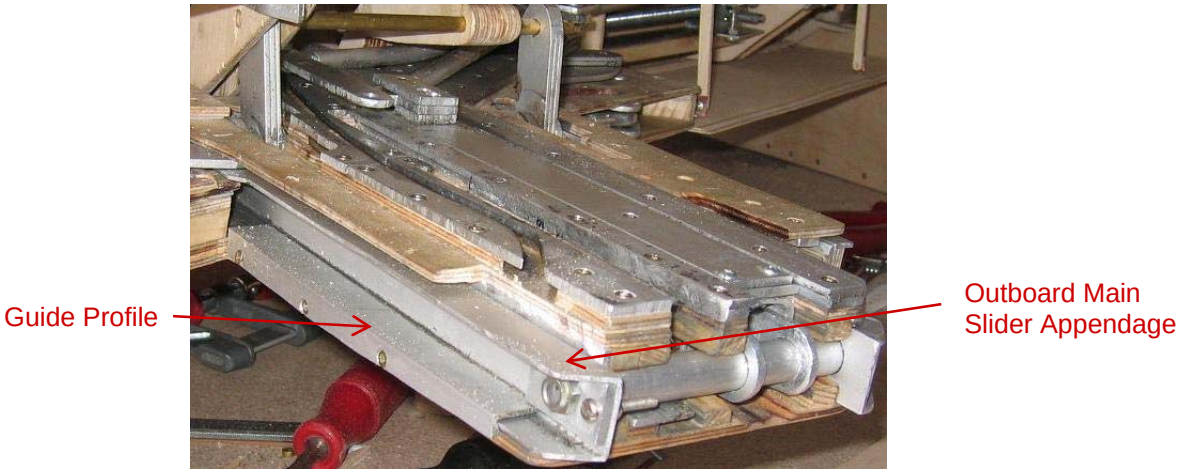

Figure 5.24 Outboard main slider appendage installed

Due to the wing sweep angle, the inboard support angle control linkage slider has its control link attachment socket farther away from the rear spar than the outboard one. On the other hand the link A attachment point needs to be set even somewhat closer to the rear spar due to constraints with the transformation locking mechanism cams (see chapter 5.4.1) Further, the inboard main slider appendage needs to be extended close to the rear spar in order to get the link C attachment point to the appropriate location. Thus, the inboard slider looks distorted when compared to its outboard counterpart.

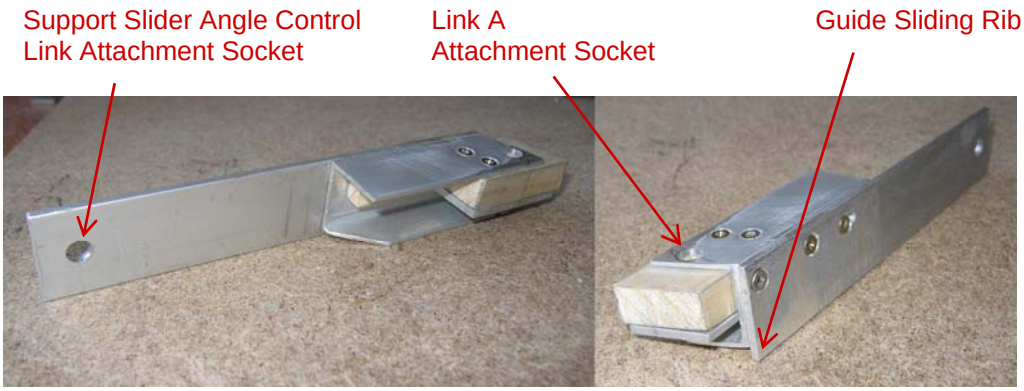

Figure 5.25 Inboard support angle control linkage slider (inboard/outboard view)

This distortion makes a simple guidance as with the outboard slider impossible. Therefore, the inboard slider has a guide sliding rib which assures a straight backward and forward motion, while it is kept from tilting by being clamped between the cover on the top and a clamping tread on the bottom, which at the same time provides the inboard boundary of the guide cam.

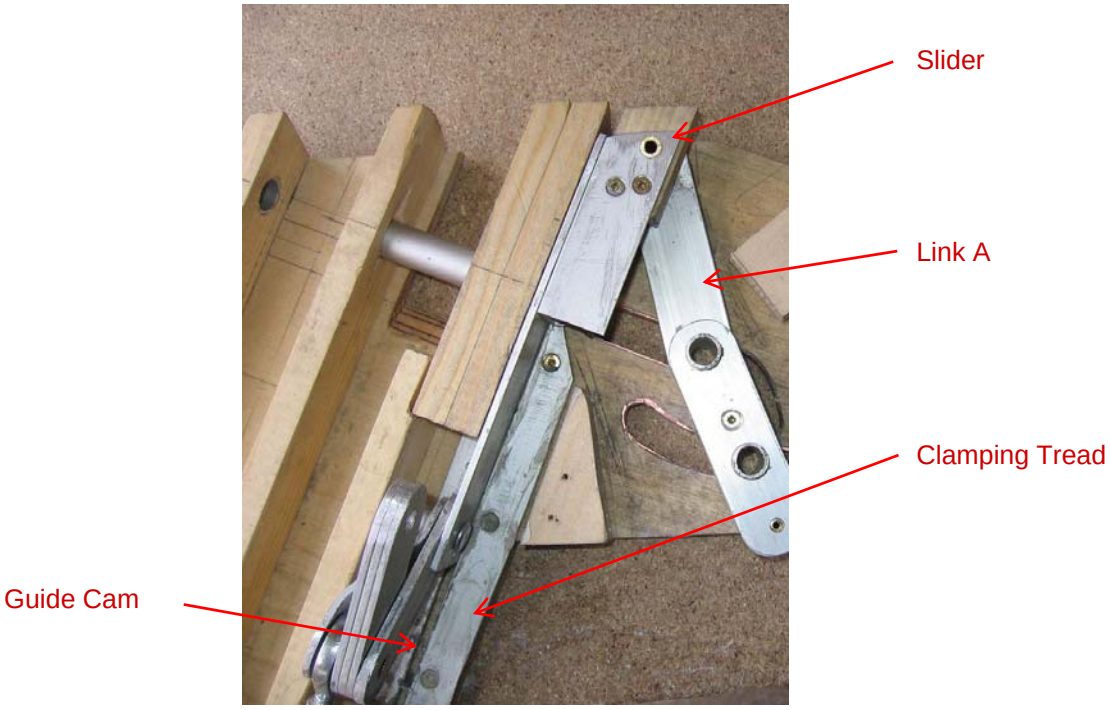

Figure 5.26 Installed inboard support angle control linkage slider

Again, the main slider appendage follows basically the same profile in order to benefit from the same guide cam and also for additional flaps up blocking reasons already mentioned with the outboard counterpart.

In addition, the inboard main slider appendage must not collide with the flap's top structure due to the β flap rotation angle; i.e. the same requirement which led to chamfering of the guide structure assembly. Chapter 5.7.2 will show the collision consequences if this is not taken into consideration. The two-part design as shown in fig. 5.27 below meets the requirements; besides, the flap vane actuation linkage (further detailed in chapter 5.7) also needs an attachment point somewhere on the main slider or its surrounds and it can thus be easily accommodated between the two parts. Note: the final design of the flap vane control link is shown on fig. 5.28 and differs slightly from the layout shown in fig. 5.27 below.

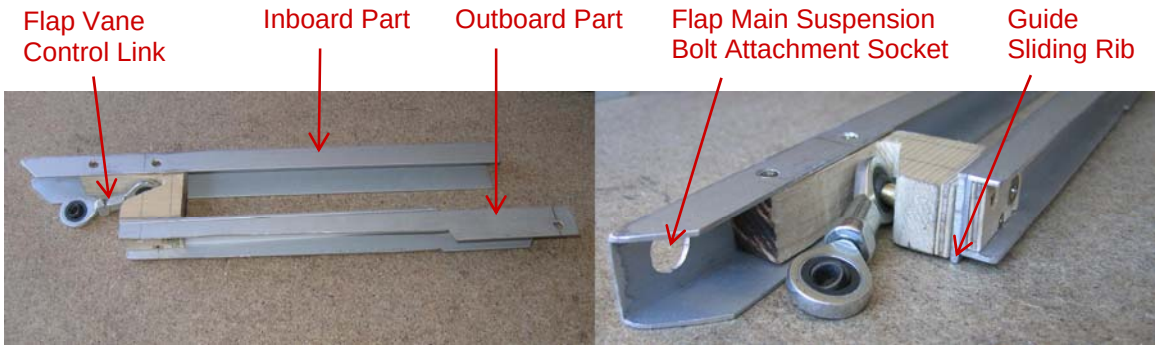

Figure 5.27 Inboard main slider appendage

This design further takes into consideration that enough space is needed for the inboard main slider angle link attachment as well as the whole inboard support angle control linkage as shown below.

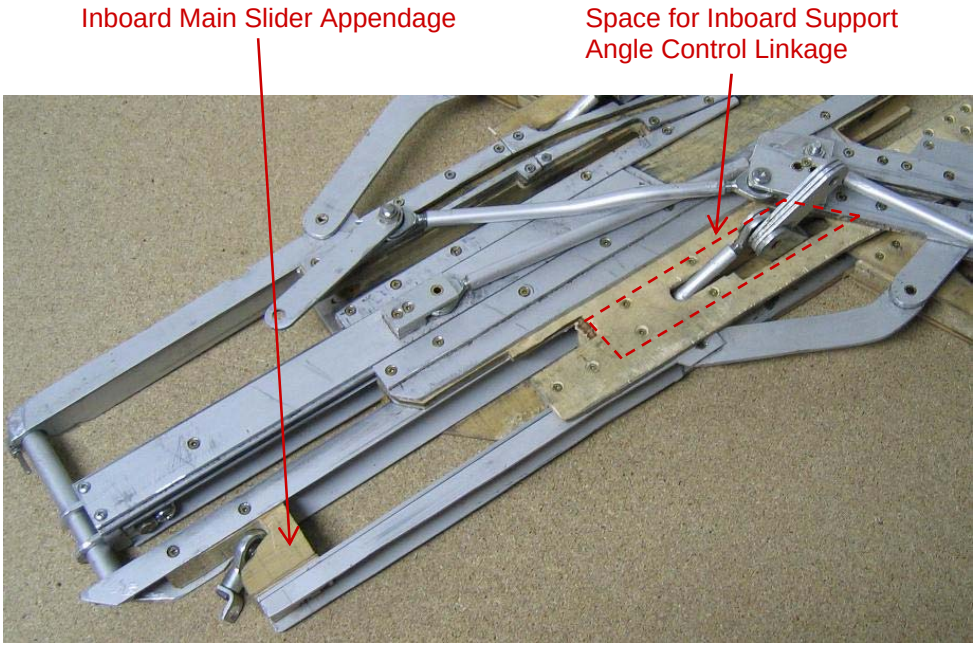

Figure 5.28 Installed inboard main slider appendage

However, this design does not allow a twofold flap angle control slider as was suggested in fig. 3.25 on page 43. This space is now needed by the outboard part of the inboard appendage, as shown above. Nevertheless, using only one flap angle control slider even simplifies the whole design; this part of the mechanism will be discussed in chapter 5.5.4.

5.3.4 Main Suspension Elements

As explained at the very beginning of this report, a requirement of this project is to demonstrate that with integrated flap tracks it is still possible to accommodate all electrical and hydraulic systems on the back of the rear spar. This means that the suspension elements need to be cut at some point, and figure 5.29 on the next page shows where this is best done. Due to constraints as explained on page 65 above, the guide structure assembly is limited anyway in its vertical dimensions. So there is enough space on top of it for other systems, and it is there where the cutouts are placed on the suspension elements. They are not structurally optimized, however. Besides, in a lightweight construction the elements are unlikely to be solid blocks as shown in figure 5.29. Chapter 6.3.4 will show a detailed and more optimized construction of them. Note the relatively long arm of the inboard suspension element; this is necessary because main slider auxiliary cam link must be stowed between this element and the guide structure assembly (see also fig. 5.45), and the suspension link attachment point is relatively far behind the rear spar.

The dashed lines in figure 5.29 show the approximate upper and lower boundaries of the guide structure assembly in the flaps retracted position.

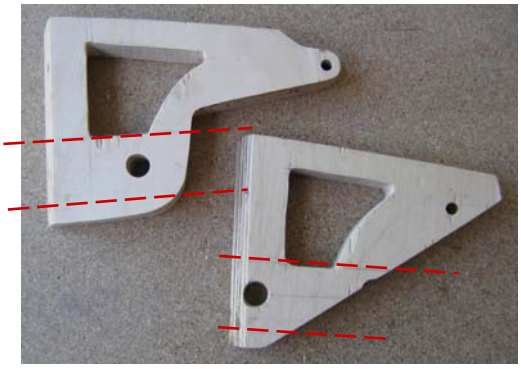

Figure 5.29 Inboard and outboard main suspension elements

Due to the wing's sweep angle these main suspension elements are not mounted perpendicular to the rear spar, but at an angle of 67°, or 23° to the normal, respectively.

Figure 5.30 Main suspension elements mounted on the rear spar

5.4 Transformation Locking Mechanism

5.4.1 Programming Cam and Sliding Bolt Placements

As mentioned on page 44 in chapter 3.3, there is a problem yet to be solved with the programming cam of the transformation locking mechanism: the cam interferes with the flap vane in the flap retracted position as shown on the next page in fig. 5.31.

While link F and G actually just fit within the limited space in front of the flap vane's leading edge, the cam itself does not since it must ensure the desired link positions also when flaps are fully extended. So far the design assumed, to simplify the construction, that the programming cam sliding bolt and the connection of link F and G are basically the same.

If the cam sliding bolt is placed somewhere in the middle of link F then the programming cam would move forward and the collision problem can be solved; however, this could now lead to a collision with the transformation and locking cam (depending on the sliding bolt diameters). The ratios as shown in fig. 5.32 represent an appropriate trade-off meeting these constraints.

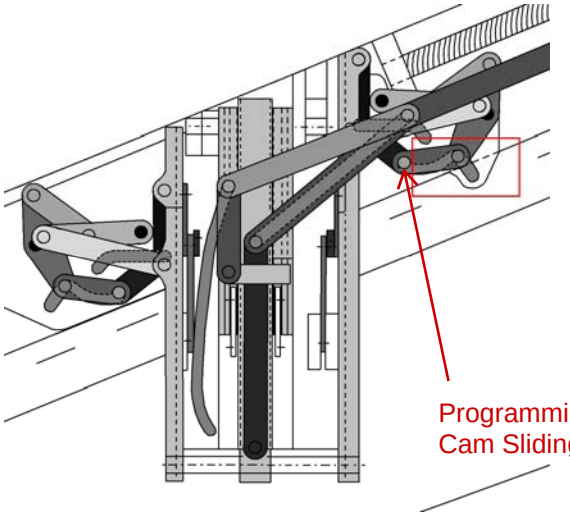

Figure 5.31 Collision: programming cam and flap vane

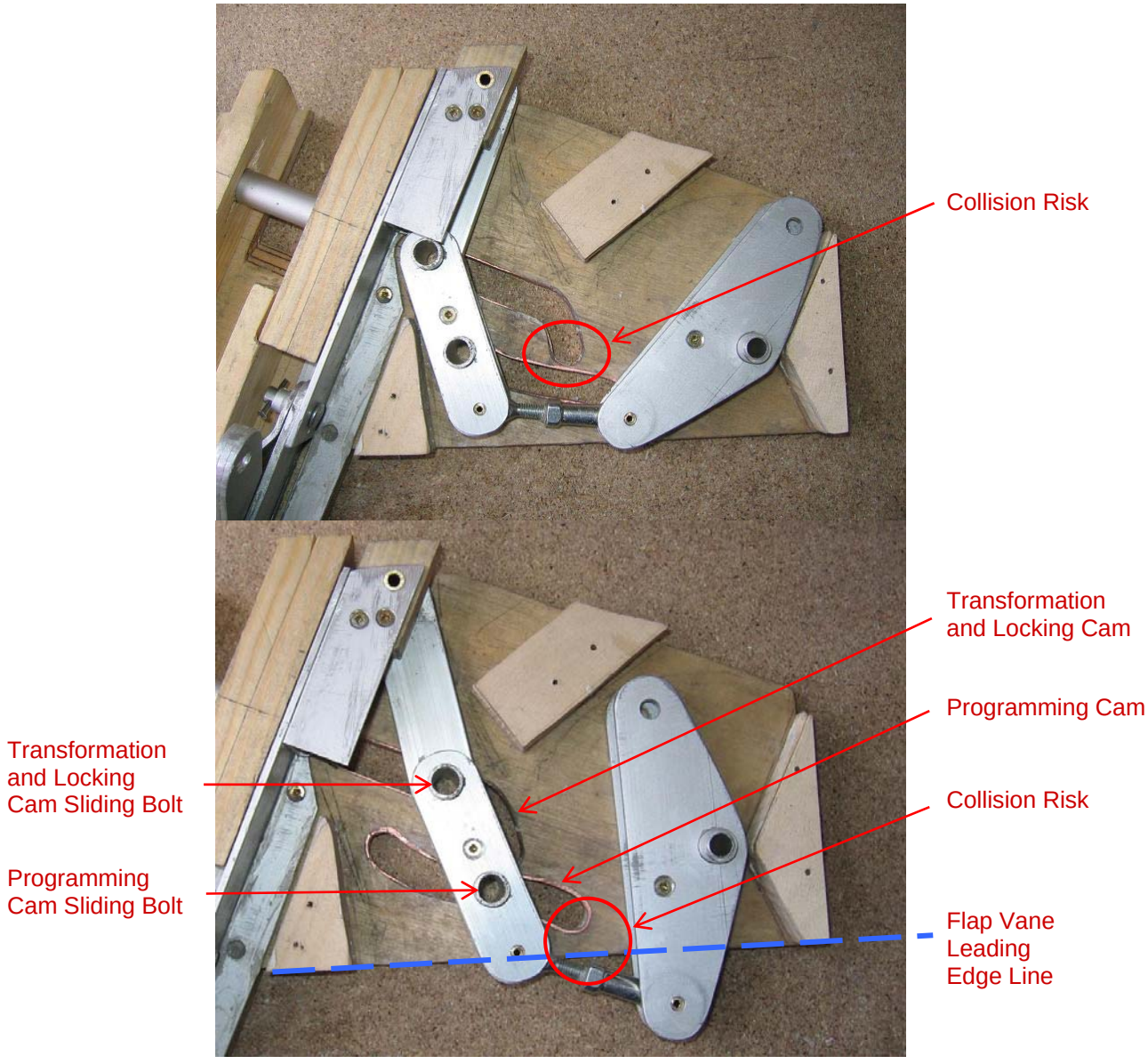

Figure 5.32 Programming cam sliding bolt placement and collision problems

5.4.2 Vertical Layering and Fitting

To accommodate all links of this rather complex mechanism it is divided in two parts, a lower and an upper one.

For maintenance and production cost reasons the transformation locking mechanism uses identical parts placed symmetrically for the inboard and outboard side. This entails much design and trade-off work to find the most appropriate lengths and ratios for each of the parts. In particular they must all fit within the space between flap vane and rear spar in the flaps retracted position.
Figure 5.33 shows a satisfactory approach where this requirement is met; the dashed blue line represents the flap vane leading edge line.

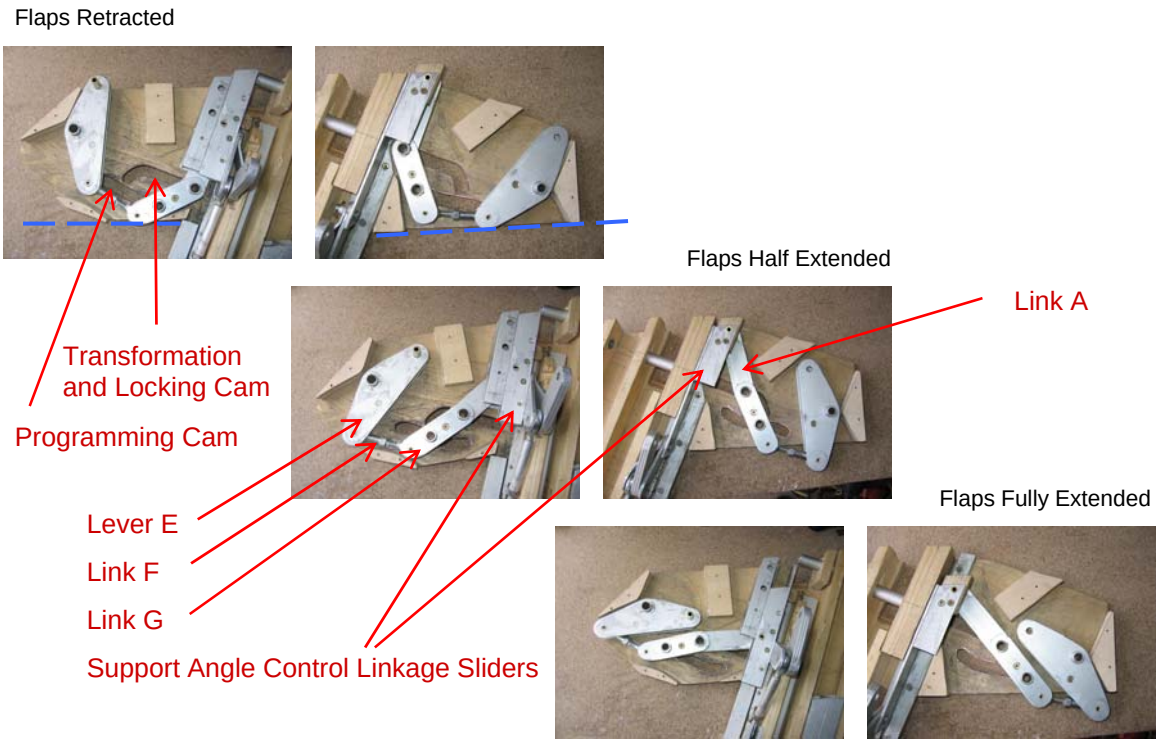

Figure 5.33 Transformation locking mechanism (lower part)

Since the intention of the transformation locking cam is to transform small loads on link G into high loads on link A and the connected slider, rather high loads are expected to act on this cams' sliding bolt, which acts at the same time as the connection of links G and A. A symmetrical load transmission from this bolt into the guide structure assembly would therefore be highly desirable to prevent the bolt and link from tilting and punctiform overstressing of the cam surface. Similar considerations apply to the lever E bolt. Therefore the same two cams are included in a plate which is added to the guide structure assembly right on top of these links, but somewhat lower than the cover already discussed in chapter 5.2.4 above. These mounting plate top counterparts are shown in figure 5.34 on the following page.

This figure shows as well the top part of the transformation locking mechanism. It is designed very thin so that it does not consume much space in the vertical direction; it just fits within the top cover and the mounting plate top counterparts.

To allow this compact design, however, the link C needs to be curved to avoid collision with link D. If it were still straight, other constraints could not be met (this is again the result of an iterative process). This is shown on the right of fig. 5.35 below, where the dashed lines represent hidden link edges. The concept and design of the linkage is such that link C will not be stressed very much in comparison with other parts. Therefore such a bend is considered to be tolerable.

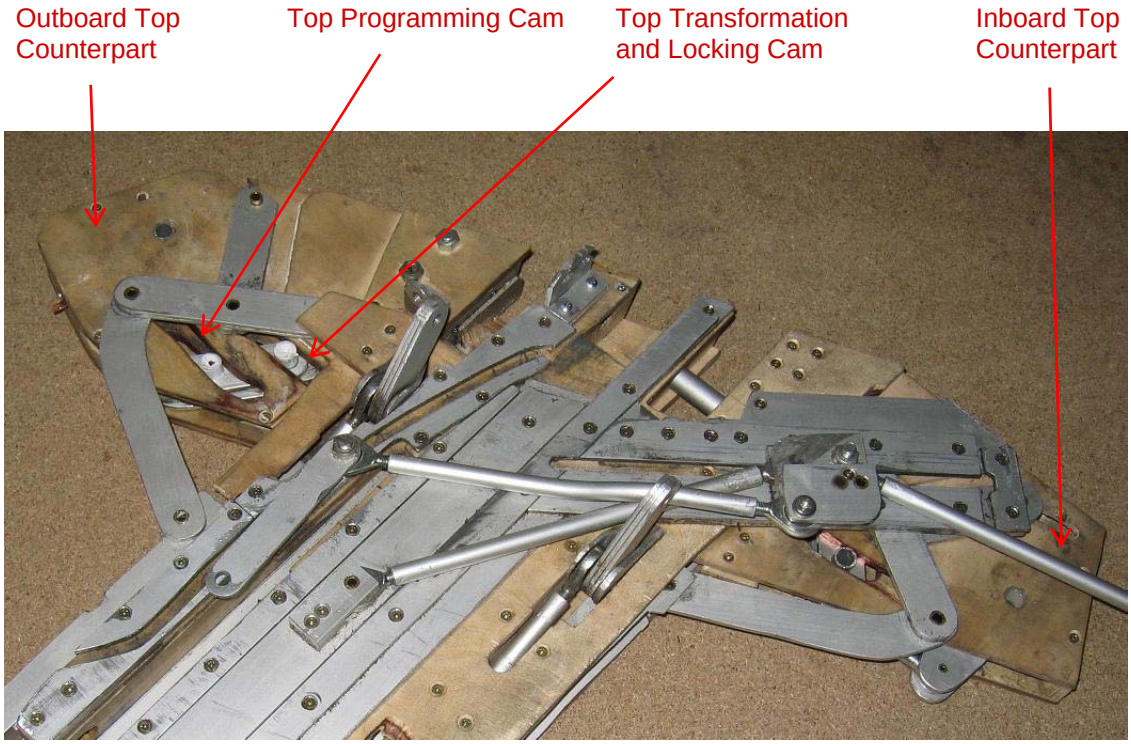

Figure 5.34 Mounting plate top counterparts

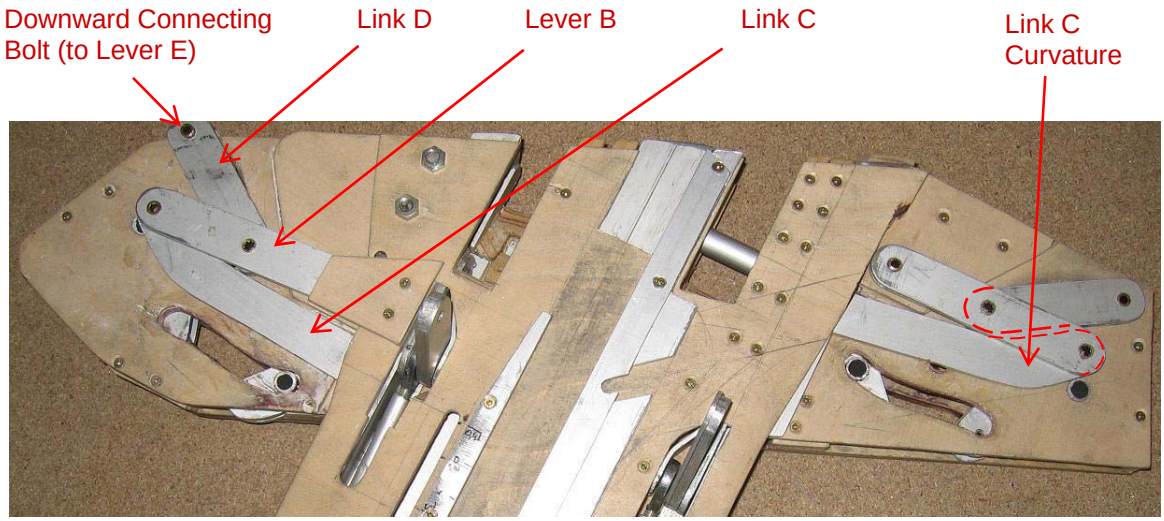

Figure 5.35 Transformation locking mechanism (upper part, flaps retracted)

The specific programming cam shape was found by setting the desired main suspension angle and corresponding main slider extension for various configurations, then locating the appropriate cam sliding bolt positions. For an actual airliner design this hands-on approach would of course be replaced by an exact 3D mathematical curve calculation.

5.5 Main and Flap Angle Control Slider Linkage

5.5.1 Main Slider Actuation

As mentioned on page 44 in chapter 3.3, the main slider is actuated via an additional link (dark red in figures 3.24 and 3.25) which is connected at about the position of the main flap support bolt. Due to the nature of the linkage, near the flap retracted position there is a high sideward force acting on this additional link as the connected main slider link pushes/pulls at a rather large angle. However, the main slider should not be stressed further laterally since its task is to mainly bear the regular flap load which acts in the z and y direction. Therefore, the connection of the additional link (which will now be called main slider control slider) and the main slider should be such that no lateral forces are transferred between the two, but only the extension motion. This is accomplished by a twofold thorn which is clamped between main slider profiles and main flap support bolt, but otherwise is able to move freely. The main slider control slider has its own guides mounted on the cover, which absorb lateral forces acting on it. Smooth motion is ensured by a guide sliding rib on each side of the slider.

Figure 5.36 Main slider control slider

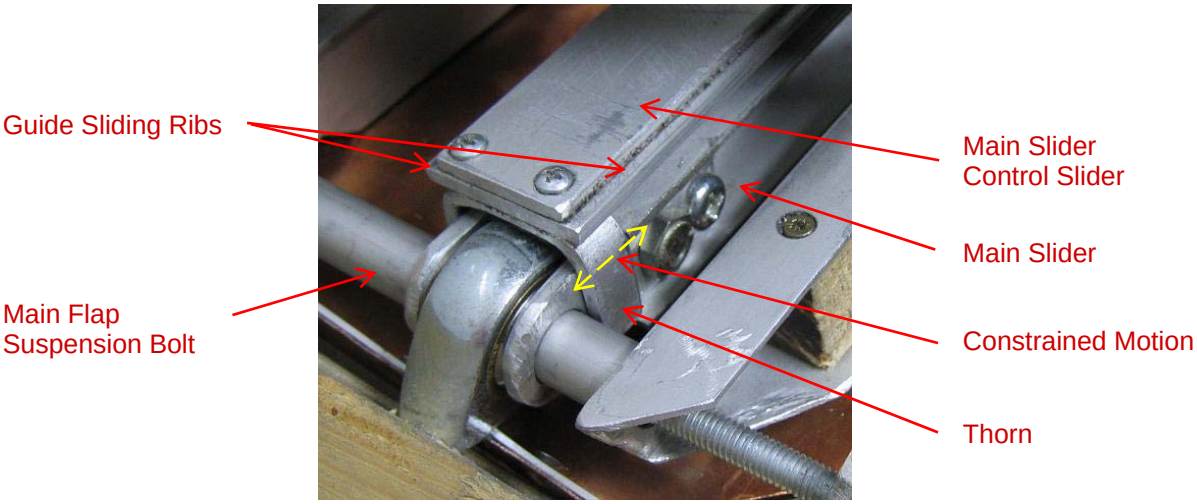

Figure 5.37 Main slider control slider installed

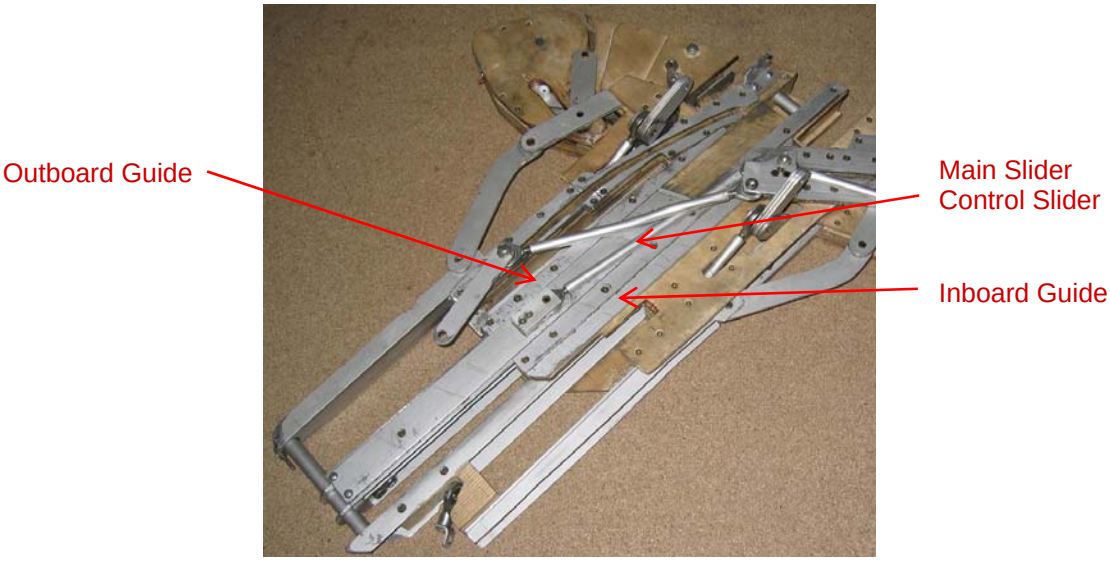

Figure 5.38 Main slider control slider guides

The main slider link is designed as a straight standard part with a ball joint at each end. It is connected to the main slider control slider through a bolt/crank element at the appropriate location.

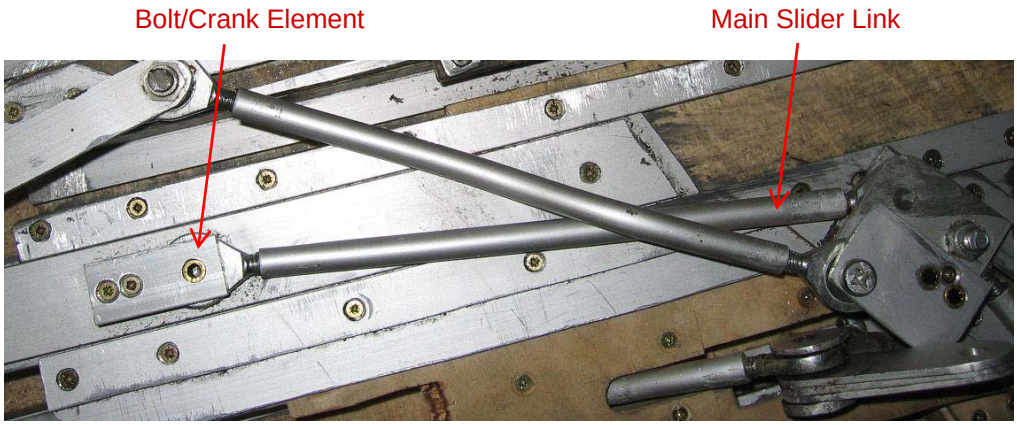

Figure 5.39 Main slider link

This attachment location depends on a number of constraints such as the main (linear) cam position, the main slider link and the collision risk with the inboard support angle control linkage as shown in figures 5.40 and 5.41 on the following page. Attention must be paid to the main slider link motion, which in fact forms a hyperbola, i.e. a collision risk with the support angle control linkage arises, not at the flaps fully extended or retracted positions, but somewhere in the middle.

The following figure shows the configuration with the main slider about 20% extended. Since the support slider angle control link is still fairly down the main slider link just passes without colliding.

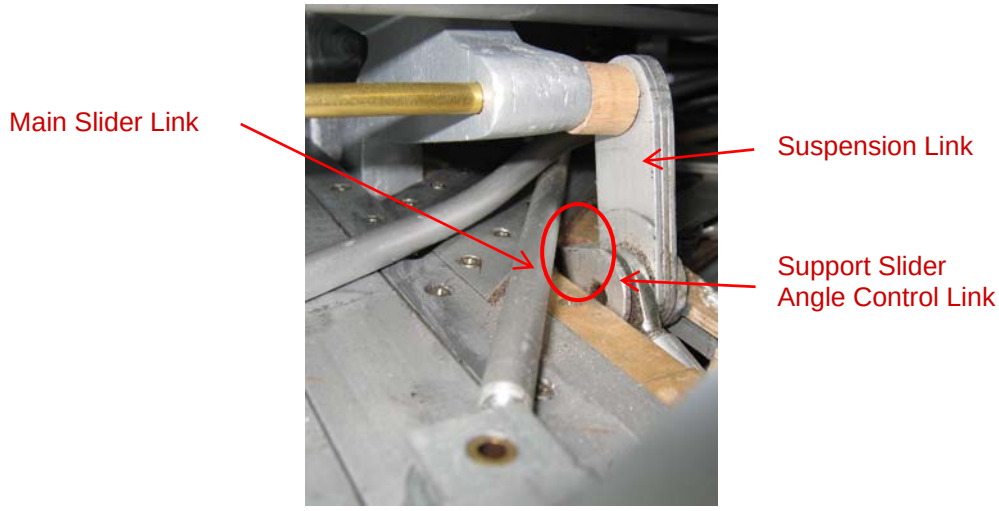

Figure 5.40 Main slider link collision risk (main slider about 20% extended)

When flaps are further extended the support slider angle control link comes up and leaves no more space for the main slider link to pass. But since the main slider link has moved further on the hyperbola it still fits in without collision, also due to the support slider angle control link's design which is bent to one side (see also fig. 5.18) and therefore leaves enough space for the main slider to pass by, as shown in fig. 5.41 below.

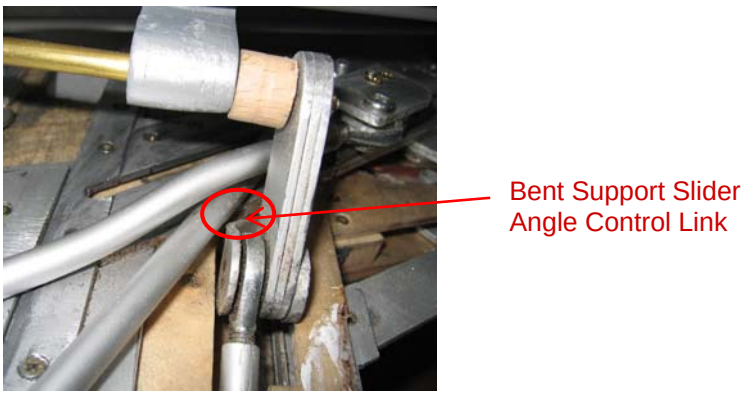

Figure 5.41 Main slider link collision risk (main slider about 70% extended)

5.5.2 Main Cam and Sliding Element

The main slider link is attached to a main cam sliding element instead of a main cam sliding bolt as was suggested in chapter 3.2.2 on page 29. Due to various constraints explained in the next chapter the auxiliary cam link needs to be attached somewhat offset as shown in fig. 5.44. This also requires that rotation of this element be blocked; this is done by a cam sliding rib which extends along the element.

The cross section shown in fig. 5.42 on the following page corresponds roughly to the location indicated by the cyan dashed line in fig. 5.43.

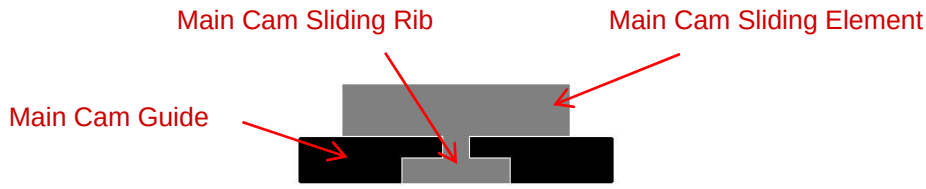

Figure 5.42 Main cam and sliding element cross section

The main linear cam is very thin (only about the main slider control slider's thickness) and mounted on the cover. The upper part of the transformation locking mechanism just fits in beneath that cam.

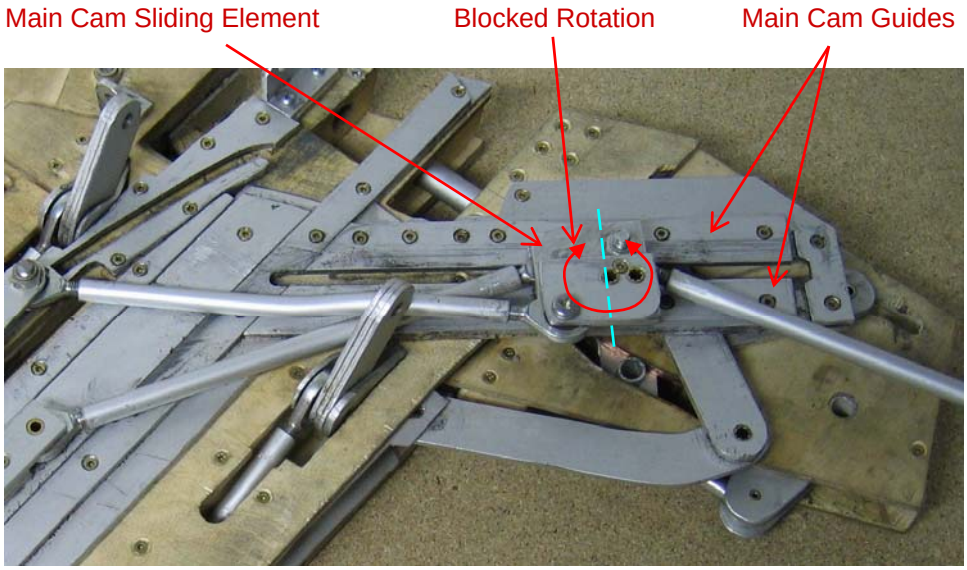

Figure 5.43 Main cam sliding element

5.5.3 Auxiliary Cam and Links

As mentioned above there are several constraints which the auxiliary cam slider and link must meet. The design process has shown that within the given setting this is not possible if the auxiliary and main slider links are attached at the same location on the main cam slider. However, they can be met by offsetting and bending the auxiliary cam link as shown in fig. 5.44. Since the design concept is such that the auxiliary cam link does not experience loads of the same magnitude as the main slider link the bending does not adversely affect structural weight too much.

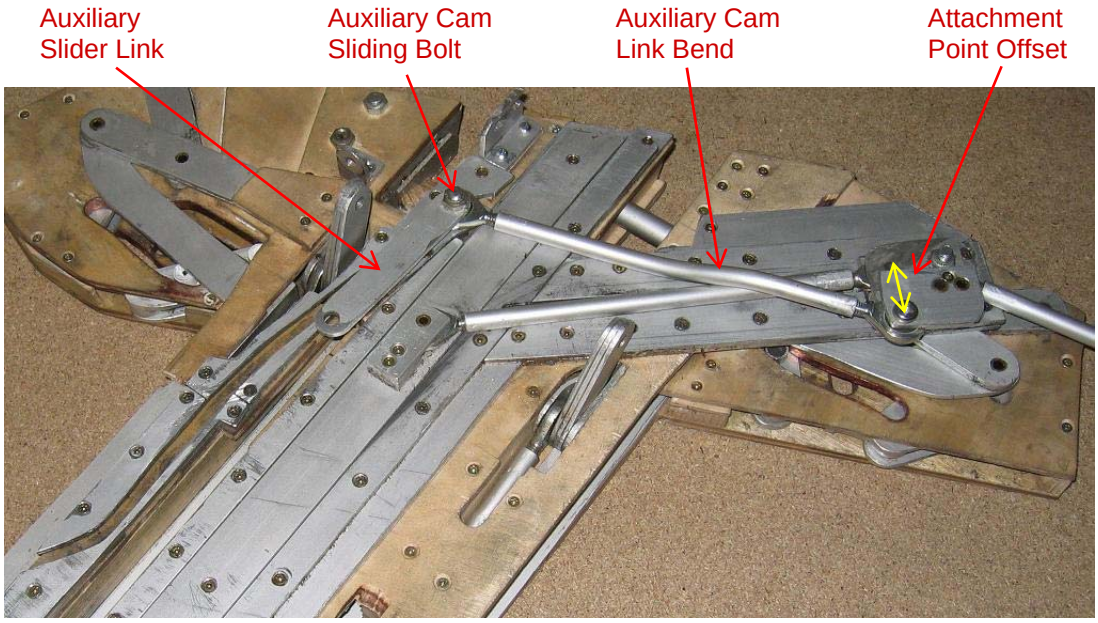

Figure 5.44 Auxiliary cam link layout and attachment

The following figures and explanations outline the set of constraints which led to this design, starting at the flaps retracted position and then listing the various collision risks encountered upon flap extension. All of these requirements are to be combined with the main intention of the auxiliary cam as a programming cam, i.e. to set the respective desired flap angle throughout the flap extension motion.

In the retracted position the auxiliary cam link must, together with the main slider link, fit in between the inboard main suspension element and the main cam mounted on the guide structure assembly. The main suspension element should be cut only where absolutely necessary, so as not to affect its structural behavior too adversely. This means that the element's arm should be as large as possible in the z-direction, this size being limited by the space needed for the auxiliary cam link (therefore the bend in the link). Furthermore, the sharp curve in the element should be as far away from the rear spar as possible to avoid interference with the cutout, and also for structural reasons; by offsetting the auxiliary cam link attachment point on the main cam slider this distance can be increased.

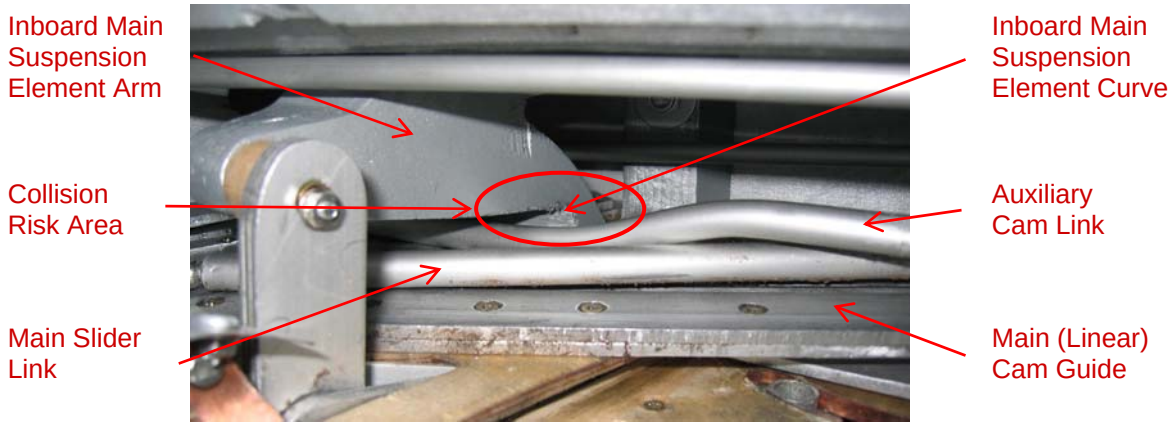

Figure 5.45 Auxiliary cam link (retracted position, view from inboard)

The same collision risk area marked in fig. 5.45 above is shown again in the following fig. 5.46, seen from the other side and referred to as collision risk area 1.

Further, the auxiliary cam sliding bolt must neither collide with the outboard main suspension element (collision risk area 2) nor with the main slider control slider (collision risk area 3).

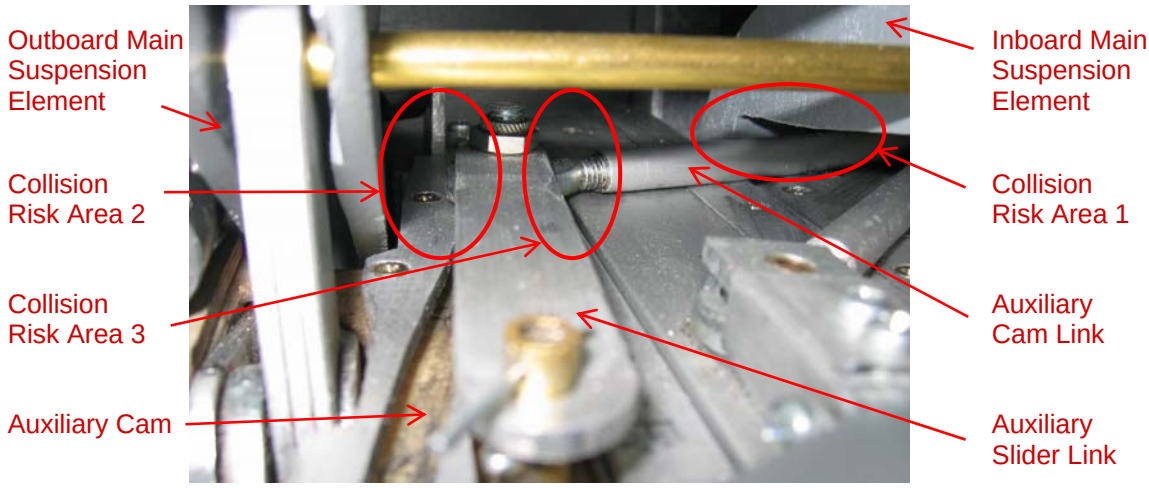

Figure 5.46 Auxiliary cam link (retracted position, view from back outboard)

When the flaps are extended the auxiliary cam sliding bolt travels along the cam and reaches the outboard support angle control linkage. At this point of extension, the support slider angle control link stays just below the auxiliary cam and thus does not interfere with the auxiliary cam link. It likewise just passes the outboard suspension link; this is possible since at this extension point the suspension link is still near the vertical position.

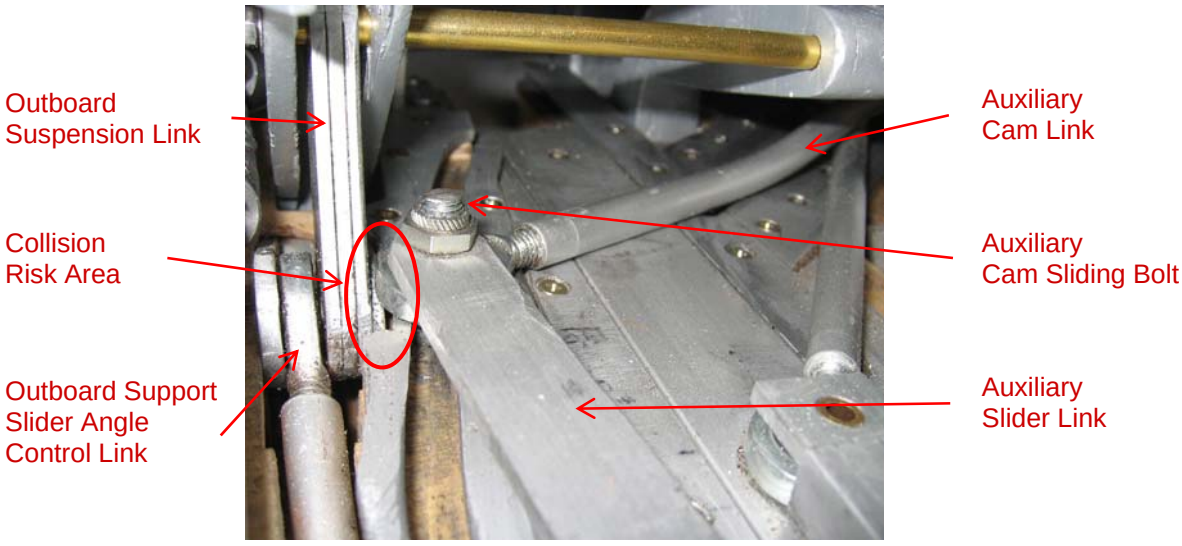

Figure 5.47 Auxiliary cam link (main slider 30% extended, view back outboard)

Figure 5.48 shows that support slider angle control link moves upward and the suspension link rotates backward soon after the auxiliary cam link passage; thus the auxiliary cam link could no longer pass now.

The figure shows as well a collision risk referred to as collision risk area 1 between the auxiliary (programming) cam and the slot in the cover which is needed for the flap angle control slider actuation bolt (see next subchapter). Note that the cam must also provide for the support slider angle control link passing.

While the suspension link's backward rotation may create problems with the outboard part, it is even necessary for the inboard part where just this additional space is needed for the auxiliary cam link to pass (referred to as collision risk area 2).

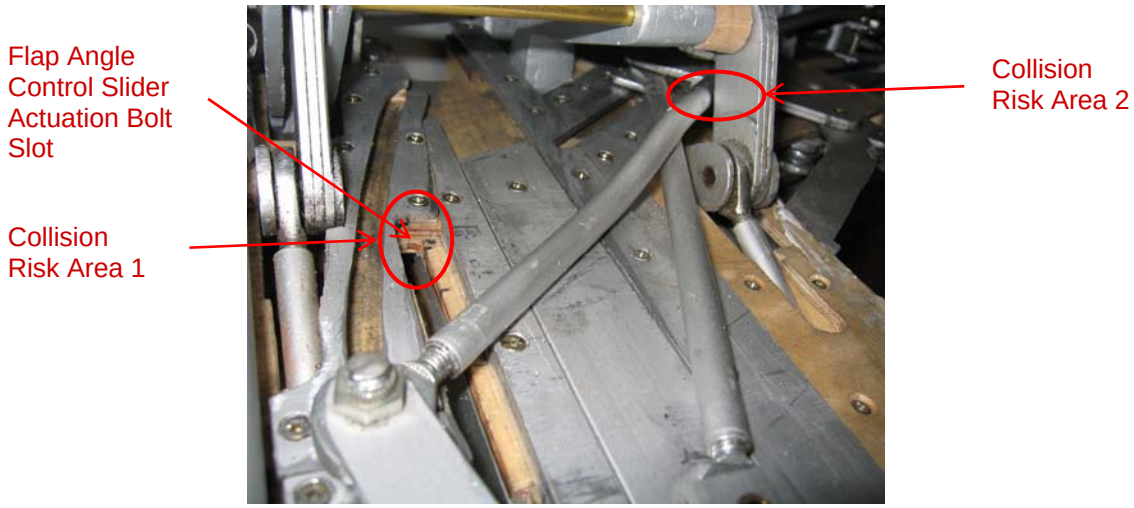

Figure 5.48 Auxiliary cam link (main slider 75% extended, view back outboard)

As the flaps are extended further, the inboard suspension link rotates further backward too. Again, this extra space is needed for the passage of the auxiliary cam link's ball joint end, as shown in fig. 5.49 below. Note that there is only enough space near the vertex of the angle (green dashed lines) formed by the suspension link and support slider angle control link. The attachment point's vertical location on the main cam sliding element must be chosen accordingly.

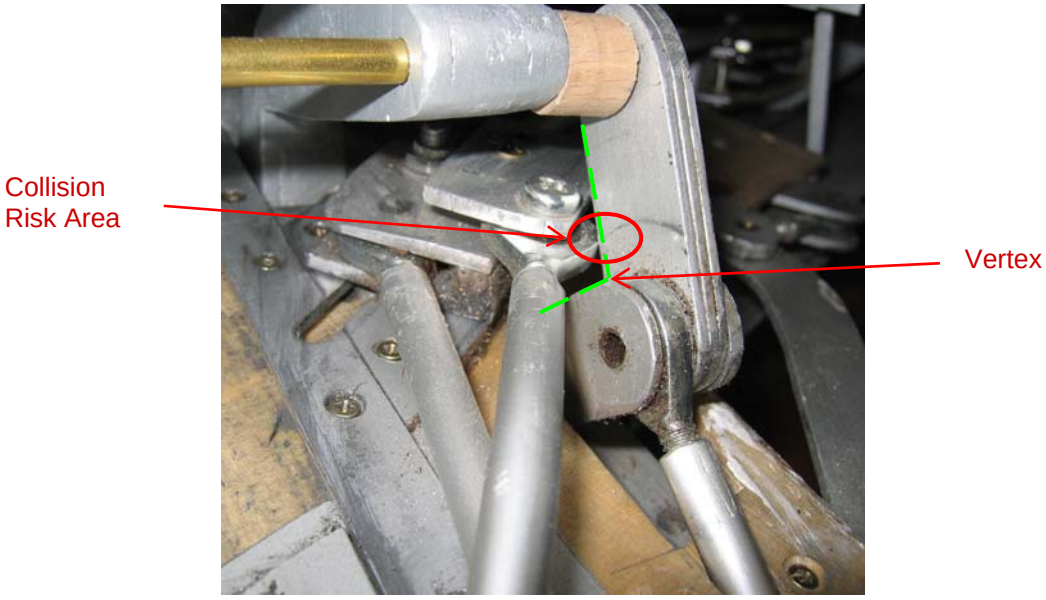

Figure 5.49 Auxiliary cam link (main slider 95% extended, view back outboard)

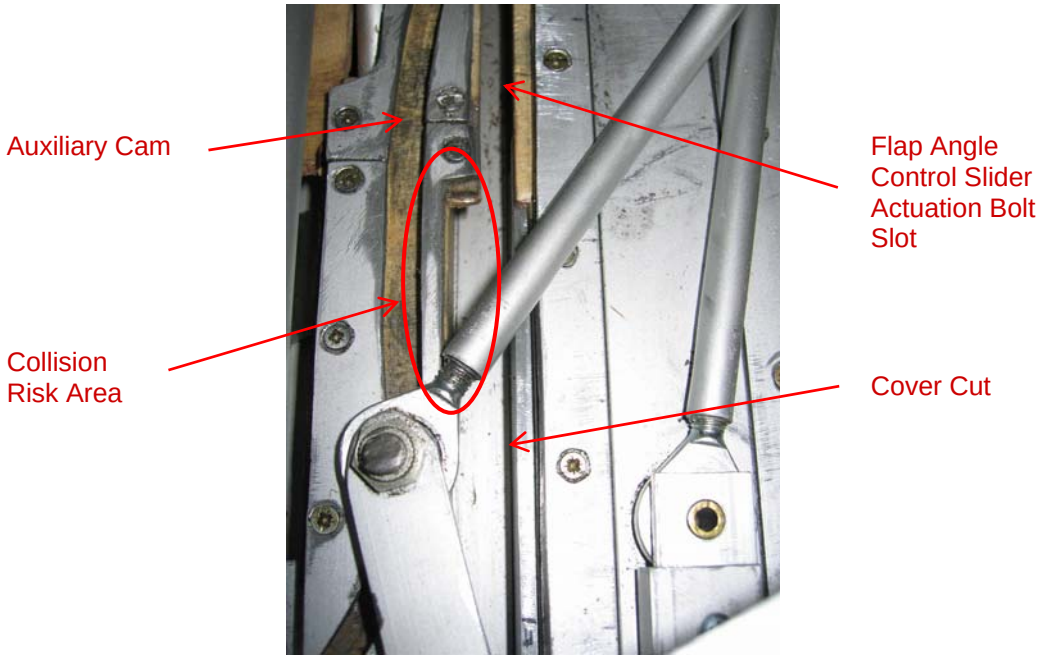

Figure 5.50 Auxiliary cam (back part, top view)

Adjacent to the slot already mentioned, there is a relatively large cut in the cover. This is needed for the flap angle control link and attachment as will be explained in the next chapters. The auxiliary cam therefore needs to be placed in a way that it does not interfere with this cut, as shown in fig. 5.50 above.

5.5.4 Flap Angle Control Slider

As mentioned above there is only one flap angle control slider in the demonstrator. A flap is suspended on at least two flap track stations, and with two attachment points per station there are at least four such points in total. Three are sufficient for the flap being suspended statically determinate, so one of the four can fail without the system getting dramatically unstable. Therefore, a design with only one flap angle control slider per station is still considered to be fail-safe.

The slider is basically an L-profile. The flap angle control link is clamped to the L-profile through an element which at the same time serves as the actuation force transfer element for the slider.

Note that due to the flap's complex 3D rotation the flap angle control link must feature ball-joints at each end. The flap angle control slider must allow for, to a certain degree, free motion of this link; the same applies to its counterpart on the flap.

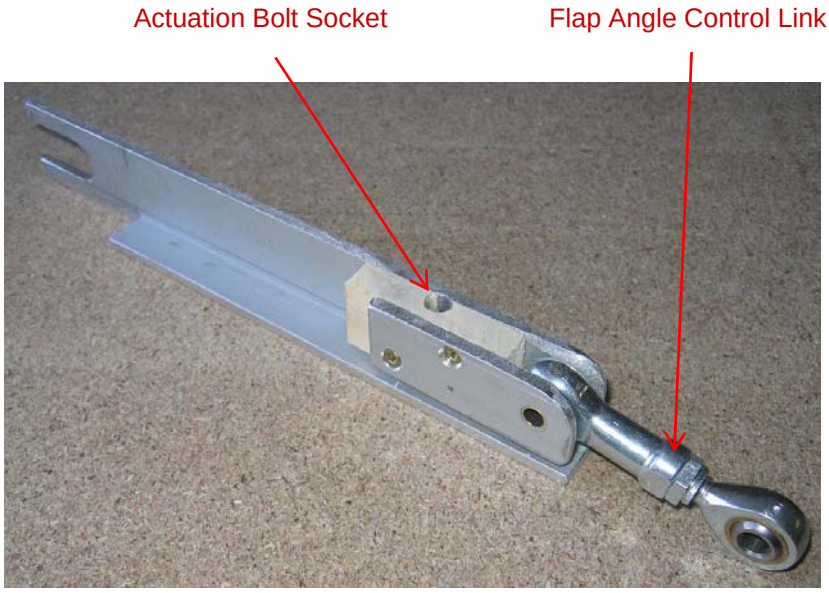

Figure 5.51 Flap angle control slider and link

Note the cuts in the profile at its end. They are needed to avoid collision (in the flaps retracted position) with the main flap track suspension and respective bolts as shown below; the dashed yellow arrows show the features which come in contact in the flaps retracted position. The profile could be cut straight instead, but the appendage to the back still gives the flap angle control slider some extra guidance stability.

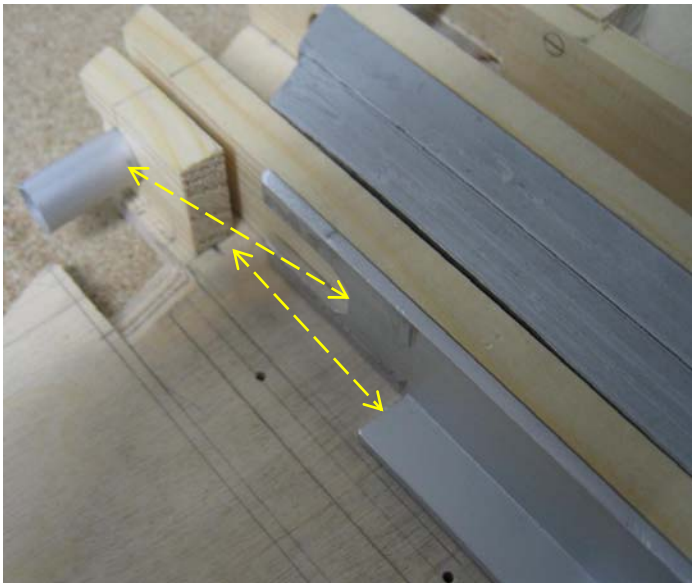

Figure 5.52 Flap angle control slider cuts

The flap angle control slider is retained and bound by a guiding band, a part of the guide structure assembly. The build-up process of this band is shown in fig. 5.53 on the following page.

Figure 5.53 Flap angle control slider guide build-up

However, this design requires a cut in the cover, which, as explained in chapter 5.5.3 above, is responsible for many collision risks. Still they can be resolved and this design as well allows for the flap angle control link attachment element to be stowed in the flaps retracted position (further explained in chapter 5.6.3).

The flap angle control slider is attached (and secured) to the auxiliary slider link through a bolt as shown in fig. 5.54 below.

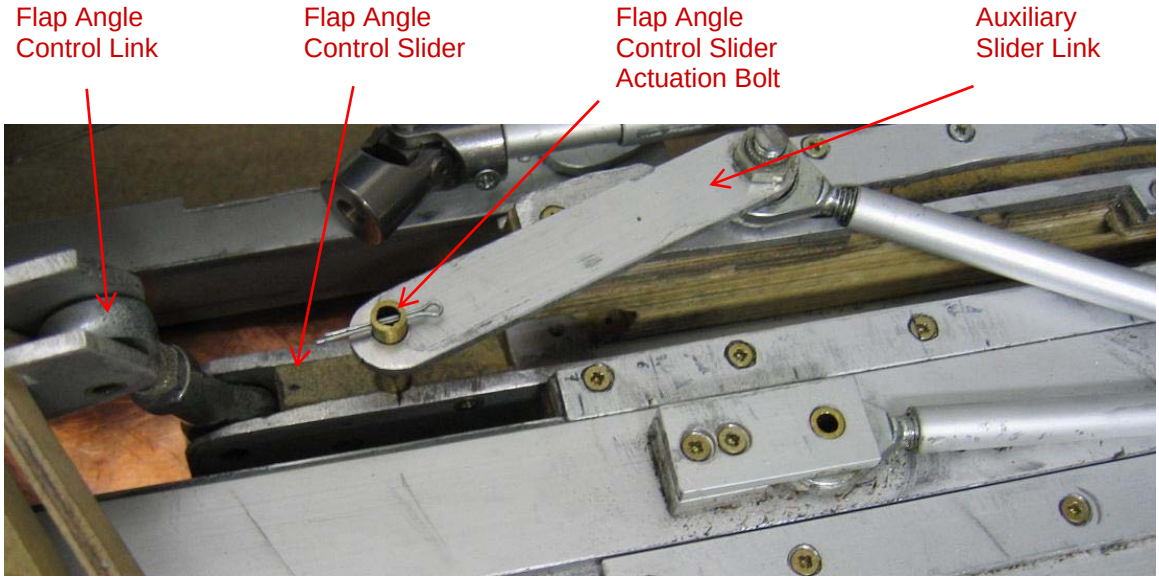

Figure 5.54 Flap angle control slider attachment

5.6 Flap Body

5.6.1 Structural Considerations

As mentioned on page 56 in chapter 4.3.1, with this integrated flap track concept a cut in the bottom of the flap structure cannot be avoided. Still, its impact can be kept at a minimum by choosing a cut shape which does not worsen the situation further by a strong notch effect. Therefore right or even acute angles in the force flow should be avoided.

Fig. 5.55 below shows the basic structural layout lines, which depict the front and rear spar, the rectangular ribs and the main flap suspension attachment location. The rear spar is continuous as was suggested in chapter 4.3.3. This cannot be fully applied to the front spar which is made up of two sections, at least in the lower part, to avoid collision with the guide structure assembly.

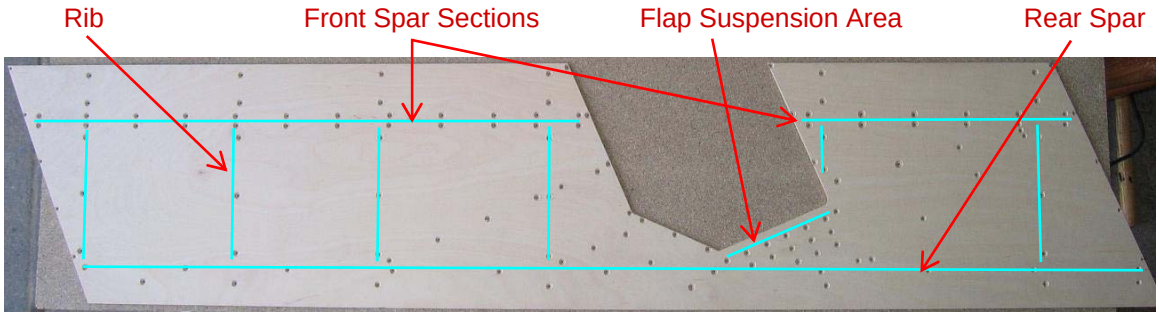

Figure 5.55 Flap bottom shell (lower side shown): structure layout

The following figure shows the anticipated force flow lines. Here it becomes evident that one of the reasons for chamfering a corner of the guide structure assembly is to be found in flap structural considerations. A force concentration is expected at the flap suspension area. Note, though, that such a substantial concentration applies to the flap bottom only; the flap top is mainly not cut so the force flow will be much smoother.

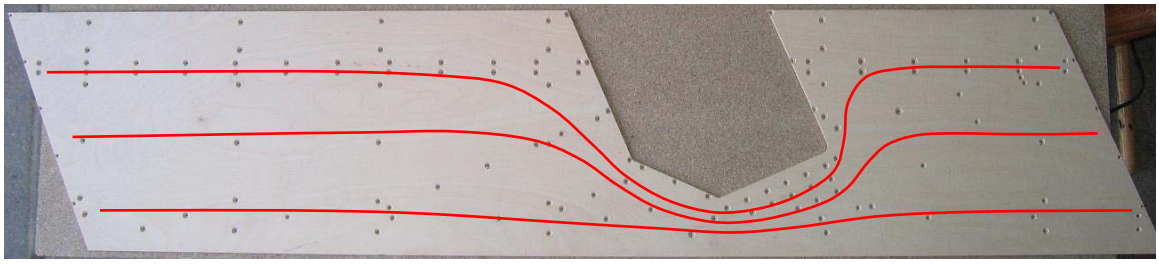

Figure 5.56 Flap bottom shell (lower side shown): force flow lines

The following figure shows the basic flap build-up; note the continuous top part of the front spar.

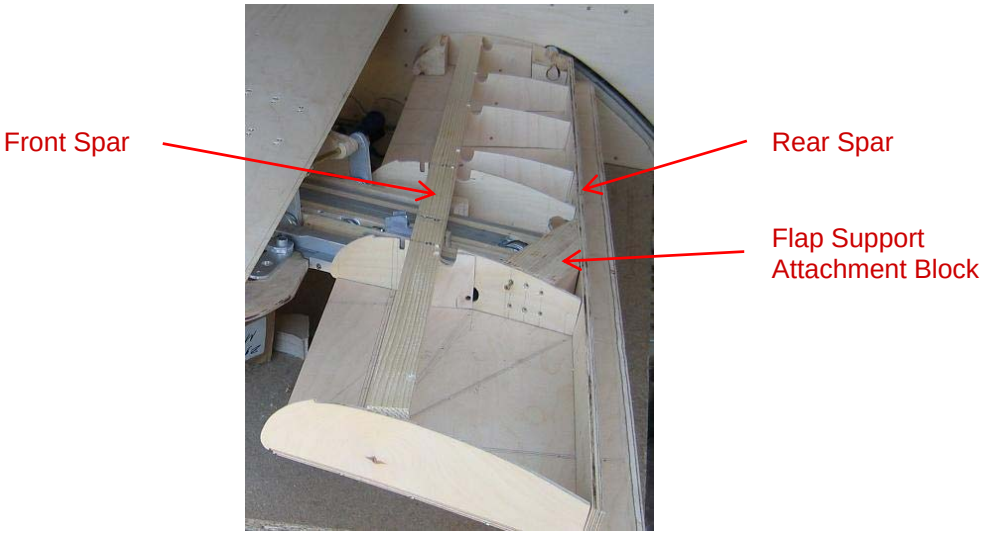

Figure 5.57 Basic flap build-up

5.6.2 Flap Main Support Attachment

Since almost the full flap load flows through the flap main support attachment, this element must be designed very robust. In an actual airliner application a shear field design could be considered rather than a solid block. The following figure shows the ball joint mounted onto the attachment block.

Figure 5.58 Flap support attachment block

To allow an evenly distributed load transmission from the flap body into this block it must be attached to as many parts as possible. Therefore it is attached to the rear spar, to the outboard boundary rib (non-rectangular), and to the bottom shell via a set of rivet fields.

Of course it would also need to be riveted to the top shell in a real airplane, but in the demonstrator this is not done for the following reason: to allow for inspection and installation a general requirement for a structure like a wing is that each section (like a 'box' between two ribs) be accessible through access panels in the skin. To keep the work for the demonstrator at a reasonable level, the whole top shell is easily detachable and thus serves as a single access panel rather than several access panels distributed all over the flap body; it is only attached to the front and rear spars by means of relatively few screws.

Figure 5.59 Installed flap support attachment block (flaps extended position)

5.6.3 Flap Angle Control Link Attachment

Besides setting the flap angle itself, the flap angle control link also bears the load due to basic flap moments. The main flap support was roughly set such that aerodynamic loads act at this point, so almost no additional moments due to these loads are added to the flap moment. Still, the distance between main flap support and flap angle control link attachment point is a lever arm and should thus be as long as possible to reduce the load on the link. However, this point must not be too far to the front as the link should fit in the cover cut and collision particularly with the auxiliary cam must be avoided. So selecting the right point is again a highly iterative process. The attachment block for the flap angle control slider is mounted on the top part of the flap front spar, as can be seen in figures 5.60 and 5.61.

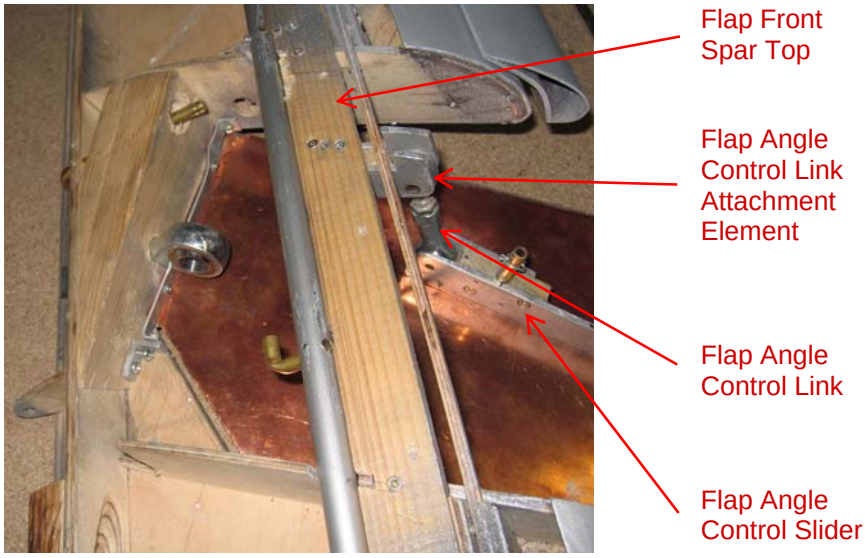

Figure 5.60 Flap angle control link and attachment

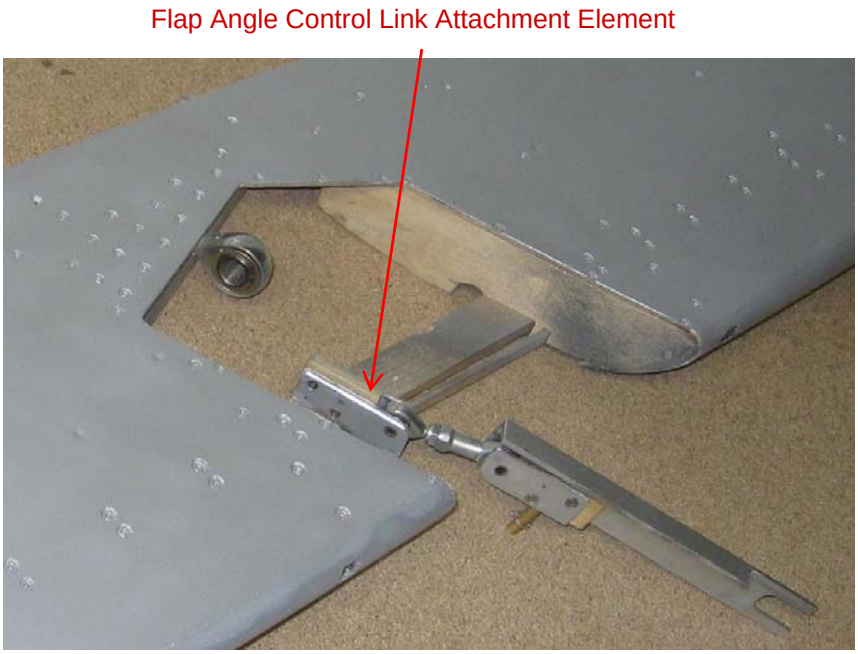

Figure 5.61 Flap angle control link and attachment (bottom view)

Figure 5.62 shows the mounted flap fully retracted. The flap angle control link attachment element just fits into the gap of the guide structure assembly.

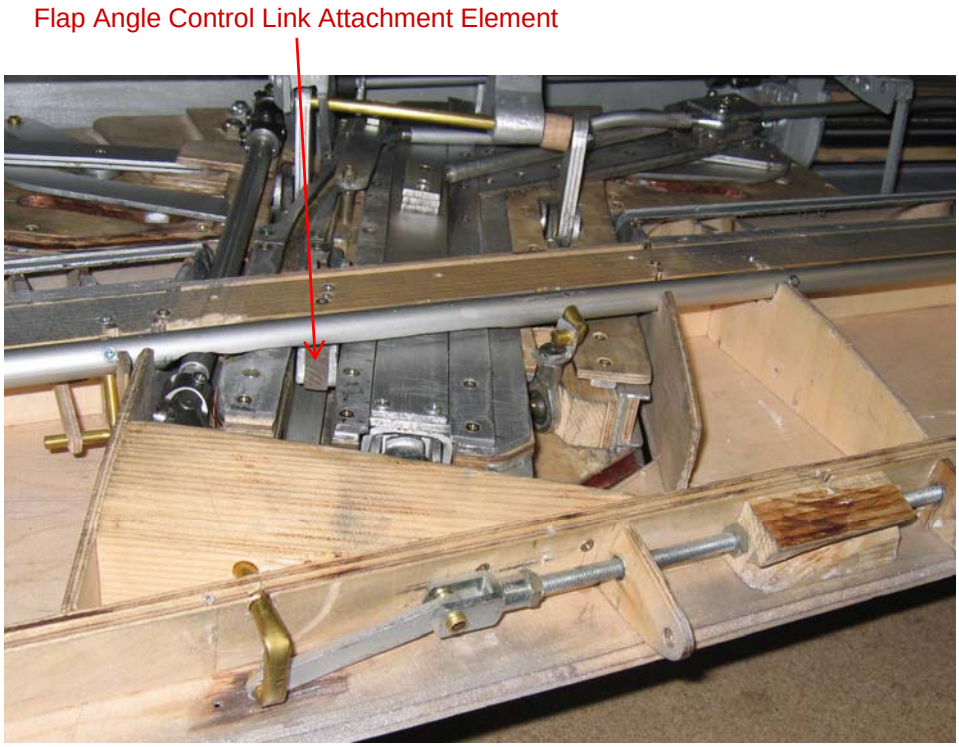

Figure 5.62 Flap angle control attachment in the flaps retracted position

5.7 Flap Vane

5.7.1 Improved Actuation Mechanism

A flap vane actuation mechanism has been presented on page 40 in chapter 3.2.7. This mechanism, however, creates problems in the detailed design process, since it requires a link being attached somewhere in the middle of the main slider or its appendages. Attaching it that much in front of the main flap support point requires the guide structure assembly to be cut further and be built wider in the x direction.

The approach shown in fig. 5.63 allows the flap vane actuation mechanism to be attached near the flap main support. A flap vane actuation rod performs a rotation controlled by a flap vane control link as the angle between flap and main slider is increased. This motion is passed on to a flap vane actuator link which controls the flap vane extension.

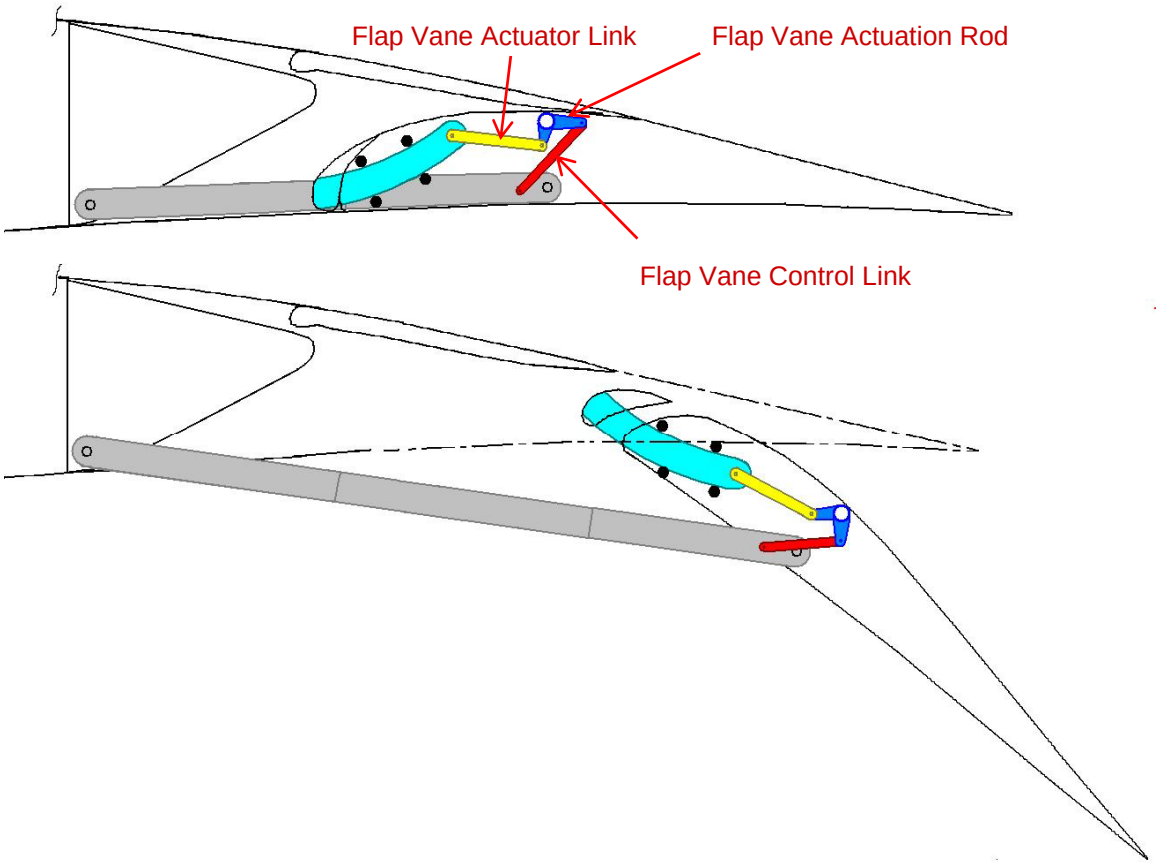

Figure 5.63 Flap angle control attachment in flaps retracted position

For simplification the mechanism as shown does not feature any programming device. However, it is possible to split the flap vane actuator link in two links, the connecting bolt of which sliding on a programming cam.

This simplification will also be applied to the demonstrator model. Still, the flap vane extension characteristics are very close to ideal: the angle between flap and main slider is increased considerably only in the final flap extension process and thus it is only then the flap vane will be extended notably, which is exactly the projected behavior.

5.7.2 Application to Demonstrator

The flap vane is split into two sections, as otherwise it would collide with the guide structure assembly in the flaps retracted position. The flap vane sliders and ribs are built as one part, so the flap vanes and sliders are rigidly connected. It is possible, however, to introduce an additional degree of freedom by designing a pivotal flap vane support (see B767 slat system in fig. 3.1).

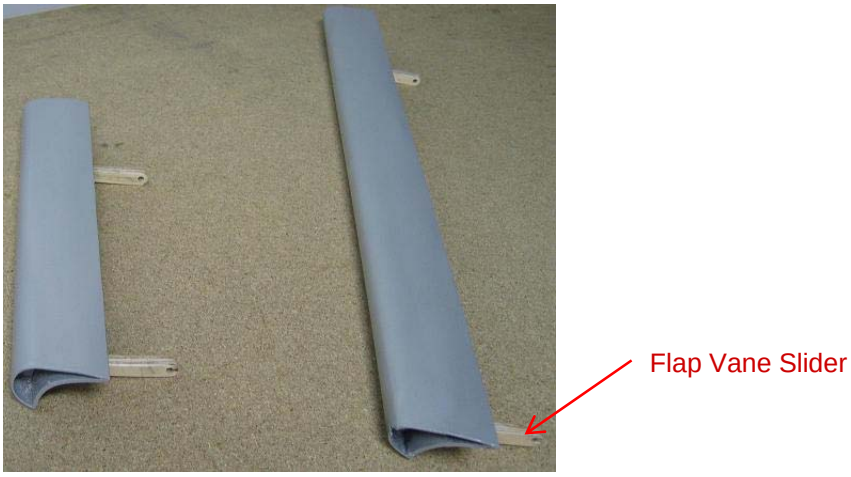

Figure 5.64 Outboard and inboard flap vane section

Each flap vane section must be supported by at least two guide stations, or receptacles, as shown in fig. 5.65 below. They are attached at the front spar and act at the same time as nose ribs. In order to avoid forced loads on the flap vanes, the lateral degree of freedom is only restrained at one receptacle. Nevertheless, the flap vane still extends straight as both sliders of one section are controlled simultaneously and thus chocking is prevented.

Note that the flap vanes must be extended perpendicular to the flap leading edge, as they are rigidly connected to their sliders. This means they are somewhat displaced sideward when extended. This effect is not considered to have a detrimental effect on performance.

Figure 5.65 Outboard flap vane receptacles (nose cover removed)

The flap front spar must be cut behind each receptacle to accommodate the sliders in the retracted position, and for the actuator link to pass.

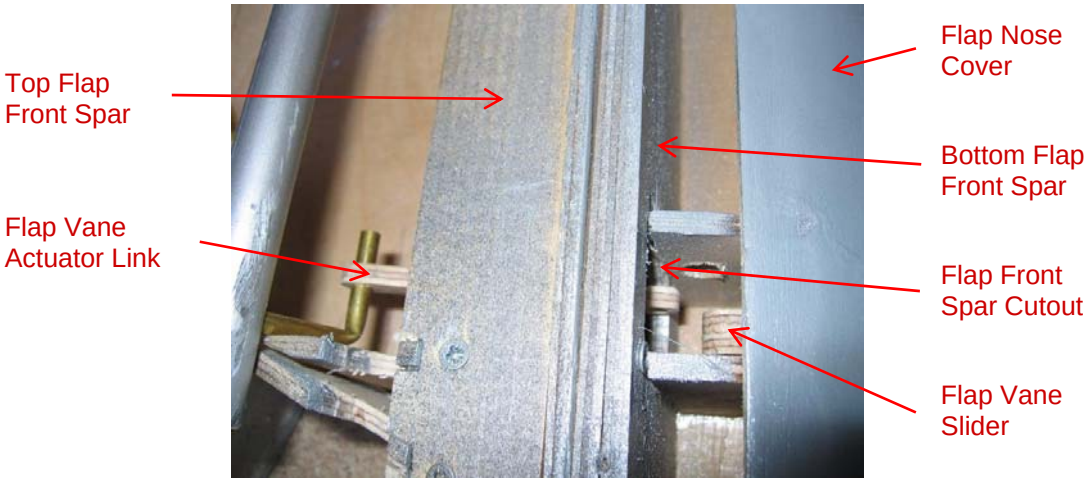

Figure 5.66 Flap vane actuation

In the figure above the actuator link and the flap vane slider are not yet connected; the full flap vane montage process can be seen on page 190 appendix G.

The nose covers need to be cut as well; in order to avoid aerodynamic problems like resonances the cuts are just large enough for the flap vane sliders.

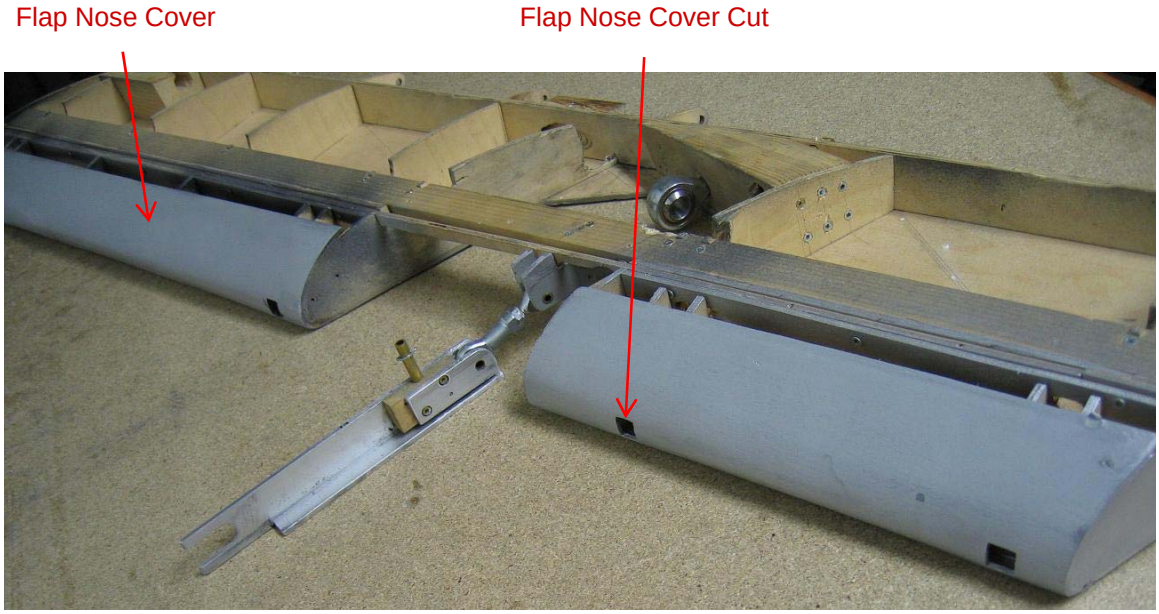

Figure 5.67 Attached and cut flap nose covers

The flap vane actuation rod extends over the flap span and is located right behind the top of the flap's front spar. The flap ribs are designed to act as bearings for this rod, and the flap top shell is part of this bearing system.

Figure 5.68 Flap vane actuation rod with actuator links attached

This flap vane actuation rod is now being attached to the flap vane control link which has already been introduced on page 78 in chapter 5.3.3. As with the flap angle control link, the flap vane control link too needs to allow for a complex 3D rotation of the flap, which entails a ball joint support approach also for this link. Production problems led to the design of this link as shown in fig. 5.28, with only the bottom part being a real ball joint and the top part allowing a minimal tilt.

The connection point between flap actuation rod and control link should be as close to the front spar as possible, since the stringers on the flap's top shell should be distributed as evenly as possible to keep the original structure as shown in chapter 4.3.1. The flap vane actuation rod too has a stiffening effect and thus acts, to a certain extent, as an extension to the front spar top. The demonstrator model does not feature the stringers, however.
Another constraint limiting the control link length is collision with the flap top shell in the flaps retracted position.

Figure 5.69 on the next page shows the flap vane actuation mechanism and the general situation, particularly stowing of the guide structure assembly in the flaps retracted position. The bottom picture shows that the front spar's top part just fits in above the guide structure assembly. The top picture shows another reason for chamfering the inboard main slider appendage and thus also the guide structure assembly: due to the flap's beta rotation the appendage would collide with the flap's top shell and stringers if it is too wide. By choosing the two-slider appendage design this problem can be solved and the flap vane control link can be attached conveniently.

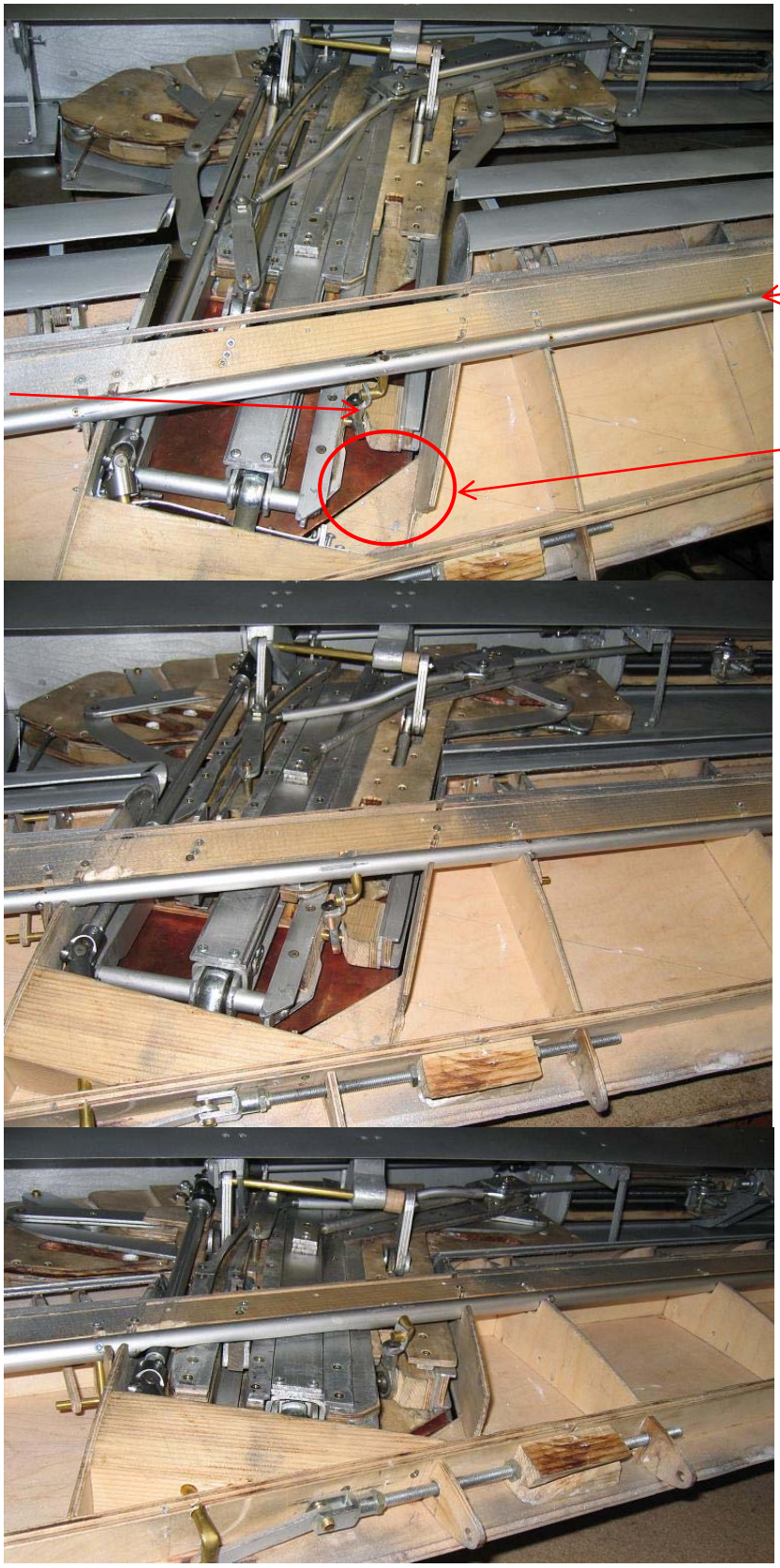

Figure 5.69 Flap vane control link attached
(fully extended, half extended, retracted)

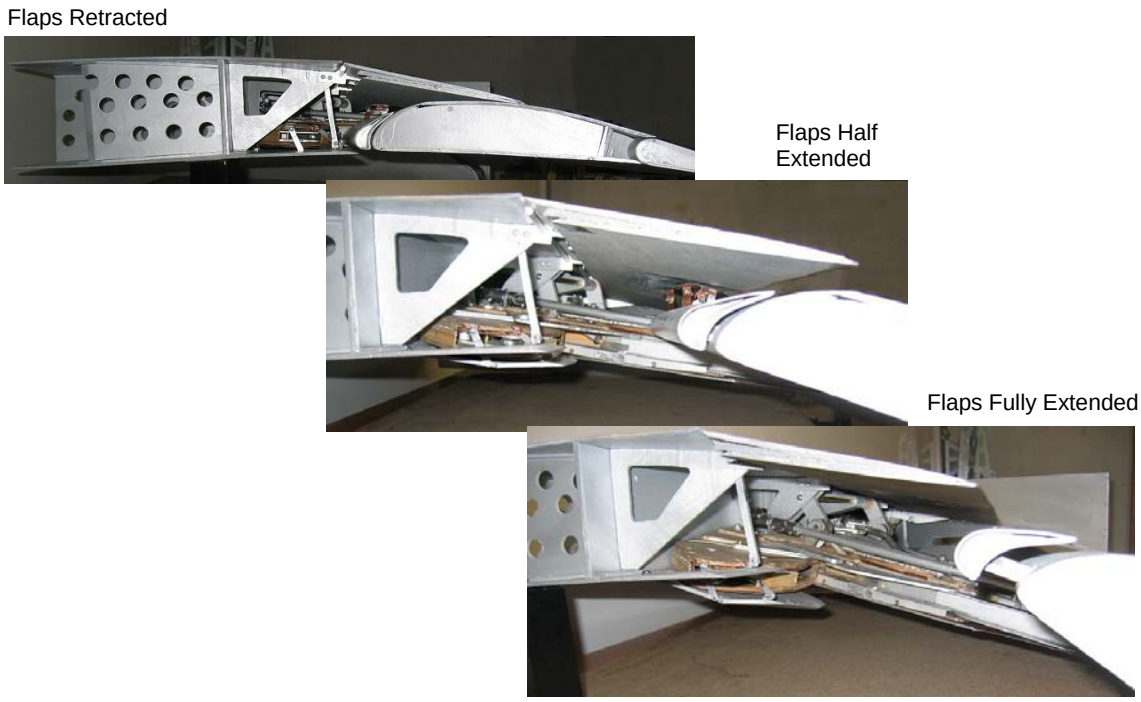

Figure 5.70 Flap vane extension characteristics

5.8 Flap Vane Gap Cover

As mentioned in the preceding chapter the flap vane comes in two sections. Besides, the flap body nose is cut at the guide structure assembly location. This leaves a large gap between the spoiler trailing edge and the flap near the fully extended position; and since the flap top shell acts like a sharp leading edge this would produce unacceptable problems such as resonance (the flap would basically act similar to a flute). To avoid this, a cover is introduced to bridge this gap and allow a smooth airflow at the wing's top side. The slot opened by the flap vane is not continuous and will therefore reduce the flap effectiveness. However, the airflow through such a slot there would be blocked anyway due to the presence of the guide structure assembly.

Figure 5.71 Flap vane gap cover (flaps fully extended)

The gap cover is suspended and actuated by a set of links. The right extension characteristics are attained by appropriately placing an aft and fore link at the inboard and outboard side and mounting them on the flap's in- and outboard boundary ribs. The corresponding attachment points and link lengths depend on the desired extension characteristics, which are constrained by the flaps fully extended position, the clearance needed towards the spoiler, and the space needed by the guide structure assembly in the flaps fully retracted position (see figure 5.75 on the next page).

The rear and fore links are bent so they fit in the small gap left between the guide structure assembly and the flap boundary ribs, and that they do not collide with each other during the extension process.

Figure 5.72 Flap vane gap cover top and bottom view

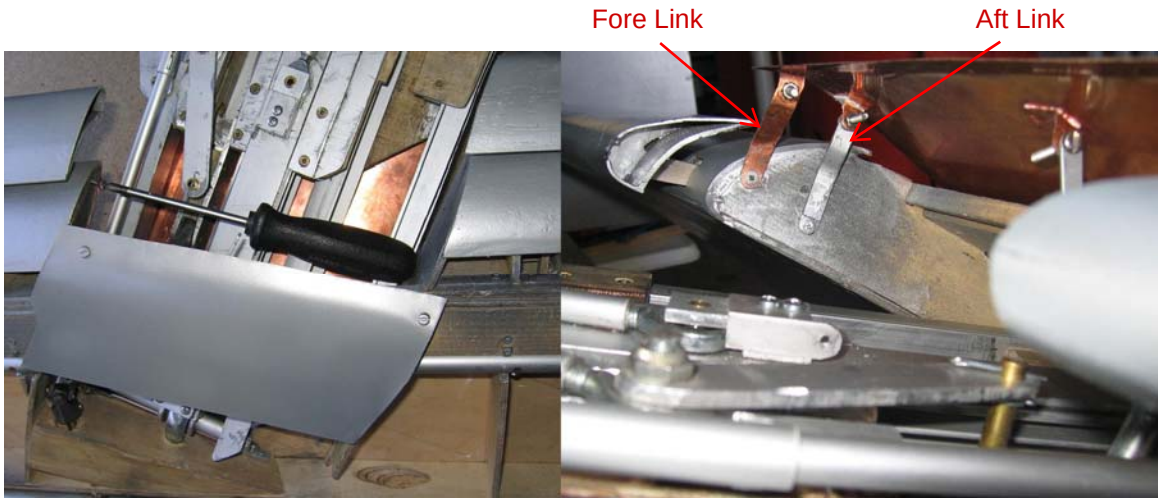

Figure 5.73 Flap vane gap cover suspension links

Due to the 3D flap rotation the actuation link needs to feature ball joints at its ends, but for this project this is replaced by just leaving enough allowance at the attachment holes. The link's length and attachment point (ideally selected on the main slider control slider) depend on of the gap cover extension characteristics.

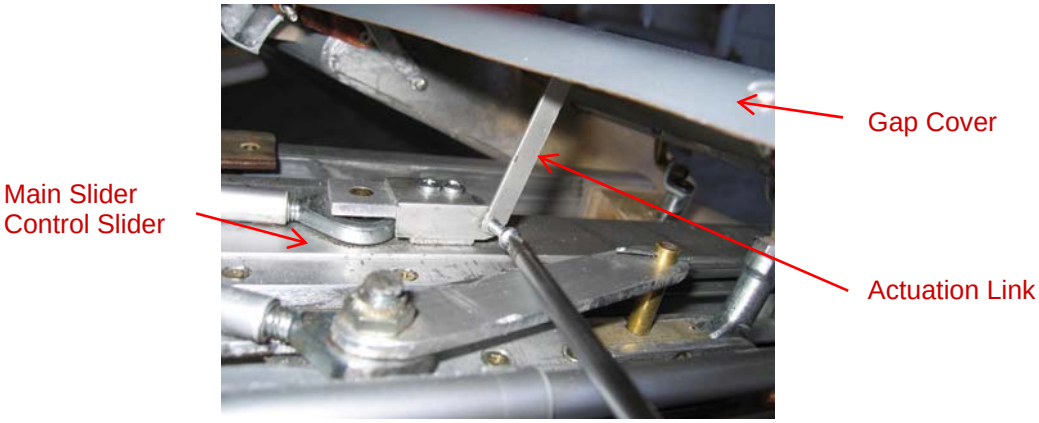

Figure 5.74 Gap cover actuation link attachment (flaps fully extended)

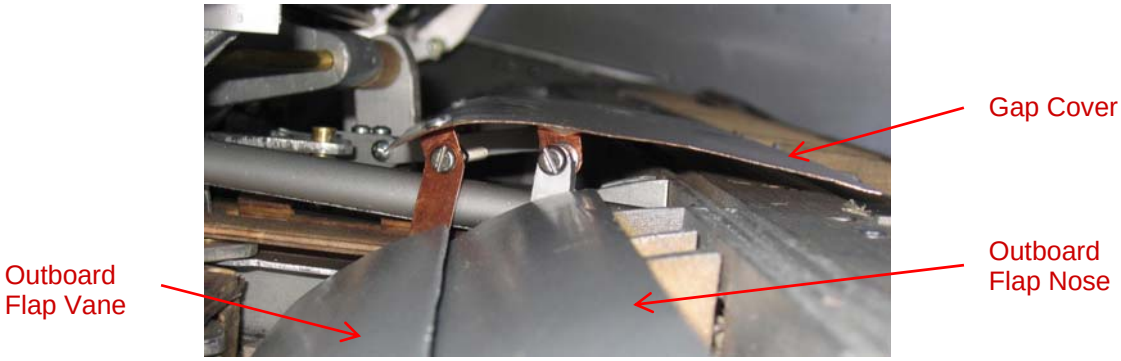

Figure 5.75 Gap cover (flaps fully retracted position, view from outboard)

Figure 5.76 Flap vane gap cover motion

5.9 Main Mechanism Actuation

5.9.1 Actuation Screw

As described in chapter 3.2.2 the main actuation screw is directly attached to the rear spar. There is a suspension at each side of the screw; as opposed to the main flap track suspension elements they are mounted perpendicular to the rear spar. Since the wing is subject to bending and the screw should not be bent if ever possible, it is essential that the screw bearings be attached to the suspension elements by means of ball joints. Still, for the purpose of the demonstrator, standard axial bearings are used.

As shown in fig. 5.77 below, there are two guides to keep the screw jack from deviating upwards or downwards when forces acting on it are not parallel to the screw axis.

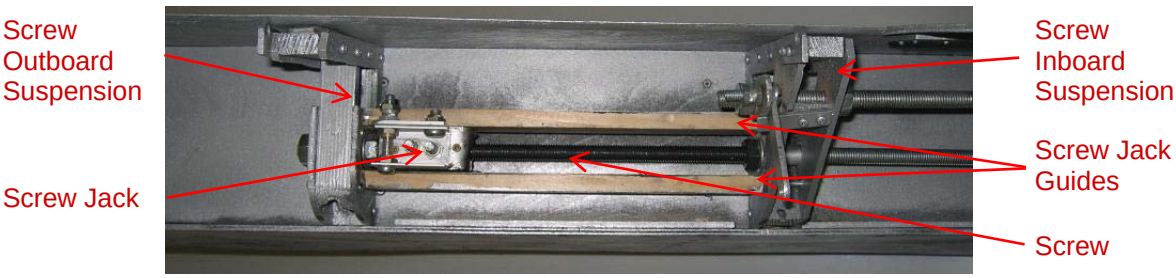

Figure 5.77 Actuation screw

The wing section with the screw attached is shown next.

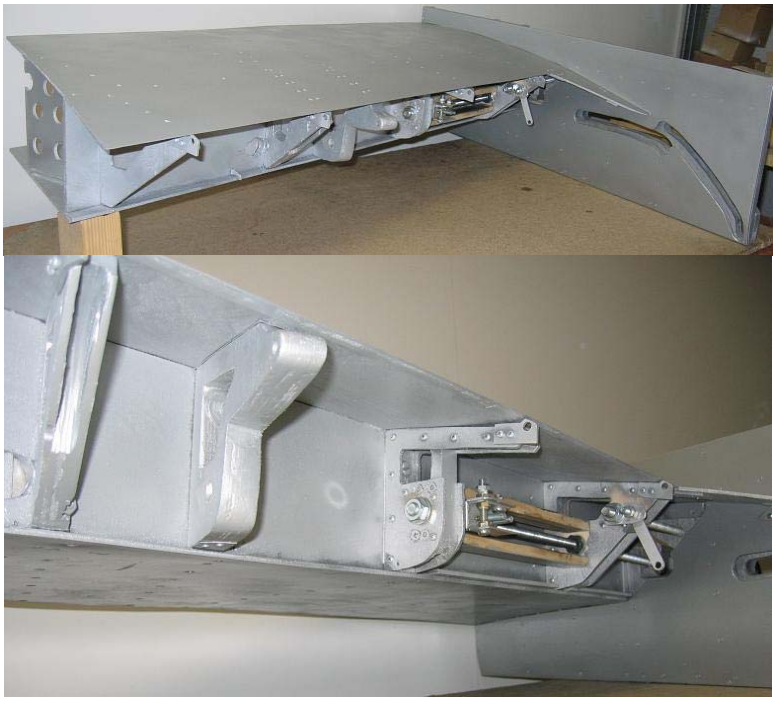

Figure 5.78 Wing section views

5.9.2 Force Transmission

The motion and force produced by screw rotation is transmitted to the main screw jack link via the screw jack. The other end of the link is attached to the main cam sliding element. The hinged screw jack main link attachment problem as depicted in fig. 3.8 on page 30 is solved by simply using ball joints at each end of the main screw jack link.

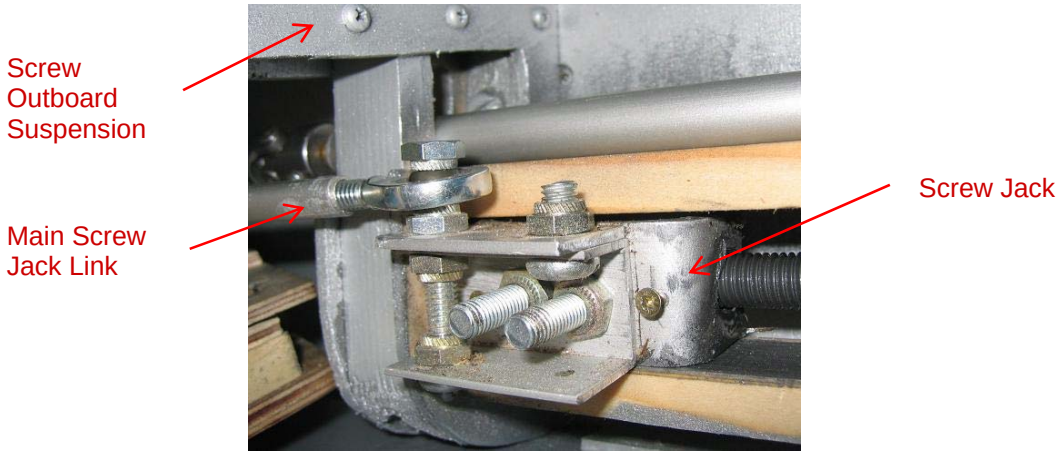

Figure 5.79 Screw jack with main screw jack link attached

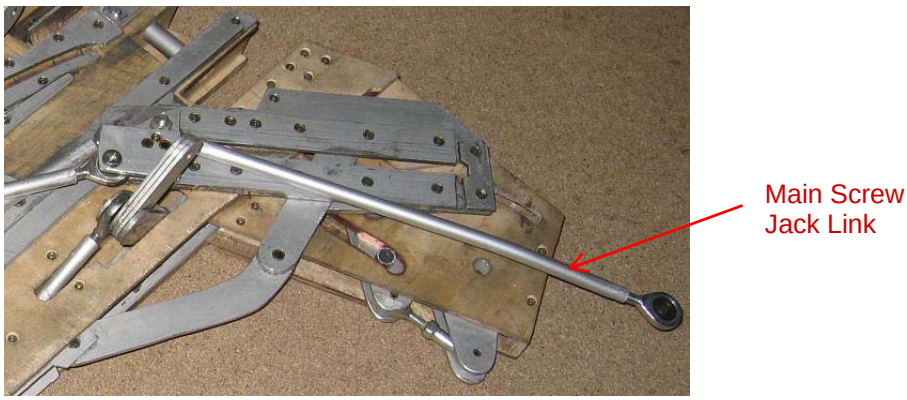

Figure 5.80 Main screw jack link attached to main cam sliding element

Fig. 5.78 above showed the outboard screw suspension cut in the backward part. This is necessary to avoid collision with the main screw jack link, which, like the main slider link, performs a hyperbolic motion during extension.

Fig. 5.81 shows the environment of the main screw jack link with the assembled mechanism and attached flap.

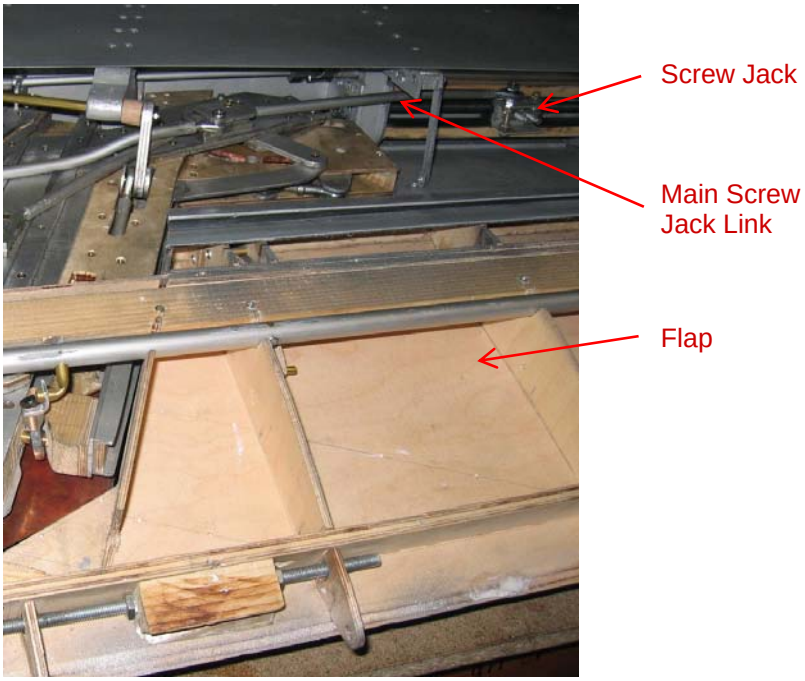

Figure 5.81 Assembled mechanism and flap (half extended position)

5.10 Wing Fixed and Moving Bottom Covers

To ensure a smooth airflow the bottom wing surface gap between the wing rear spar and the flap vane leading edge needs to be closed. This is usually done by attaching covers right behind the rear spar and suspending them at the spoiler suspension elements.

Due to its downward motion, the guide structure assembly would collide with these covers; this is why they must be designed to follow the motion. On the other hand, downward motion of the covers interferes with a smooth airflow and therefore likely reduces flap effectiveness, so they must be designed in a way to reduce this impact wherever possible.

Figure 5.82 Fixed and moving bottom covers attached

The main cover is the part located directly under the cut in the flap body. It is attached to the wing section by a hinge line and to the guide structure assembly by means of a sliding crank. The sliding design of this crank is necessary as the main cover and the guide structure assembly have different hinge lines (the crank could also be replaced by a link).

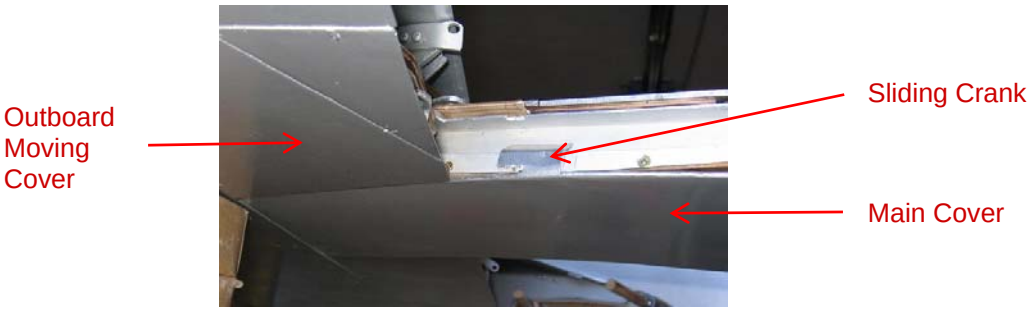

Figure 5.83 Moving bottom covers in flaps retracted position

When the flaps are extended, parts such as the main slider and appendages are openly exposed to the environment, particularly water spray on wet runways, or snow which would likely get lumpy in the mechanism. Besides, the cut flap bottom is likely to disturb the airflow significantly. For these reasons the main cover features an extendable part which is attached to the flap body and protects the mechanism at each flap extension position. Due to the 3D flap rotation this extendable part must be somewhat flexible (the demonstrator model uses a thin copper sheet for this part).

Figure 5.84 Main cover extendable part attached to flap body

This extendable part slides in cams on the main cover; it thus fulfills its purpose to protect the mechanism and ensure a smooth airflow, as shown in fig. 5.85.

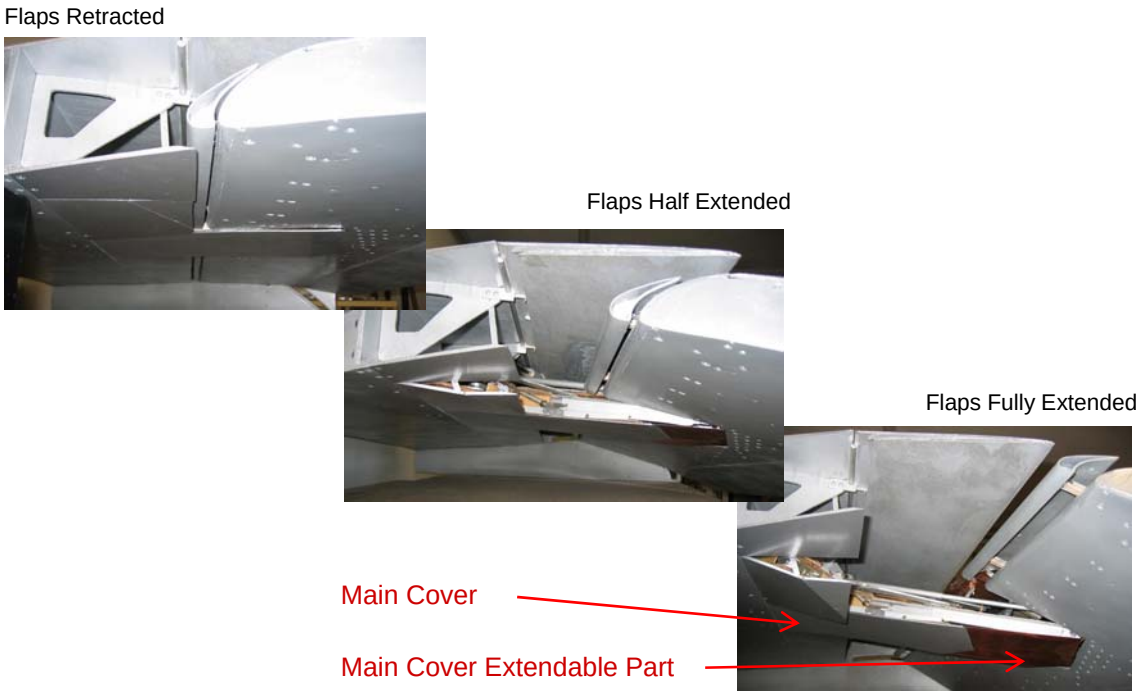

Figure 5.85 Wing bottom covers (side view)

The outboard part of the guide structure assembly has a shape which allows the cover to be designed in two sections. This cover chamfering reduces the negative impact on flap performance. By setting the control link attachment points appropriately the extension as shown in figures 5.85 and 5.86 can be obtained.

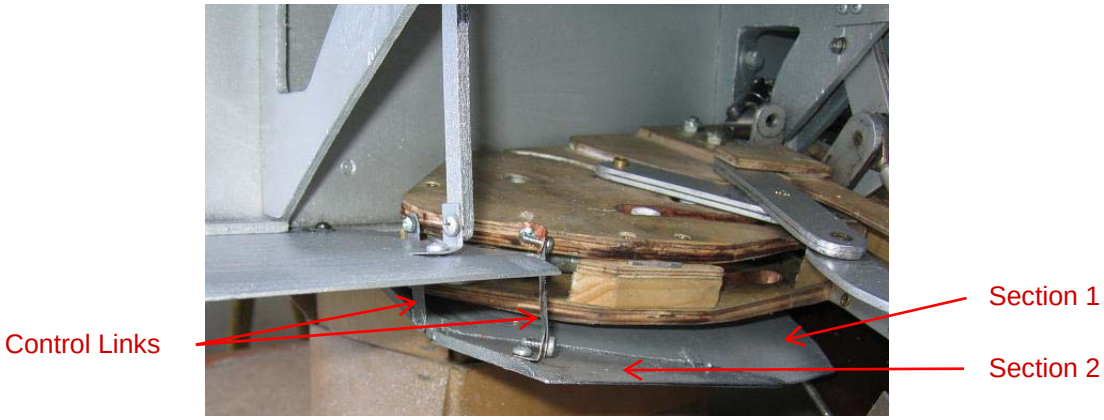

Figure 5.86 Outboard wing bottom cover

Since the inboard guide structure assembly moves downward only minimally the corresponding moving cover has one section only, and one control link.

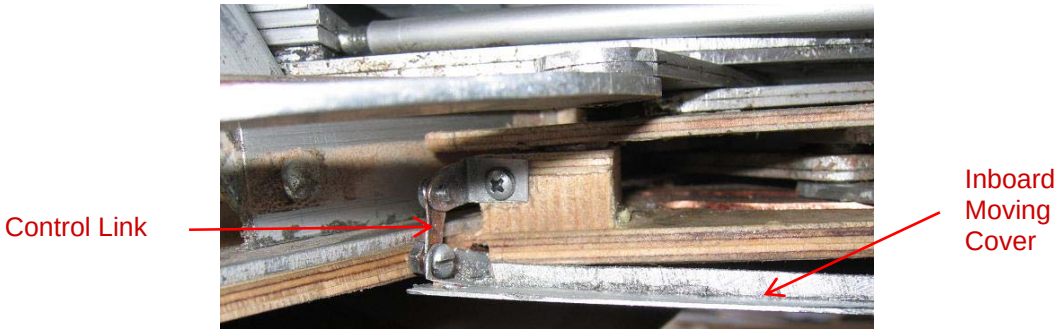

Figure 5.87 Inboard wing bottom cover

The front views shown in fig. 5.88 below demonstrate the good protection of the mechanism in all extension states.

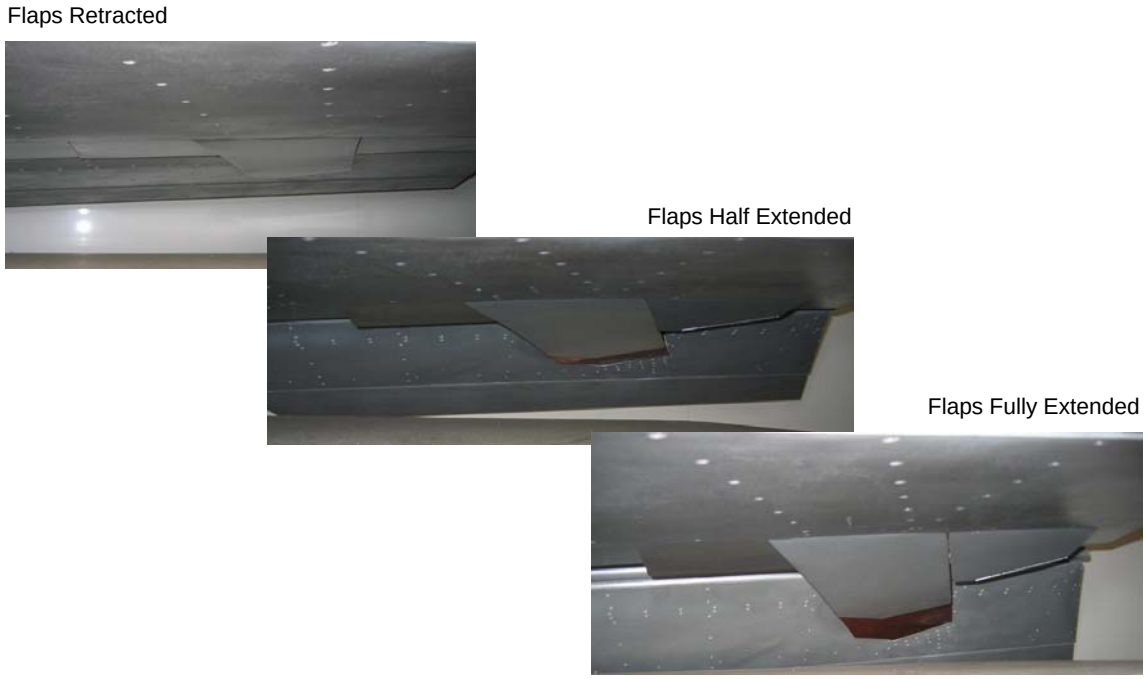

Figure 5.88 Wing bottom covers (front view)

5.11 Tab Layout and Actuation

5.11.1 Tab Layout

The tab layout is a standard rib-shell structure. One of the ribs is the tab actuation rib with its spike. However, in an actual airliner such trailing edge tabs would be designed as honeycomb structures.

The whole tab is supported by a single rod which is inserted from one side. The ribs are doubled; the attachment elements on the flap just fit within them.

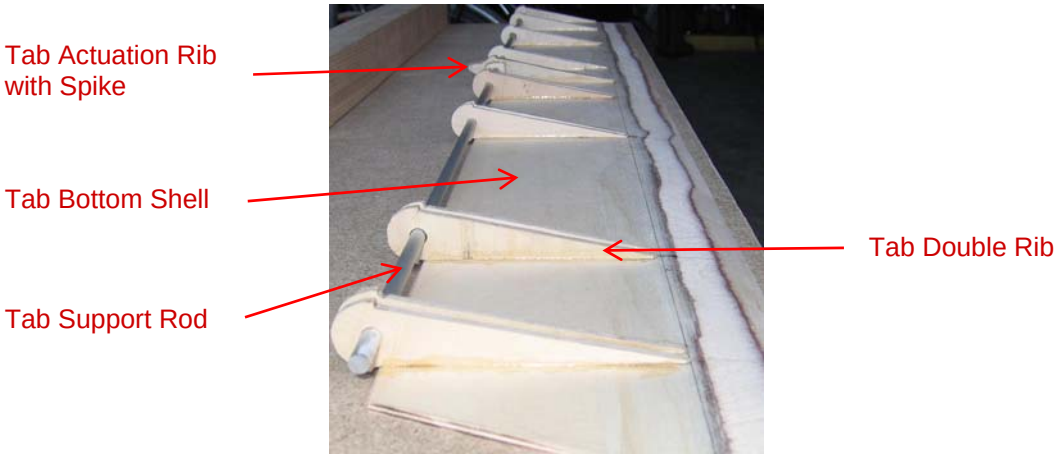

Figure 5.89 Basic tab structure

Figure 5.90 Finished tab

5.11.2 Tab Angle Control Slider

The slider and its actuation mechanism are identical to the approach described in chapter 3.2.6, except that the leverage is upside down. The tab control lever is located as close as possible to the flap's top shell, the reason will be outlined later. The lever extends through the flap rear spar and the flap support attachment block.

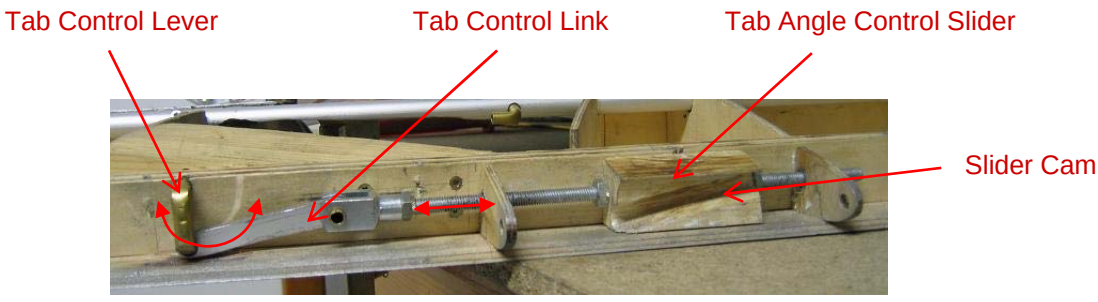

Figure 5.91 Tab actuation slider and leverage

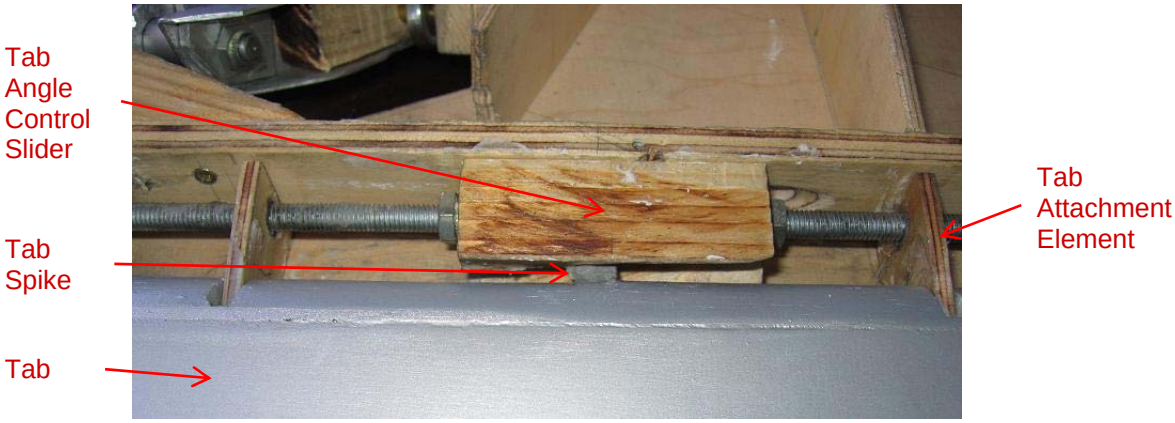

Figure 5.92 Tab actuation slider with tab spike inserted

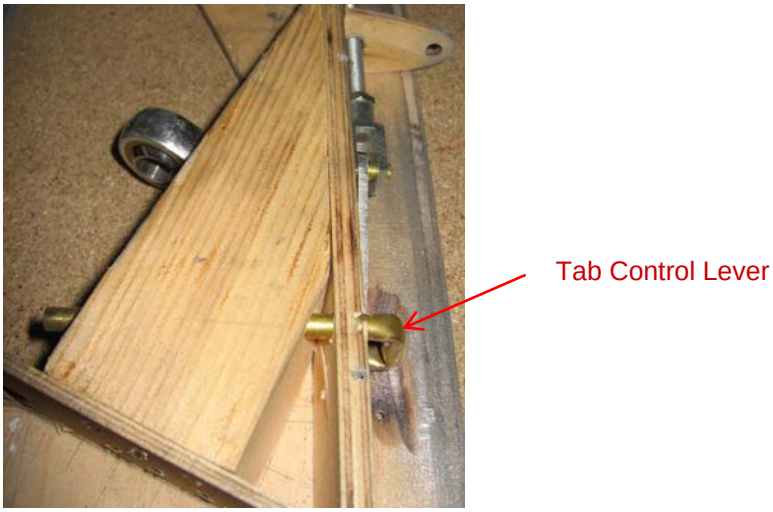

Figure 5.93 Tab control lever inserted

5.11.3 Tab Actuation Rods

An extendable rod is attached to this lever and a bearing on the guide structure assembly via cardan joints; this design allows tab operation at each flap extension position and takes the 3D flap rotation into account.

Figure 5.94 Extendable tab actuation rod (fully extended)

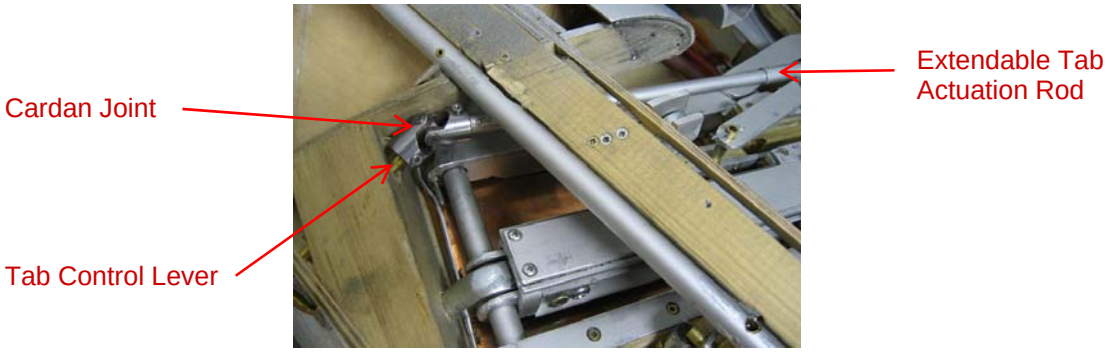

Figure 5.95 Extendable tab actuation rod attached to tab control lever

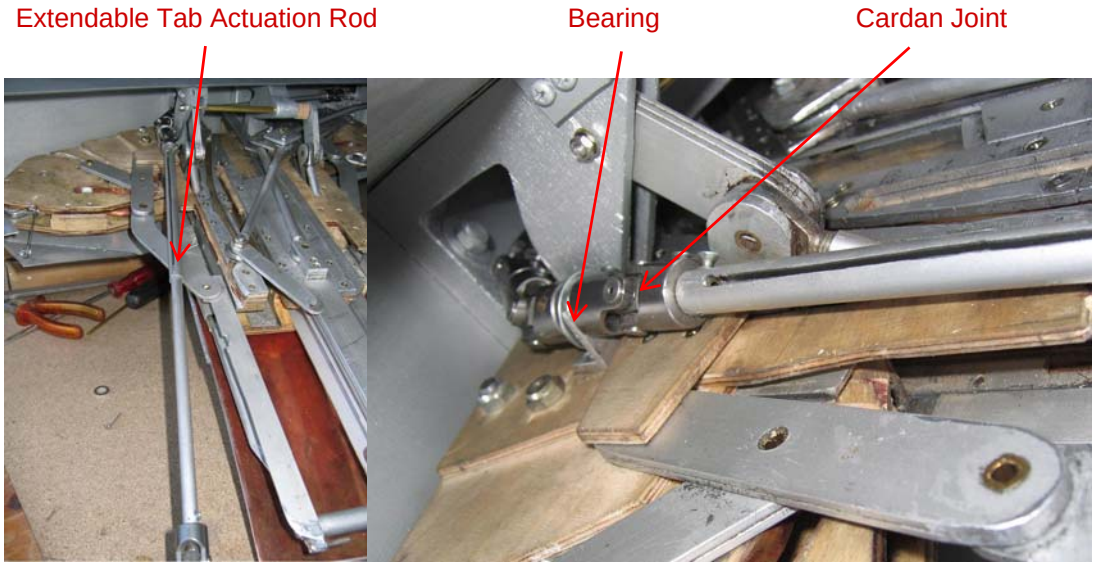

Figure 5.96 Extendable tab actuation rod attached

The extendable rod is attached to another part which is eventually parallel to the rear spar; it is there the actual actuator (electric or hydraulic) could be mounted. In the demonstrator this rod is directly attached to a lever.

The rod bearing on the guide structure assembly is not mounted exactly at the main flap track suspension bolt location. This entails a backward motion of this bearing when the guide structure assembly moves downward. Therefore, the tab actuation rod is made up of two sections, one parallel to the rear spar and the other moving forward and backward with the bearing.

Figure 5.97 Tab actuation rod

Due to the multiple cardan joints the moving rod section would become unstable if a torque is applied. Therefore, the moving section needs to be restrained in the vertical direction, with a free forward and backward motion being ensured. This restraint is a simple fork mounted on the guide structure assembly, as shown in fig. 5.99 below.

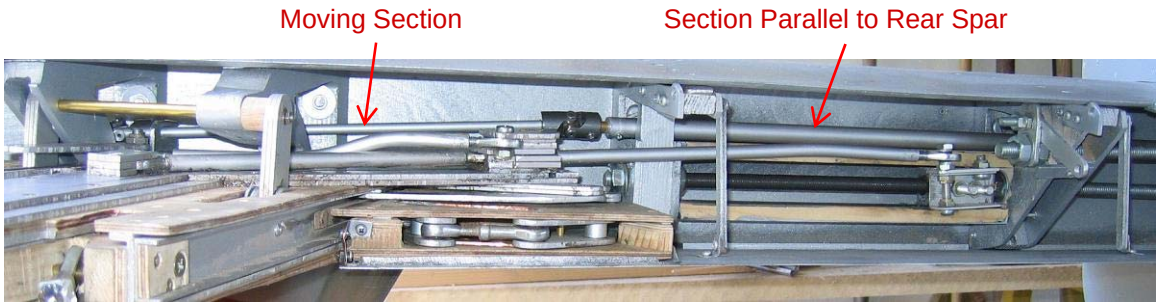

Figure 5.98 Tab actuation rod installed

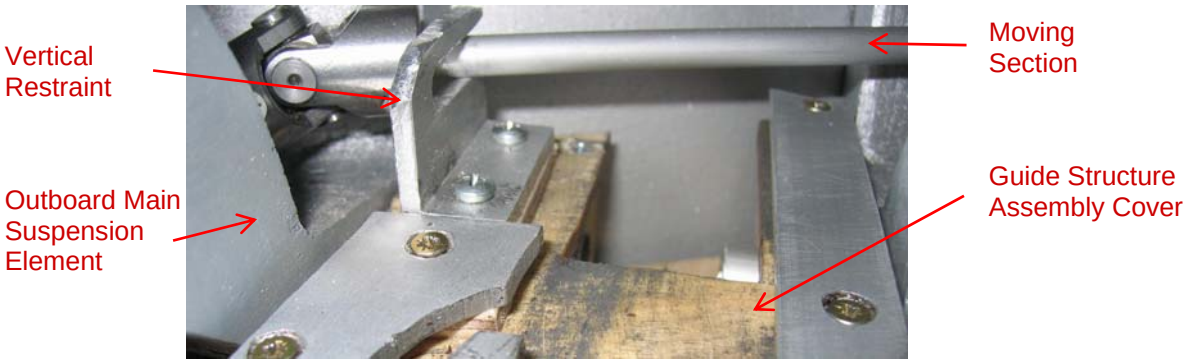

Figure 5.99 Tab actuation rod vertical restraint

5.11.4 Tab Operation Overview

With the tab actuation mechanism as outlined in the preceding chapters it is possible to operate the tab at every flap position and particularly as well during the extension process. This is important to ensure stability of an aircraft with an adaptive wing where rolling is controlled only by means of such tabs.

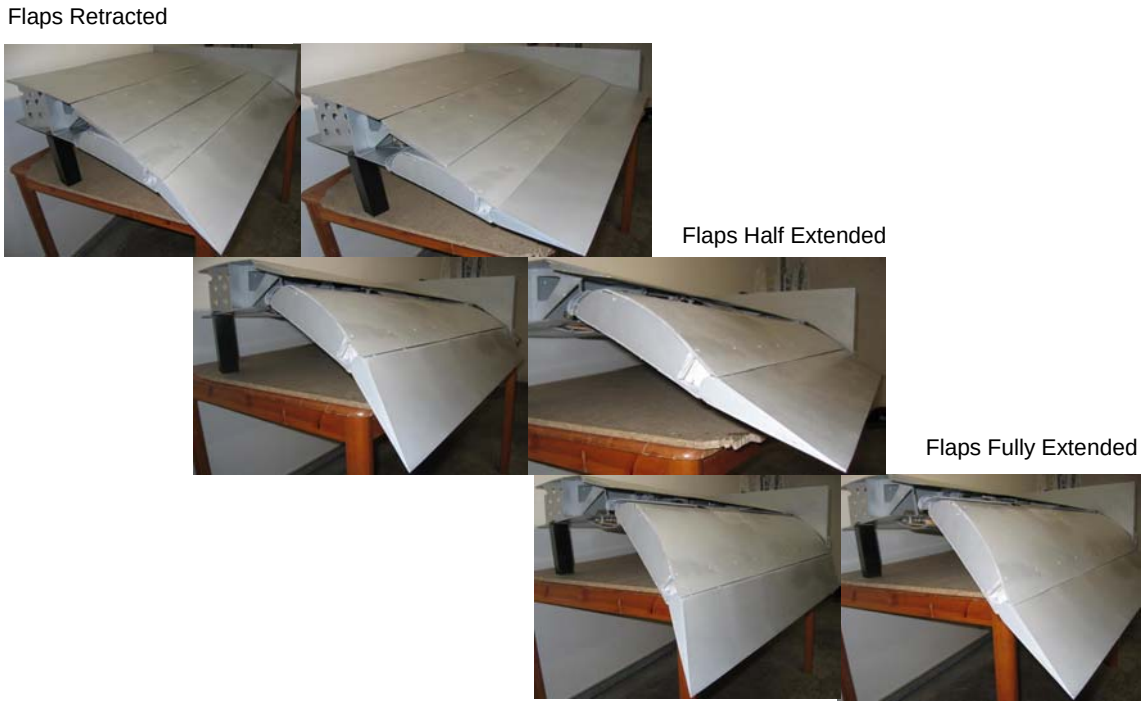

Figure 5.100 Tab operation over the full flap extension range

5.12 Spoiler

Although not the main subject of this thesis it is still important to have a short look at the integration of spoilers (or also speed brakes, depending on the purpose). A collision risk with the inboard main suspension element and support angle control linkage has already been discussed in chapter 5.3.1.

To cut down on weight wherever possible the suspension elements already installed will serve as well as suspensions for the spoiler.

Figure 5.101 Spoiler top and bottom side

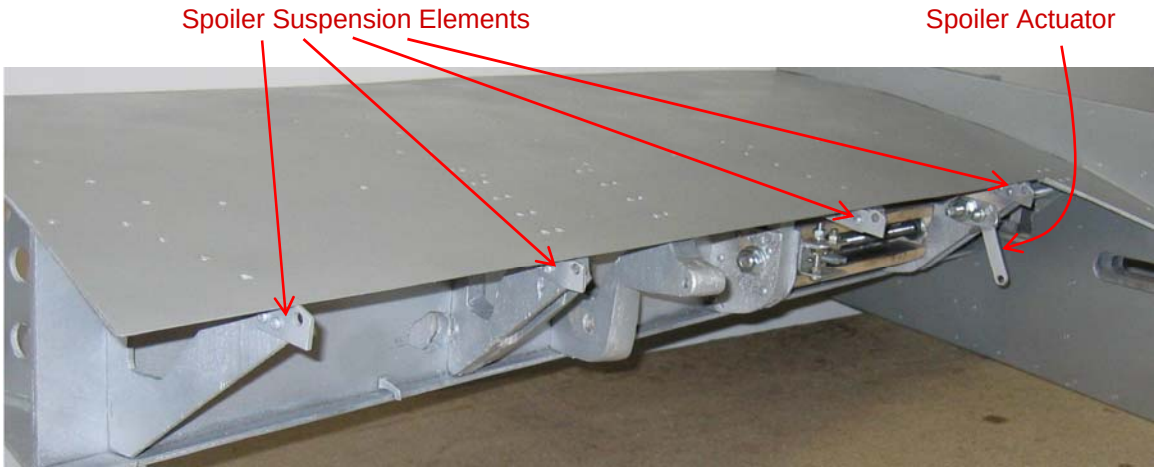

Figure 5.102 Spoiler suspension elements and actuator

In the demonstrator model the spoiler is attached by means of a single rod inserted into the spoiler suspension and attachment elements, similar to the tab attachment system. The rotary actuator element and its link are attached to the corresponding attachment element on the spoiler.

Figure 5.103 Spoiler attachment rod inserted

Figure 5.104 Spoiler actuation

5.13 Inboard Flap Track Station

5.13.1 State of the Art

In practically every modern airliner the number one flap track station is integrated in the fuselage.

The Airbus A330/340 system as shown in fig. 5.105 below uses a system with programming cams and sliders. This system requires a slot in the fuselage structure; for aerodynamic efficiency reasons it is closed in the flaps retracted position.

To keep this slot as small as possible there is a single attachment block (carriage) for the flap; the block is suspended on and controlled by two programming cams.

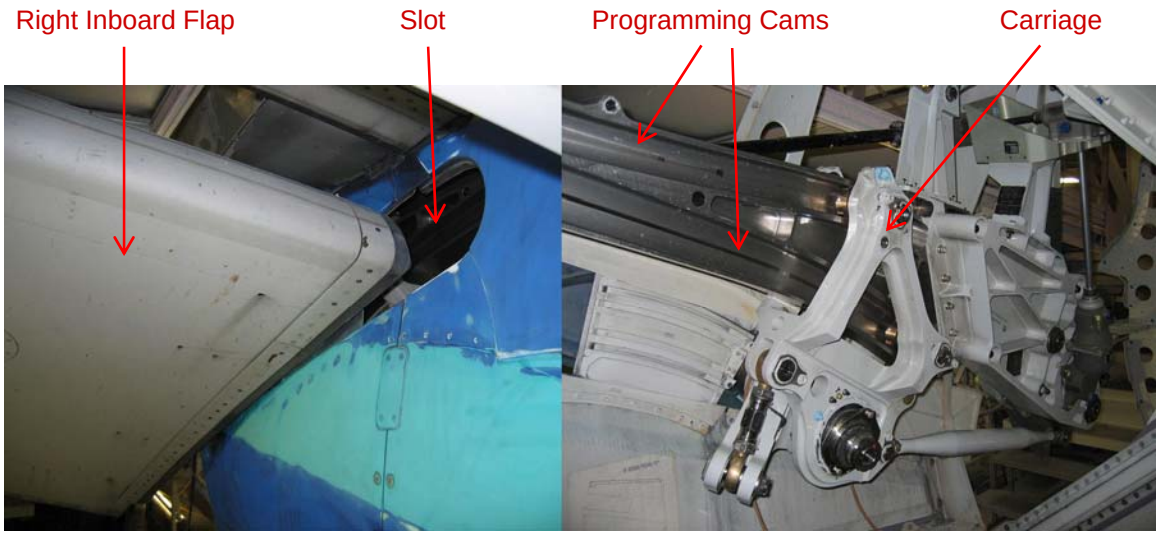

Figure 5.105 A330/340 #1 flap track station (right side), view from out- and inboard

5.13.2 Simplified Demonstrator Approach

Since the intention of using such a flap track in the demonstrator model is to reduce work, a somewhat simplified system is used; the slot remains open. There are two bolts sliding along two cams instead of a single carriage. This requires cutting the fuselage section more than with a single carriage, but facilitates the programming cam placement. They need to be chosen such that they do not collide with each other, but nonetheless provide for the desired flap extension characteristics. Furthermore, they must be set such that the corresponding attachment points on the flap body do not collide with other structural boundaries, like the flap's rear spar, nose, top and bottom shell.

The sliding bolts are at the same time ball joints attached to the flap. Rigid attachment elements can not be used here due to the flap's 3D rotation. The fuselage slot needs to be large enough to accommodate these ball joints. The sliding bolts are kept perpendicular to the cams by attaching them to a panel sliding on the fuselage section's inboard surface.

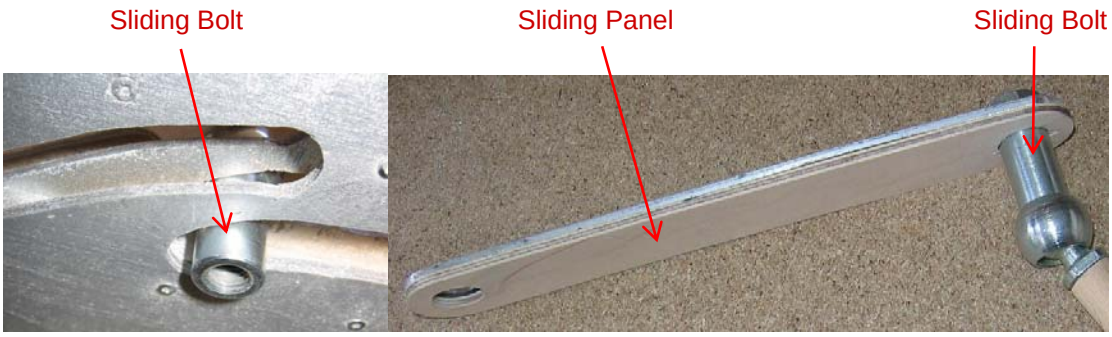

Figure 5.106 Sliding bolt inserted in cam, and attached to sliding panel

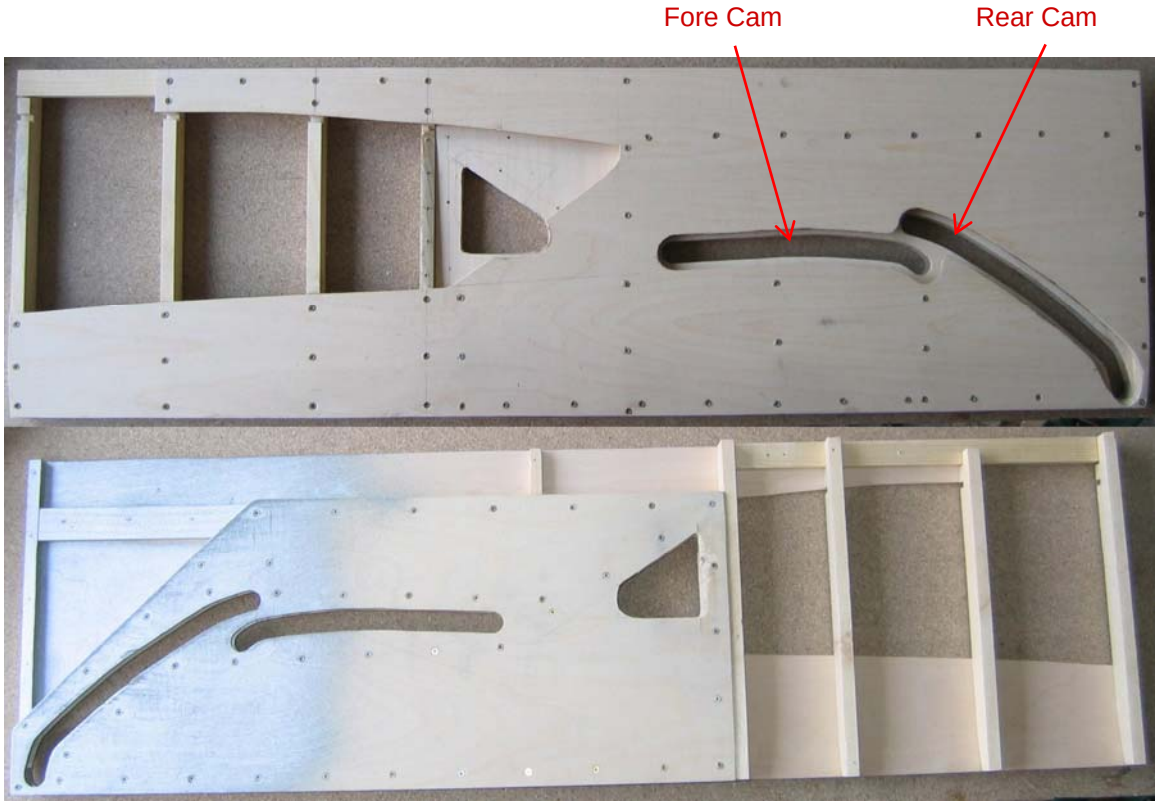

Figure 5.107 Fuselage section with inboard flap track cams (outboard/ inboard view)

Due to the flap's beta rotation the flap body top moves somewhat to the inboard and thus into the slot with full flap extension. Figure 5.108 shows that the slot is just large enough to avoid a collision. Due to its extension perpendicular to the leading edge, the flap vane moves somewhat to the outboard which is just enough to avoid collision with the fuselage section.

Actuation is accomplished via the same screw as is being used for the integrated flap track station. The motion is transferred to the linear cam on the fuselage section by means of a link and then transferred to the sliding panel via a programming cam and linkage to ensure the correct flap position corresponding to the extension state of the other flap track station.

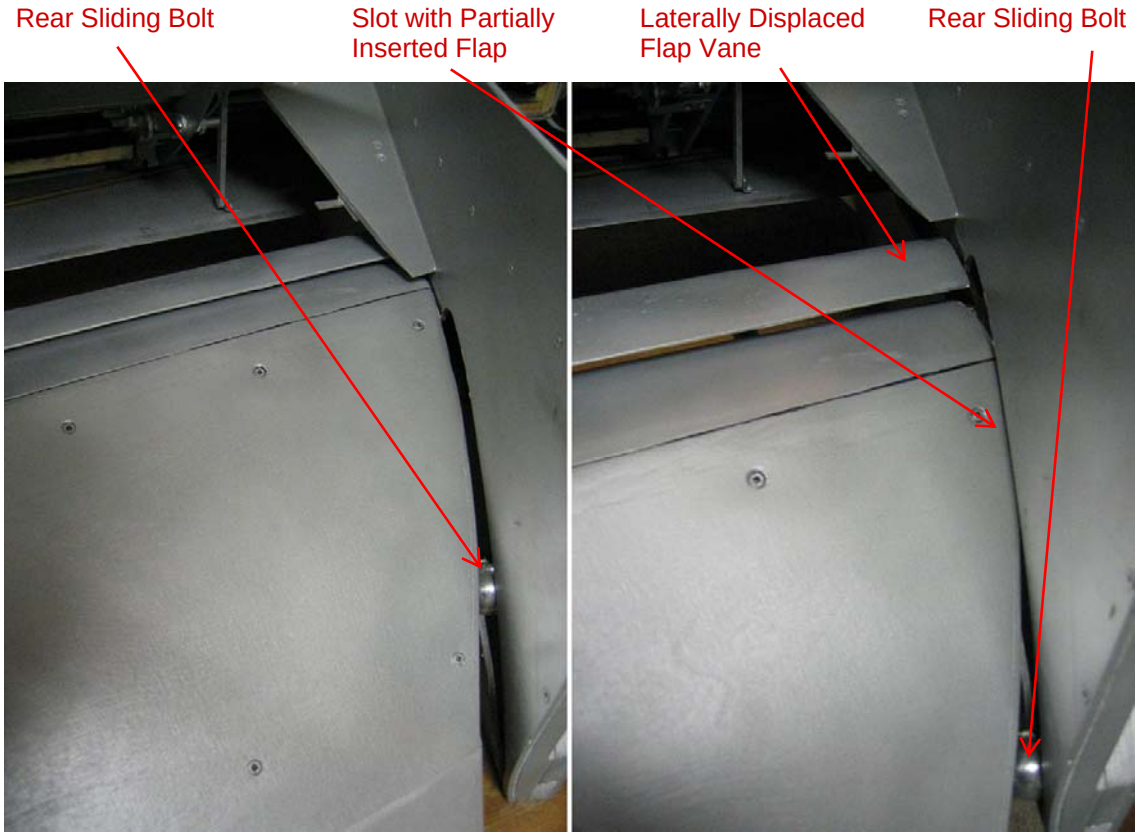

Figure 5.108 Inboard flap track (half and fully extended positions)

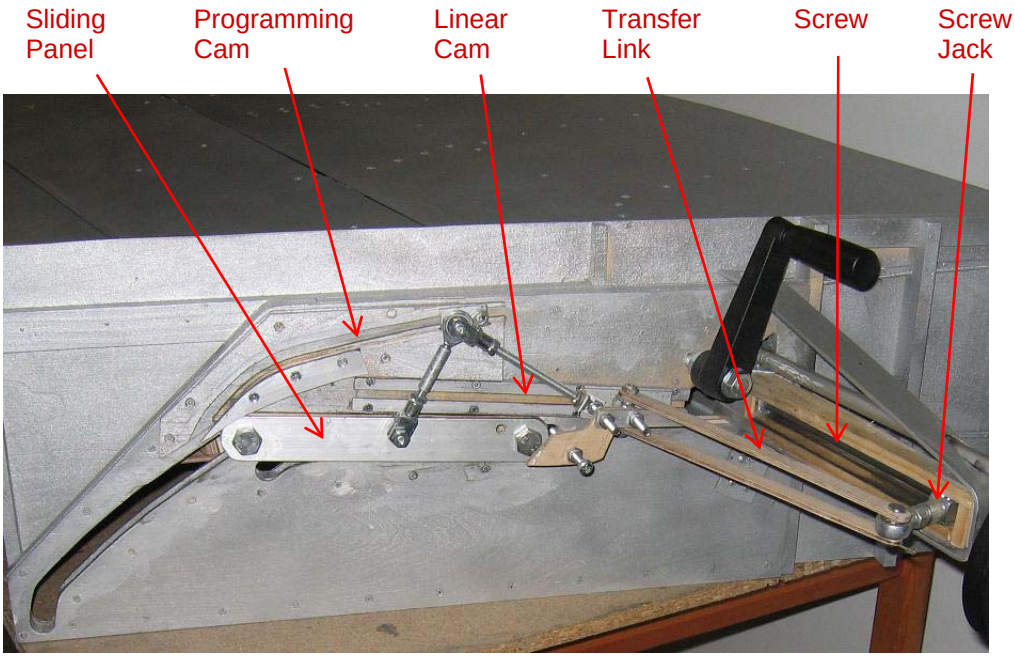

Figure 5.109 Inboard flap track actuation system

Figure 5.110 shows the actuation mechanism in different flap extension positions. The figure also shows all three operation devices on the demonstrator.

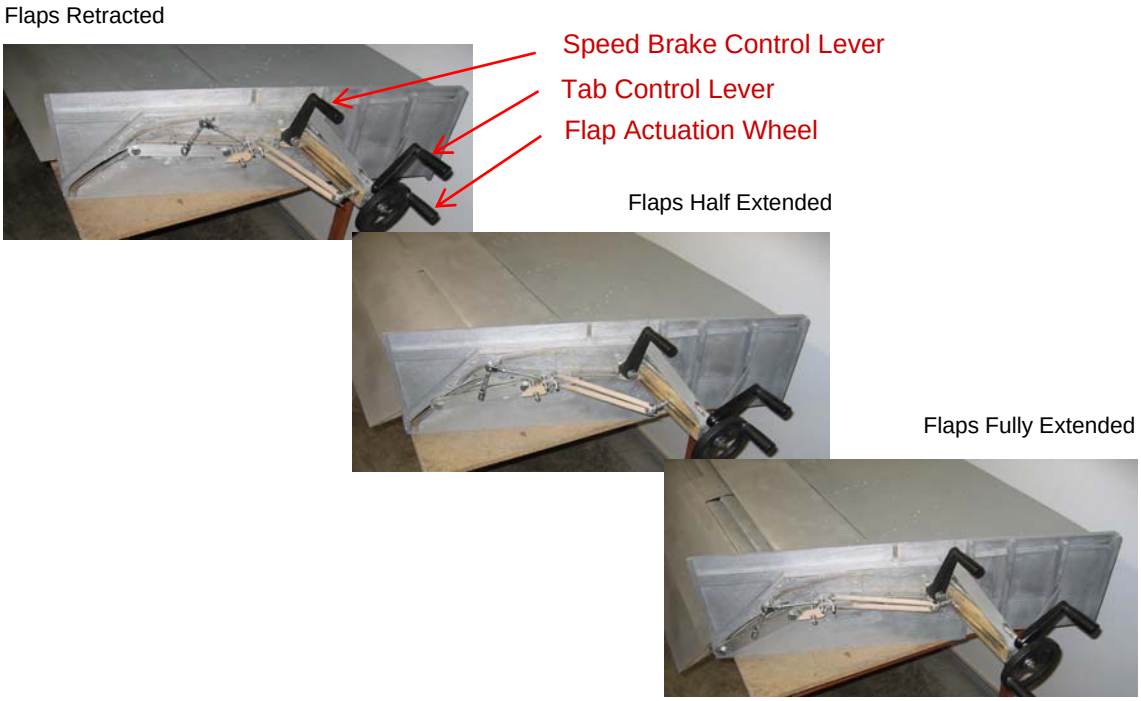

Figure 5.110 Inboard flap track actuation system and demonstrator operation devices

Chapter 6

Structural Details and CAD Model

6.1 Overview

The intention of the CATIA V5 CAD model as presented in this chapter is to provide the basis for movies of the working main mechanism, and for some basic and simple FE analyses of selected parts. For some parts there is a higher level of detail compared to the demonstrator model, such as lightweight shear field design approaches applied to suitable parts. Some minor modifications are carried out, such as improved moving bottom covers. Emphasis is set on the main mechanism, however, so many parts like rivets etc are not modeled, and neither are the tab actuation mechanism and wing internal structure.

As opposed to the demonstrator model, two identical flap track stations are being used in the CAD model to simulate an outboard flap configuration. The wing section and dimensions used are similar to the B767 outboard flap region (see also figure 4.3). The section has a span of about 6 meters, which is considered to be the minimum to accommodate two integrated flap track stations, i.e. with this dimension the outboard station's actuation screw and suspension do not collide with the inboard guide structure assembly.

From this chapter onward, only one design step will be done, i.e. no iterations are carried out to optimize the respective design. This particularly applies to flange dimensioning and other tasks the results of which highly depend on actual loads and circumstances of the aircraft, factors which are not known accurately enough in this project to make extensive optimization steps reasonable.

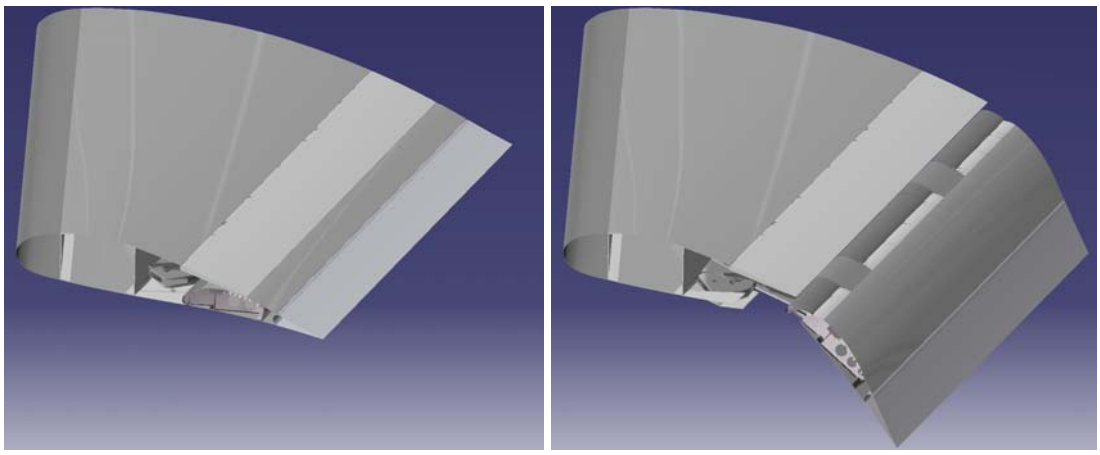

Figure 6.1 Wing section with flaps fully retracted and extended

Figures 6.1 and 6.2 present snapshots of the assembled model. Note that the main cover's extendable part is not featured since modeling of flexible parts creates problems in the CAD model.

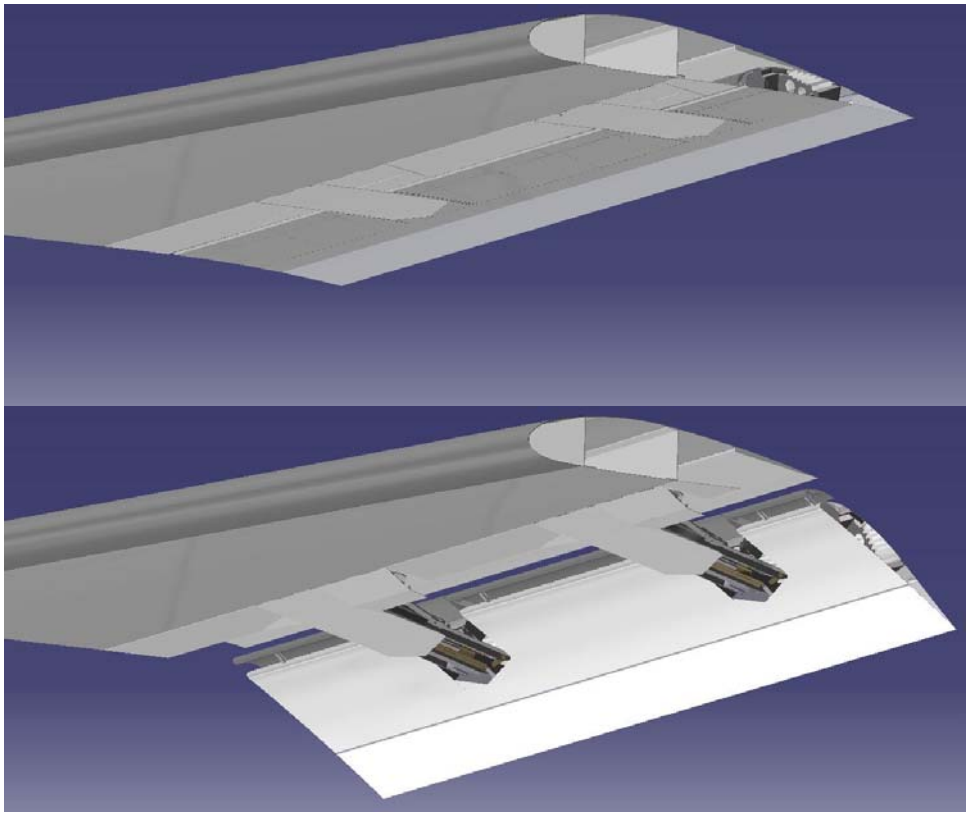

Figure 6.2 Wing section bottom view with flaps fully retracted and extended

6.2 Guide Structure Assembly

6.2.1 Mounting Plate

As with the demonstrator model the mounting plate is made up of a single part, which also contains the programming cams as well as transformation locking cams, lever E axis attachment sockets and distance block attachment points.

The bottom view in fig. 6.3 shows that the plate's inboard and outboard parts are designed as shear fields, using pockets to minimize weight; the flanges are set such that there are no bends in the force flow wherever possible.

In the middle part no such pockets are applied, since due to the level of detail chosen the attachment rivets and holes for the guides are not featured, but they would have a significant effect on pocket placements.

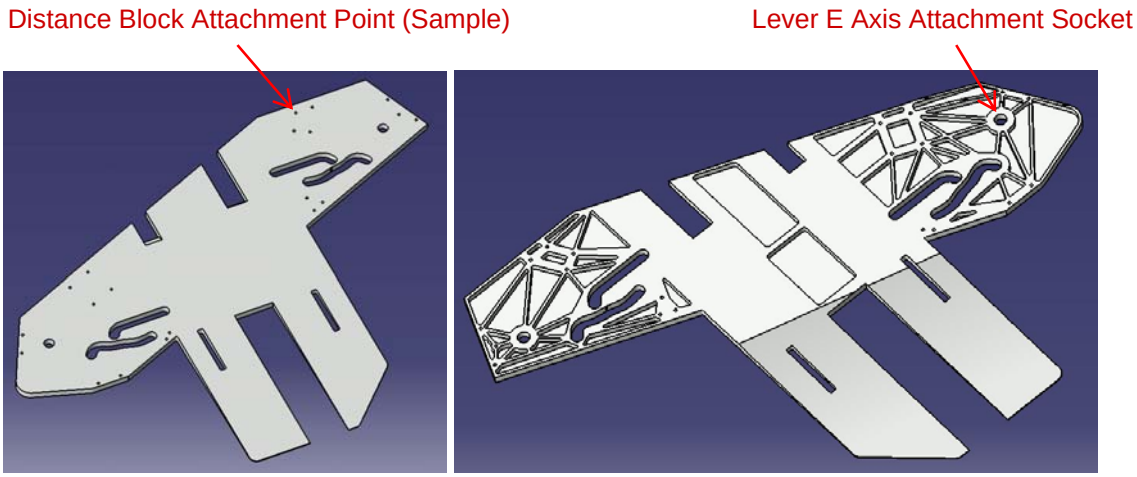

Figure 6.3 Mounting plate top and bottom view

6.2.2 Main Slider Roll Support and Other Structures

So far all slider contacts and guides have been designed as floating bearings. For highly loaded parts such as the main slider, however, it does make sense to apply roll supports as mere lubrication may not be sufficient to allow a smooth extension. Although such roll supports are ideally applied to all sliding elements, it is done exemplarily for the main slider only in this project. The main loads are in vertical direction, while the slider needs guidance in the lateral direction as well, but there much smaller loads apply.

The main slider support rolls are fixed to the inboard and outboard main slider guide profiles by means of clamps as shown in fig. 6.4 on the next page. To ensure firm support in all flap extension states these rolls are mounted only at the main slider overlap area of the guide structure assembly, which can be seen in fig. 6.5. Otherwise, when the main slider moves off such a support roll and bends due to flap load, it could block when being retracted.

Main slider lateral guidance is accomplished by fixed and moving rolls. The fixed rolls are attached to a U-profile which is mounted on the inboard and outboard guide profiles and fits within the main slider profiles (see figures 6.5 and 6.6). Two additional rolls are attached at the main slider fore end (see fig. 6.7) which provide lateral guidance near the flaps retracted position. They also serve as an additional blockage so that the main slider and attached flap cannot completely detach from the wing should all other links fail. To separate the main slider from the guide structure assembly these rolls would need to be detached first.

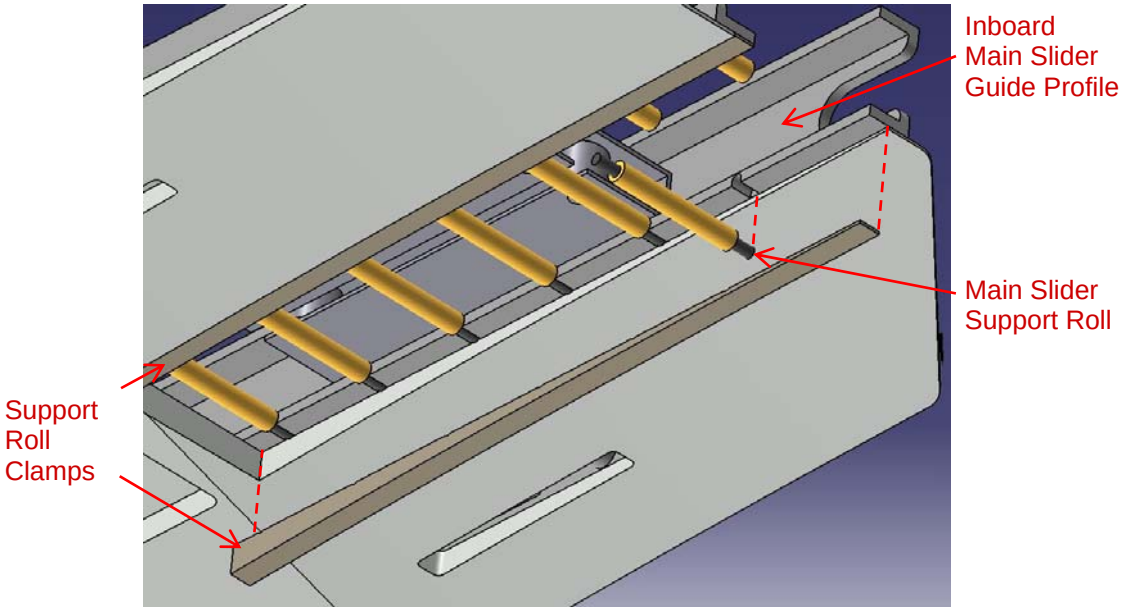

Figure 6.4 Mounting plate bottom view

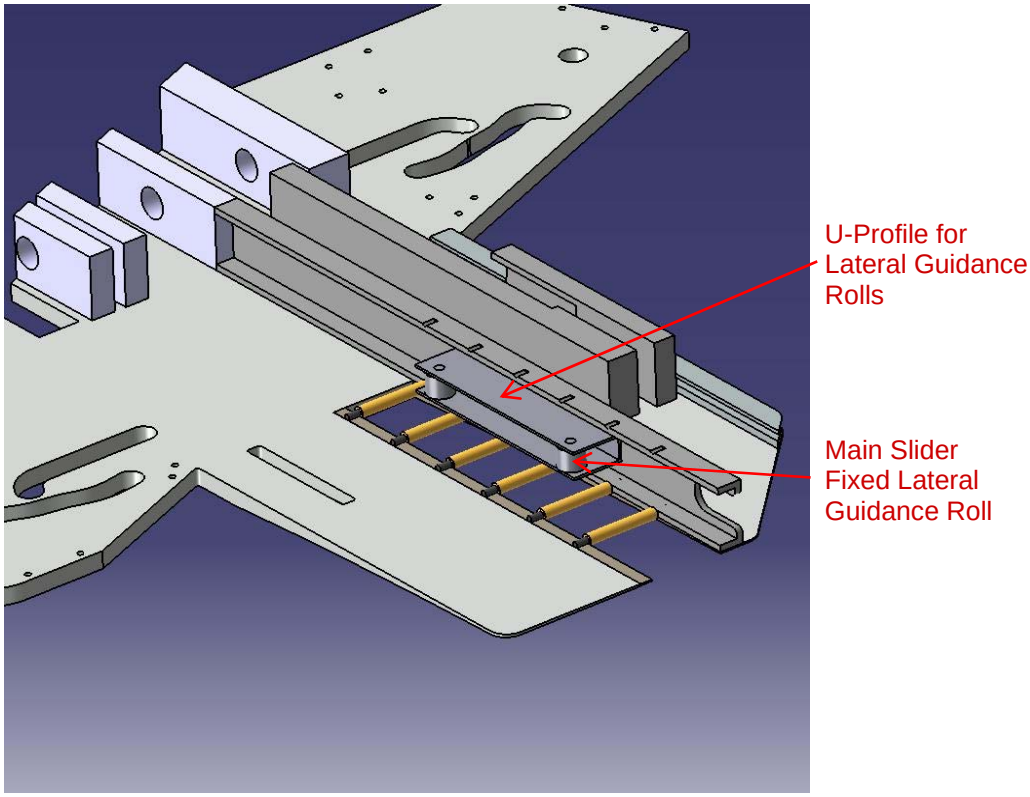

Figure 6.5 Mounting plate top view, structures partially shown

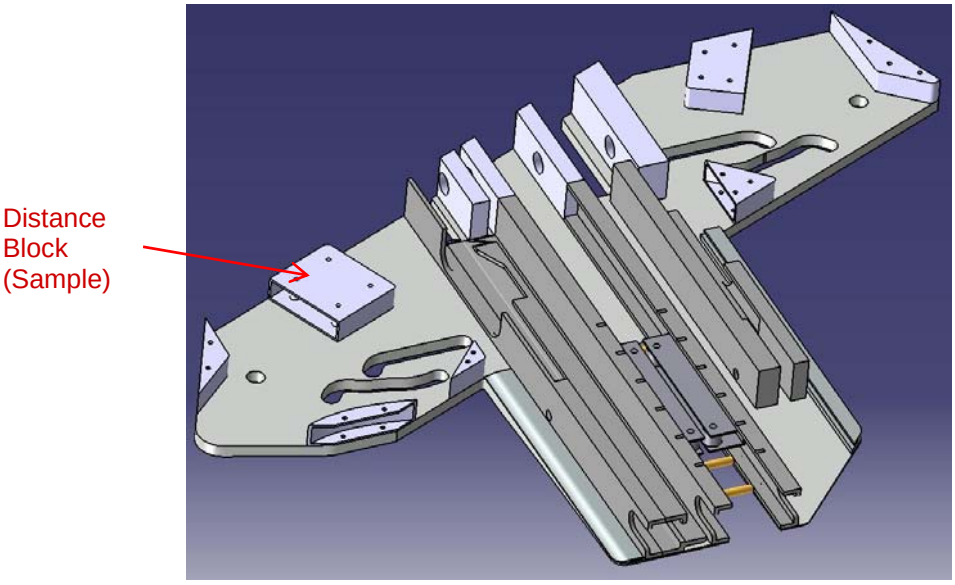

Figure 6.6 Mounting plate top view, all structures shown

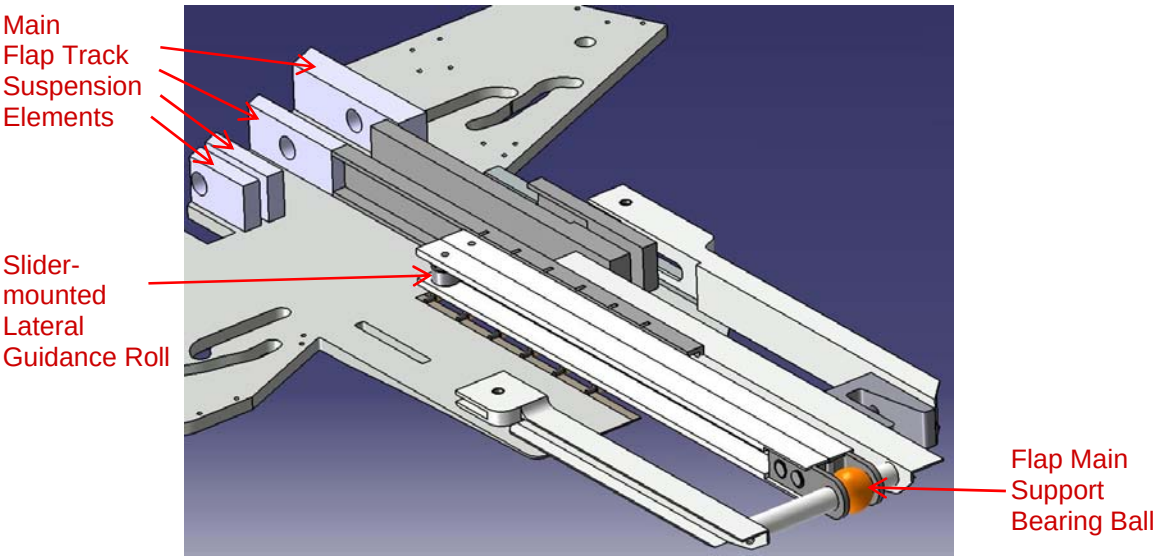

Figure 6.7 Mounting plate with main slider and appendages (flaps extended)

Mounting of the top main slider support rolls is much similar to the bottom part, but now the clamps are at the same time the guides for the main slider control slider, as shown on the following page. To replace any of these top support rolls the main slider control slider needs to be removed first followed by the clamps.

This design requires another large cut in the cover, as seen in figure 6.9. The entailing reduction of guide structure assembly bending stiffness is counteracted somewhat by the guides mounted on the cover.

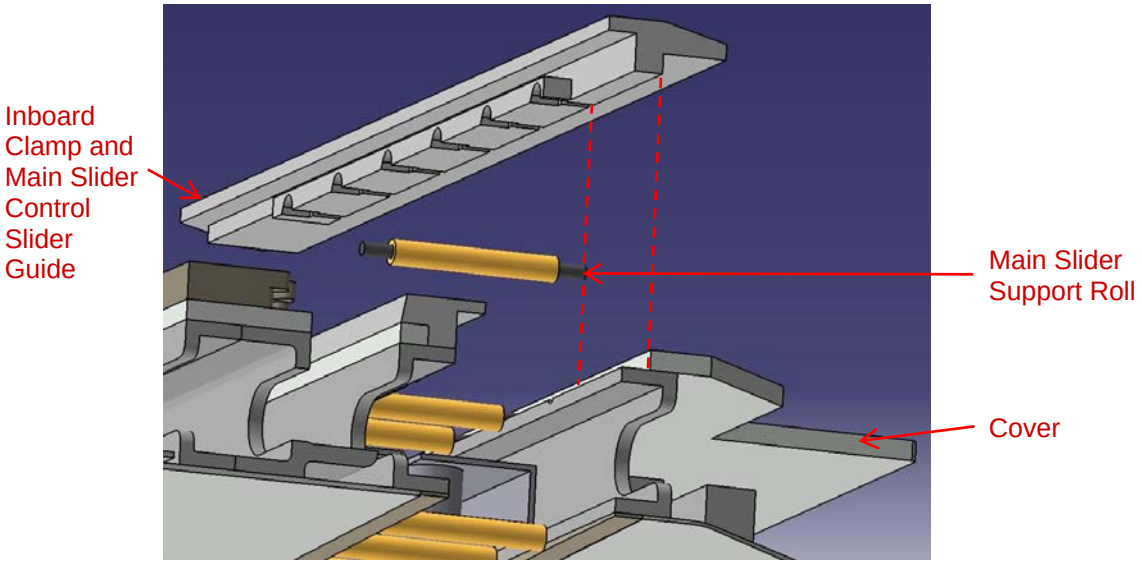

Figure 6.8 Main slider top support roll clamp

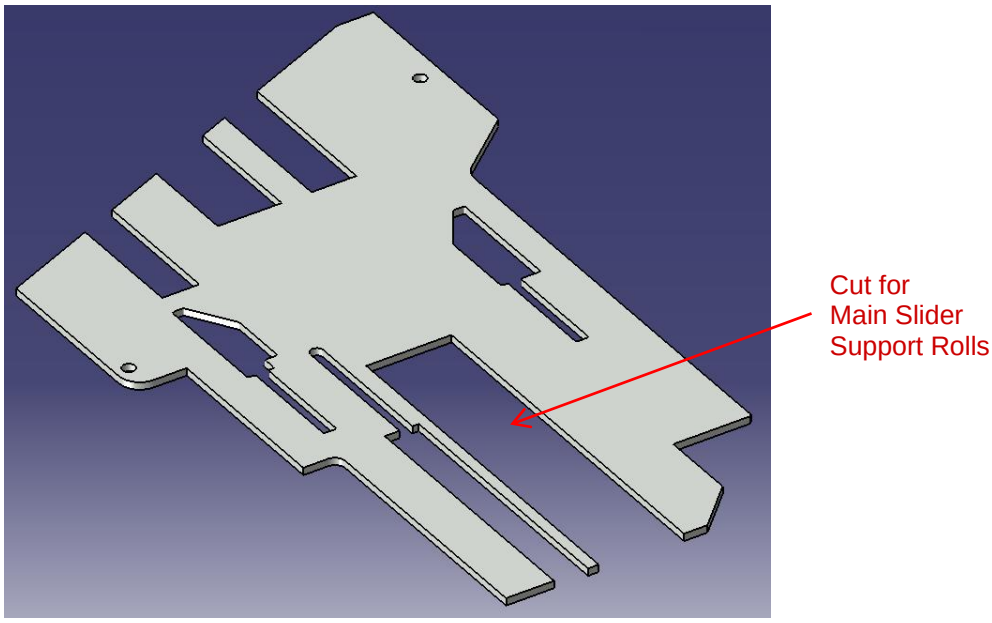

Figure 6.9 Guide structure assembly top cover

Finally, the guide structure assembly contains all guides, supports and rolls needed to accommodate all other moving parts of the mechanism.

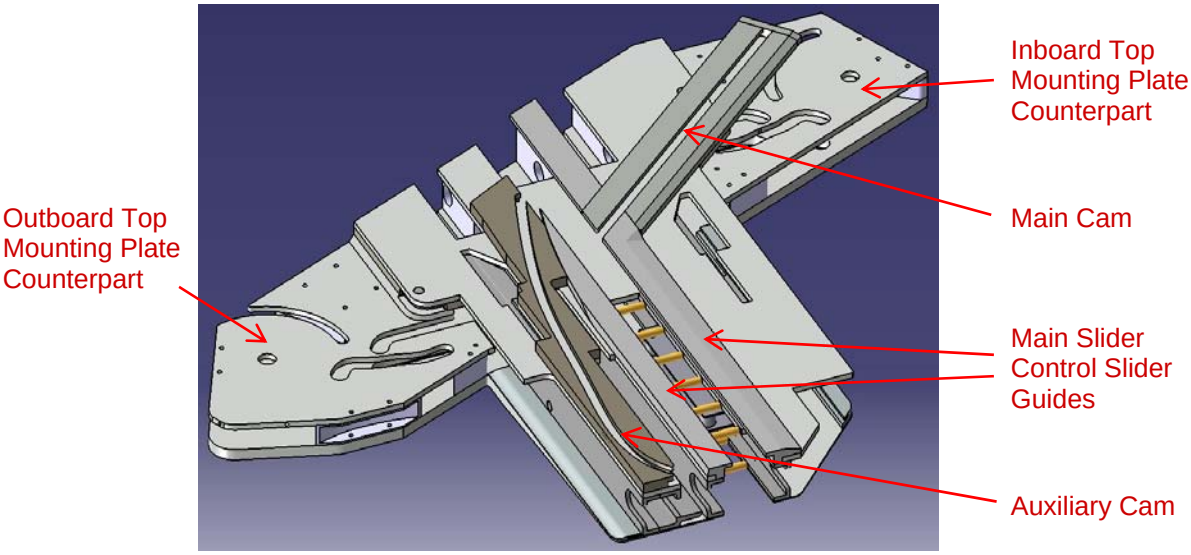

Figure 6.10 Full guide structure assembly

6.3 Support Angle Control Linkage

6.3.1 Suspension Link

As explained in chapter 5.3.2, the suspension link needs axial bearings to prevent the whole linkage from bending. These bearings need to be securely fixed to the link also in the axial direction and doubling them on each side represents a fail-safe approach. The design with securing flanges as shown in fig. 6.11 below meets these requirements, and the link itself as well is made up of a positive and a negative part screwed together. Note the chamfer on the negative part which is considered necessary for ensured collision avoidance with various links (compare detailed explanations in chapter 5).

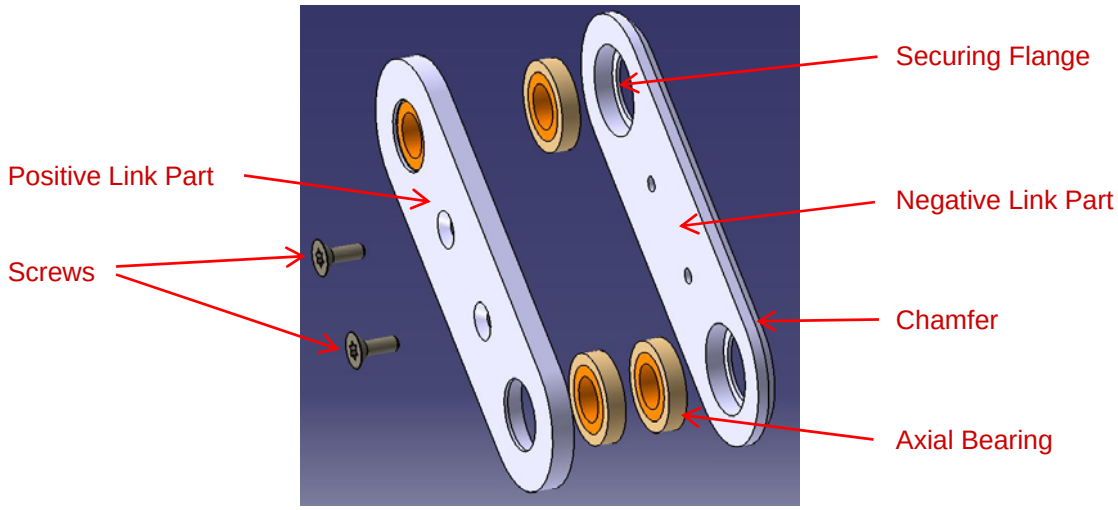

Figure 6.11 Suspension link (exploded view)

6.3.2 Main Slider Angle Link

In fig. 5.18 a simple rod with ball-joint ends has been suggested for this part. However, since it is highly loaded with a pressure force (outlined in chapter 7), it is susceptible to bending and a moment of inertia increase should therefore be envisaged. So almost the identical approach as with the suspension link is applied to the main slider angle link, but here ball joints are used rather than axial bearings, which renders doubling impossible. As explained, mainly pressure loads act on the linkage. Since the main slider angle link is longer than the suspension link the positive and negative parts are more susceptible to bending; this effect may be counteracted somewhat by applying more than the two screws shown to fasten them together.

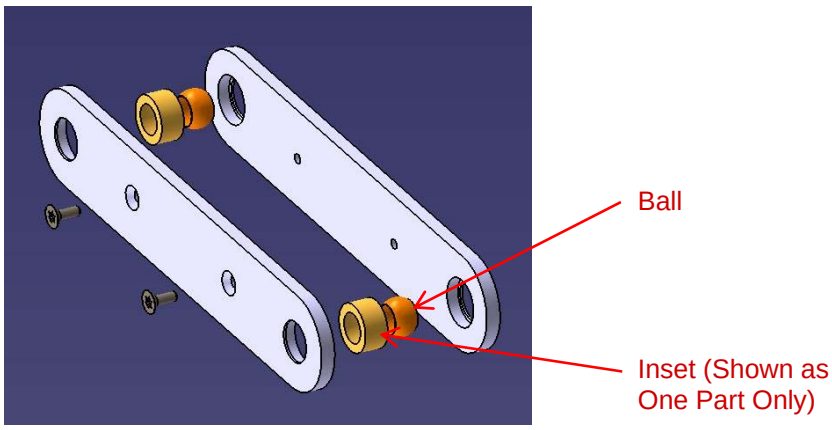

Figure 6.12 Main slider angle link (exploded view)

6.3.3 Support Angle Control Linkage Sliders

As depicted in figures 5.22 and 5.25, the support angle control linkage sliders are somewhat complicated parts from a geometrical point of view. Nevertheless, they can be manufactured from single raw blocks. As shown below, pockets can easily be introduced.

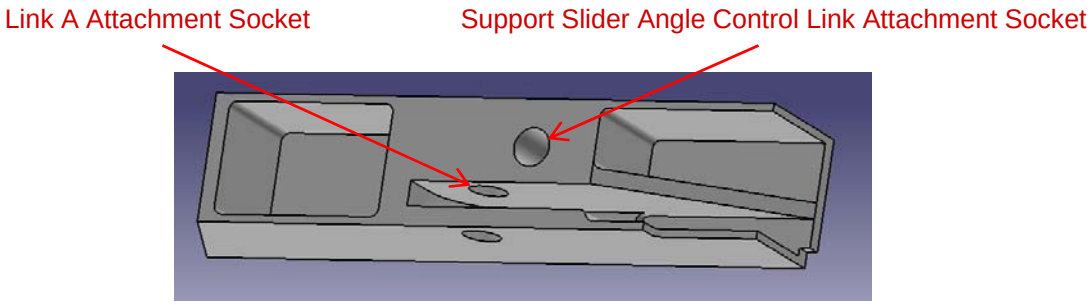

Figure 6.13 Outboard support angle control linkage slider

There are some peculiarities with the inboard slider, however. First, a boss is added at the socket for the support slider angle control link attachment bolt. This guides the bolt and prevents it from snapping off with high loads.

Second, there is a relatively large hole behind the link A attachment socket. This is needed for assembly of the full mechanism: the guide structure assembly would normally be attached to the wing with all links and sliders already mounted, but the main flap track suspension bolts still need to be handled. As the inboard slider covers the main flap track suspension elements and their bolt sockets, it must therefore have a hole with the dimension of a main flap track suspension bolt to handle these bolts conveniently. Since attaching the guide structure assembly is best done with the mechanism in the flaps fully extended position, this hole must be located accordingly on the inboard slider, i.e. slightly behind the link A attachment socket as shown in fig. 6.14 below.

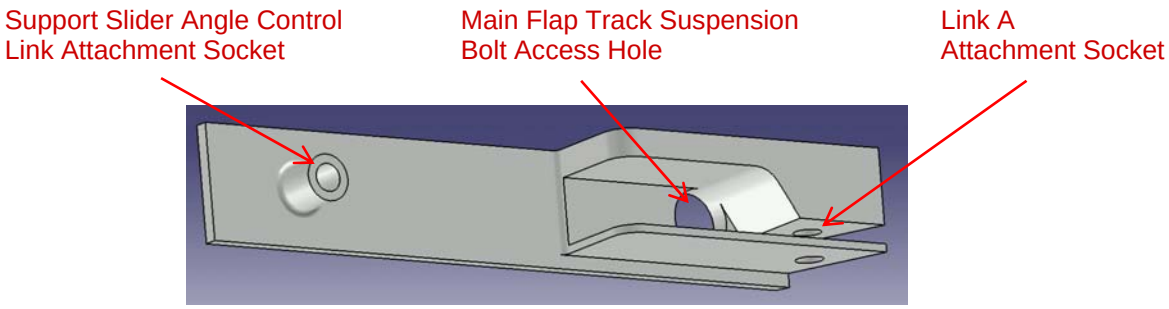

Figure 6.14 Inboard support angle control linkage slider

6.3.4 Main Suspension Elements

Leaving the main suspension elements as presented in chapter 5 would lead to a prohibitive weight. In aerospace engineering such parts are often designed using a shear field/flange approach, and this is done too for the main suspension elements. The white lines in fig. 6.15 below show the basic flange lines applied, particularly the indicated main flange lines should not be bent since otherwise high stress concentrations would occur as they represent the main load paths.

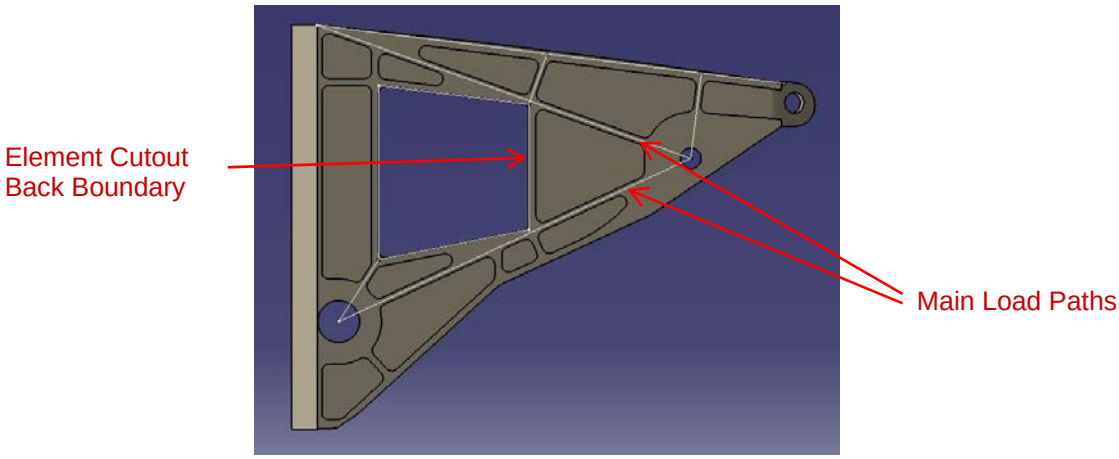

Figure 6.15 Outboard main suspension element basic flange lines

The flange widths are set arbitrarily, but with some optical reference to similar such parts in actual airliners. The given main load path flange widths give the backward position limit of the element cutout as shown above.

A number of additional flanges are introduced to avoid too large shear fields applied to reduce weight at various locations. Further, a spoiler attachment element is introduced at the element's rear end.

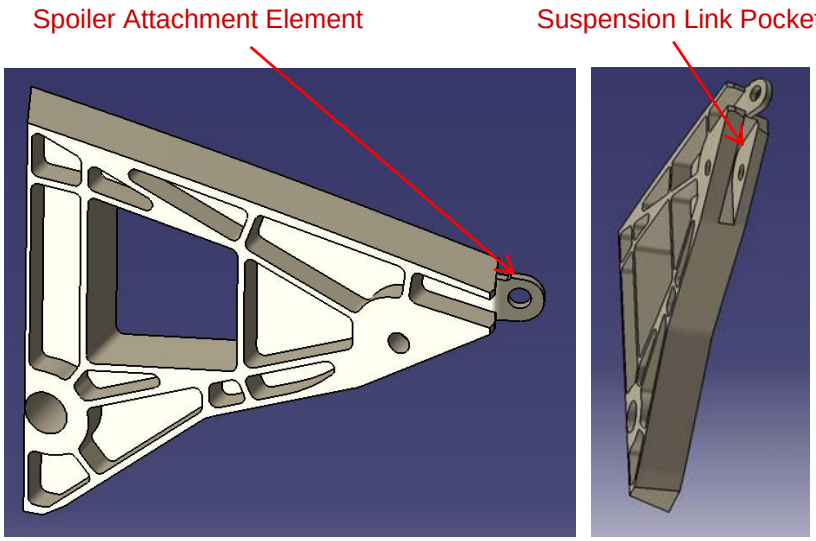

Figure 6.16 Outboard main suspension element

The element is fixed to the main wing rear spar by an array of screws or rivets (holes shown only for the inboard main suspension element below). High stress concentrations are expected particularly at the cutout aft corners which are close to the main load paths. They can be reduced by a corner radius increase at these locations.

For the inboard main suspension element, because of design and collision constraints as outlined in chapter 5 it is not possible to place the lower main load path in a way that it connects the main flap track suspension point to the suspension link attachment point. Therefore the corresponding flange is placed as much downward as possible such that it extends from the suspension link attachment point and passes right above the sharp curve of the element. The element cutout is placed such that this flange remains straight right up to the wing rear spar.

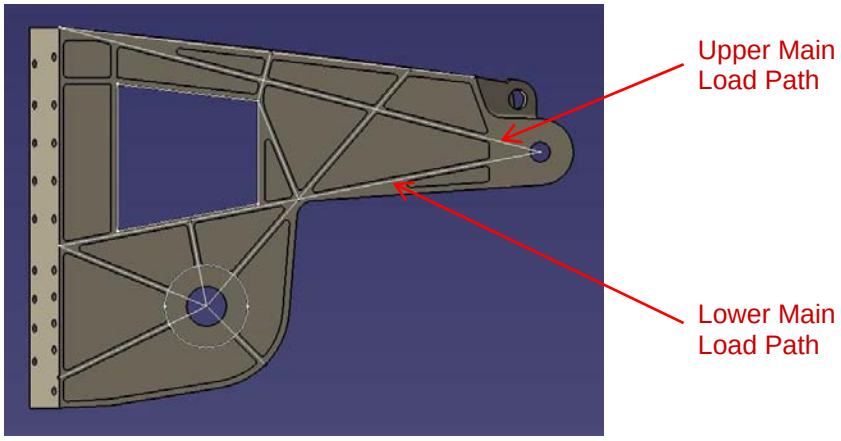

Figure 6.17 Inboard main suspension element basic flange lines

Since the inboard suspension link is mounted somewhat away from the inboard suspension element, the corresponding attachment socket features a boss up to the needed distance.

The inboard main suspension element is wider than its outboard counterpart, so there is enough space for two spoiler attachment elements, as shown below.

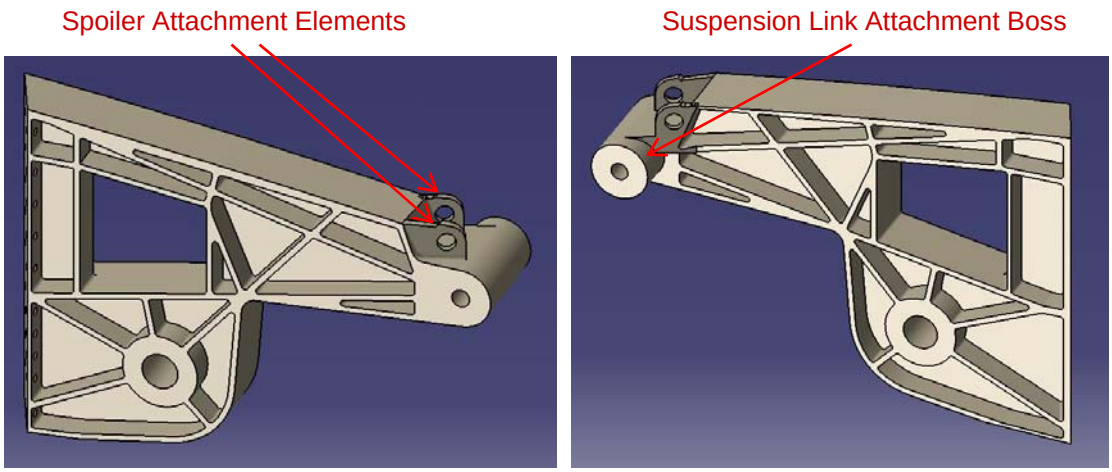

Figure 6.18 Inboard main suspension element (outboard and inboard view)

The structure of these suspension elements makes them suitable for thixoforming, as this production process work particularly well for thin-walled cast parts, produces plane surfaces and, thanks to an uniform microstructure, minimizes internal stress in the part.

6.4 Transformation Locking Mechanism (TLM)

6.4.1 Upper Part

Chapter 5.4.2 presented the TLM layering, suggesting a very flat design of the top part so that it fits in between the main cam and mounting plate top counterpart. It was suggested to arrange the links C and D below lever B. A symmetrical load distribution would be beneficial, however, and this allows for a convenient integration of bearings (same approach as with the suspension link) as shown on the next page; cutouts and screws need to be included to allow full motion of links C and D.

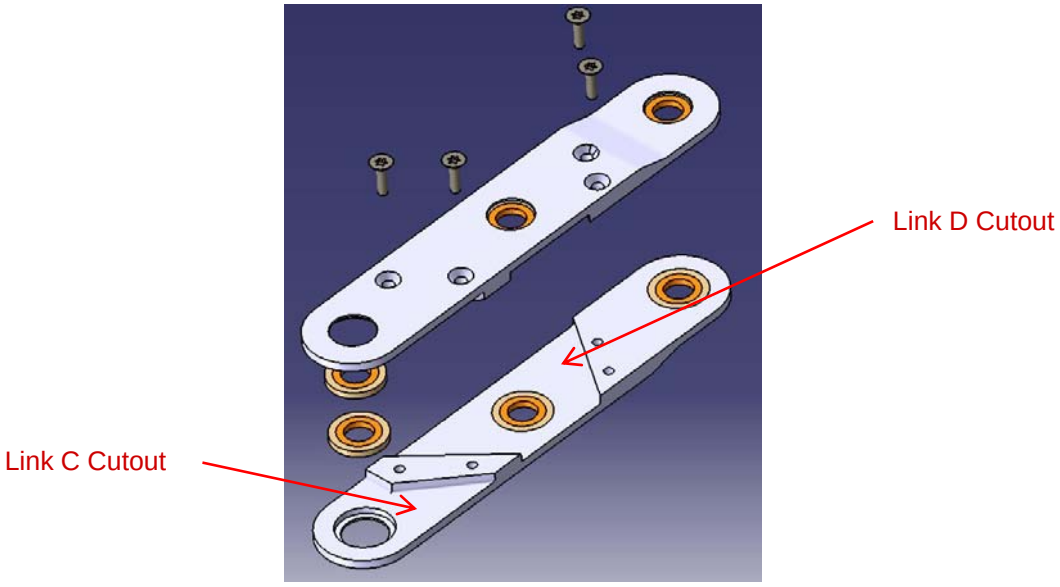

Figure 6.19 Lever B (exploded view)

Links C and D again follow the same design approach as the suspension link, they both just fit into lever B.

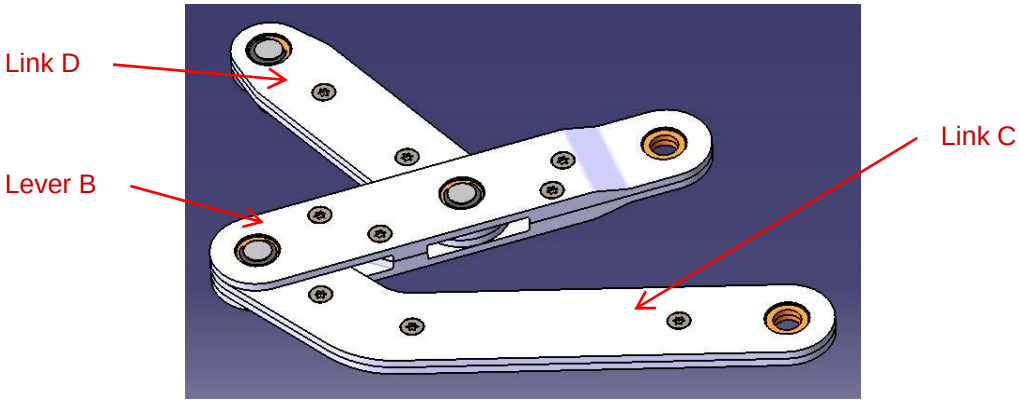

Figure 6.20 TLM upper part

6.4.2 Lower Part

Lever E and link G are both made of one raw block, respectively, as shown in fig. 6.21 on the following page; they are connected by the ball-joint supported link F. This is basically the same design as has been suggested in chapter 5.

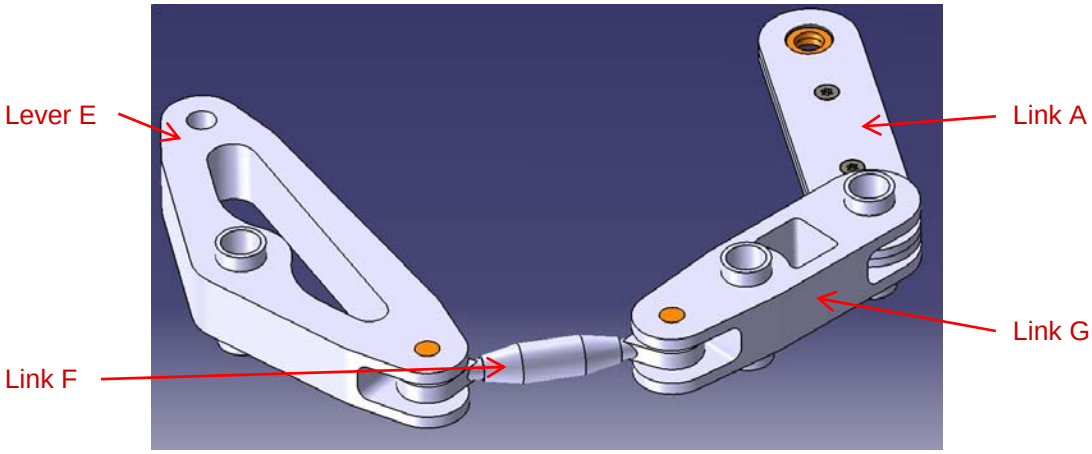

Figure 6.21 TLM lower part

For the CATIA assembly to work properly, link G must be constrained in a way that it follows both the programming and transformation locking cam. For this purpose two points are introduced at the respective bolt socket midpoints on the link. These points are then set congruent with the cam datum lines.

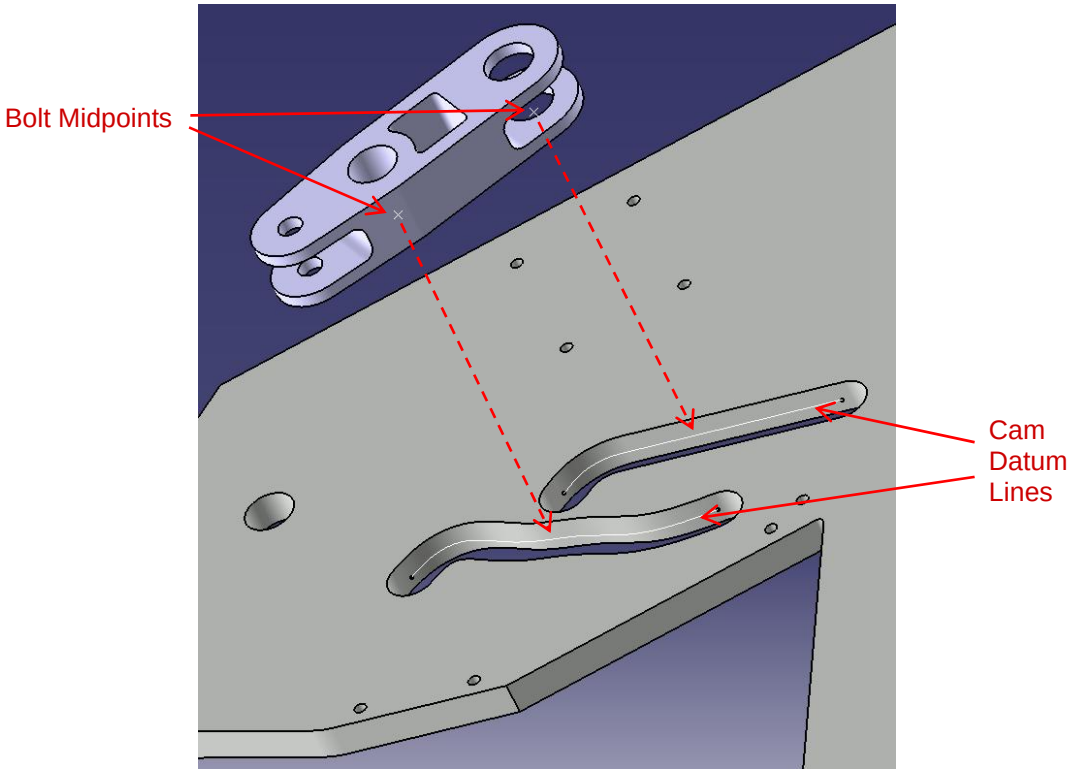

Figure 6.22 Link G guidance in CATIA assembly

The fully assembled outboard TLM and support angle control linkage look as follows, with flaps approximately 25% extended.

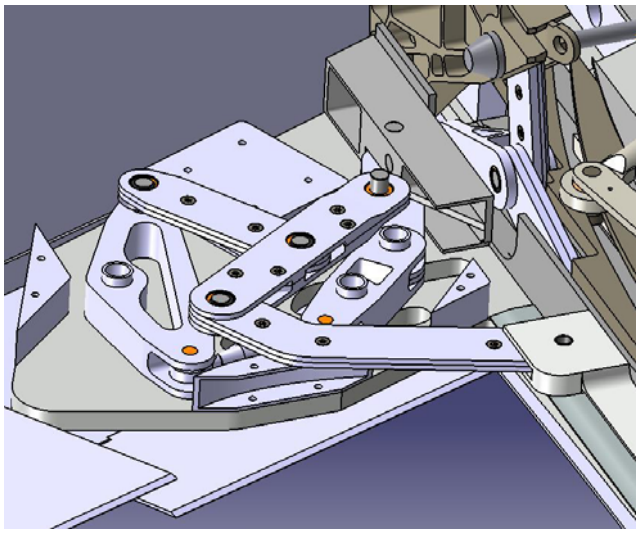

Figure 6.23 Full outboard TLM (top counterpart and cover removed)

6.5 Wing Bottom Covers

6.5.1 Fixed Covers

Basically, the fixed bottom covers should be as large as possible as this entails the least negative impact on aerodynamics. Figure 6.24 below shows the main wing structures with attached main suspension and screw suspension elements for both stations, as well as the fixed bottom covers.

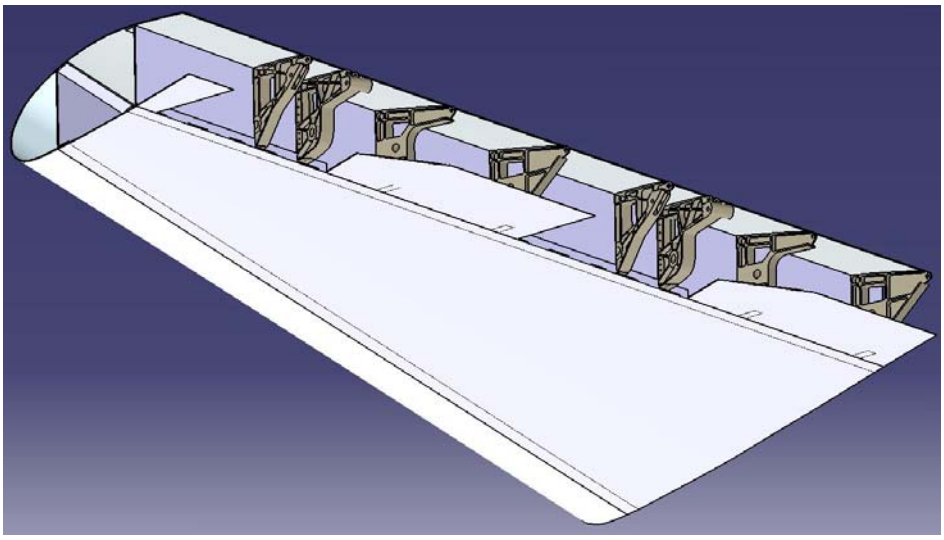

Figure 6.24 Main wing assembly with fixed parts attached

6.5.2 Moving Covers

Moving bottom covers disturb the airflow, so besides being as small as possible they should be shaped in way which minimizes airflow deflection and separation. The cover designs as can be seen for example in figure 5.88 can be improved in this respect. Figure 6.25 below show these improved covers.

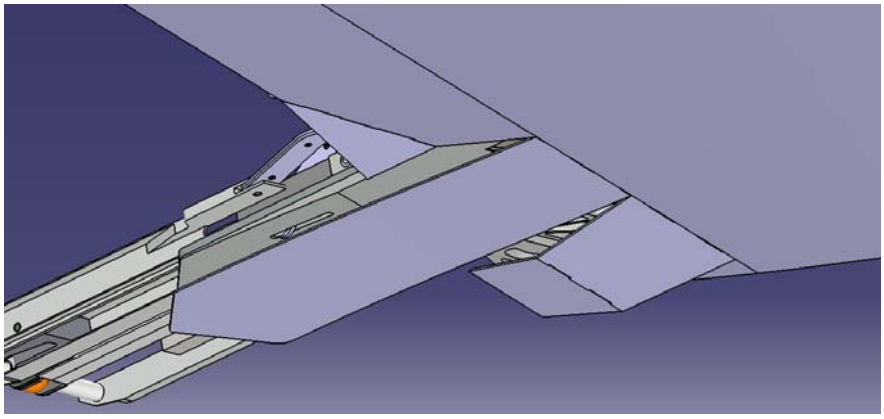

Figure 6.25 Wing bottom covers

As mentioned already, the main cover's extendable part is not featured since modeling of flexible parts creates problems in the CAD model. The flexible modeling would be needed to account for the complex flap 3D rotation, especially the beta angle. There is an angle of 23° between the main bottom cover hinge line and the guide structure assembly hinge line, which upon extension leads to a tilt of the main cover in the desired beta direction, as shown in figure 6.26 below. This reduces the angle greatly by which the extendable cover would need to be twisted. The corresponding link is not modeled, but indicated by a green dashed line.

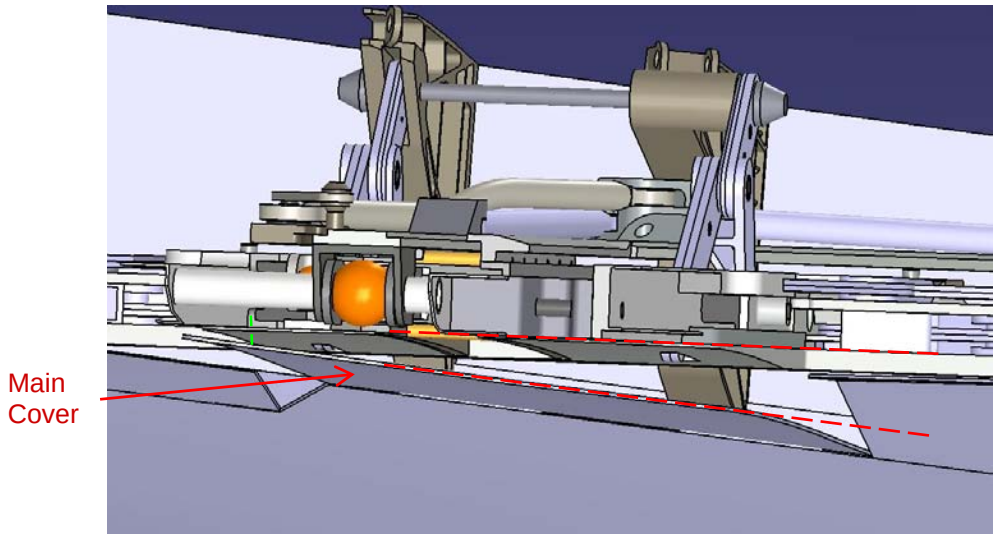

Figure 6.26 Main bottom cover tilt (view from back, flap not shown)

The inboard cover need not be square shaped, but a small triangle is sufficient to avoid collision with the guide structure assembly, as shown in fig. 6.27. Again, the corresponding link is not modeled, but indicated by a green dashed line.

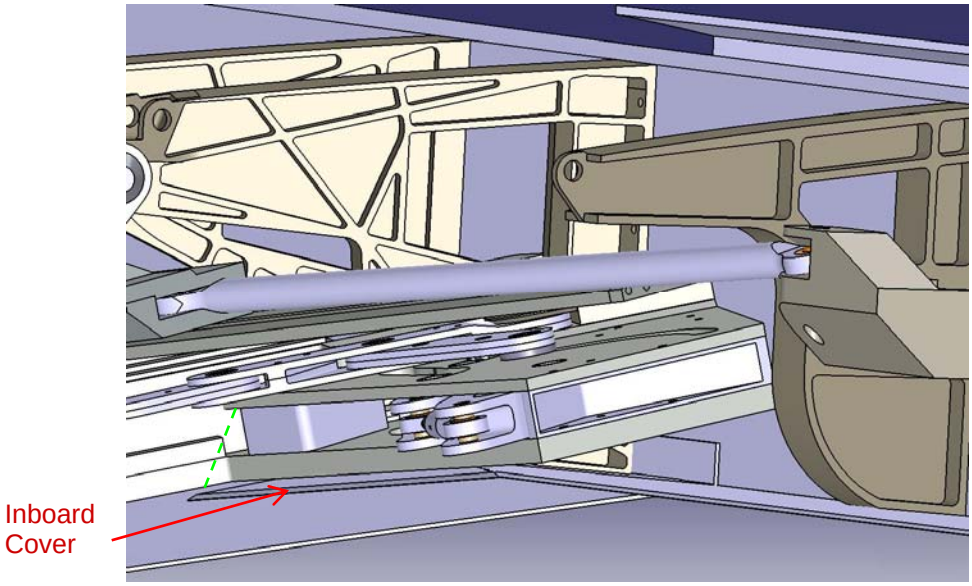

Figure 6.27 Inboard bottom cover (flaps fully extended position)

While in fig. 5.88 the second section of the outboard moving cover is only a small triangle at the outer corner, this section can be enlarged to a more rectangular shape, without collision, as shown below.

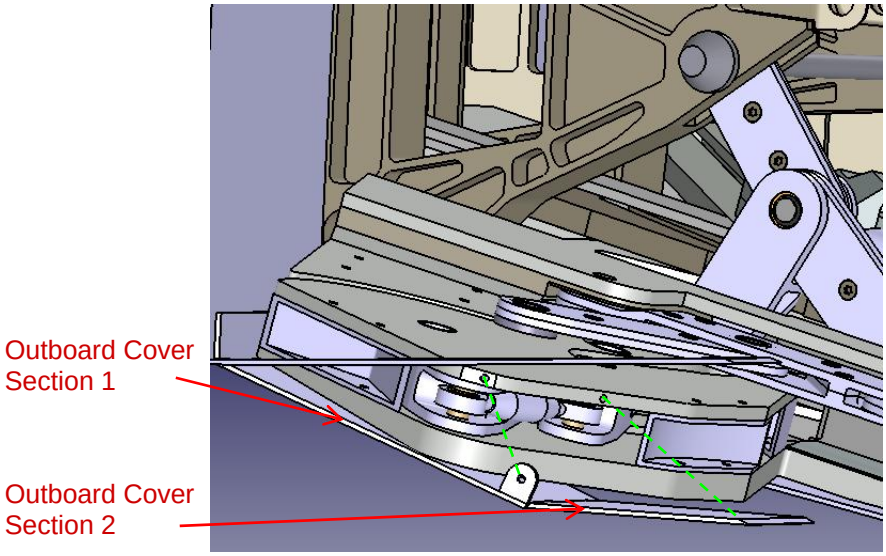

Figure 6.28 Outboard multi-section bottom cover (flaps fully extended position)

6.6 Flap Body

6.6.1 Rib Placement

The layout as described in chapter 5.6 is applied, apart that now two identical cuts are needed for the two flap track stations. The rectangular ribs contain cutouts typical for any such construction. As shown in fig. 6.29 below, some of the nose ribs are doubled; there they are designed as flap vane receptacles.

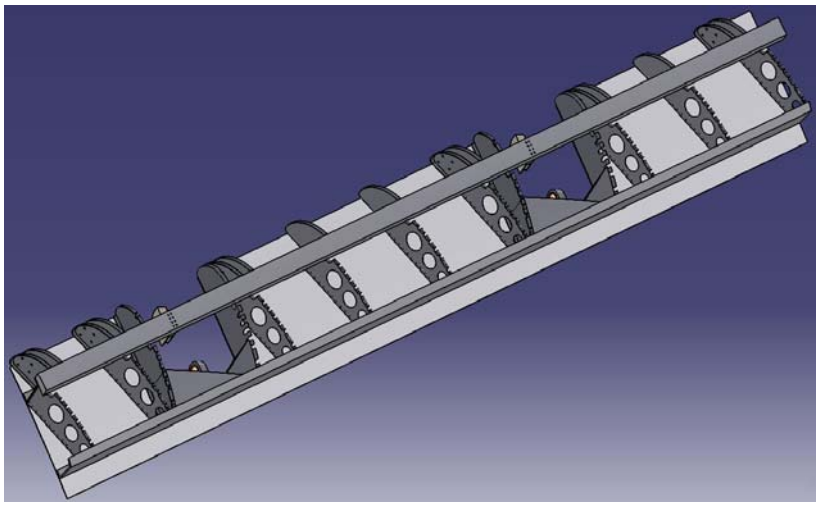

Figure 6.29 Flap body basic layout ─ spars and ribs

6.6.2 Top Shell Stringers

The stringers must be fitted in a way so that they do not collide with the guide structure assembly in the retracted position. As shown in fig. 6.30 below, somewhat distorted stringers cannot be avoided to prevent collision, but the design as displayed keeps fairly much of the standard lightweight structure. The stringers are indeed continuous as fig. 6.31 demonstrates, which is considered to give an acceptable overall stiffness of the flap body top shell.

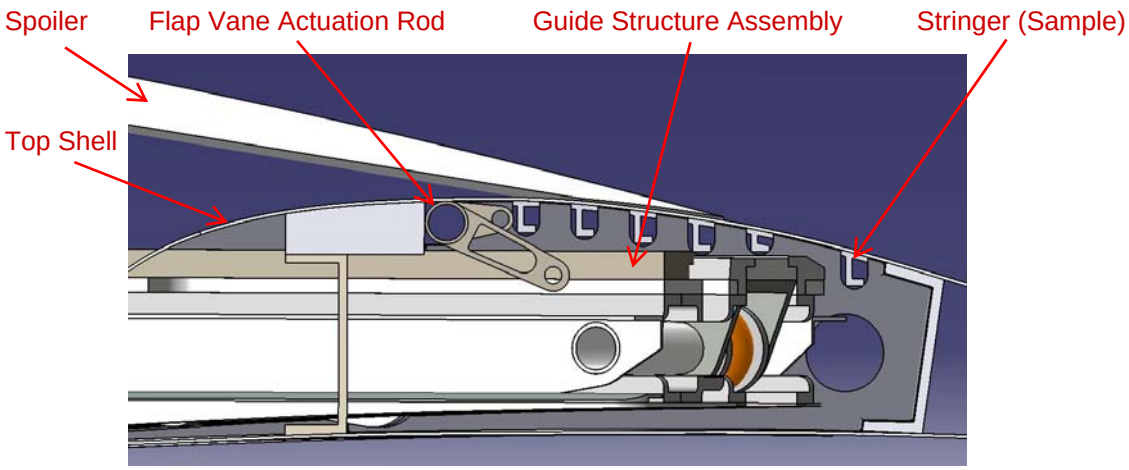

Figure 6.30 Top shell stringer fitting (some parts removed)

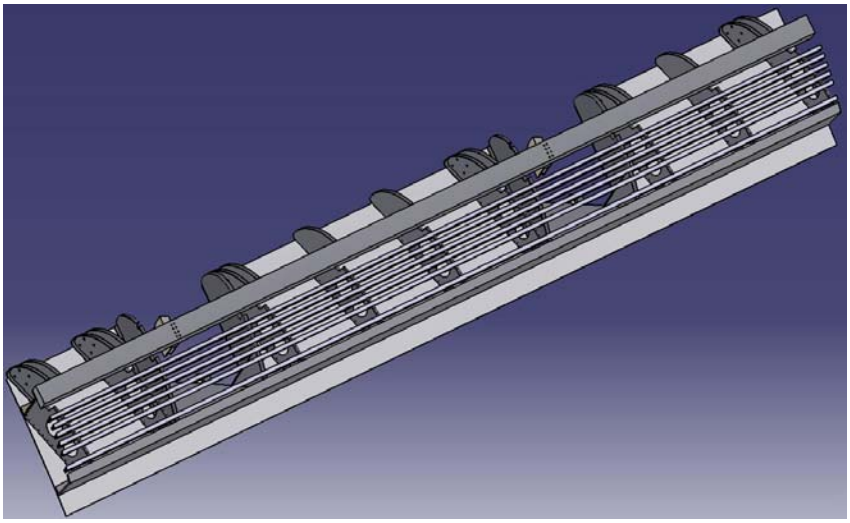

Figure 6.31 Flap body basic layout ─ top shell stringers

6.6.3 Flap Vane Gap Cover

In chapter 5.8 a simple two-link approach has been suggested for the flap vane gap cover. However, the use of programming cams gives more flexibility to avoid collisions in the adaptation of this flap track system to other dimensions and constraints. An approach made up of a link and a cam could be designed, or made up of two cams as shown in fig. 6.32 below. The cams would be integrated in the inboard and outboard boundary ribs of the flap structure; the actual cams are not modeled here but indicated by their datum lines, and the sliding bolt locations are marked with crosses.

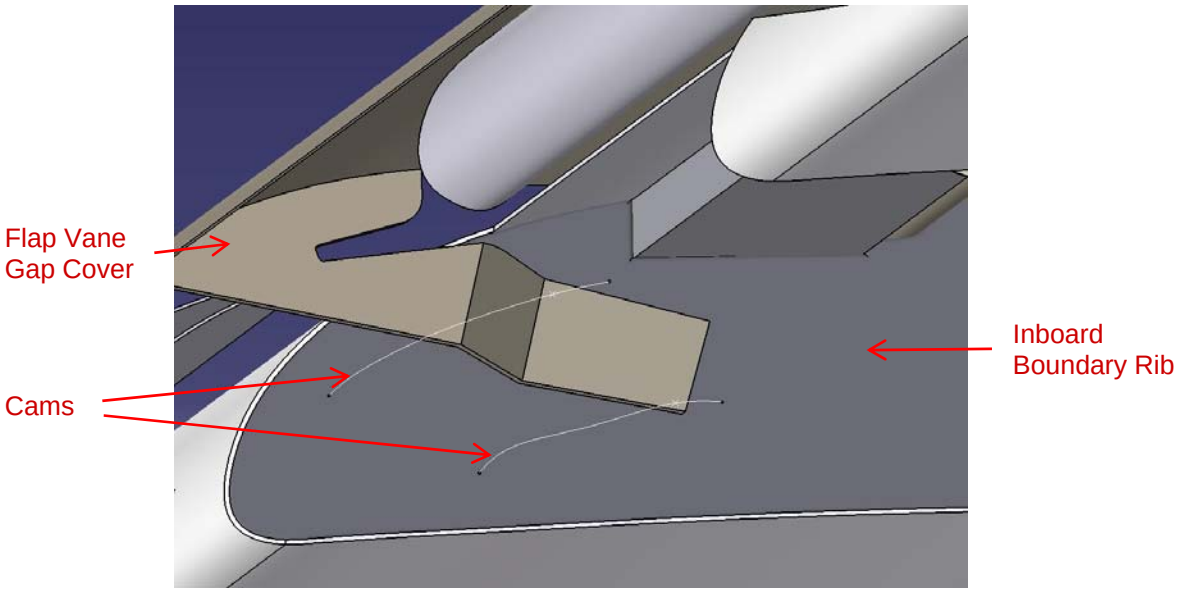

Figure 6.32 Flap vane gap cover ─ cam guidance approach

6.7 Miscellaneous Views

The following array of figures shows the main mechanism in fully retracted, half extended and fully extended state. The amber parts are the joint balls for the flap angle control link and main flap support, respectively. Note that the screw jack guides (as has been shown in fig. 5.77) are not modeled.

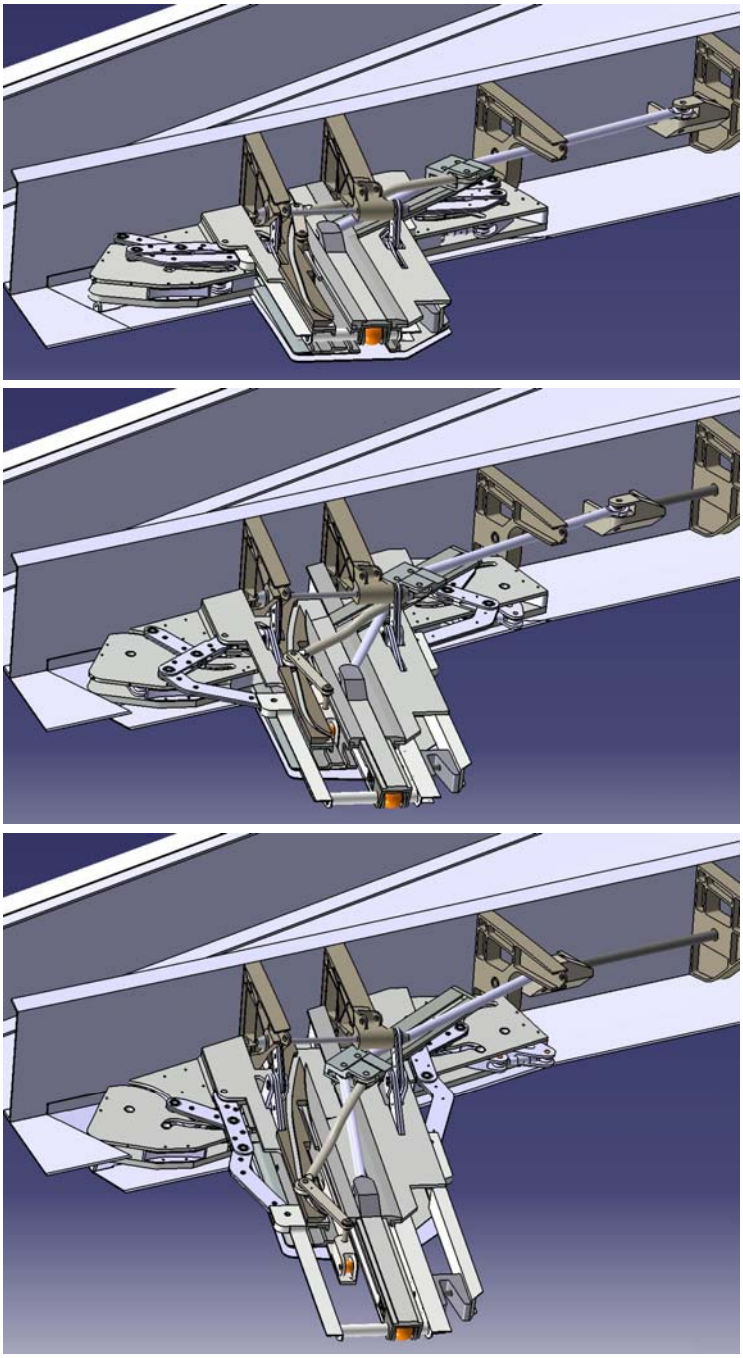

Figure 6.33 Main mechanism

As a basic requirement for this project, there must be enough space behind the rear spar for various systems and wiring. Figure 6.34 below shows there is indeed enough such space thanks to the main and screw suspension element cutouts.

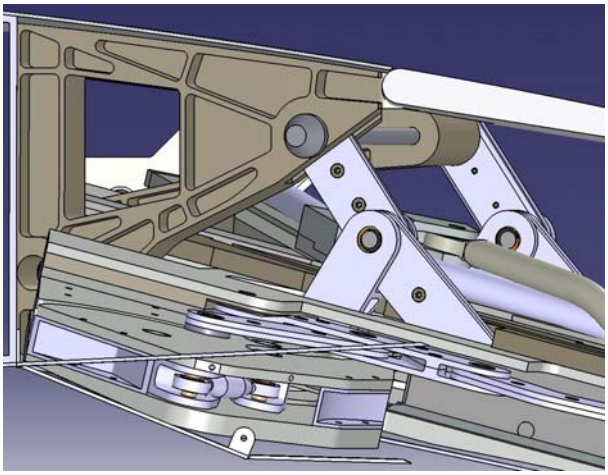

Figure 6.34 Cutouts overlay view

The flap beta rotation, as well as the flap vane lateral displacement, become particularly visible in views from behind, as shown in fig. 6.35 below.

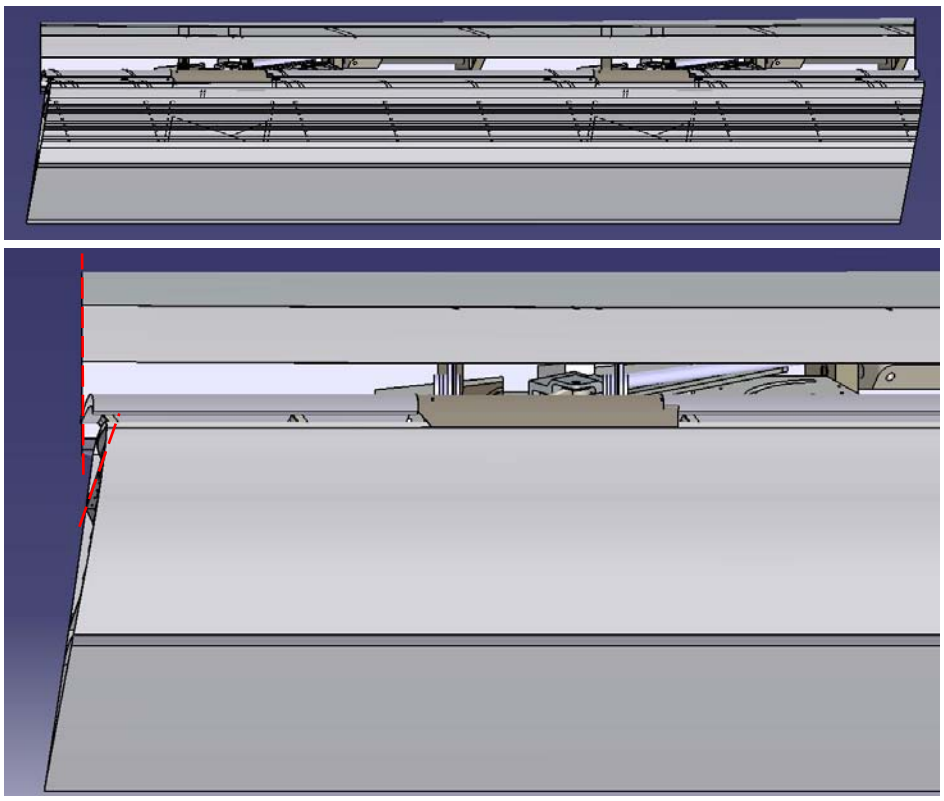

Figure 6.35 Flap beta rotation angle (views from behind)

Chapter 7

FE Analysis

This chapter will give a brief overview and rough structural analysis of some selected parts which are considered to be stressed at a critical level. It is not the intention of this chapter to present the results of a thorough static and dynamic analysis, since they would largely depend on the actual airplane and a very high number of loading cases need to be considered for certification. The loading cases considered in this chapter are those outlined in chapter 4.2.5 on page 54.

7.1 Main Slider

7.1.1 Loads

The design is such that the main slider absorbs normal loads only: parallel loads (mainly due to drag) are eventually directed to the screw via the main slider control slider. This also applies to jamming loads, so main slider calculations will not take them into account.

The loading case '+2.5g and tab down 30°' is dimensioning, as it produces the highest normal load. The corresponding basic lift and drag values are L = 81kN and D = 46.5kN, and the same safety factor considerations as outlined in chapter 4.2.5 apply (apart of jamming), i.e. an overall factor of 2.5*0.5 = 1.25 is applied. Therefore, L=101kN and D=58kN will be used and the normal force acting on the slider is calculated as follows:

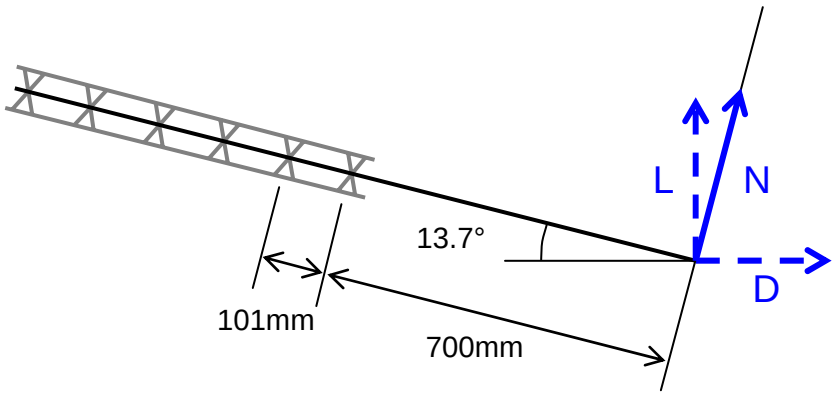

N= L*cos(13.7°) + D*sin(13.7°)

Result with L=101kN and D=58kN: N=112kN

Although not actually known in this project, the main slider and flap weights are considered negligible for an FE analysis when compared to these high aerodynamic loads and will therefore not be considered any further.

7.1.2 Modeling

The originally two main slider profiles are merged to one part. The roll bearings are modeled as rigid line clamps; to allow such restraints to be modeled in the CATIA analysis tool the following approach can to be followed.

Clamps can only be applied to full surfaces or edges, but the respective roll bearing lines are located within the main slider's top and bottom surface. So edges must be introduced, while not altering the mechanical behavior. This can be accomplished by applying very small pockets, as they produce the required edges but are still not taken into account by the meshing algorithm due to their small size.

Figure 7.1 below shows the raw sketches for the pockets at the roll support bearing locations in the flaps fully extended position.

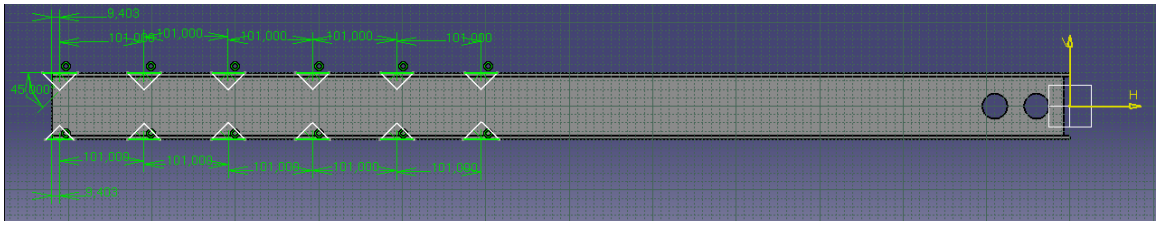

Figure 7.1 Sketches for small edge-producing pockets

The basic dimensions having been set, the sketch sizes now need to be reduced to a minimum as shown below.

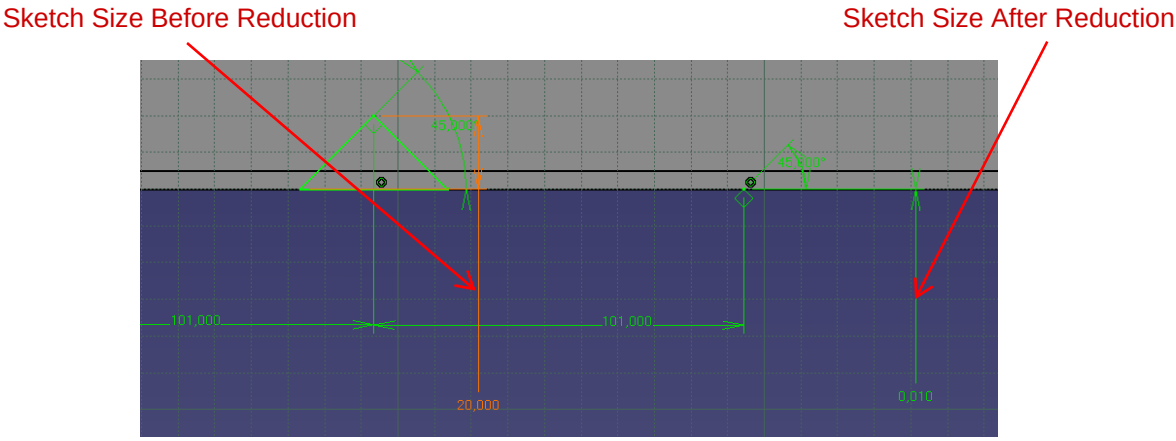

Figure 7.2 Sketch size reduction

However, it is likely that clamps applied on such sharp notches would lead to unrealistically high stress values in an FE analysis. Applying clamps to small surfaces (representing a contact surface between roll bearing and main slider pressed together) gives a more realistic behavior. Fig. 7.3 shows such an approach, with the sketch sized unreduced.

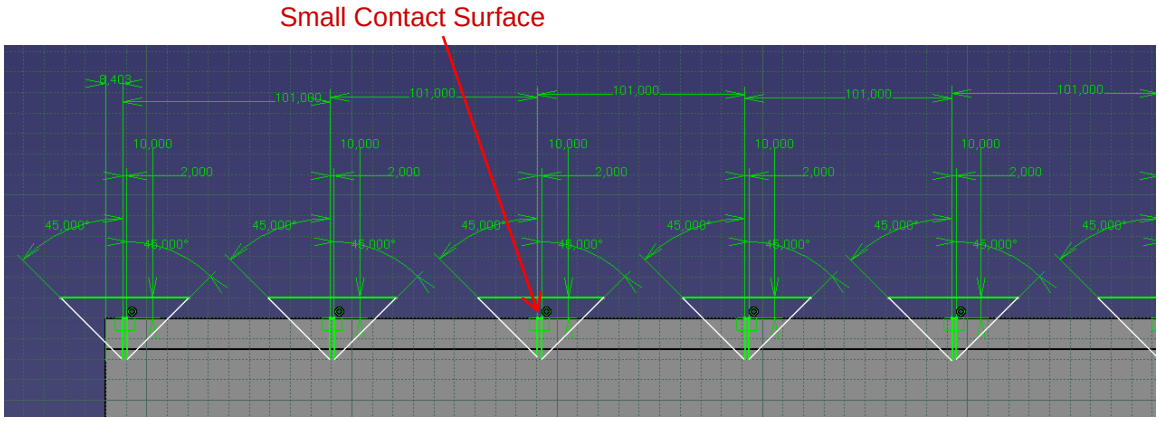

Figure 7.3 Improved pocket sketches

Applying these sketches to the main slider by means of the pocket function yields the needed edges, as figure 7.4 below demonstrates. Clamps and force are applied to this model, the mesh size is set to 9mm (a larger mesh creates problems at the edge locations).

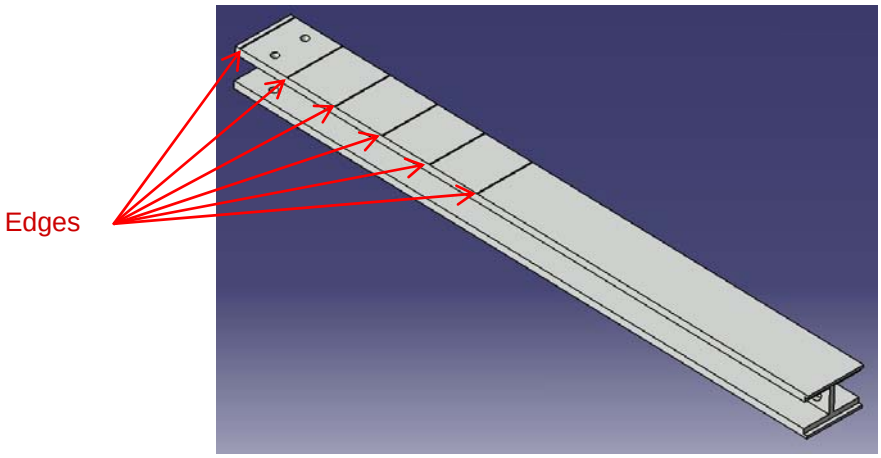

Figure 7.4 Main slider with edges

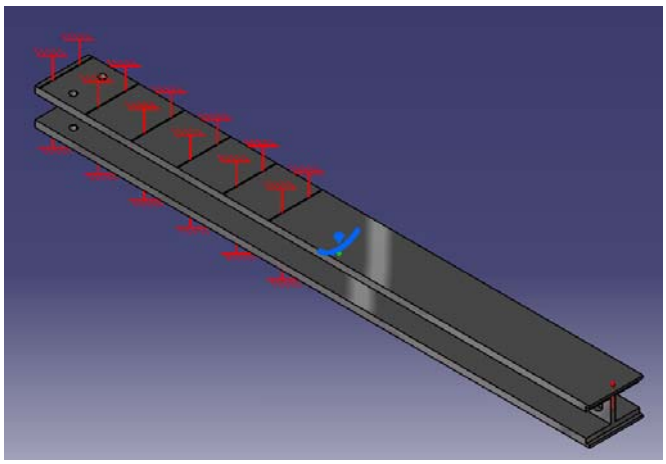

Figure 7.5 Main slider FE constraints

7.1.3 Results

FEM computations yield stresses close to 4000MPa, which is about ten times the value obtained by the rough calculation in chapter 5.2.3. But these high stresses occur only very close to the two rear roll bearings, as shown by the color distributions in the two figures below. This corroborates the assumption that the clamp modeling distorts reality, the more so since stress rapidly decreases in the slider z (vertical) direction.

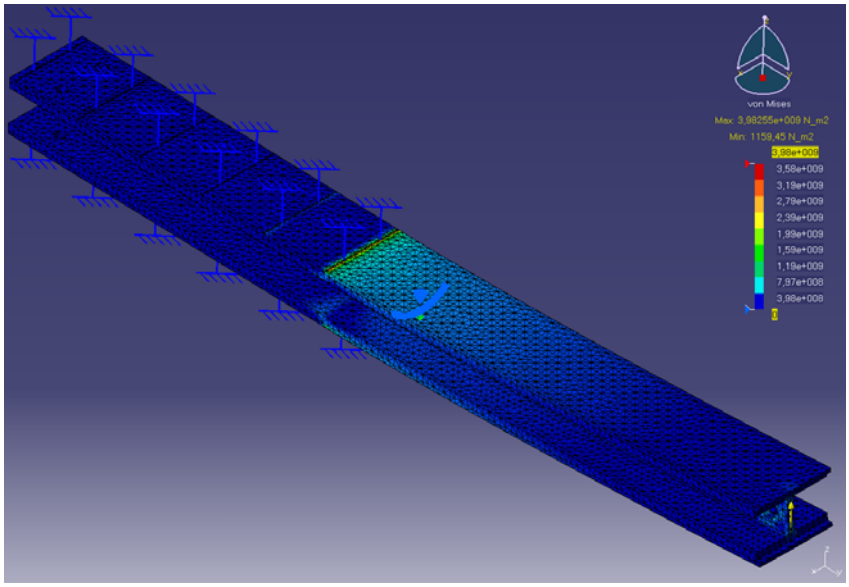

Figure 7.6 Main slider stress

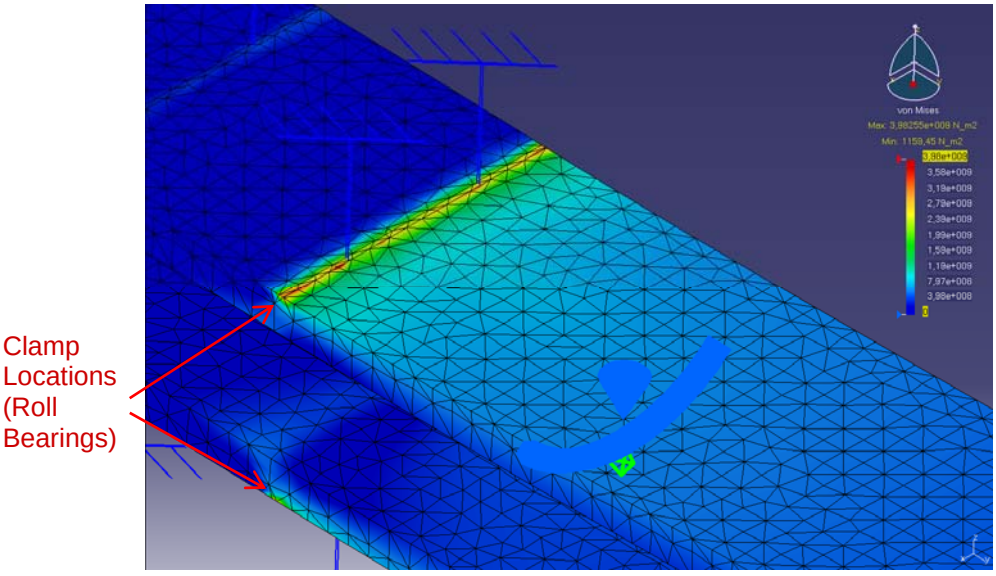

Figure 7.7 Main slider stress near the back roll bearing

To get a more realistic view the color scale maximum value is set to 1500MPa, and a more realistic stress distribution becomes visible.

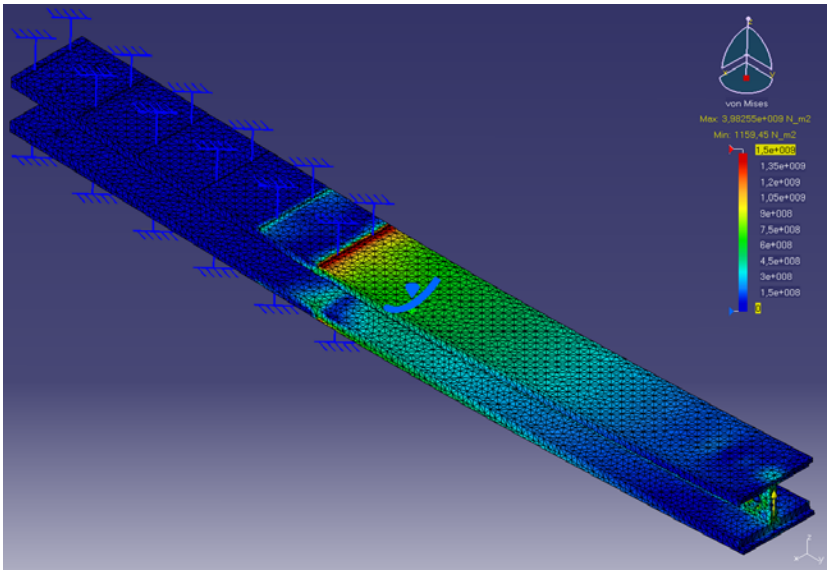

Figure 7.8 Main slider stress with adjusted color scale

A closer examination of the area around the bearing shows again the huge local stress increase at the clamp location. Stresses in the flange go up to 750MPa, but only close to the outer side; at the inner side they are about the same as the predicted 450MPa by the rough calculation in chapter 5.2.3.

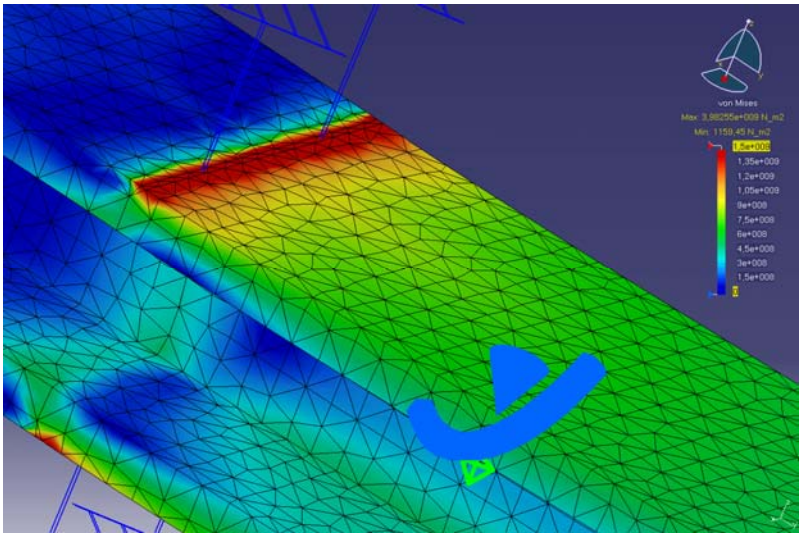

Figure 7.9 Main slider stress near the back roll bearing

Taking the mentioned modeling inaccuracies into consideration as well as that the load applied is in effect much higher than encountered in normal flight, it can be assumed that this first rough main slider dimensioning is correct. There are materials which can bear these and much higher stresses; for example special tempered steels with tensile strength values up to 2400MPa (such as 100Cr6) can be used for the main slider. A basic safety factor of 1.1 can therefore be met. Using steel, the flap attachment point displacement is about 20mm for this very high and unlikely load, which is acceptable.

7.2 Flap Angle Control Slider

7.2.1 Loads

Due to the design approach chosen it is assumed that the main aerodynamic load is absorbed in the main flap support only. Therefore, only flap/tab moments will be considered in the flap angle control slider analysis. Further, only the moment produced by the deflected tab will be used since it is much higher than the bias aerodynamic moment with the tab not deflected. The calculation in appendices C and D yield a moment of -10.4kNm for the tab deflected by 30°, and the same (but positive) value for -30°.

A factor of 2.5 (due to the operation range up to 2.5g) is applied to the moment as well. Since jamming of the flap angle control slider is possible a jamming factor of 1.7 applies, which at the same time serves as a fatigue safety factor (again introduced as a load multiplier rather than a reduction of material constants). This is considered acceptable since jamming is a one-off event that would entail thorough inspection and maintenance, and adding an extra factor of 2 for fatigue would probably require a more robust and heavy slider than really necessary. Therefore the overall factor is 2.5*1.7 = 4.25 and the moment is set to ±44.2kNm. Because of fail safe design considerations as outlined in chapter 5.5.4, this load is applied to one slider only and not distributed for the purpose of this calculation.

In the flaps fully extended state the flap angle control slider protrudes about 200mm from the guide structure assembly and thus bending is the dimensioning factor, with shear playing a subordinate role only.

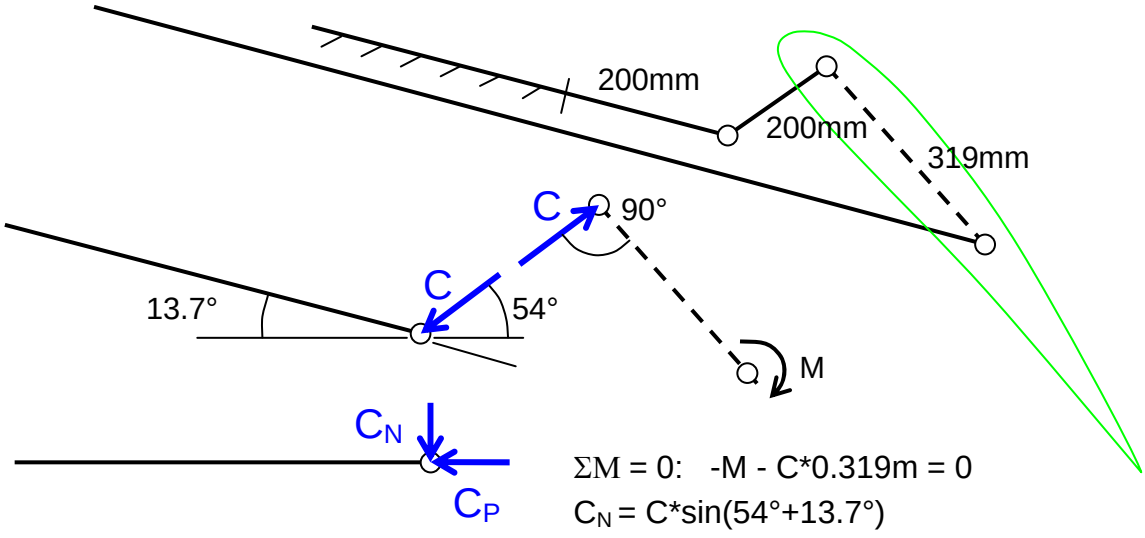

$\Sigma M = 0: \quad -M - C*0.319m = 0$

$C_N = C*\sin(54°+13.7°)$

$C_P = C*\cos(54°+13.7°)$

Results for M = ±44.2kNm:

$C = \pm 138.6kN \begin{cases} C_{Normal} = \pm 128kN \\ C_{Parallel} = \pm 53kN \end{cases}$

7.2.2 Modeling

Similar to the main slider, the protruding of the flap angle control slider requires a surface division and edge introduction to attach a clamp correctly. Figure 7.10 below shows the edges as they are obtained by simply ‘fining down’ the respective surfaces by 0.01mm.

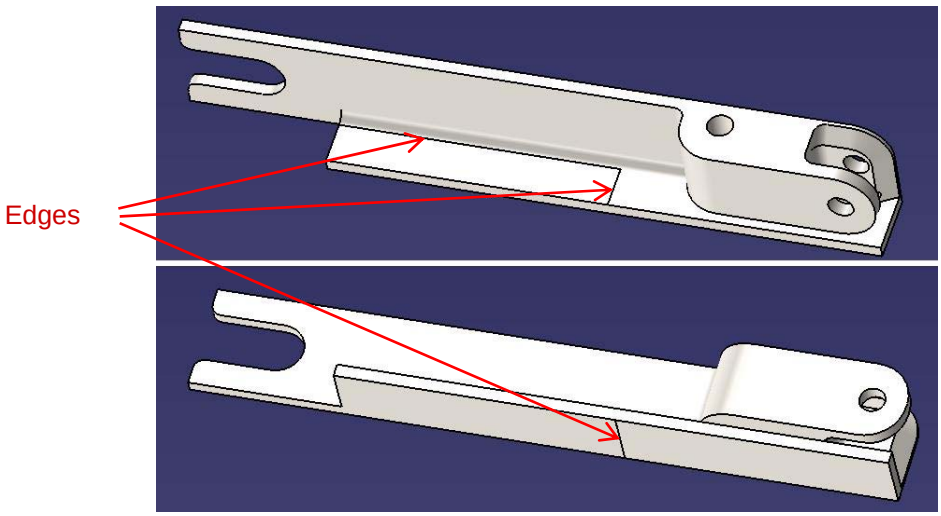

Figure 7.10 Flap angle control slider with edges

The load is distributed to the flap angle control link attachment holes as shown in fig. 7.11.

Floating surface bearings are applied to all surfaces in contact with the guide structure assembly (particularly the guiding band on the top side), and to the actuation bolt socket. As otherwise constraint problems arise in the computation, an additional floating bearing is added to the fore end face; the effect of this is minimal since parallel forces are mainly absorbed in the actuation bolt socket.

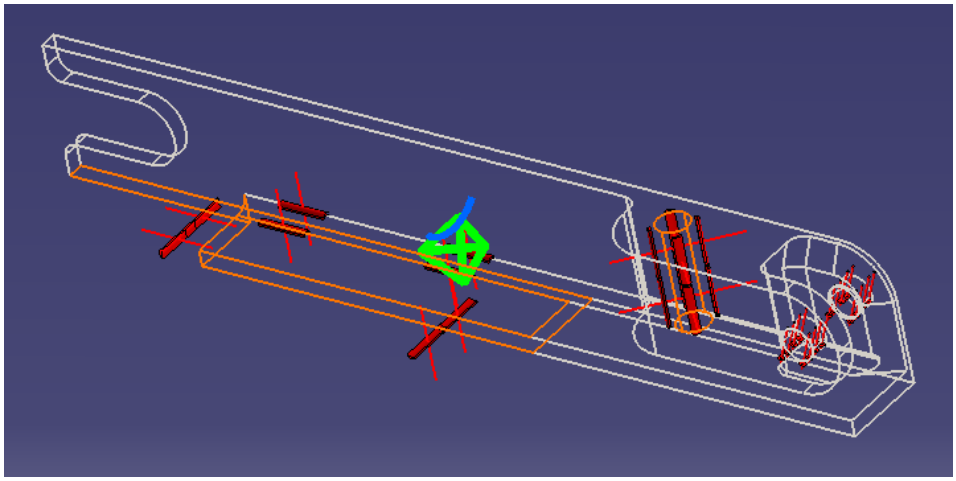

Figure 7.11 Flap angle control slider FE constraints

7.2.3 Results for -30° Tab deflection

Figures 7.12 and 7.13 again show some stress concentrations due to the modeling approach. Stresses go up to 900MPa at these locations, while the average is between 100 and 200MPa.

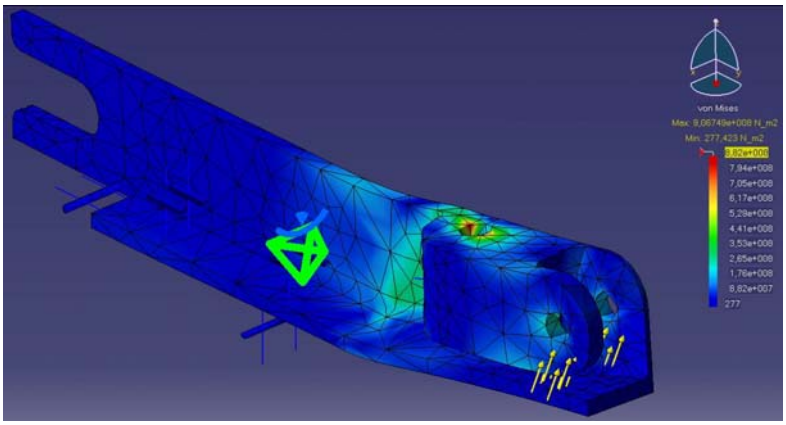

Figure 7.12 Flap angle control slider stress (outboard view)

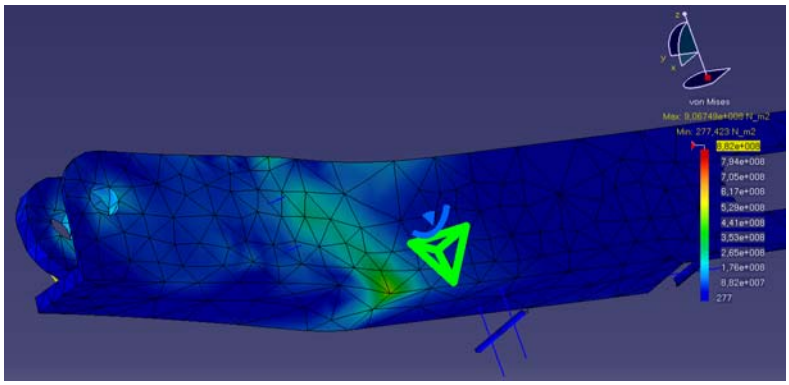

Figure 7.13 Flap angle control slider stress (inboard view)

Setting the color scale maximum to 300MPa gives a more helpful picture as shown in figures 7.14 and 7.15. While the stress values remain between a maximum easily met by tempered steels, there is a rather uneven stress distribution near the actuation bolt socket. This time it does not result from FE modeling inaccuracies but from the structure of the flap angle control slider. A redesign may be considered to get a less sharp curve at this location which may finally lead to a lighter part.

When using steel the displacement at the flap angle control link attachment point is about 0.6mm, which is small enough to be acceptable.

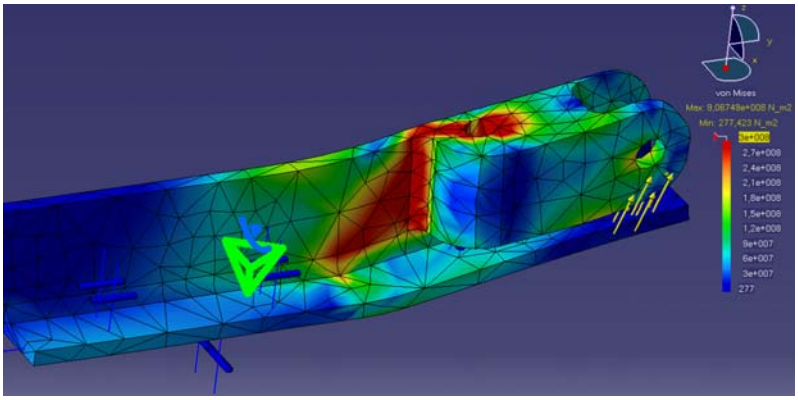

Figure 7.14 Flap angle control slider stress (outboard view), adjusted color scale

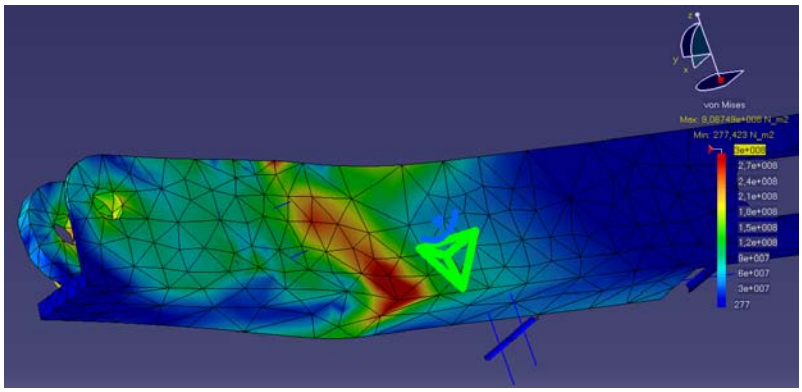

Figure 7.15 Flap angle control slider stress (inboard view), adjusted color scale

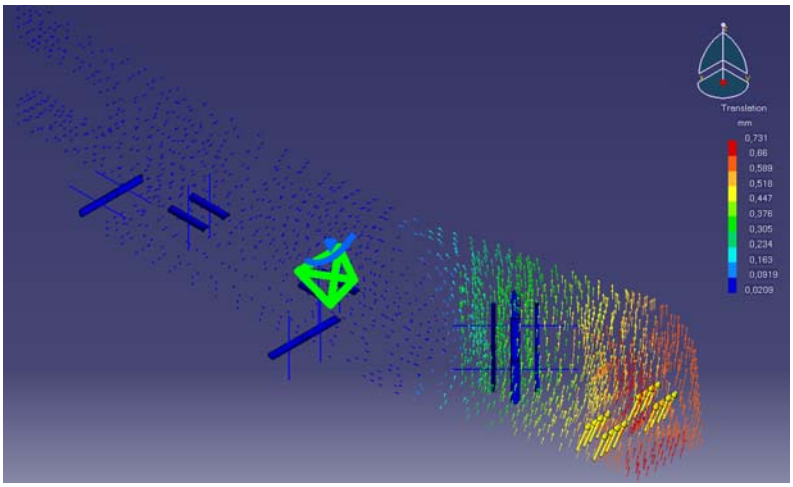

Figure 7.16 Flap angle control slider translation vectors (outboard view)

7.2.4 Results for +30° Tab deflection

Very similar results are computed with the tab deflected to the other side. The problems remain the same and so do the improvement suggestions as explained in the preceding subchapter.

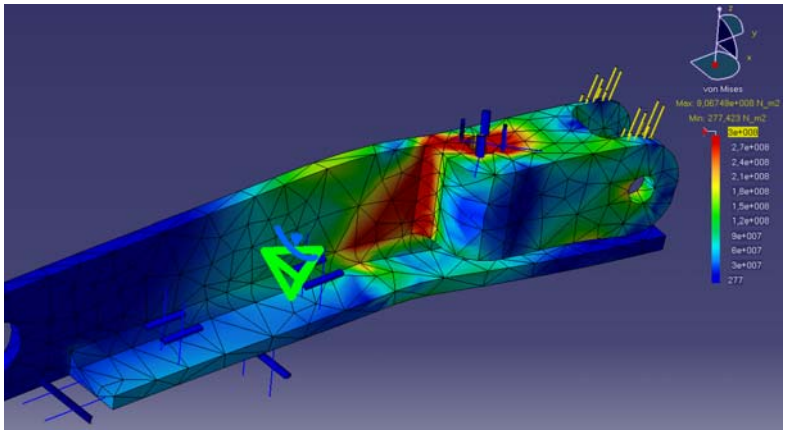

Figure 7.17 Flap angle control slider stress (outboard view), adjusted color scale

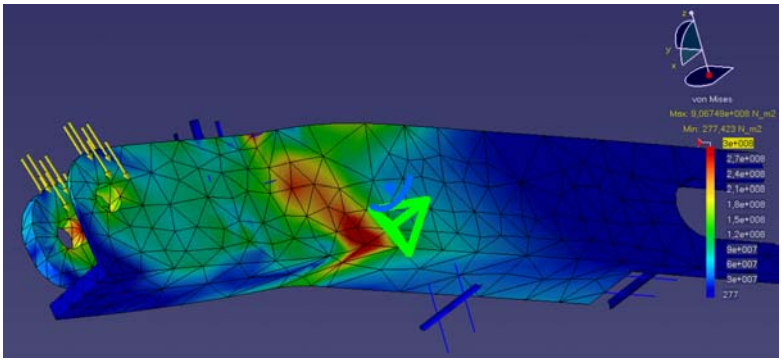

Figure 7.18 Flap angle control slider stress (inboard view), amended color scale

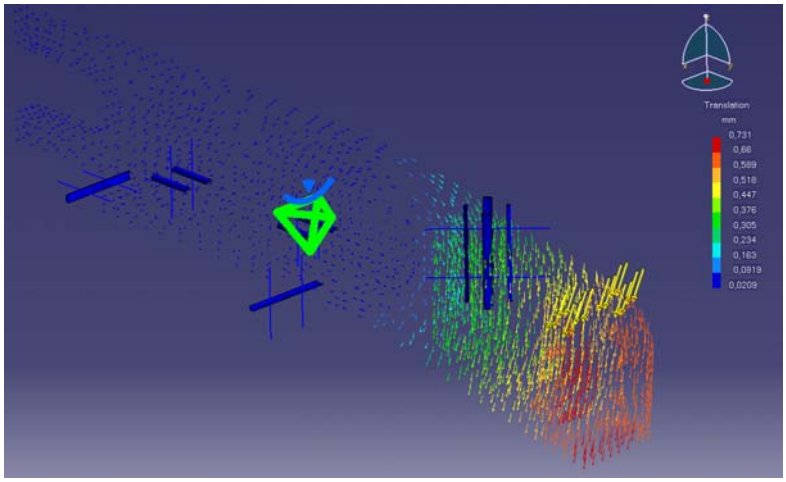

Figure 7.19 Flap angle control slider translation vectors (outboard view)

7.3 Main Suspension Elements

7.3.1 Loads

Bearing forces acting on the main suspension elements are calculated as follows:

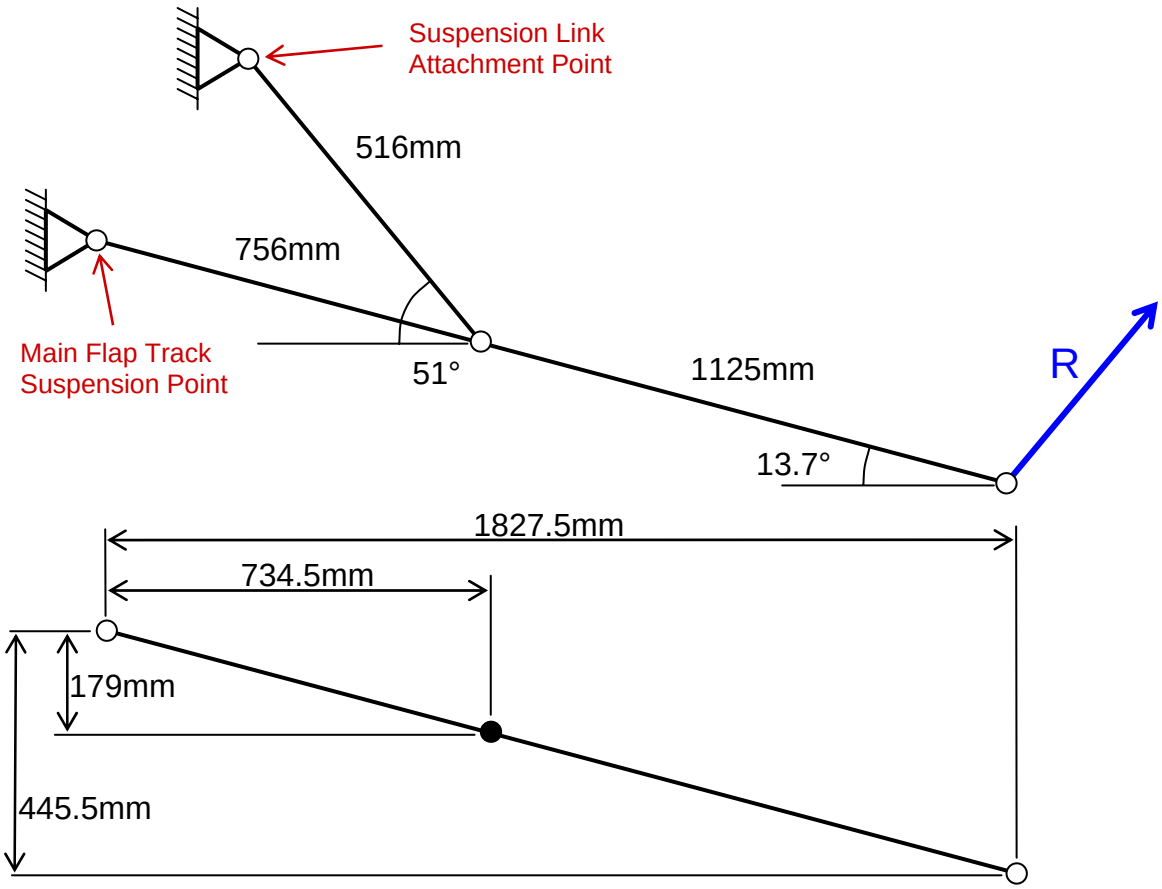

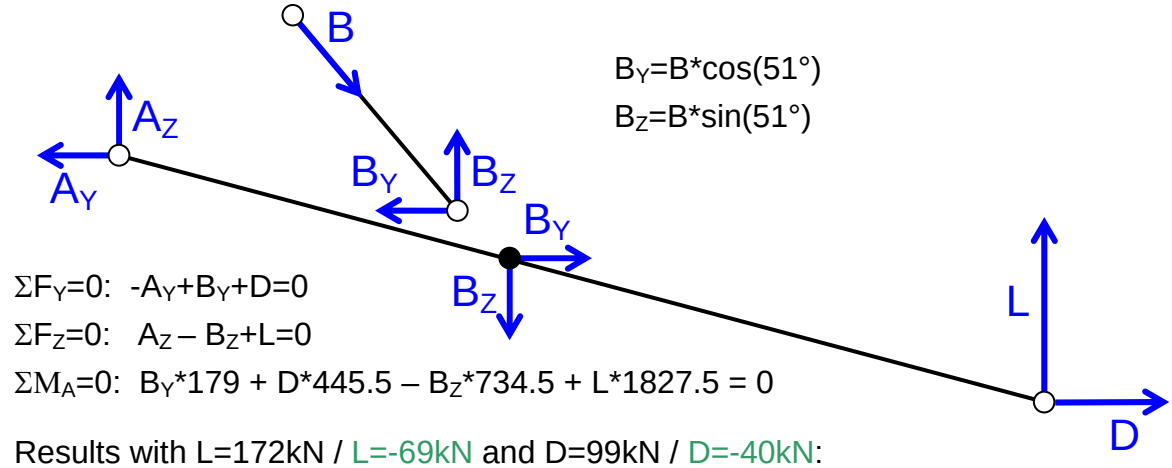

$B_Y = B*\cos(51°)$

$B_Z = B*\sin(51°)$

$\Sigma F_Y = 0$: $-A_Y + B_Y + D = 0$

$\Sigma F_Z = 0$: $A_Z - B_Z + L = 0$

$\Sigma M_A = 0$: $B_Y*179 + D*445.5 - B_Z*734.5 + L*1827.5 = 0$

Results with L=172kN / L=-69kN and D=99kN / D=-40kN:

A_Y=591kN / A_Y=-238kN B_Y=492kN / B_Y=-198kN

A_Z=436kN / A_Z=-175kN B_Z=608kN / B_Z=-244kN

} B=782kN / B=-314kN

As with the flap angle control slider, factors 2.5 and 1.7 apply to account for operating range requirements and jamming loads. Only tab deflection +30° will be considered as this position produces the highest load magnitude. Since it is unlikely that both suspension elements on one flap track station fail at the same time and thus fail safe design is ensured, the flap load is distributed evenly to both stations. The overall factor applied thus is 2.5*1.7*0.5 = 2.125. It is not evident how the suspension elements would behave at -1.0g, so this loading case must be examined as well. The resulting overall factor for this case is -1.0*1.7*0.5 = -0.85.

Hence, with the lift and drag values (81kN and 46.5kN, respectively) as calculated in appendices C and D, L = 172kN/L = -69kN and D = 99kN/D = -40kN are being used for the calculations as outlined on the preceding page (the values for -1.0g are green), the y and z directions correspond to those introduced in chapter 4.2.1.

As a simplification the main slider angle link attachment point in assumed to be on the line connecting the main flap track suspension and flap support bolt, in spite of the actual design where this point is located somewhat downward.

Figure 5.21 on page 75 showed that the inboard and outboard support angle control linkages are not exactly at the same distance from the middle reference line (which runs through the main flap support ball joint), and neither are the two suspension elements. This entails a slightly uneven distribution of the loads calculated above. Still, as these are rough calculations only, the bearing forces are assumed to be evenly distributed to both suspension elements. So the values above must be divided before applying them to the respective FE models. Note that the actual force direction must be reversed on the suspension elements.

Spoiler loads are not taken into account for these calculations, although they do have an impact also for the flap fully extended position: usually they are deployed immediately after touchdown, now in the function of speed brakes and mainly as lift dumpers. Since at this time +1.0g automatically prevails, the safety factor obtained by considering the loading case +2.5g is considered sufficient to account for this configuration right after touchdown. For the aim of this project this gives the needed results for a first assessment. However, for some detailed design tasks, mainly of the spoiler suspension points, more accurate calculations would need to be carried out.

7.3.2 Modeling

The design as presented in the demonstrator and CAD models is such that the main suspension elements are attached to both the main wing rear spar and main wing top shell. Attachment to the top shell provides for increased stability in the case of very high lateral loads not encountered during normal operations. The main flap load and moment is absorbed in the rear spar, however. This is the reason why only the rear spar attachment planes of the main suspension elements receive a clamp as shown in figures 7.20 and 7.21. The bearing forces are introduced as distributed loads.

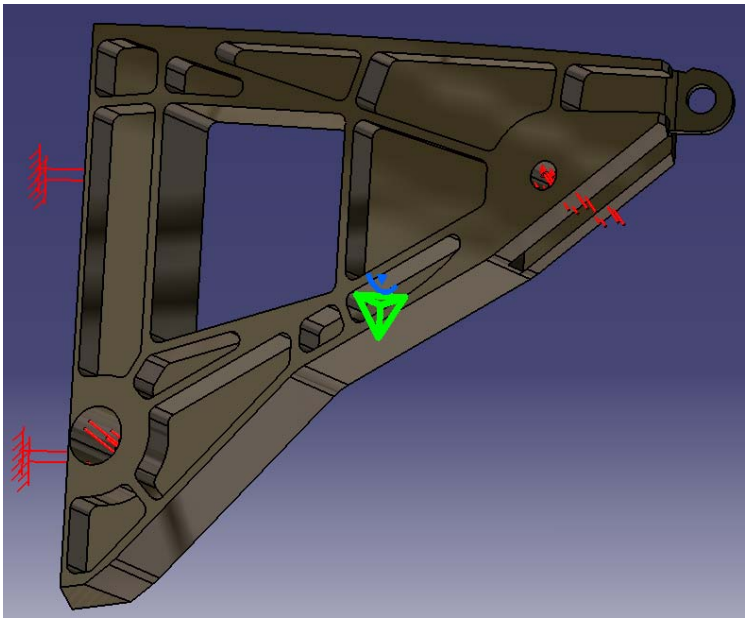

Figure 7.20 Outboard main suspension element
FE constraints (loads shown for +2.5g)

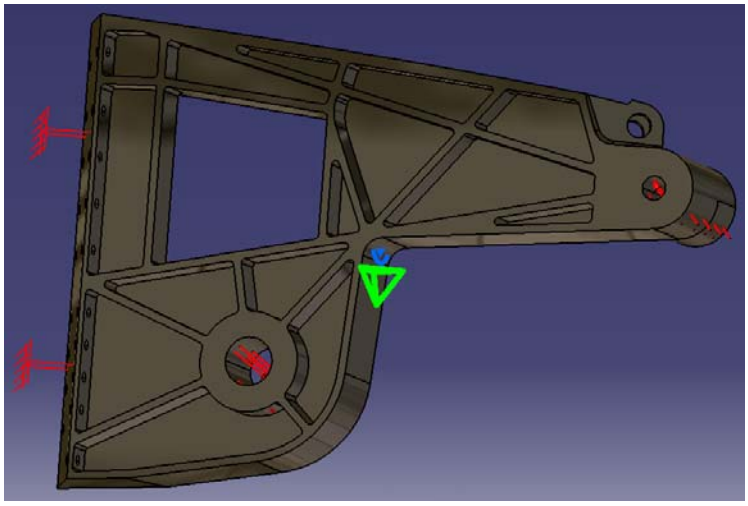

Figure 7.21 Inboard main suspension element
FE constraints (loads shown for +2.5g)

7.3.3 Results for +2.5g

Figure 7.22 on the next page shows that the shear field approach used for these elements basically works and the chosen dimensions are not grossly off the mark. aluminum has been used for these calculations, and the average stresses are within material limits. The design and flange/field dimensions were chosen intuitively in chapter 6, far from being optimized. The FE analysis now shows optimization potential: with the current design of the outboard element some parts are much more stressed than others. Weight economization is possible at various locations. No extreme stress concentrations have been detected in the model, so the results obtained are close to real.

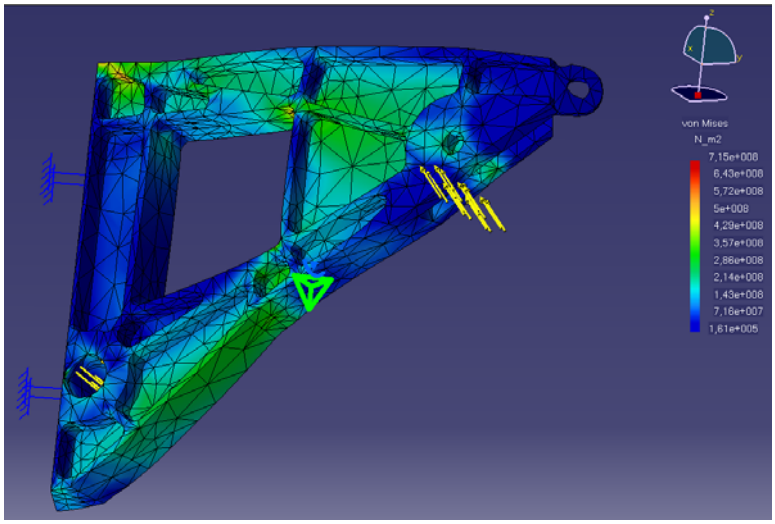

Figure 7.22 Outboard main suspension element (outboard view)

There are some locations where the stresses are very high for aluminum, up to 715MPa, particularly at the cutout's two aft corners. This problem could be solved by increasing the radius at these corners.

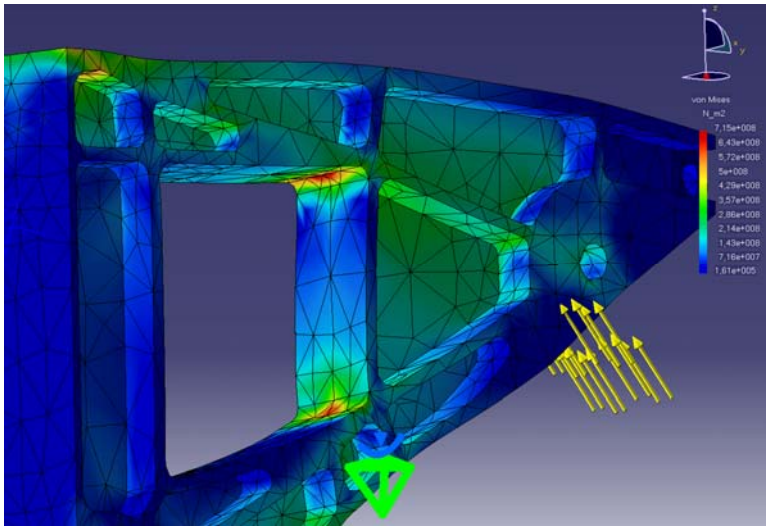

Figure 7.23 Outboard main suspension element, cutout detail

At the spoiler attachment point vertical displacement is about 4mm when using aluminum, which is acceptable given that the applied load is about four times as high as encountered in normal flight.

For the inboard main suspension element the situation is somewhat different. Fig. 7.24 reveals a stress concentration up to 3700MPa near the spoiler attachment element. Two factors contribute to this problem: on one hand, the radius at the respective corner is too small to be meshed properly; this can be improved by increasing the radius. On the other hand, the suspension link attachment bolt socket is placed in a way that a load from the suspension link induces a moment into the element.

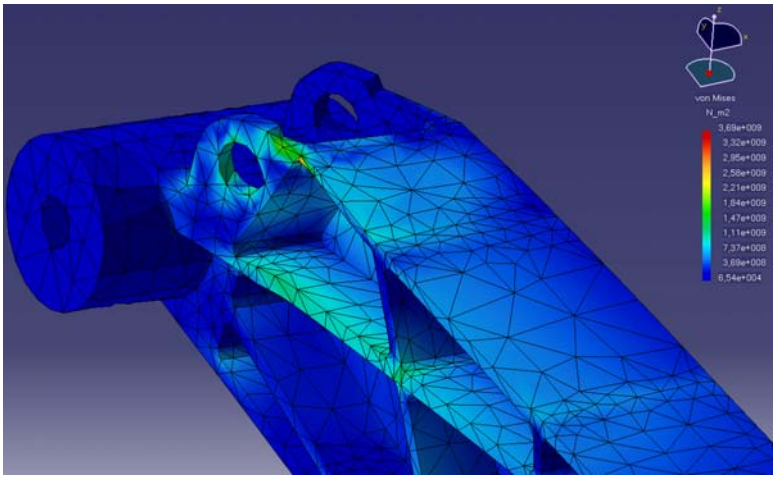

Figure 7.24 Inboard main suspension element aft part

Adjusting the color scale produces a more informative stress distribution picture. Figure 7.25 below shows that the induced torsion indeed poses a problem at the middle flange, where stresses are very high.

A local redesign of this part of the inboard main suspension element may be appropriate to attain a more homogenous stress distribution; particularly thickening the flange will improve the results.

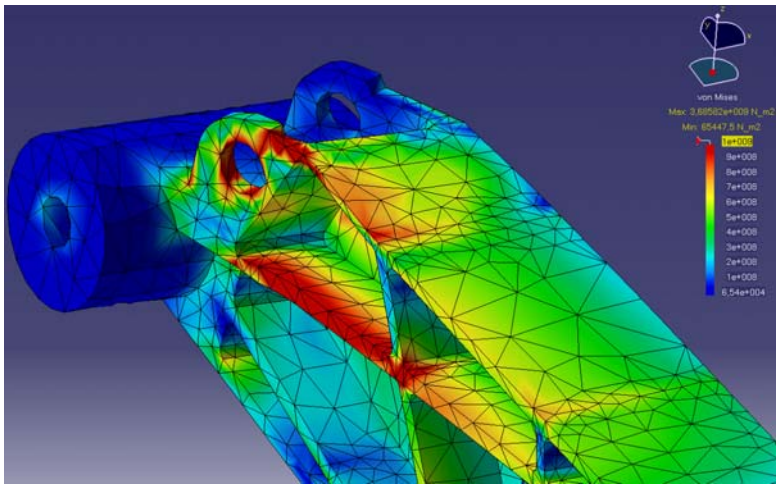

Figure 7.25 Inboard main suspension element aft part (adjusted color scale)

However, overall views of the element show the stress distributions on the other parts to be within acceptable limits and, as intended, mainly pass through the flanges. In the fore part around the main flap track suspension point shear field stresses are evenly distributed.

As expected there are high stresses at the sharp curve between the fore and aft part of the element. A slight radius increase there may reduce them, but attention must be paid to the collision risk with the auxiliary cam link (see also fig. 5.45 on page 88).

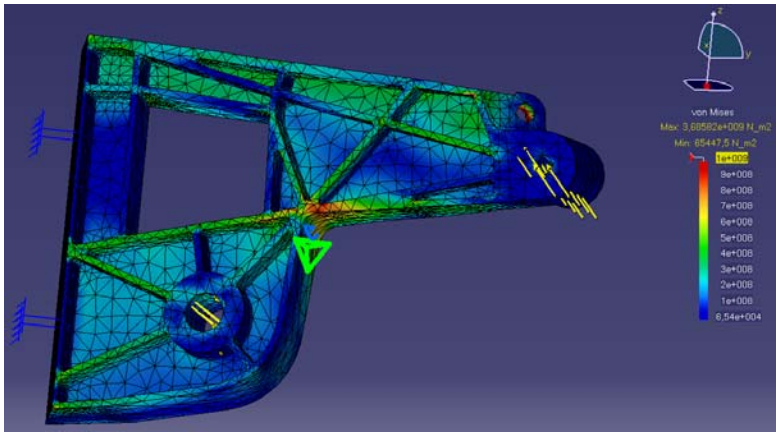

Figure 7.26 Inboard main suspension element (outboard view), adjusted color scale

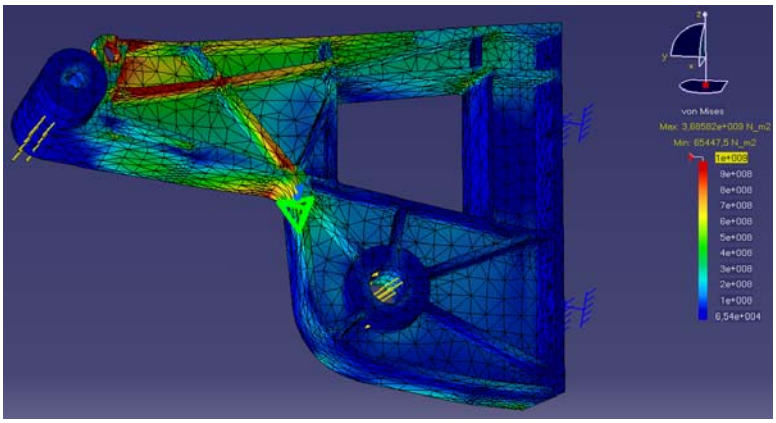

Figure 7.27 Inboard main suspension element (inboard view), adjusted color scale

Mainly due to torsion, displacement is up to 20mm at the inboard suspension link attachment point, which is too high given then rather small dimensions of the element. Replacing aluminum by steel reduces this value by about 50%. It must be noted, though, that the two main suspension elements and suspension links are connected by a rod (compare demonstrator model, see for example fig. 5.19 on page 74). This reduces actual torsion and stresses as the rod has a stiffening effect.

7.3.4 Results for -1.0g

Almost exactly the same observations are made for -1.0g, although the stresses are not of the same magnitude since the applied loads are much smaller than with +2.5g.

For the outboard main suspension element, again no critical problems are identified, apart of the too small radius at the two cutout aft corners. For aluminum, maximum downward displacement is about 2mm at the spoiler attachment element, which is acceptable.

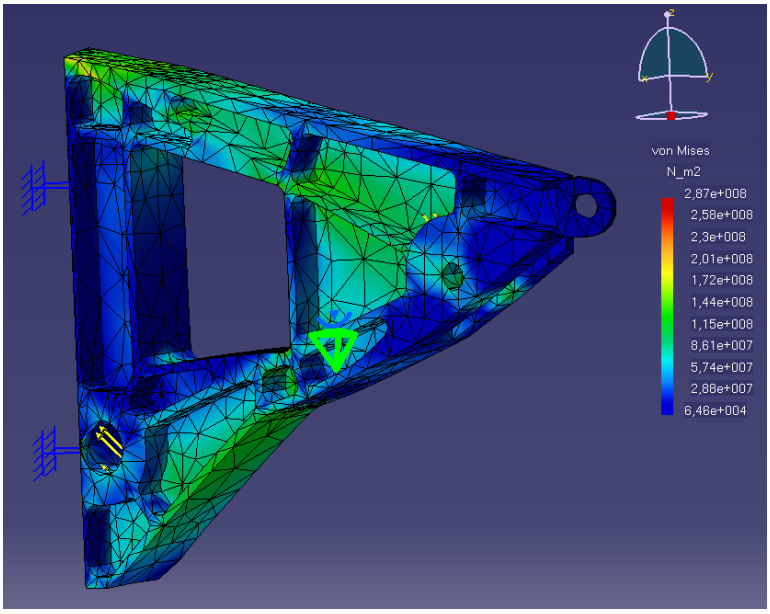

Figure 7.28 Outboard main suspension element (outboard view)

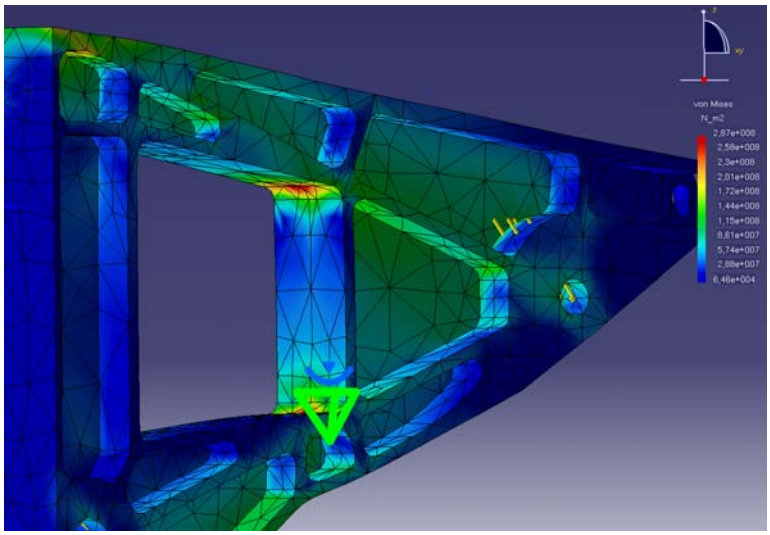

Figure 7.29 Outboard main suspension element, cutout detail

As with +2.5g, a stress concentration appears in the corner at the spoiler attachment element, and the flange is particularly stressed at its inboard side as shown in fig. 7.31 on the next page. Again, torsion is responsible for this problem. Maximum downward displacement is about 10mm at the suspension link attachment point.

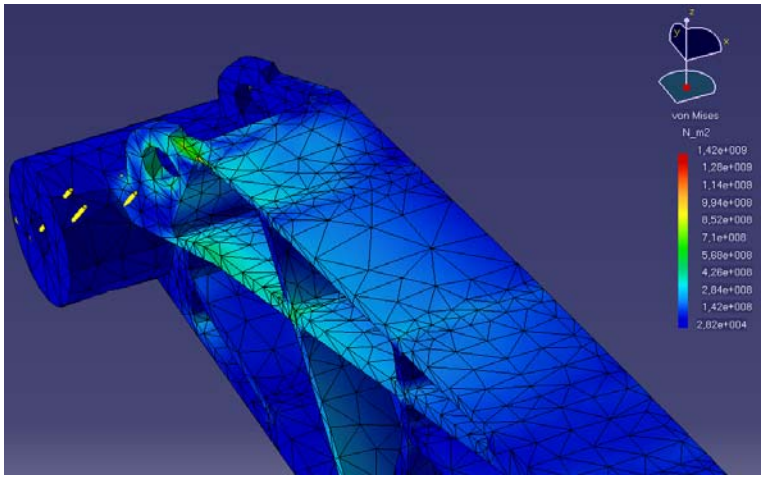

Figure 7.30 Inboard main suspension element aft part

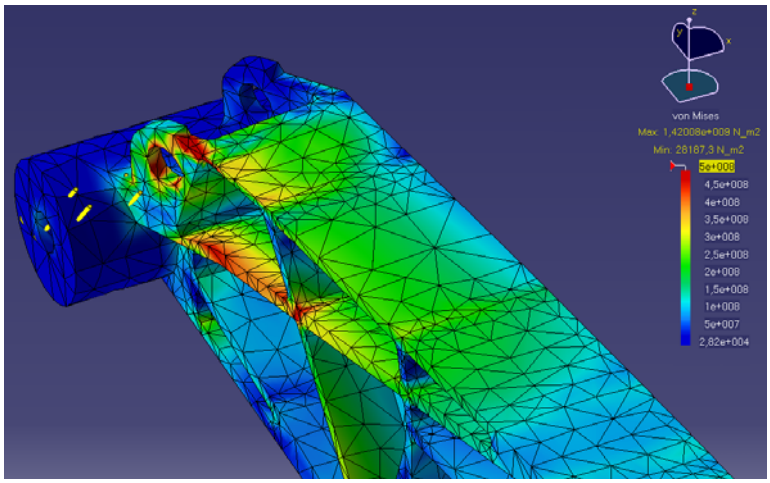

Figure 7.31 Inboard main suspension element aft part (adjusted color scale)

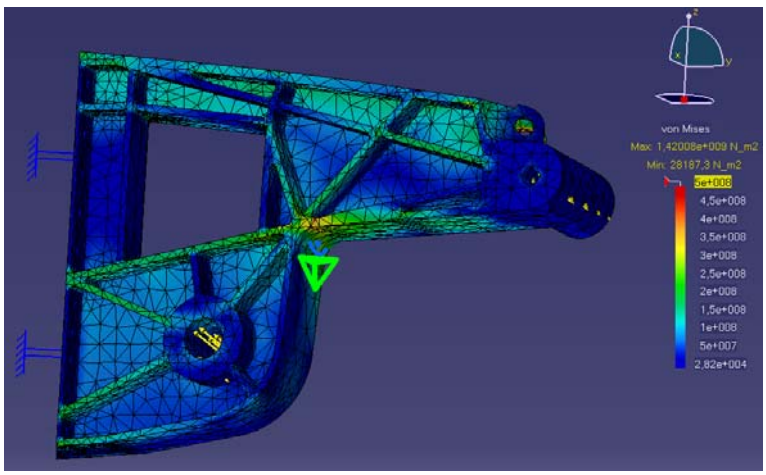

Figure 7.32 Inboard main suspension element (outboard view), adjusted color scale

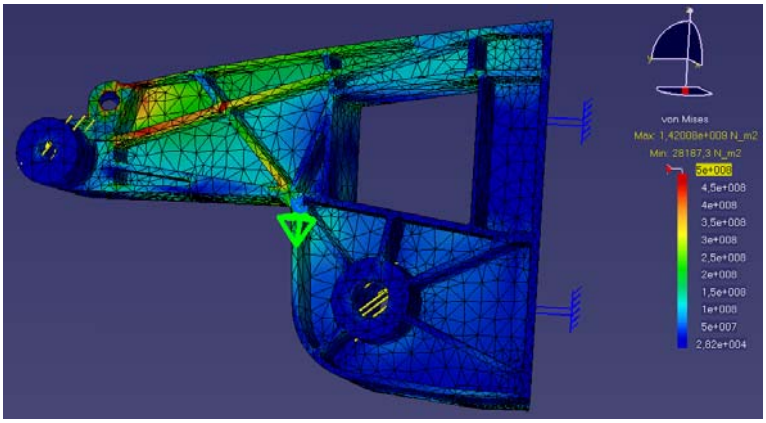

Figure 7.33 Inboard main suspension element (inboard view), adjusted color scale

As a summarization no entirely new insights are gained from the loading case -1.0g discussion. The same improvement and redesign suggestions apply, and the problems as discussed for both loading cases may be solved by only one redesign approach.

7.4 Support Angle Control Linkage

7.4.1 Loads

The same considerations as with the main suspension elements apply to the support angle control linkage, and the same loading cases are being used. Therefore, B = 782kN/B = -314kN are distributed evenly to the inboard and outboard support angle control linkage, coming up with $B_{\text{Per Linkage}}$ = 391kN/$B_{\text{Per Linkage}}$ = -157kN.

It becomes evident that with the loading case +2.5g a high pressure force acts on the linkages. This makes the suspension links and main slider angle links susceptible to buckling, a loading case which poses problems for many FEM algorithms. Therefore, buckling strength will be evaluated manually.

Although both the suspension link and main slider angle link have almost the same cross section, the latter is more susceptible to buckling as it is longer and features ball joints at its ends whereas there are axial bearings on the suspension link.

According to Euler, a maximum buckling load can be estimated using a simple formula:

$$F_E = k \cdot \frac{\pi^2 \cdot E \cdot I}{L^2}$$

where E is the material's young modulus, I the smallest moment of inertia perpendicular to the force axis, and L the link length. k is a factor representing the bearing type (clamp, floating etc).

For a ball joint support at each end, as is the case with the main slider angle link, k = 1.0 applies. The situation is depicted in fig. 7.34 below.

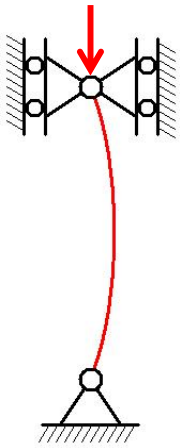

Figure 7.34 Buckling with ball joint bearings

The link cross section is 80mmx24mm. So the smallest moment of inertia is

$$I = \frac{80mm \cdot (24mm)^3}{12} = 92160mm^4$$

A typical young modulus for tempered steels (as could be used for such highly stressed parts) is 200kN/mm^2; the link length is 346mm.

$$F_E = 1.0 \cdot \frac{\pi^2 \cdot 200000 \frac{N}{mm^2} \cdot 92160mm^4}{346^2 mm^2} = 1520kN$$

This is almost four times the actual pressure load of 391kN on the link, so there is a comfortable reserve should one of the linkages fail.

An FE model is still done mainly to investigate the -1.0g loading case effect, but also to see how the bolt sockets perform with both loading cases.

7.4.2 Modeling

The two parts of the link are merged, as has been done with the main slider. To avoid singularity problems in the FE calculations, one of the bolt sockets is provided with a clamp, even though this does not represent a ball joint accurately. Therefore, only the results at the other socket will be considered further, where the load is introduced as a distributed bolt load.

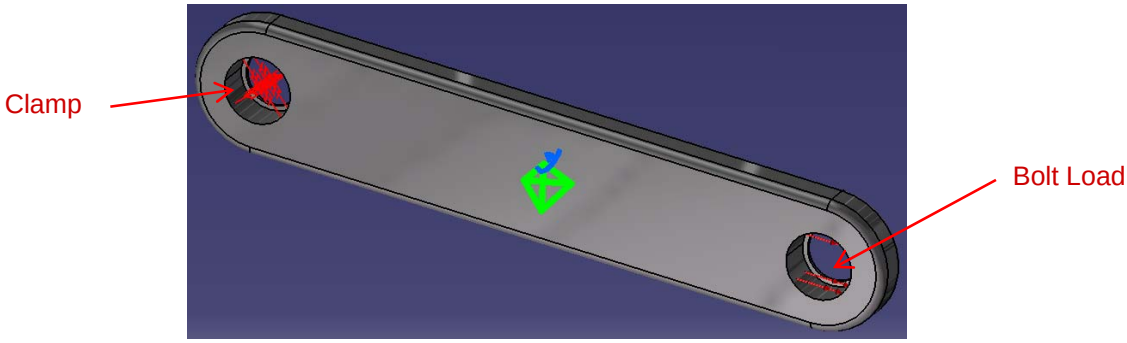

Figure 7.35 Main slider angle link FE constraints

7.4.3 Results

With -1.0g stresses at the socket surface are about 300MPa, which poses no problems for tempered steels. The high stresses are only very close to the surface and rapidly decrease to the outside of the link, where less stressed material acts as a support for the inside.

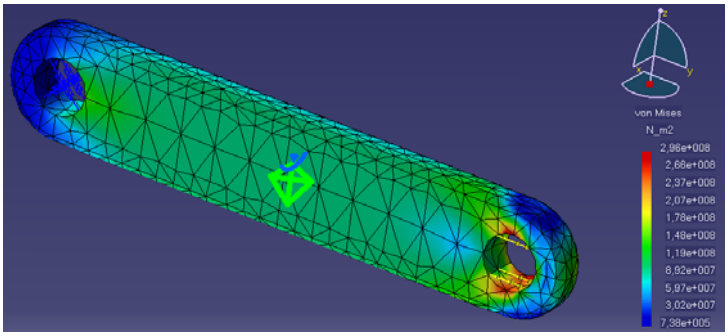

Figure 7.36 Main slider angle link stresses with -1.0g

With +2.5g a pressure load acts on the link, and as explained above FE results should be viewed at with caution for such loading cases. Still, the analysis shows the socket stresses to be up to 735MPa; this is not an unsolvable problem either for tempered steels. Besides, since the load acts as a pressure load, the ring which forms the bolt socket is not at risk to break due to this load.

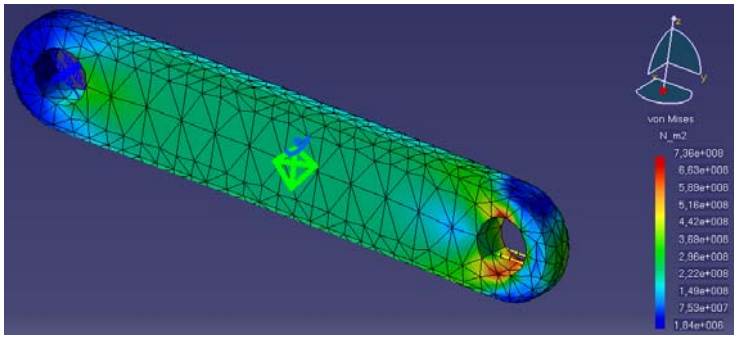

Figure 7.37 Main slider angle link stresses with +2.5g

Intentionally left blank

Chapter 8

Conclusion

An all new flap track mechanism has been successfully developed and applied to a realistic environment. The various constraints and problems encountered in the course of the project have been taken into account and solved to a high degree. The main goal of this project as described in chapter 1, i.e. to investigate whether it is at all possible to fully integrate a flap track mechanism into the wing strake, has thus been attained.

There are various tasks which remain to be done, but to provide meaningful results a somewhat more concrete application than in this project needs to be specified. At least data obtained through the preliminary design part of an aircraft's development process, such as approximate masses, loads, wing span and area, need to be known.

Particularly to be investigated remain weight and materials, as well as maintenance and production expenditure. The latter should be compared to more complex Boeing systems rather than those of Airbus, and the obvious advantages of integrated flap tracks must be taken into account. The same applies to reliability and availability considerations. Further, an exact jamming investigation must be done as well as an analysis of aerodynamic efficiency, issues which have not been addressed in this project.

The following advantages and disadvantages have been identified; where applicable the disadvantages come with measures taken to reduce their respective negative impact.

Advantages

- No fairing drag during cruise ─ the main goal of integrated flap tracks.
- Thanks to usage of programming cams, flap extension characteristics are exactly as required by aerodynamics, not only approximately as with current systems.
- Noise is reduced due to less turbulent airflow at the wing lower side.
- Flap extension not exactly in flight direction poses no problem. No wider fairing due to off-axis track mounting is needed.
- Tab collision with fairing is not an issue anymore ─ which could prove the combination of integrated flap tracks with adaptive wing technologies to be very promising, even though an integrated flap track system may likely be heavier than current systems.

- Although a complex mechanism, convenient maintenance and replacement is possible as the main elements of the mechanism are quickly detachable (the main mechanism assembly is connected to flap and main wing by only seven bolts), which allows them to be serviced individually and reduces aircraft turnaround time due to a quick part replacement. Also in the built-in state most of the mechanism is easily accessible for inspection without any part removal needed. This is a clear advantage compared to current systems where the removal of fairings is avoided unless absolutely necessary, as mounting of such fairings is quite laborious.

Disadvantages

- Weight ─ although not investigated closely in this project it is evident that a flap track mounting on the main wing rear spar only and cutting the flap body structure will lead to a heavier system. However, the latter effect has been reduced by a more or less intact flap top structure with continuous stringers, as well as an intact flap rear spar and a partly continuous flap front spar.

- Reliability and availability decrease with increasing complexity of a system. Fail-safe design is essential to ensure reliability and has been applied in this project, but more and especially moving parts lead to decreased availability.

- Manufacturing and maintenance expenditure likewise increase with complexity. However, many parts are very simple, such as the guides which are basically extruded profiles, and many parts are identical for the inboard and outboard side (such as the levers and links of the transformation locking mechanism). The complexity of the system may lead to higher maintenance costs, but as explained above there are still several advantages with this approach.

- With any flap track system there is a conflict of aims between cruise qualities, i.e. attaining the least drag possible, and landing qualities where a high drag is needed to ensure a steep descent angle. By removing extra fairing drag the descent angle gets smaller; however, this problem could for example be solved by deflecting the inboard tabs fully downward (thus being almost perpendicular to the airflow and producing a high drag), and using the outboard tabs for roll control.

- The airflow through the flap slot above the track is blocked more than with conventional systems, where the fairing is located considerably downward in the flap extended position, which allows at least a partial airflow around the fairing and through the flap slot behind it. This reduces flap effectiveness somewhat, but is counteracted by using a flap vane on the other parts of the flap.

- Particularly the outboard moving bottom cover interferes with a smooth airflow, which further deteriorates flap effectiveness. This effect is reduced by using a two-section cover; further, the problem is substantial only near the flaps fully extended position where high drag is needed anyway (see above) so it is considered to be acceptable.

- The tab actuation mechanism as presented in chapters 3 and 5 creates problems as to the material characteristics needed. The slider and tab spike must bear very high pressures due to the spike's short lever arm. This problem could be solved by using an array of several such sliders per tab, weight permitting. Another approach could be using a highly efficient Guerney flap acting as a servo rudder for the tab. Nevertheless, the described actuation system for transferring a rotary motion from the wing into the flap is still applicable.

The above considerations show that a meaningful conclusion can be made only on the basis of an overall trade-off. Particularly with flap track systems, the decision for a specific system may seem implausible from one single discipline's viewpoint, but an overall view may prove it to be advantageous and optimal for a given application. The results of this project give a good basis for further tradeoff studies.

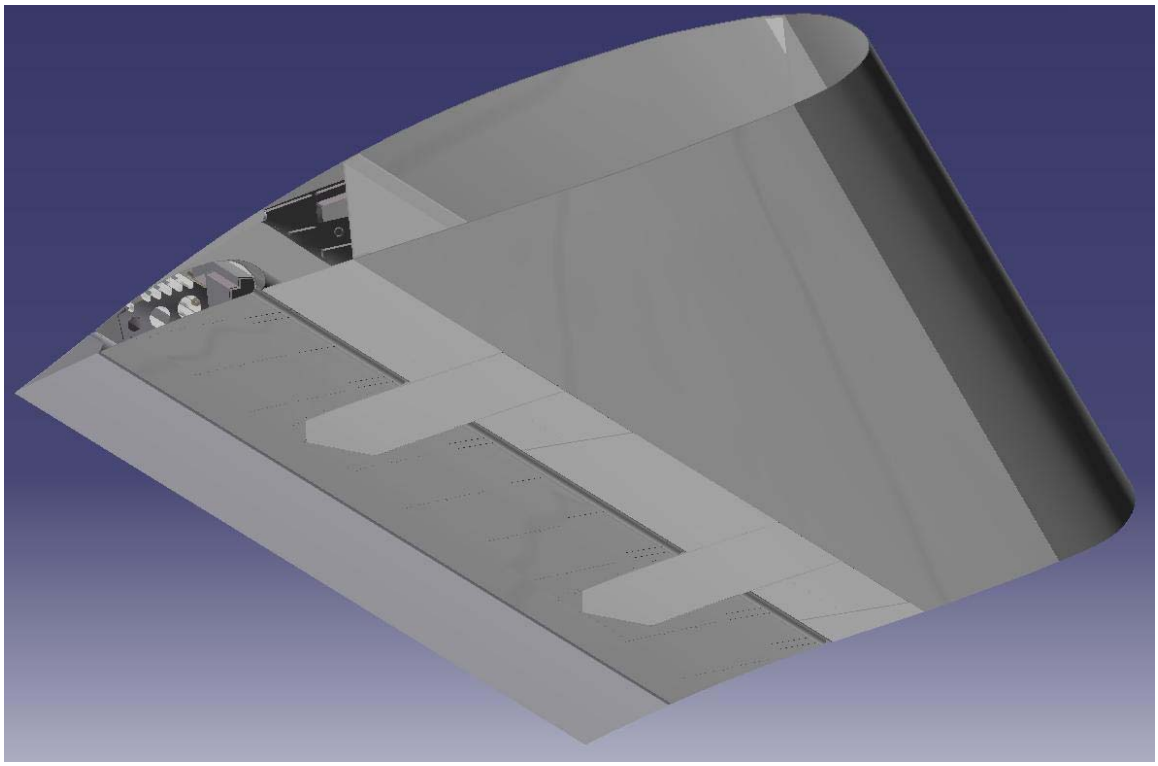

Figure 8.1 A fully integrated flap track mechanism ─ task accomplished!

Appendix

Appendix A: Relevant FARs (as obtained from [14])

FAR25.697 Lift and drag devices, controls.

(a) Each lift device control must be designed so that the pilots can place the device in any takeoff, en route, approach, or landing position established under §25.101(d). Lift and drag devices must maintain the selected positions, except for movement produced by an automatic positioning or load limiting device, without further attention by the pilots.

(b) Each lift and drag device control must be designed and located to make inadvertent operation improbable. Lift and drag devices intended for ground operation only must have means to prevent the inadvertant operation of their controls in flight if that operation could be hazardous.

(c) The rate of motion of the surfaces in response to the operation of the control and the characteristics of the automatic positioning or load limiting device must give satisfactory flight and performance characteristics under steady or changing conditions of airspeed, engine power, and airplane attitude.

(d) The lift device control must be designed to retract the surfaces from the fully extended position, during steady flight at maximum continuous engine power at any speed below *V*F +9.0 (knots).

[Amdt. 25–23, 35 FR 5675, Apr. 8, 1970, as amended by Amdt. 25–46, 43 FR 50595, Oct. 30, 1978; Amdt. 25–57, 49 FR 6848, Feb. 23, 1984]

FAR25.699 Lift and drag device indicator.

(a) There must be means to indicate to the pilots the position of each lift or drag device having a separate control in the cockpit to adjust its position. In addition, an indication of unsymmetrical operation or other malfunction in the lift or drag device systems must be provided when such indication is necessary to enable the pilots to prevent or counteract an unsafe flight or ground condition, considering the effects on flight characteristics and performance.

(b) There must be means to indicate to the pilots the takeoff, en route, approach, and landing lift device positions.

(c) If any extension of the lift and drag devices beyond the landing position is possible, the controls must be clearly marked to identify this range of extension.

[Amdt. 25–23, 35 FR 5675, Apr. 8, 1970]

FAR25.701 Flap and slat interconnection.

(a) Unless the airplane has safe flight characteristics with the flaps or slats retracted on one side and extended on the other, the motion of flaps or slats on opposite sides of the plane of symmetry must be synchronized by a mechanical interconnection or approved equivalent means.

(b) If a wing flap or slat interconnection or equivalent means is used, it must be designed to account for the applicable unsymmetrical loads, including those resulting from flight with the engines on one side of the plane of symmetry inoperative and the remaining engines at takeoff power.

(c) For airplanes with flaps or slats that are not subjected to slipstream conditions, the structure must be designed for the loads imposed when the wing flaps or slats on one side are carrying the most severe load occurring in the prescribed symmetrical conditions and those on the other side are carrying not more than 80 percent of that load.

(d) The interconnection must be designed for the loads resulting when interconnected flap or slat surfaces on one side of the plane of symmetry are jammed and immovable while the surfaces on the other side are free to move and the full power of the surface actuating system is applied.

[Amdt. 25–72, 55 FR 29777, July 20, 1990]

Appendix B: Mathematica Notebook 'FlapRotation.nb'

Definitions

Norm function and COS base vectors:

```
norm[vector_] := Sqrt[(vector[[1]])^2 + (vector[[2]])^2 + (vector[[3]])^2]
XVector = {1, 0, 0}
{1, 0, 0}
YVector = {0, 1, 0}
{0, 1, 0}
ZVector = {0, 0, 1}
{0, 0, 1}
```

Rotation matrices:

```
RotationMatrixXAxis[XAngle_] := {{1, 0, 0}, {0, Cos[XAngle * Pi / 180], -Sin[XAngle * Pi / 180]},
  {0, Sin[XAngle * Pi / 180], Cos[XAngle * Pi / 180]}}
RotationMatrixYAxis[YAngle_] := {{Cos[YAngle * Pi / 180], 0, Sin[YAngle * Pi / 180]}, {0, 1, 0},
  {-Sin[YAngle * Pi / 180], 0, Cos[YAngle * Pi / 180]}}
RotationMatrixZAxis[ZAngle_] := {{Cos[ZAngle * Pi / 180], -Sin[ZAngle * Pi / 180], 0},
  {Sin[ZAngle * Pi / 180], Cos[ZAngle * Pi / 180], 0}, {0, 0, 1}}
```

Swept wing back structure edge line (sweep angle 23°):

```
WingStructureEdgeLine = {-Cos[23. * Pi / 180], -Sin[23. Pi / 180], 0}
{-0.920505, -0.390731, 0}
```

Flap vane leading edge line parallel to wing structure back edge (retracted position)

```
FlapVaneLine = WingStructureEdgeLine
{-0.920505, -0.390731, 0}
```

Alpha Rotation

Set Alpha = extended flap angle 38.2755° (rotation axis = XVector):

```
AlphaAngle = 38.2755
38.2755
```

Beta Rotation

Calculate beta rotation axis (green dashed line to red dashed line in fig. 4.10)

```
FlapSurfaceBetaRotationLine = RotationMatrixXAxis[-AlphaAngle].YVector
{0., 0.785041, -0.619443}
```

Calculate flap surface normal direction (uncorrected gamma rotation axis, before Beta rotation)

```
FlapSurfaceNormalVector = Cross[FlapSurfaceBetaRotationLine, -XVector]
{0., 0.619443, 0.785041}
```

Calculate desired flap surface normal direction (corrected Gamma rotation axis, after Beta rotation); norm resulting vector:

```
TargetedFlapSurfaceNormalVector = Cross[FlapSurfaceBetaRotationLine, WingStructureEdgeLine]
{-0.242036, 0.570201, 0.722634}
norm[TargetedFlapSurfaceNormalVector]
0.951793
TargetedFlapSurfaceNormalVector =
 1 / norm[TargetedFlapSurfaceNormalVector] * TargetedFlapSurfaceNormalVector
{-0.254295, 0.59908, 0.759235}
norm[TargetedFlapSurfaceNormalVector]
1.
```

Perform beta rotation such that desired flap surface normal direction is obtained, i.e. set Beta=14.7318°:

```
BetaAngle = 14.7318
14.7318
RotationMatrixXAxis[-AlphaAngle].(RotationMatrixYAxis[-BetaAngle].ZVector)
{-0.254295, 0.59908, 0.759234}
```

Gamma Rotation

Calculate uncorrected flap vane direction (green in fig. 4.11, before Gamma rotation)

```
FlapVaneLineBeforeGamma =
 RotationMatrixXAxis[-AlphaAngle].(RotationMatrixYAxis[-BetaAngle].FlapVaneLine)
{-0.890245, -0.451739, 0.0582737}
```

Calculate flap vane direction (red line in fig. 4.11, after Gamma rotation), i.e. obtain original retracted flap vane direction with Gamma=5.137°:

```
FlapVaneLine
{-0.920505, -0.390731, 0}
GammaAngle = 5.137
5.137
FlapVaneLineAfterGamma = RotationMatrixXAxis[-AlphaAngle].
  (RotationMatrixYAxis[-BetaAngle].(RotationMatrixZAxis[-GammaAngle].FlapVaneLine))
{-0.920504, -0.390733, 1.1609 × 10^-6}
```

Appendix C: Flap Load Estimation

Since flap force and aerodynamic data is not freely available for actual airliners, an approximate calculation is carried out in this project in order to obtain at least a somewhat realistic estimate of these forces.

For all of these calculations the flap is being treated like a free wing and the tab acting as a standard camber flap. The actual wing influence is neglected for these very rough calculations.

Formulas used in this appendix are taken from [2] and [3]. The following steps shown in 'pretty print' format are exactly the same as carried out in the Mathematica Notebook FlapLoad.nb, which is presented in Appendix D.

Dynamic Pressure Data

A typical configuration with flaps fully extended is on final approach, where a large airliner flies at a speed of 140knots or about 70m/s. ISA conditions are assumed.

V = 70m/s

$\rho = 1.225 kg/m^3$

Therefore, the following dynamic pressure results:

$$q = \frac{\rho}{2} \cdot V^2 = 3001.25 N/m^2$$

Flap and Tab Basic Data

The maximum tab deflection angle is set to 30°, as defined in chapter 4.2.2.

$\xi_{max,tab} = 30°$

The minimum drag for a standard aerofoil is about 0.011, according to [2]. The actual flap drag coefficient (including induced drag) will be calculated later.

$C_{W0,flap} = 0.011$

Additional drag due to tab deflection is introduced. For a standard camber flap, which the tab is considered to act as for the flap body, the following maximum additional drag is obtained with a fully deflected tab:

$$\Delta C_{CW0,max,tab} = \left(0.07 - C_{W0,flap}\right) \cdot \frac{\xi_{max,tab}}{45} = 0.0393$$

Now the different flap dimensions need to be specified. According to fig. 4.4 on page 48 they are as follows:

Flap span: b = 8.75m
Flap chord inboard: $l_i = 1.815$m
Flap chord inboard: $l_o = 0.619$m

A mean flap chord results:
$l = (l_i - l_o)/2 + l_o = 1.217$m

The tab chord is set to 1/3 of the full flap chord, i.e.
$l_k = 0.405$m

Relative tab chord:
$\lambda_k = l_k/l = 0.33$

Flap taper:
$\lambda = l_o/l_i = 0.341$

Reference flap chord:
$$l_\mu = l_i \cdot \frac{2}{3} \cdot \frac{1+\lambda+\lambda^2}{1+\lambda}$$

Flap surface:
$$S = b \cdot l = 10.648 m^2$$

The flap's Oswald factor is set to a standard value (see [2] and [3]):
e = 0.7

Flap aspect ratio:
$\Lambda = b^2/S = 7.3145$

For induced drag calculations the following coefficient is needed:
$$k_{Flap} = \frac{1}{\pi \cdot \Lambda \cdot e} = 0.0622$$

Flap and Tab Position Samples

A set of main flap suspension coordinates for various flap extension states is now defined in FlapLoad.nb so that it represents the characteristics as shown in fig. 4.6. A position array is defined for the tab as well. These samples later serve as a basis for mathematical curve fitting.

Flap and Tab Characteristics

From the flap and tab data defined above, the lift, drag and moment coefficients produced by tab deflection can be derived. η_k is the tab deflection angle, measured in radians; note that in flight mechanics a downward deflection is defined to be positive.

Calculating the lift coefficient with a deflected tab is a multiple-step process as defined in [2] for a wing with deflected camber flap (in this case the flap with deflected tab). First, a change of the acting angle of attack due to tab deflection must be calculated:

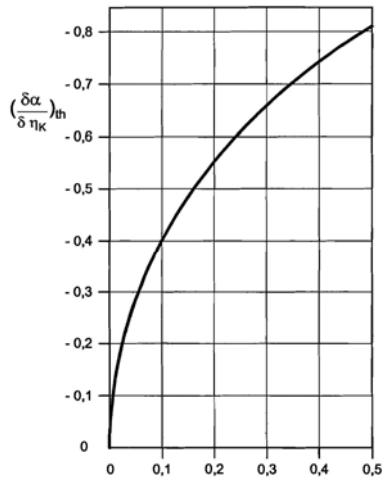

Figure C.1 Theoretic flap effectiveness, from [2]

$$\left(\frac{\partial\alpha}{\partial\eta_k}\right)_{th} = -\frac{2}{\pi}\cdot\left(\sqrt{\lambda_k\cdot(1-\lambda_k)}+\arcsin\sqrt{\lambda_k}\right) = -0.689$$

This is a theoretical value; the actual value is obtained through a flap effectiveness coefficient f_η:

$$\left(\frac{\partial\alpha}{\partial\eta_k}\right)_{actual} = \left(\frac{\partial\alpha}{\partial\eta_k}\right)_{th}\cdot f_\eta$$

f_η depends on a number of variables, one of which is the tab deflection angle. Fig. C.2 below shows the correlations. In this project there is no slot between the flap and the tab so the solid lines apply. The Mathematica Notebook FlapLoad.nb extracts and approximates the curve for the given $\lambda_k = 0.33$ for further use.

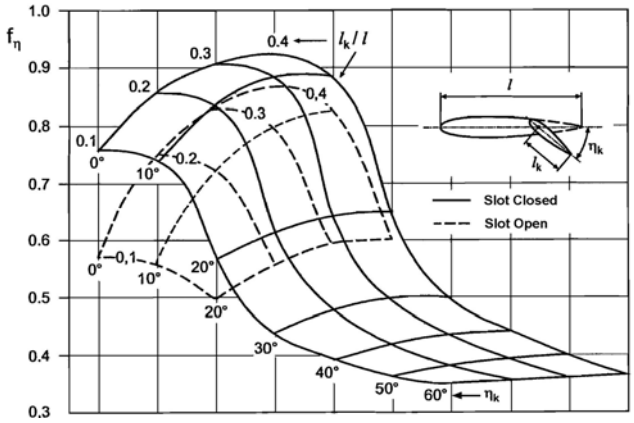

Figure C.2 Flap effectiveness coefficient f_η, from [2]

C_l is defined as follows for the flap with deflected tab:

$$C_l = \frac{\partial C_l}{\partial \alpha}\left(\alpha - \frac{\partial \alpha}{\partial \eta_k}\eta_k\right)$$

α is the AOA of the flap, with the flap lift coefficient derivative $\frac{\partial C_l}{\partial \alpha} = C_l'$

This derivative is a function of $C_l(\alpha)$ of the flap, which in turn greatly depends on the aerodynamic characteristics of its aerofoil and a number of other constraints.

For a flat plate the derivative can be calculated as follows, using Λ for the dimensions as defined for the flap at hand:

$$C_l' = \frac{2 \cdot \pi \cdot \Lambda}{\Lambda + 3} = 4.43$$

This gives at least a first indication for the $C_l(\alpha)$ function gradient near an AOA of 0°. At higher AOA, however, this gradient decreases because of beginning stall. Figure C.3 shows a realistic $C_l(\alpha)$ function taking this into account.

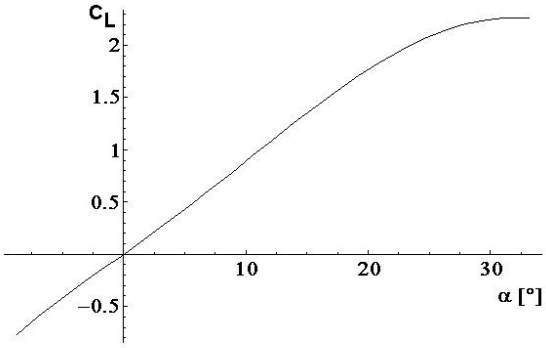

Figure C.3 Typical $C_l(\alpha)$ function

The notebook extracts this function in radians for further use.

The derivative function can be approximated by the following formula:

$$C_l'(\alpha) \approx \frac{C_l(\alpha + 0.1)}{\alpha + 0.1}$$

With the formulas as depicted above the function $C_l(\alpha, \eta_k)$ is obtained.

Now the drag needs to be calculated. Adding induced drag to the standard minimum drag is done using the following equation:

$$C_{D,Flap} = C_{W0,Flap} + k_{Flap} \cdot C_{l,Flap}^2$$

This formula produces an accurate drag function at small AOA, but at high AOA where C_l decreases again the drag decreases as well, which is not very realistic. Therefore, the notebook corrects the drag function to be steadier at high AOA.

This basic drag now needs to be combined with the drag encountered by tab deflection.

$$C_D = C_{D,Flap} + \Delta C_{W0,\max,tab} \cdot \xi_{Tab}$$

Finally, the flap moment coefficient needs to be calculated. Its theoretic derivative is defined as follows:

$$\left(\frac{\partial C_M}{\partial \eta_k}\right)_{th} = -2 \cdot \sqrt{\lambda_k \cdot \left(1-\lambda_k\right)^3} = -0.630$$

with the actual measured moments usually being about 75% of these values (see [2]):

$$\left(\frac{\partial C_M}{\partial \eta_k}\right)_{actual} = 0.75 \cdot \left(\frac{\partial C_M}{\partial \eta_k}\right)_{th} = -0.473$$

which yields the flap moment function:

$$C_M = \left(\frac{\partial C_M}{\partial \eta_k}\right)_{actual} \cdot \eta_k \qquad \text{with } \eta_k = \xi_{Tab}$$

The basic flap moment is neglected in this rough estimation since normally it is much smaller than the moment induced by tab deflection.

Flap Loads and Moment Calculation

For better data and graph handling the functions as obtained above are first adjusted so that they represent values for flap extension percents rather than flap angles. This is where the position samples are needed.

$$L = C_L \cdot q \cdot S$$

$$D = C_D \cdot q \cdot S$$

$$M = C_M \cdot q \cdot S \cdot l_\mu$$

These functions can now be used for subsequent tasks.

Appendix D: Mathematica Notebook 'FlapLoad.nb'

Dynamic Pressure Data

```
Airspeed = 70
```
```
70
```
```
AirDensity = 1.225
```
```
1.225
```
```
DynamicPressure = AirDensity / 2 * Airspeed^2
```
```
3001.25
```

Flap and Tab Basic Data

```
XiMaxTabDegree = 30
```
```
30
```
```
cDragZeroFlap = 0.011
```
```
0.011
```
```
DeltacDragZeroTab = (0.07 - cDragZeroFlap) * XiMaxTabDegree / 45
```
```
0.0393333
```
```
SpanOutboardFlap = 8.75
```
```
8.75
```
```
FlapChordOutboard = 0.61875
```
```
0.61875
```
```
FlapChordInboard = 1.815
```
```
1.815
```
```
l = (FlapChordInboard - FlapChordOutboard) / 2 + FlapChordOutboard
```
```
1.21688
```
```
lk = l / 3
```
```
0.405625
```
```
LambdaK = lk / l
```
```
0.333333
```
```
FlapTaper = FlapChordOutboard / FlapChordInboard
```
```
0.340909
```
```
FlapReferenceChord = FlapChordInboard * 2 / 3 * (1 + FlapTaper + FlapTaper^2) / (1 + FlapTaper)
```
```
1.31487
```
```
SurfaceOutboardFlap = l * SpanOutboardFlap
```
```
10.6477
```
```
FlapOswaldFactor = 0.7
```
```
0.7
```
```
FlapLambda = (SpanOutboardFlap) ^2 / (SurfaceOutboardFlap)
```
```
7.19055
```
```
FlapK = 1 / (Pi * FlapLambda * FlapOswaldFactor)
```
```
0.0632397
```

Flap and Tab Position Samples

```
MainSuspensionBackMotionSample = {29.8, 32.4, 36.0, 39.6, 43.3, 45.92, 47.15}
```

```
{29.8, 32.4, 36., 39.6, 43.3, 45.92, 47.15}
```

```
MainSuspensionBackMotionDelta =
 Last[MainSuspensionBackMotionSample] - First[MainSuspensionBackMotionSample]
```

```
17.35
```

```
MainSuspensionExtensionSample =
 (MainSuspensionBackMotionSample - 29.8) / MainSuspensionBackMotionDelta * 100
```

```
{0., 14.9856, 35.7349, 56.4841, 77.8098, 92.9107, 100.}
```

```
FlapAOASample = {0, 3, 10, 18.5, 26, 33, 38}
```

```
{0, 3, 10, 18.5, 26, 33, 38}
```

```
XiTabSample = Table[i, {i, -XiMaxTabDegree, XiMaxTabDegree, 1}]
```

```
{-30, -29, -28, -27, -26, -25, -24, -23, -22, -21, -20, -19, -18, -17, -16, -15, -14,
 -13, -12, -11, -10, -9, -8, -7, -6, -5, -4, -3, -2, -1, 0, 1, 2, 3, 4, 5, 6, 7, 8, 9,
 10, 11, 12, 13, 14, 15, 16, 17, 18, 19, 20, 21, 22, 23, 24, 25, 26, 27, 28, 29, 30}
```

Flap and Tab Characteristics

fη curve extraction:

```
fEtaTabPolynom[XiTabSet_] =
 Fit[{{0, .91}, {5, .877}, {10, .87}, {20, .64}, {30, .5}, {40, .43}, {50, .39},
   {60, .365}, {70, .34}}, {1, XiTabSet, XiTabSet^2, XiTabSet^3, XiTabSet^4,
   XiTabSet^5, XiTabSet^6, XiTabSet^7}, XiTabSet]
```

$$0.908086 - 0.014923\,\text{XiTabSet} + 0.00403504\,\text{XiTabSet}^2 - 0.000486127\,\text{XiTabSet}^3 + 0.0000225074\,\text{XiTabSet}^4 - 4.98584\times10^{-7}\,\text{XiTabSet}^5 + 5.33618\times10^{-9}\,\text{XiTabSet}^6 - 2.21945\times10^{-11}\,\text{XiTabSet}^7$$

```
Plot[fEtaTabPolynom[XiTabSample], {XiTabSample, -XiMaxTabDegree, XiMaxTabDegree*2}]
```

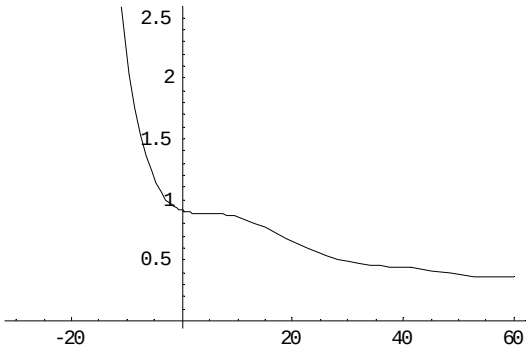


```
- Graphics -
```

C_L *Calculation:*

C_L*'tab, theoretic:*

```
cltabderivtheoretic = -2 / Pi * (Sqrt[LambdaK * (1 - LambdaK)] + ArcSin[Sqrt[LambdaK]])
```

```
-0.691932
```

C_L'tab, realistic:

```
cltabderivrealistic[XiTabAngle_] := cltabderivtheoretic * fEtaTabPolynom[Abs[XiTabAngle]]
Plot[cltabderivrealistic[XiTabSample],
 {XiTabSample, -XiMaxTabDegree * 1.5, XiMaxTabDegree * 1.5}]
```

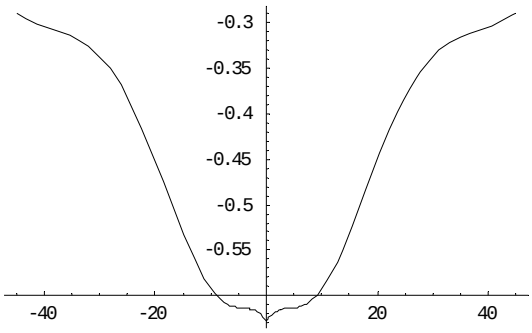


```
- Graphics -
```

C_L' flap without tab, AOA=0°:

```
clderivflapatzeroalpha = 2 * Pi * FlapLambda / (FlapLambda + 3)
4.43348
```

C_L flap without tab, standard curve extraction:

```
flapaloneclpoly[FlapAngleset_] =
 Fit[{{-10 * Pi / 180, -0.77}, {0 * Pi / 180, 0}, {10 * Pi / 180, 0.77}, {22 * Pi / 180, 1.71},
   {28 * Pi / 180, 2.05}, {33 * Pi / 180, 2.225}, {38 * Pi / 180, 2.2625}},
  {1, FlapAngleset, FlapAngleset^2, FlapAngleset^3, FlapAngleset^4, FlapAngleset^5},
  FlapAngleset]
-0.000287549 + 4.18141 FlapAngleset + 0.782618 FlapAngleset^2 +
 7.18921 FlapAngleset^3 - 24.9279 FlapAngleset^4 + 14.5857 FlapAngleset^5
Plot[flapaloneclpoly[FlapAngle], {FlapAngle, -10 * Pi / 180, 38 * Pi / 180}]
```

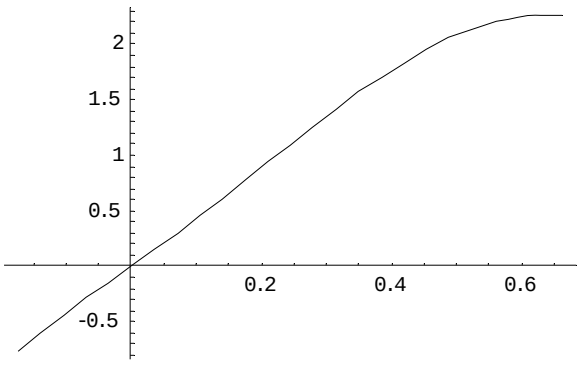


```
- Graphics -
```

C_L' flap derivative without tab calculation:

```
FlapCLDerivativePolynom[FlapAngleset_] =
 flapaloneclpoly[FlapAngleset + .1] / (FlapAngleset + .1)
        1
-------------------- (-0.000287549 + 4.18141 (0.1 + FlapAngleset) + 0.782618 (0.1 + FlapAngleset)^2 +
0.1 + FlapAngleset
  7.18921 (0.1 + FlapAngleset)^3 - 24.9279 (0.1 + FlapAngleset)^4 + 14.5857 (0.1 + FlapAngleset)^5)
```

```
Plot[FlapCLDerivativePolynom[FlapAngle], {FlapAngle, 0, 40*Pi/180},
 PlotRange→{{0, 38*Pi/180}, {-5, 6}}]
```

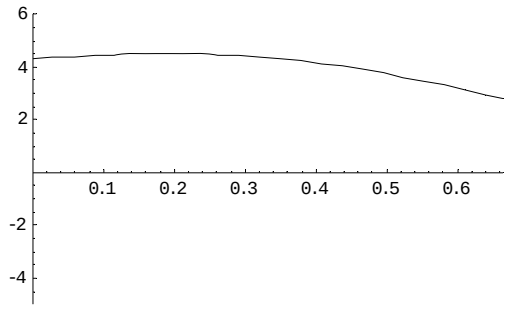

- Graphics -

```
cLiftFlap[FlapAngle_, XiTabAngle_] :=
 FlapCLDerivativePolynom[FlapAngle*Pi/180] *
  (FlapAngle*Pi/180 - cltabderivrealistic[XiTabAngle] * XiTabAngle*Pi/180)
cLiftFlap[38, 30] - cLiftFlap[38, 0]
0.499357
Plot[cLiftFlap[FlapAOA, -30], {FlapAOA, -0, 38}]
```

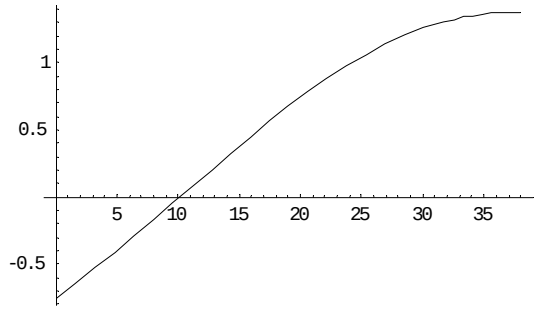

- Graphics -

C_L function for flap combined with tab:

```
Plot3D[cLiftFlap[FlapAOA, XiTabAngle], {FlapAOA, 0, 38},
 {XiTabAngle, -XiMaxTabDegree, XiMaxTabDegree}]
```

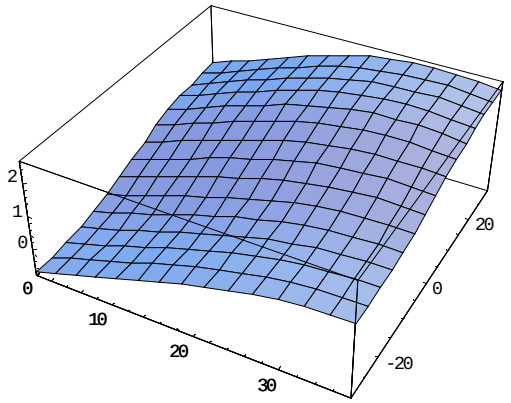

- SurfaceGraphics -

```
Plot3D[cLiftFlap[FlapAOA, XiTabAngle], {FlapAOA, 0, 38},
 {XiTabAngle, -XiMaxTabDegree, XiMaxTabDegree}]
```

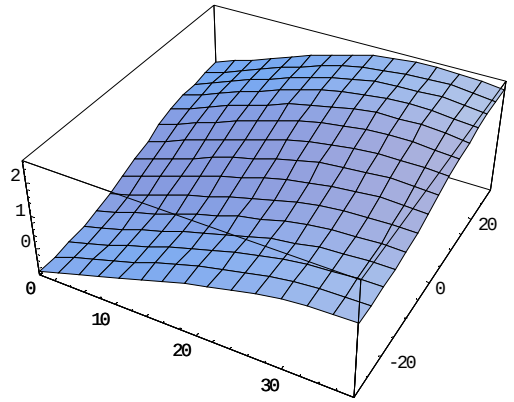

- SurfaceGraphics -

C_D Calculation:

Basic C_D:

```
cDragFlapBasic[FlapAngle_] := cDragZeroFlap + FlapK * cLiftFlap[FlapAngle, 0]^2
Plot[cDragFlapBasic[FlapAOA], {FlapAOA, 0, 38}, PlotRange -> {{0, 38}, {0, 0.4}}]
```

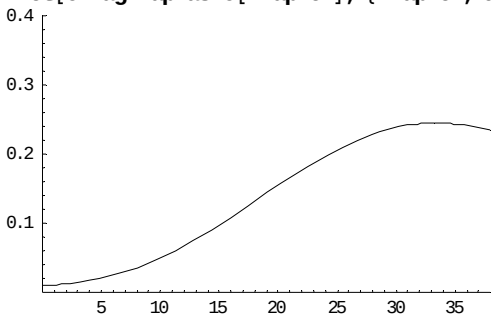

- Graphics -

C_D Correction at high AOA:

```
cDragFlapBasicPolynom[FlapAngleset_] =
 Fit[{{0, cDragFlapBasic[0]}, {5, cDragFlapBasic[5]}, {10, cDragFlapBasic[10]},
   {15, cDragFlapBasic[15]}, {20, cDragFlapBasic[20]}, {38, .36}},
  {1, FlapAngleset, FlapAngleset^2, FlapAngleset^3, FlapAngleset^4, FlapAngleset^5},
  FlapAngleset]
```

$0.011 + 0.000319146\,\text{FlapAngleset} + 0.000219667\,\text{FlapAngleset}^2 + 0.0000248959\,\text{FlapAngleset}^3 - 1.2586\times10^{-6}\,\text{FlapAngleset}^4 + 1.61284\times10^{-8}\,\text{FlapAngleset}^5$

```
Plot[cDragFlapBasicPolynom[FlapAOA], {FlapAOA, 0, 38}]
```

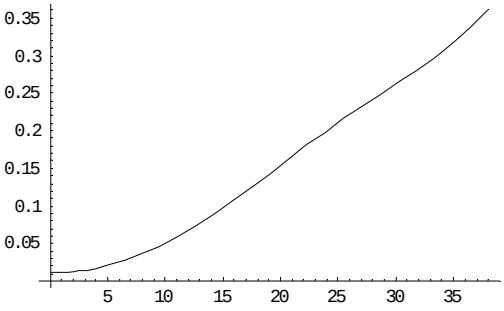

- Graphics -

C_D with tab deflection:

```
cDragFlap[FlapAngle_, XiTabAngle_] :=
 cDragFlapBasicPolynom[FlapAngle] + DeltacDragZeroTab * Abs[XiTabAngle]
Plot3D[cDragFlap[FlapAOA, XiTabAngle], {FlapAOA, 0, 38},
 {XiTabAngle, -XiMaxTabDegree, XiMaxTabDegree}]
```

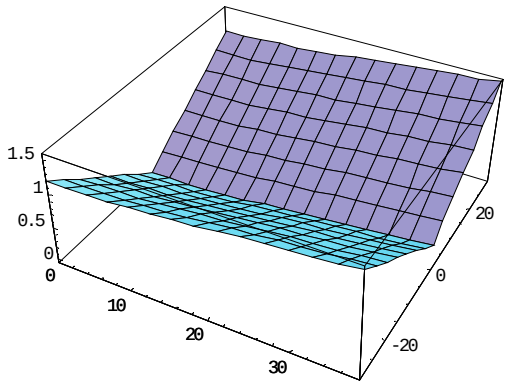


```
- SurfaceGraphics -
Plot3D[cDragFlap[FlapAOA, XiTabAngle], {FlapAOA, 0, 38},
 {XiTabAngle, -XiMaxTabDegree, XiMaxTabDegree}]
```

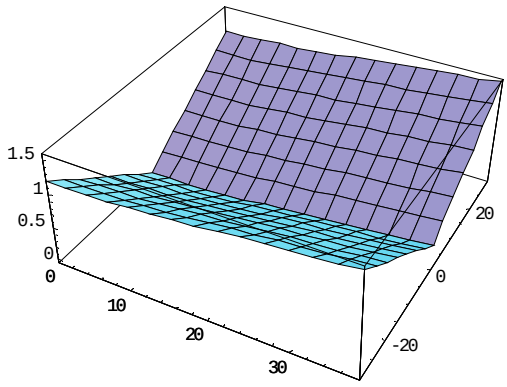


```
- SurfaceGraphics -
```

C_M Calculation:

```
cMomentTabDerivativeTheoretic = -2 * Sqrt[LambdaK * (1 - LambdaK) ^3]
-0.628539
cMomentTabDerivativeRealistic = 0.75 * cMomentTabDerivativeTheoretic
-0.471405
cMomentFlap[XiTabAngle_] := cMomentTabDerivativeRealistic * XiTabAngle * Pi / 180
Plot[cMomentFlap[XiTabAngle], {XiTabAngle, -30, 30}]
```

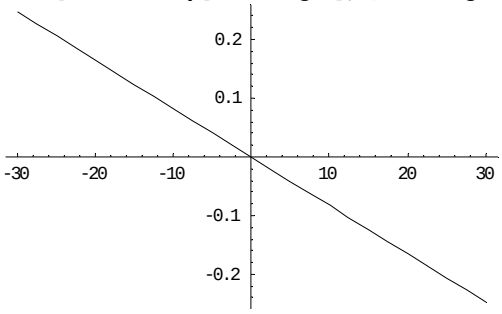


```
- Graphics -
```

Flap Loads and Moment Calculation

Function argument transfer from AOA to extension percents:

```
FlapAOASampleListFunction[FlapSetting_] :=
 {Extract[MainSuspensionExtensionSample, FlapSetting], Extract[FlapAOASample, FlapSetting]}
FlapAOASampleList = Table[FlapAOASampleListFunction[i], {i, 1, 7, 1}]
{{0., 0}, {14.9856, 3}, {35.7349, 10},
 {56.4841, 18.5}, {77.8098, 26}, {92.9107, 33}, {100., 38}}
FlapAOApoly[ExtensionPercents_] =
 Fit[FlapAOASampleList, {1, ExtensionPercents, ExtensionPercents^2, ExtensionPercents^3,
   ExtensionPercents^4, ExtensionPercents^5, ExtensionPercents^6}, ExtensionPercents]
9.81753 × 10^-6 + 0.216736 ExtensionPercents - 0.00645327 ExtensionPercents^2 +
 0.00048324 ExtensionPercents^3 - 9.50132 × 10^-6 ExtensionPercents^4 +
 7.46911 × 10^-8 ExtensionPercents^5 - 1.9916 × 10^-10 ExtensionPercents^6
FlapAOApoly[MainSuspensionExtensionSample] - FlapAOASample
{9.81753 × 10^-6, 7.05473 × 10^-6, 4.87222 × 10^-6,
 7.14121 × 10^-6, 9.19688 × 10^-6, 0.0000111921, 0.0000118946}
GraphicsArray[{Plot[FlapAOApoly[perc], {perc, 0, 100}], ListPlot[FlapAOASampleList]},
 PlotRange → {{0, 100}, {0, 14}}]
```

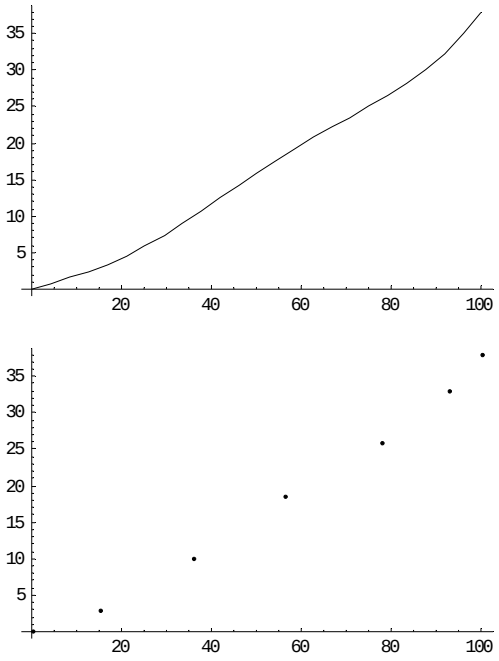


```
- GraphicsArray -
```

Flap Lift:

```
FlapLift[perc_, XiTab_] := cLiftFlap[FlapAOApoly[perc], XiTab] * DynamicPressure *
   SurfaceOutboardFlap
Plot3D[FlapLift[ExtensionPercents, xideg], {ExtensionPercents, 0, 100},
 {xideg, -XiMaxTabDegree, XiMaxTabDegree}]
```

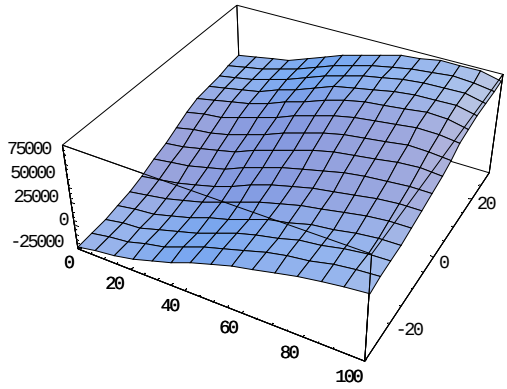

- SurfaceGraphics -

```
FindMinimum[-FlapLift[ExtensionPercents, 30], {ExtensionPercents, 80, 100}]
{-81082.6, {ExtensionPercents → 87.3708}}
Plot[FlapLift[0, xideg], {xideg, -30, 30}]
```

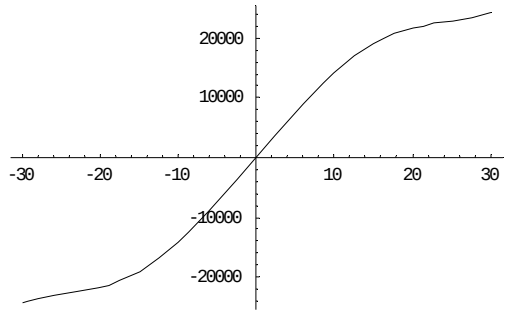

- Graphics -

Flap Drag:

```
FlapDrag[perc_, XiTab_] := cDragFlap[FlapAOApoly[perc], XiTab] * DynamicPressure *
  SurfaceOutboardFlap
Plot3D[FlapDrag[ExtensionPercents, xideg], {ExtensionPercents, 0, 100},
 {xideg, -XiMaxTabDegree, XiMaxTabDegree}]
```

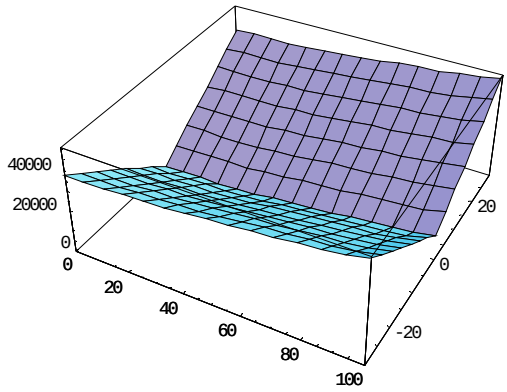

- SurfaceGraphics -

```
FlapDrag[100, 30]
49212.7
```

Flap Resultant Force:

```
FlapLoadResultant[perc_, XiTab_] :=
 Sqrt[(FlapLift[perc, XiTab])^2 + (FlapDrag[perc, XiTab])^2]
Plot3D[FlapLoadResultant[ExtensionPercents, xideg], {ExtensionPercents, 0, 100},
 {xideg, -XiMaxTabDegree, XiMaxTabDegree}]
```

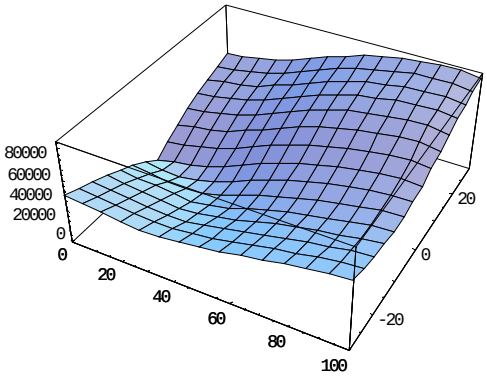

- SurfaceGraphics -

Flap Moment:

```
FlapMoment[XiTabAngle_] := cMomentFlap[XiTabAngle] * DynamicPressure * SurfaceOutboardFlap *
   FlapReferenceChord
Plot[FlapMoment[XiTab], {XiTab, -30, 30}]
```

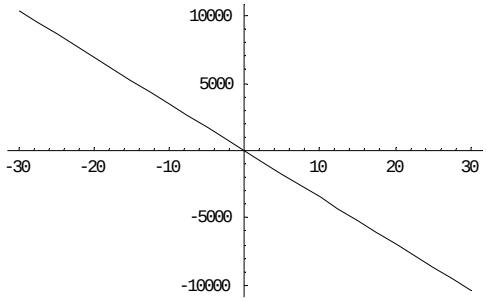

- Graphics -

Maximum Loads (Xi,tab = +30°):

```
FindMinimum[-FlapLoadResultant[ExtensionPercents, 30], {ExtensionPercents, 80, 100}]
{-93361.3, {ExtensionPercents → 89.5094}}
FlapLift[89.5, 30]
80981.6
FlapDrag[89.5, 30]
46457.6
```

Maximum Moments:
Xi,tab = +30°

```
FlapMoment[30]
-10371.3
```

Xi,tab = -30°

```
FlapMoment[-30]
10371.3
```

Appendix E: Main Flap Support Size Estimation

Only high-quality materials are to be considered for a highly loaded part such as the flap main suspension joint. Quenched and tempered steels are such materials, for example 100Cr6 the data of which is taken from [19] as follows:

100Cr6, tempered:

$E_{100Cr6} = 208000\ N/mm^2$
$\nu_{100Cr6} = 0.3$
$\rho_{100Cr6} = 7850kg/m^3$
$\sigma_{100Cr6} = 2200\ N/mm^2$

For a ball joint like the flap main support, basically two spheres press against each other, with one of the spheres having a negative radius (i.e. a concave shape). For such cases the maximum pressure encountered is calculated by the following formula taken from [20]:

$$p_{\max} = \left(\frac{6 \cdot F \cdot \left(\frac{1}{r_1} + \frac{1}{r_2} \right)^2}{\pi^3 \cdot \left(1 - \upsilon^2\right)^2 \cdot \left(\frac{1}{E_1} + \frac{1}{E_2} \right)^2} \right)^{1/3}$$

with F being the pressure load, r_1 and r_2 the radius of the respective sphere (note that one of them is negative), ν the Poisson ratio and E_1 and E_2 the Young's moduli. To simplify the calculation the same material is used for both parts.

In ball joints there is always a small radius difference between ball and inset; it should be as small as possible since this reduces pressure. For this calculation the difference is set to 1mm, which is a rather large play and therefore a conservative assumption.

According to [20] the maximum allowable pressure is $p_{\max,allow} = \frac{\sigma_{\max,allow}}{0.62}$

with $\sigma_{\max,allow} = \frac{\sigma_{100Cr6}}{S}$

S is a safety factor made up of the basic safety factor and another for jamming, i.e. $S = 1.1 \cdot 1.7 = 1.87$

For the force applied the considerations as outlined on page 143 apply. The force resulting from lift and drag is
$F = \sqrt{L^2 + D^2} \approx 116.5kN$

The following appendix yields a bearing radius of about 14mm. At least doubling of this value is needed for the inset and ring of the ball-joint bearing. Another safety factor of 2 is appropriate to account for lower quality materials and assumption inaccuracies. So a bearing radius of about ***60mm*** should be used for an initial design.

Appendix F: Mathematica Notebook 'FlapJointDim.nb'

Flap Support Joint Dimensioning

```
SafetyFactor = 1.1 * 1.7
```

```
1.87
```

```
MaxMainSuspBoltLoad = 116500
```

```
116500
```

```
RadiusDelta = 1
```

```
1
```

```
E1 = 208000
```

```
208000
```

```
E2 = 208000
```

```
208000
```

```
nu = 0.3
```

```
0.3
```

```
SigmaMax = 2200
```

```
2200
```

```
SigmaVMaxAllow = SigmaMax / SafetyFactor
```

```
1176.47
```

```
pmaxAllow = SigmaVMaxAllow / 0.62
```

```
1897.53
```

```
SupportRadiusSolutions =
 Solve[
  pmaxAllow ==
   ((6 * MaxMainSuspBoltLoad *
        (1 / SupportRadius + 1 / (-(SupportRadius + RadiusDelta)))^2) /
      (Pi^3 * (1 - nu^2)^2 * (1 / E1 + 1 / E2)^2))^(1 / 3), SupportRadius]
```

```
{{SupportRadius → -14.9169}, {SupportRadius → -0.5 - 14.3996 i},
 {SupportRadius → -0.5 + 14.3996 i}, {SupportRadius → 13.9169}}
```

```
SupportRadius = SupportRadius /. SupportRadiusSolutions[[4]]
```

```
13.9169
```

Appendix G: Demonstrator Parts and Assembly Manual

Parts & Nomenclature: Flap

Flap Body (Top Side, Cover Removed)

Flap Body Nose

Flap Angle Control Slider

Flap Angle Control Link

Outboard and Inboard Flap Vanes

Flap Vane Receptacles (Nose Cover Removed)

Flap Body (Lower Side)

Flap Vane Actuation Rod

Tab

Tab Actuation Slider

Parts & Nomenclature: Wing Section

Wing Structure Section

Flap Track Suspensions (View From Inboard)

Flap Track Suspensions (View From Outboard)

Covers (Lower Side)

Covers (Top Side)

Tab Actuation Rod

Tab Actuation Rod (Extendable Part)

Flap Actuation Screw & Screw Jack

Assembly Manual: 1/7; complete assembly time approx. 60 mins.

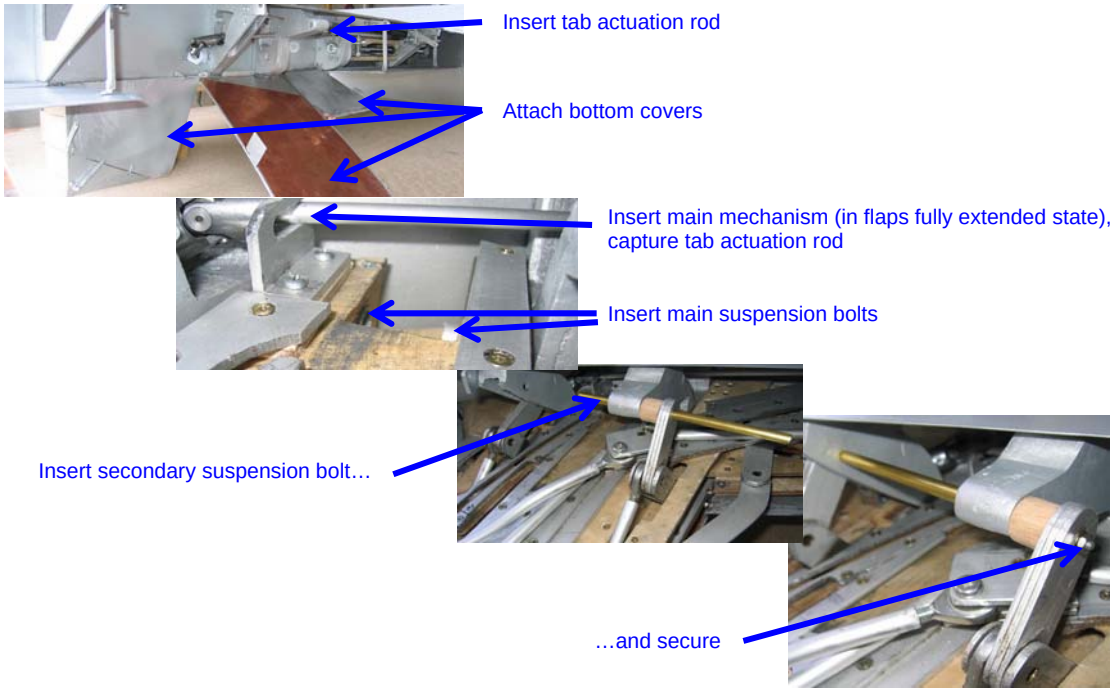

Assembly Manual: 2/7

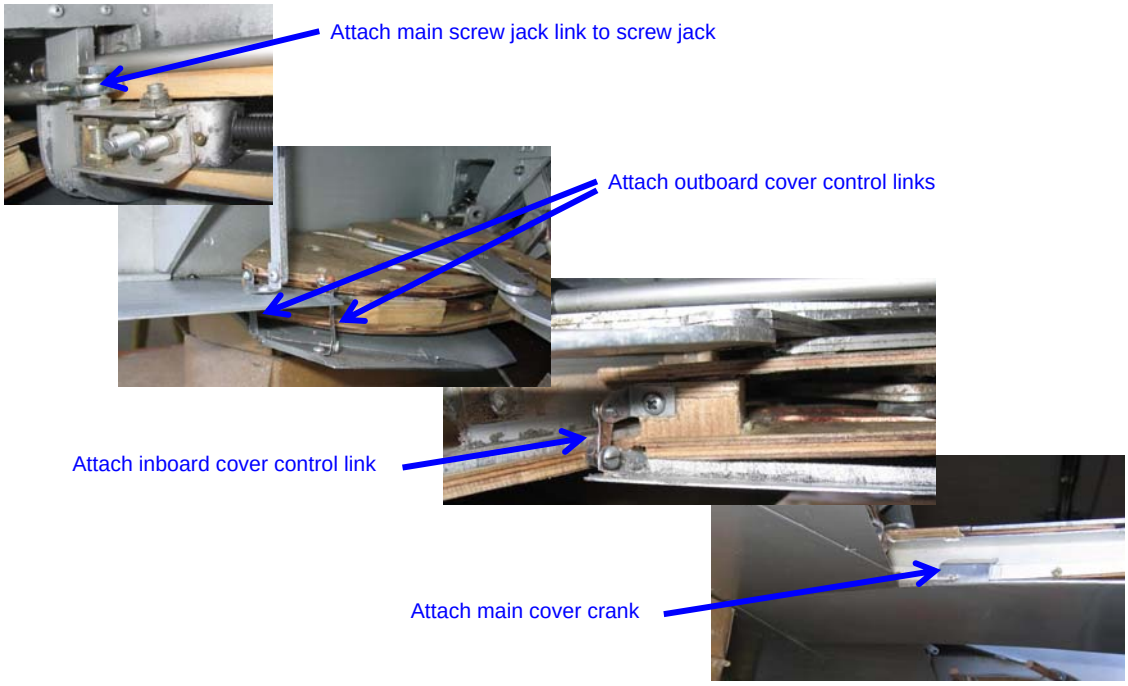

Assembly Manual: 3/7

Insert inboard & outboard flap vanes

Place flap vane
actuation rod links

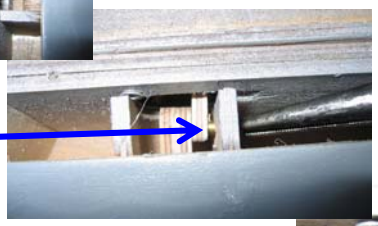

Connect links to flap
vane by inserting bolts…

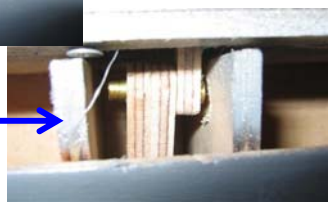

…at each of the four flap vane receptacles

Assembly Manual: 4/7

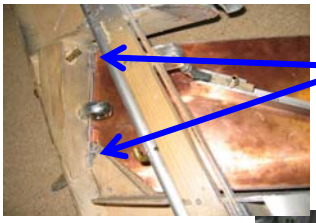

Attach extendable main cover to flap body

Insert flap angle
control slider;
insert extendable
cover into main cover

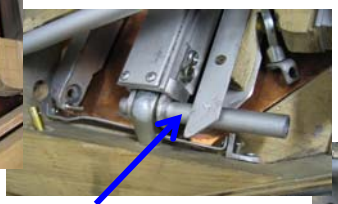

Insert main flap support bolt

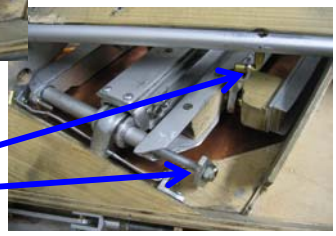

Attach flap vane actuation rod and
secure main flap support bolt with screw

Assembly Manual: 5/7

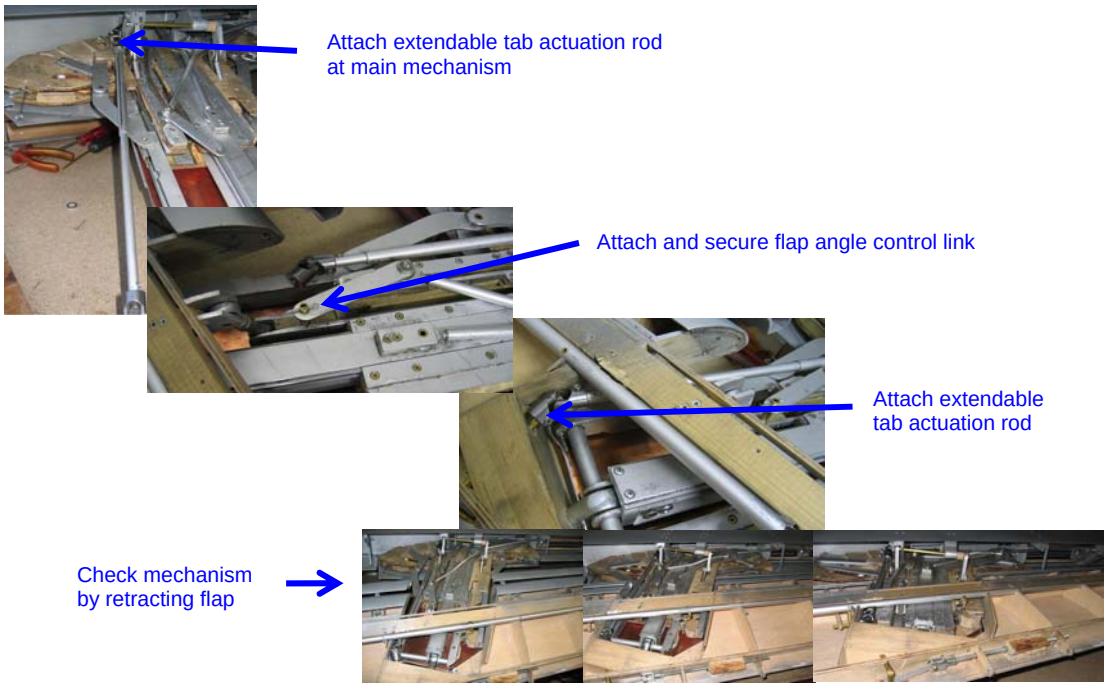

Assembly Manual: 6/7

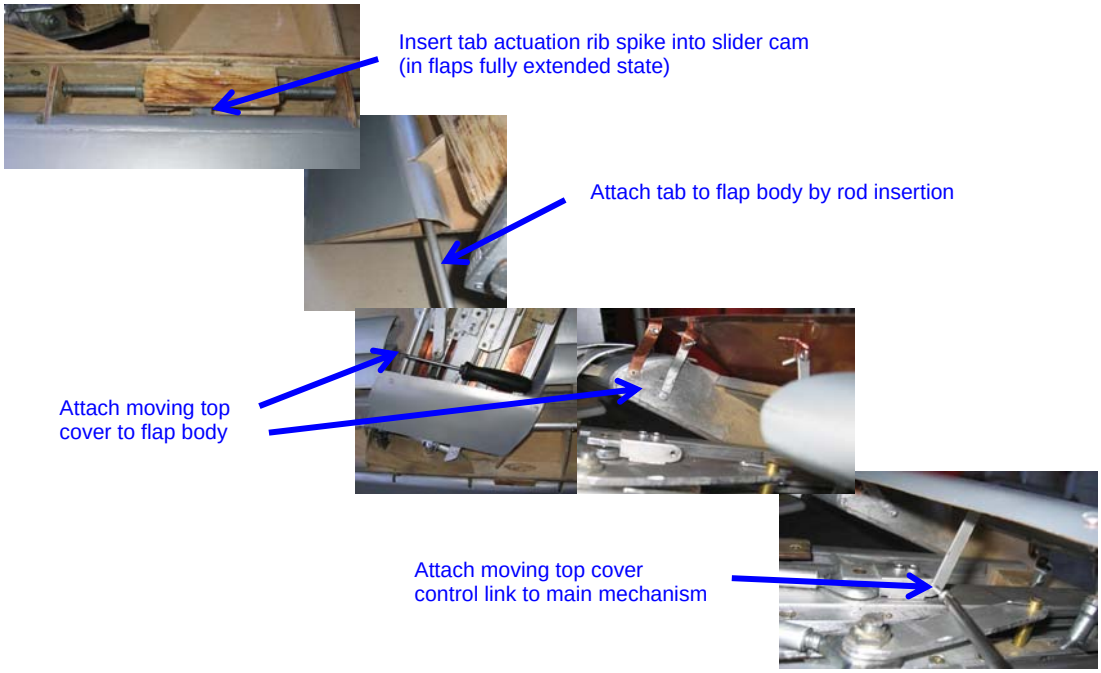

Assembly Manual: 7/7

Attach flap body fixed top cover;
attach speed brake to main wing section by rod insertion

Attach speed brake
control lever

Finished!

Bibliography

[1] Rudolph, P. K., *High-Lift Systems on Commercial Subsonic Airliners*, NASA Contractor Report 4746, National Aeronautics and Space Administration, Ames Research Center, Moffet Field, CA, USA, 1996

[2] Voit-Nitschmann, R., *Einführung in die Luftfahrttechnik*, Lecture Notes, Institute for Aircraft Design, University of Stuttgart, Germany, 2001

[3] Voit-Nitschmann, R., *Flugzeugentwurf*, Lecture Notes, Institute for Aircraft Design, University of Stuttgart, Germany, 2003

[4] Sigolotto, C., *Auslegung von Flugzeugsystemen*, Lecture Notes, Institute for Aircraft Design, University of Stuttgart, Germany, various editions

[5] Müller, C., *Flugzeuge der Welt*, NZZ Verlag, Zurich, Switzerland, 1997

[6] Gunston, B., *The Cambridge Aerospace Dictionary*, Cambridge University Press, Cambridge, United Kingdom, 2004

[7] *The Encyclopedia of World Aircraft*, Orbis Publishing Ltd. and Aerospace Publishing Ltd., 1997

[8] Niu, M.: *Airframe Structural Design*, Conmilit Press, Burbank, CA, USA, 1999.

[9] Rudolph, P.K.: *Mechanical Design of High Lift Systems for High Aspect Ratio Swept Wings*, NASA Contractor Report 196709, National Aeronautics and Space Administration, Ames Research Center, Moffett Field, CA, USA,1998.

[10] Bellam, J.E.: *Airplane Flap Supporting and Control Mechanism*, The Boeing Company, United States Patent No. 2,609,166; filed December 22, 1945 (obtained through www.depatisnet.de)

[11] Butler, V.B., and Cook, W.H.: *Airplane Flap Control Mechanism*, The Boeing Company, United Kingdom Patent No. 712,028; filed November 10, 1952 (obtained through www.depatisnet.de)

[12] Hansen, H.: *Multifunktionales Klappensystem für zukünftige Anwendungen*, Vortragsreihe 99: Start-/Landekonfigurationen, DaimlerChrysler Aerospace Airbus, Bremen, Germany, 1999

[13] Behrens, G.: *Systemkonzepte zu Mechanisierung: Hochauftriebssystem FLAP/SLAT*, Vortragsreihe 99: Start-/Landekonfigurationen, DaimlerChrysler Aerospace Airbus, Bremen, Germany, 1999

[14] *Electronic Code of Federal Regulations (eCFR)*, Title 14: Aeronautics and Space, Part 25 (obtained through http://ecfr.gpoaccess.gov)

[15] Stinton, D.: *Anatomy of The Aeroplane*, Blackwell Science Ltd, Oxford, United Kingdom, 1998

[16] Stinton, D.: *Flying Qualities and Flight Testing of The Aeroplane*, Blackwell Science Ltd, Oxford, United Kingdom, 1996

[17] Stinton, D.: *The Design of The Aeroplane*, Blackwell Science Ltd, Oxford, United Kingdom

[18] Beitz, W., Grothe, K.-H.: *Dubbel Taschenbuch für den Maschinenbau*, Springer Verlag, Berlin, Germany, 1997

[19], Paland, E.-G.: *Technisches Taschenbuch*, INA-Schaeffler KG, Herzogenaurach, Germany, 2002

[20] Meier, M., *Produkte-Entwicklung*, Lecture Notes, Institute for Mechanical Systems, ETH Zurich, Switzerland, 2002

[21] Reissner, J., *Werkstoffe*, Lecture Notes, Department of Materials, ETH Zurich, Switzerland, 2002

[22] Engmann, K., Meier, P.: *Technologie des Flugzeuges*, Leuchtturm Verlag/LTV Press, Alsbach/Bergtrasse, Germany, 2000

[23] Airbus Industries: *A330 Structural Repair Manual*

The following websites are valuable sources of aircraft pictures:

www.airliners.net
www.myaviation.net
www.planepictures.net
www.flugzeugbilder.de